Fixed-structure Control of LTI Systems with Polytopic-type Uncertainty:
Application to Inverter-interfaced Microgrids

THÈSE N^O 6799 (2016)

PRÉSENTÉE LE 12 FÉVRIER 2016
À LA FACULTÉ DES SCIENCES ET TECHNIQUES DE L'INGÉNIEUR
LABORATOIRE D'AUTOMATIQUE
PROGRAMME DOCTORAL EN GÉNIE ÉLECTRIQUE

ÉCOLE POLYTECHNIQUE FÉDÉRALE DE LAUSANNE

POUR L'OBTENTION DU GRADE DE DOCTEUR ÈS SCIENCES

PAR

Mahdieh Sadat SAD ABADI

acceptée sur proposition du jury:

Prof. D. Bonvin, président du jury
Dr A. Karimi, directeur de thèse
Prof. G. Ferrari Trecate, rapporteur
Prof. H. Karimi, rapporteur
Dr D. Gillet, rapporteur

EPFL

ÉCOLE POLYTECHNIQUE
FÉDÉRALE DE LAUSANNE

Suisse
2016

In loving memory of my dear mother

Acknowledgements

First and foremost, I would like to express my sincere gratitude to my PhD supervisor Dr. Alireza Karimi for accepting me in his research team and for his support, help, and immense knowledge. Indubitably, this thesis would have not been possible without him.

Besides my supervisor, I would like to thank my collaborator and external examiner, Prof. Houshang Karimi for introducing me to the active research area of microgrids. His motivational support, encouragement, and insightful comments brought a new spirit to this thesis.

I would also like to thank the rest of my thesis committee: Dr. Denis Gillet and Prof. Giancarlo Ferrari Trecate for their helpful suggestions, constructive feedbacks, and smart questions. I am grateful to Prof. Dominique Bonvin, the president of the thesis jury and the director of Automatic Control Lab (LA) at EPFL for all his continuous support, positive attitude, and advices.

My sincere thanks also go to Dr. Dimitri Peaucelle at LAAS-CNRS and Dr. Qobad Shafiee at the University of Aalborg for a short but fruitful collaboration. Their help and guidance are very much appreciated.

I am truly thankful to all current and past members of the Automatic Control Lab who provided a friendly and positive atmosphere, which indeed helped me during my PhD studies. Particularly, I wish to thank Ruth and Eva for their friendly and valuable administrative support, Christophe Salzmann for his precious help with laboratory setups and IT, Sandra for her kindness and support, Philippe for all technical and non-technical discussions and his regular help, Sriniketh for his friendship and help during my PhD studies, Jean-Hubert and Gabriel for translating the abstract of the thesis into French and their help. Many thanks go to my previous and current officemates (alphabetically ordered) Achille, Alejandro, Basile, David, Diogo, Gene, Ivan, Predrag, Sean, Sriniketh, Willson, and Zlatko. Special thanks go to Christoph K and Zlatko for their friendship, help, and interesting and enriching discussions about different aspects of my thesis.

Furthermore, I would like to thank my dear Iranian friends in Lausanne for all their help, support, and our unforgettable memories.

Lastly, I wish to thank my dear family. My utmost gratitude goes to my father, Jalal, for his unconditional love and continuous support at all stages of my life. I am thankful to my lovely sisters and brother, Yassaman, Zohreh, and Saeed, for their pure love, kindness,

Acknowledgements

encouragement, and unlimited support.

Abstract

This thesis focuses on the development of robust control solutions for linear time-invariant (LTI) interconnected systems affected by polytopic-type uncertainty. The main issues involved in the control of such systems, e.g. sensor and actuator placement problem, control configuration selection, and robust fixed-structure control design are included.

The problem of fixed-structure control is intrinsically non-convex and hence computationally intractable. Nevertheless, the problem has attracted considerable attention due to the great importance of fixed-structure controllers in practice. In this thesis, necessary and sufficient conditions for fixed-structure H_∞ control of polytopic systems with a single uncertain parameter in terms of a finite number of bilinear matrix inequalities (BMIs) are developed. Increasing the number of uncertain parameters leads to sufficient BMI conditions, where the number of decision variables grows polynomially. Convex approximations of robust fixed-order and fixed-structure controller design which rely on the concept of strictly positive realness (SPRness) of transfer functions in state space setting are presented. Such approximations are based on the use of slack matrices whose duty is to decouple the product of unknown matrices. Several algorithms for determination and update of the slack matrices are given.

It is shown that the problem of sensor and actuator placement in the polytopic interconnected systems can be formulated as an optimization problem by minimizing cardinality of some pattern matrices, while satisfying a guaranteed level of H_∞ performance. The control configuration design is achieved by solving a convex optimization problem whose solution delivers a trade-off curve that starts with a centralized controller and ends with a decentralized or a distributed controller.

The proposed approaches are applied to inverter-interfaced microgrids which consist of distributed generation (DG) units. To this end, two important control problems associated with the microgrids are considered: (i) Current control of grid-connected voltage-source converters with L/LCL-type filters and (ii) Voltage control of islanded microgrids. The proposed control strategies are able to independently regulate the direct and quadrature (dq) components of the converter currents and voltages at the point of common couplings (PCCs) in a fully decoupled manner and provide satisfactory dynamic responses. The important problem of plug-and-play (PnP) capability of DGs in the microgrids is also studied. It is shown that an inverter-interfaced microgrid consisting of multi DGs under plug-and-play functionality can be cast as a system with polytopic-type uncertainty. By virtue of this novel description and use of the results from theory of robust control, the stability of the microgrid system under PnP operation of DGs is preserved. Extensive case studies, based on time-domain simulations

Résumé

Cette thèse porte sur le développement de méthodes de commande robuste pour des systèmes linéaires interconnectés sujets à une incertitude polytopique. Les principaux problèmes qui existent pour le contrôle dans ces systèmes sont inclus, tels que le problème de positionnement des capteurs et actionneurs, la sélection de la configuration des contrôleurs et la synthèse robuste de structure fixe.

Le problème de la synthèse robuste de structure fixe est non-convexe et donc difficile à résoudre en pratique. Néanmoins, ce problème a attiré une grande attention à cause de l'importance de contrôleur à structure fixe dans la pratique. Cette thèse développe des conditions nécessaires et suffisantes pour le contrôle H_∞ à structure fixe applicable à des systèmes polytopiques avec un seul paramètre incertain sous forme d'un nombre fini d'inégalités matricielles bilinéaires (BMI). Augmenter le nombre de paramètres incertains conduit à des conditions suffisantes sous forme des BMIs où le nombre de variable croît de façon polynomiale. On présente aussi des approximations convexes des régulateurs robustes d'ordre fixe et de la synthèse de régulateurs de structure fixe basée sur le concept de positivité réelle stricte (SPR-ness) des fonctions de transfert dans l'espace d'état. De telles approximations sont basées sur des matrices de relaxation qui découplent le produit des matrices inconnues. Plusieurs algorithmes pour le calcul et la mise à jour des matrices de relaxation sont présentés.

Il est démontré que le problème du positionnement de capteurs et d'actionneurs dans les systèmes polytopiques interconnectés peut être formulé comme un problème d'optimisation dont l'objectif est la minimisation de la cardinalité de certaines matrices sous des contraintes de performance H_∞. La conception de la configuration du régulateur est réalisée par la résolution d'un problème convexe dont la solution produit une courbe de compromis qui commence avec un régulateur centralisé et finit par un régulateur distribué ou décentralisé.

Les approches proposées sont appliquées sur des micro-réseaux avec unités de génération distribuées (DG). On aborde deux problèmes importants de régulation associés au micro-réseaux : (i) la régulation de courant de convertisseurs en source de tension avec des filtres L/LCL (ii) la régulation de tension pour des micro-réseaux îlotés. Les stratégies de contrôle proposées permettent de réguler les composantes directes et de quadratures (dq) des tensions et courants du convertisseur au point de couplage commun (PCC) d'une façon complètement découplée et donnent une performance dynamique satisfaisante. On étudie aussi le problème du plug-and-play (PnP) d'unités de génération distribuées dans la micro-réseau. On montre qu'une micro-réseau consistant d'unités de génération distribuées sous des fonctionnalités de plug-and-play peut être modélisée comme un système sous des incertitudes

de type polytopique. En vertu de cette nouvelle description et de résultats de commande robuste, la stabilité de la micro-réseau en opération PnP est préservée. Des études de cas en MATLAB/SimPowerSystems sont présentées pour évaluer la performance des régulateurs proposés dans différents cas, tels que des variations de la charge, de la tension et du courant. Des études de cas avec hardware-in-the-loop en temps réel (RT-LAB OPAL-RT Technologies) sont aussi analysées pour évaluer la performance des méthodes proposées et leur sensibilité au bruit et aux défauts des PWM. Les simulations et résultats expérimentaux montrent une performance satisfaisante des régulateurs synthétisés.

Mots-clés : Régulation à structure fixe, régulation à ordre fixe, incertitude polytopique, optimisation convexe, régulation distribuée et décentralisée, synthèse de structures de régulation, micro-réseaux.

List of Abbreviations

2DOF   Two-Degree-of-Freedom
BMI   Bilinear Matrix Inequality
d   direct
DC   Direct Current
DER   Distributed Energy Resource
DG   Distributed Generation
DOE   Department of Energy
dq   direct-quadrature
QS   Quadratic Stability
QSL   Quasi Stationary Line
IEEE   Institute of Electrical and Electronics Engineers
IMP   Internal Model Principal
GPS   Global Positioning System
HIFOO   H-Infinity Fixed-Order Optimization
HIL   Hardware-In-the-Loop
HPPD   Homogeneous Polynomially Parameter-Dependent
KYP   Kalman-Yakubovich-Popov
L   Inductive(L)
LCL   Inductive(L)-Capacitive(C)-Inductive(L)
LFT   Linear Fractional Transformation
LMI   Linear Matrix Inequality
LPD   Linearly Parameter-Dependent
LTI   Linear Time-Invariant
MIMO   Multi-Input Multi-Output
NP   Non-deterministic Polynomial-time
PCC   Point of Common Coupling
PI   Proportional-Integral
PID   Proportional-Integral-Derivative
PLL   Phase-Locked Loop
PMS   Power Management System
PnP   Plug-and-Play
PPD   Polynomially Parameter-Dependent
PR   Proportional Resonant

PV	Photovoltaics
PWM	Pulse-Width Modulation
q	quadrature
RL	Resistive(R)-Inductive(L)
RLC	Resistive(R)-Inductive(L)-Capacitive(C)
SDP	Semidefinite Programming
SISO	Single-Input Single-Output
SOF	Static Output Feedback
SPR	Strictly Positive Real
THD	Total Harmonic Distortion
VSC	Voltage-Source Converter

Contents

Contents

Contents

List of Figures

List of Tables

1 Introduction

1.1 Research Context

1.1.1 Fixed-structure Control of Uncertain Systems

Classical controller design methods usually lead to full-order controllers which have same order as that of a generalized plant, i.e. plant plus frequency weighting functions [1]. The implementation of such controllers result in high cost in terms of both memory and processing power, difficult commissioning, and potential problems in maintenance [2]. Low-, fixed-order controllers are always preferred, particularly in many practical applications with limited available memory and computational power, such as embedded control systems for space and aeronautics industries [3, 4].

The classical control techniques cannot also cope with fixed-structure controllers in which some structural constraints are imposed on the controllers. Constraints on the control structure are mainly rooted in different sources. The first source comes from the well-known Internal Model Principle (IMP) [5] which states that for tracking and disturbance rejection, the dynamics of persistently exciting references and/or disturbances must be replicated in the structure of the controller. Furthermore, the well-known proportional-integral (PI)/proportional-integral-derivative (PID) controllers, widely used in industrial control systems, inherently have a fixed structure. Finally, the last main source results from a need for decentralized or distributed control of large-scale interconnected systems due to cost, reliability issues, and limitations on communication links among local controllers. All these reasons highlight the paramount importance of fixed-structure control design.

The problem of fixed-order and fixed-structure control still remains as an open issue. In fact, the non-convexity of the set of all fixed-order and fixed-structure stabilizing controllers for a given plant is the major root of difficulty in solving such a problem [4, 6]. Furthermore, if the problem is formulated in the space of the controller parameters, it becomes nonsmooth [4]. Nevertheless, due to the great importance of fixed-structure controllers in practice, several approaches for fixed-structure control design have been developed which are briefly reviewed

in the next section.

Fixed-structure control design becomes more complicated for the systems affected by uncertainties. The main sources of model uncertainties usually arise from unmodeled dynamics, parameter uncertainty, and neglected nonlinearities [7]. In the case of uncertain systems, the fixed-structure controller must be able to guarantee stability and performance specification of the whole family of models in the uncertainty domain.

This dissertation centres around the development of new fixed-structure controller design strategies for linear time-invariant (LTI) systems subject to unmodeled dynamics and parameter uncertainty. More specifically, it focuses on the following main objectives:

- Development of robust fixed-order and fixed-structure control techniques
- Control structure design of LTI interconnected systems with parameter uncertainty
- Application to inverter-interfaced microgrids consisting of distributed generation (DG) units

It is assumed that the LTI systems with uncertain parameters belongs to a polytope which is the convex hull of parameters of a set of models called as the vertices of the polytope. The polytopic-type uncertainty is one of the most general ways to present the physical parameter uncertainty without any conservatism. In fact, this type of uncertainty can cover interval, linear parameter, and multi-model uncertainties.

1.1.2 Inverter-interfaced Microgrids

Nowadays the growth of electricity demand, the critical shortages of fossil fuels, and global warming caused by greenhouse-gas-effect have negatively impacted on conventional power systems. The problems have been tackled alternatively through an efficacious integration and coordination of distributed generation (DG) units among which, in terms of their potential for energy generation, renewable energy sources such as photovoltaics (PV), wind power, and hydropower are the most important ones.

Reliable integration of DGs into power systems can be achieved by means of microgrids which are small electrical networks heterogeneously composed of DGs, loads, and energy storage systems [8]. Renewable energy sources are normally interfaced to the microgrids through power electronic converters acting as voltage sources [9].

Microgrids normally operate in grid-connected mode where they are connected to the main grid at Point of Common Coupling (PCC). Under this connection scheme, the voltage and frequency of the microgrids are predominantly determined by the main grid while the microgrid control system accurately shares active and reactive power among DGs and controls the power exchange between the microgrid and the main grid. Due to intentional (scheduled)/unintentional reasons, the microgrids can experience islanding conditions where they

are disconnected from the main grid [10]. In this case, due to a power mismatch between the DGs and the loads, voltage and frequency of the loads deviate from their rated values and the islanded microgrid eventually becomes unstable. This operation mode of the microgrids is more challenging than the grid-connected mode because accurate load sharing mechanisms are required to balance the power mismatch [8]. Therefore, upon the islanding condition, a new microgrid control strategy must come into service in order to provide voltage and frequency stability as well as a proper power sharing among DGs [11].

In spite of the potential benefits that the use of DGs may bring, their increasing penetration challenges an appropriate control strategy to ensure stable and reliable operation of microgrids in both grid-connected and islanded modes and smooth transition between them [12]. The main challenges arise from basic differences existing between the physical characteristics of the conventional electrical generators and the inverter-interfaced microgrids [13]. Conventional power networks feature a large fraction of generation from traditional synchronous generators that present large rotational inertia and play a key role in maintaining frequency and voltage stability. Given current and future trends in the cost and regulation of distributed photovoltaic systems, the future power network will feature deep penetration of inverter-interfaced microgrids (see, e.g., the SunShot Initiative by the Department of Energy (DOE) in the USA[1]). While larger renewable penetration is desirable, current power-electronic inverters behave as low-inertia devices and are not designed to contribute to grid-wise stability.

The application part of this dissertation aims to develop new control strategies for stable and efficient operation of microgrids in both grid-connected and islanded operation modes. A brief summary of the most relevant existing works organized by research topic is provided in the following section.

1.2   State of the Art

1.2.1   Current State of the Research in Fixed-structure Control

Fixed-structure control design is a theoretically challenging issue in control theory and it has attracted considerable attention due to its great importance in practice. However, so far, there has been no exact solution to this prominent problem and only rough approaches are available to approximately solve such a problem. The fact is that the problem is intrinsically non-convex; furthermore, it becomes nonsmooth in the case of problem formulation in the space of the controller parameters [4].

The easiest and most straightforward technique for low-order controller design is plant and/or controller order reduction using well-known methods, e.g. balanced model reduction [1]. However, plant or controller order reduction techniques do not always guarantee that the closed-loop performance is preserved. Moreover, the order reduction approaches are not able

---

[1]http://energy.gov/eere/sunshot/sunshot-initiative

to impose any structural constraints on the controller. Therefore, the challenging problem is to directly design a fixed-structure controller.

The only existing survey of fixed-order control/static output feedback has been conducted in [14]. Nevertheless, the past two decades have witnessed much theoretical progress on fixed-order controller design which has not been covered in that survey. A large amount of research has been carried out on the development of fixed-order control via linear matrix inequalities (LMIs) that among them one can mention: cone complementarity linearization method [15], (directional) alternating projection algorithm [16, 17], min/max algorithm [18], path-following approach [19], dual iteration method [20], XY-centring algorithm [21], penalty function method [22], log-det heuristic approach [23], sequential linear programming matrix method [24], augmented Lagrangian approach [25, 26], and concave minimization approach [27, 28]. A branch and bound (BB) algorithm for solving a general class of bilinear matrix inequality (BMI) problems with application to fixed-structure control has been developed in [29]. However, the BB approach is computationally high, particularly when the number of the controller parameters increase. Although the proposed approaches cope with the fixed-order control design, they cannot handle structural constraints imposed on the controller beyond its order.

In addition to the LMI-based approaches, there exist nonsmooth non-convex optimization-based fixed-structure control strategies, see, e.g. [30–36] which focus on solving the following optimization problem:

$$
\begin{aligned}
&\min_{K} && g(K) \\
&\text{subject to} && g(K) \le \beta
\end{aligned}
\tag{1.1}
$$

where $g(K)$ is a function of the closed-loop system matrices, e.g. spectral abscissa or an H_∞ norm, and the scalar β is given. The above optimization problem is nonconvex and nonsmooth. In fact, the lack of convexity and smoothness of the spectral abscissa and other similar performance criteria make the above optimization problem difficult to solve [37].

The following software and recent MATLAB functions, available in Robust Control Toolbox, can cope with the above nonsmooth nonconvex optimization problem.

- HIFOO (H_∞-H_2 Fixed Order Optimization) [31–34]

  HIFOO is a public-domain MATLAB package for static output feedback and fixed-order stabilizing control design in state space setting with several performance objectives, e.g. H_∞, H_2, multiobjective optimization, simultaneous stabilization, spectral abscissa, and complex stability radius optimization. HIFOO relies on quasi-Newton updating and gradient sampling algorithm in [37, 38].

- MATLAB commands: *hinfstruct*, *looptune*, *systune* [30, 35, 36, 39]

  The MATLAB command *hinfstruct*, available in the Robust Control Toolbox since R2010b,

addresses the problem of fixed-structure and fixed-order H_∞ control synthesis in both state space and transfer function framework. *looptune* tunes fixed-structure and fixed-order feedback loops while satisfying the common engineering requirements including performance bandwidth, setpoint tracking, roll-off, multiloop gain, and phase margins [40]. The MATLAB routine *systune* deals with the fixed-structure and fixed-order control synthesis with time-domain, frequency domain, open-loop shape, stability margin, and closed-loop poles requirements [40]. *systune* can also handle multiple requirements as well as multiple models.

The main properties of HIFOO, *hinfstruct*, *looptune*, and *systune* are that:

1) They are purely optimization-based, i.e. the fixed-order/fixed-structure control design problem is formulated as a solution to a nonsoomth noncomvex optimization.

2) As compared to the Lyapunov-based methods, they are quite fast in terms of execution time due to the absence of the Lyapunov matrix and the slack variables.

3) The existing nonsmooth nonconvex techniques cannot deal with the problem of fixed-order/fixed-structure control of systems with parameter uncertainty.

The fixed-structure controller design problem becomes more complicated for systems subject to polytopic uncertainty. In this case, the main objective is to design a fixed-structure controller which guarantees robust stability as well as robust performance of the whole family of models in the polytopic uncertainty domain. To solve this kind of problem, several LMI-based methods have emerged in the literature, e.g. the methods of [3, 41–45] in polynomial framework and the methods of [46–58] in state space framework. The polynomial-based approaches are based on the use of a central polynomial whose duty is to convexify the nonconvex problem of fixed-structure control and develop some inner convex approximations of that problem. In the state space approaches, which inherently introduce the Lyapunov matrix, some slack variables are used as a tool to decouple the product of the closed-loop matrices and the Lyapunov matrix leading to a sequence of sufficient LMI conditions. The main drawback of the fixed-structure control approaches in the polynomial setting is that they are just limited to single-input single-output (SISO) systems and cannot be employed for multi-input multi-output (MIMO) systems.

The main issue of the state space approaches lies in their conservativeness, which is reflected by the structure of the Lyapunov matrix. According to the structure of the Lyapunov matrix, the fixed-structure control approaches in the state space setting can be categorized in four classes: (i) QS-based methods, e.g. [46, 51], which provide the robust stability (performance) of the closed-loop system by means of a parameter-independent Lyapunov matrix. (ii) LPD-based methods, e.g. [53, 58], in which the robust stability (performance) is guaranteed via a linearly parameter-dependent (LPD) Lyapunov matrix. (iii) PPD-based methods, e.g. [57], which guarantee the robust stability and robust performance via a polynomially parameter-dependent Lyapunov (PPD) matrix. (iv) HPPD-based approaches, e.g. [56], in which the robust

stability (performance) is assessed by means of the existence of a homogeneous polynomially parameter-dependent (HPPD) Lyapunov matrix.

In the fixed-structure control approaches, the first assumption is that the control structure is given *a priori.* However, the problem of controller structure selection has a great importance, especially in large scale interconnected systems. In interconnected systems with a large number of inputs and outputs, the constraints on the controller structure are associated with some reasons: cost, reliability issues, inaccessibility of the states, and limitations on communication links and information exchange among the subsystems and/or the subcontrollers.

First, it is not cost-effective to use all possible sensors and actuators in large-scale systems, e.g. power grids [59], target-tracking [60], transportation networks [61], and buildings [62]. This leads to the problem of sensor and actuator placement in which a minimal set of sensors and actuators is chosen, provided that stability and a satisfactory level of performance of the system is guaranteed. The performance of a system not only depends on the control law but also it is considerably affected by the number of sensors and actuators and their positioning. The exact solution for the problem of sensor and actuator placement is to evaluate the overall system performance for all possible choices of sensors and actuators. However, this approach is not practical for the large values of sensors and actuators since it leads to a numerically intractable combinatorial cost. Therefore, several approximate solutions have been developed, e.g. [59–65]. Recently, some approaches based on convex optimization have been proposed, e.g. [65–67]. Although the literature on sensor and actuator selection is quite vast, the proposed methods do not consider the problem in the case of uncertainty in the system parameters. In this case, the question arises is that how to place a minimal number of sensors and actuators such that a good performance for the whole set of uncertain parameters is guaranteed?

Next, the interconnected systems need an appropriate design of control configuration which entails a minimal amount of information exchange and communication links among the subsystems and the local controllers. Under a fully decentralized control scheme, a set of non-interacting local controllers is designed for each subsystem and there is no communication links between different local controllers and different subsystems [68]. In spite of many advantages of the decentralized controllers, they may not provide the desired performance or even stability for the interconnected systems. Therefore, to avoid the stability problems associated with the decentralized control approaches, a distributed control strategy is used. In the distributed control methods, there exist several communication links between the local controllers and the subsystems according to the control configuration. Most of available distributed control approaches assume that the control configuration is given *a priori* [69]. However, it is possible that the assumed control structure is not the best one which can be taken into consideration. Moreover, it is generally difficult to select the configuration of the controller in advance. Therefore, the question arises is that in an interconnected system, what is the best control configuration, in terms of the connections between the local controllers and the subsystems, to provide a trade-off between the given control objectives? This problem has been recently addressed by some researchers in [70–75] through the design of sparse

static output/state feedback controllers where the gain between the subsystems' inputs and outputs/states is sparsified. Despite considerable efforts over the past few years, the problem is still open in the case of parameter uncertainties in the interconnected systems.

Finally, decentralized/distributed state feedback controllers are not always adequate control strategies for practical large-scale interconnected systems [76]. The state variables of certain subsystems are not often available for control purposes. In such a case, it is necessary to apply output feedback controllers, particularly low-order/static output feedback control due to the ease of practical implementation and computational issues.

1.2.2 Current State of the Research in Microgrid Control Systems

Grid-connected Voltage-Source Converters

In the grid-connected operating mode of microgrids, the utility grid provides the regulated frequency and voltage for the local loads at PCCs. In this case, each DG regulates its active and reactive power exchange based on current control techniques.

Voltage-source converters (VSCs) are commonly interfaced to the grid by means of a pure L or an LCL filter in order to attenuate switching high-frequency harmonics caused by pulse width modulation (PWM) VSCs. The LCL filters are frequently used in VSCs due to their cost-effectiveness in terms of size and weight of the filters and the efficient attenuation of the switching harmonics [77]. However, the LCL filters increase the complexity of the dynamics of the DG interface system. Moreover, due to the high resonant peak of the LCL filters, incorporating the LCL filters into VSCs necessitates modifying the conventional proportional integral (PI) in stationary domain or proportional resonant (PR) current controllers in synchronous reference domain. To overcome this issue, various current control approaches have been proposed for grid-tied VSCs in the literature, which can be categorized into two major classes: passive damping [78] and active damping approaches [77, 79–88].

A common strategy in the passive damping methods is to use resistors in series with the capacitor in the filters. Although this strategy is simple and reliable, the damping resistors weaken the high-frequency harmonic attenuation property of the LCL filters and creates power losses [89].

In the active damping methods, the current control structure is modified such that the grid-connected VSC is stabilized. Active damping-based controllers are generally designed either in stationary reference frame (abc-frame)[79, 82, 83, 88, 90] or in rotating reference frame (dq-reference frame) [84, 87, 91–93]. Although the stationary reference frame does not include the coupling terms, it has some drawbacks, e.g. its sensitivity to the grid frequency changes [80, 94], complicated controller design, etc. Therefore, the dq-based controllers are generally more preferred than the abc-frame ones [80]. Nevertheless, the rotating reference frame brings the coupling terms into system equations [77]. The coupling components can be easily cancelled

in the L-type filters [91, 92]; however, in the case of the LCL filters such terms are complicated to handle.

Depending on the availability of the sensors and/or signals and from the economic and practical points of view, the active damping approaches can be classified into two main classes: (i) multi-loop and state feedback controllers[79, 82, 84, 88] and (ii) dynamic output feedback controllers (filter-based methods) [81, 85–87]. In the first group, there exist two or three control loops instead of a single current loop whereas in the second category, only one current control loop is adopted. Therefore, multiloop and state feedback controllers need more sensors leading to an increase in the overall cost of the system and a decrease in the system reliability.

Generally, in the context of current control of the grid-tied VSCs, there are several areas which can still benefit from further research: (1) robust stability and robust performance specifications against the parameter uncertainty in the grid inductance and (2) decoupling of the direct (d) and quadrature (q) components of current axes.

Islanded Microgrids

In order to standardize the operation and functionalities of microgrids, a hierarchical control strategy has been recently developed in [95]. It mainly consists of three levels with separate time-scales named as primary, secondary, and tertiary control. The first one is intended to stabilize the voltage and frequency of the microgrids and to facilitate an accurate power sharing. The second level compensates for the deviations in the voltage and frequency in the steady-state and provides global controllability of the microgrids [96]. The last level is related to the optimal operation in both islanded and grid-connected modes and the power flow control in the grid-connected mode [97].

A control strategy ubiquitously used for the primary control of microgrids is droop control which relies on the principle of power balance of a classical synchronous generator in conventional power networks (see, e.g., [9, 95, 98–106]). In the power systems based on rotating generators, frequency (rotor speed) is dependent on active power balance, i.e. the frequency is dropped when the demanded active power increases [107]. The idea of the so-called "droop" controllers has been developed by Chandorkar *et al* [108]. From a control point of view, droop control is a decentralized proportional controller maintaining the voltage and frequency stability of the microgrids [13]. The main advantage of droop-based control is the elimination of the communication links among droop controllers enabling the plug-and-play (PnP) operation in the microgrids.

In the droop control of an inverter-based microgrid with dominantly inductive lines, i.e. power lines with small R/X ratios, the active power is strongly influenced by the frequency ("$\omega - P$" droop characteristic), while the reactive power is affected by the voltage deviations ("$V - Q$" droop characteristic) [13]. The active power-frequency and reactive power-voltage droop

controllers of the ith inverter are implemented as follows [13]:

$$
\begin{aligned}
\omega_i &= \omega^* - K_{P_i}(P_i - P_i^*) \\
V_i &= V_i^* - K_{Q_i}(Q_i - Q_i^*)
\end{aligned}
$$

(1.2)

where ω^* is the desired (nominal) frequency, V_i^* is the desired (nominal) voltage amplitude, P_i and Q_i respectively are the active and reactive power injection at inverter i, and P_i^* and Q_i^* are the nominal active and reactive power injection of inverter i, respectively. The controller gains $K_{P_i} > 0$ and $K_{Q_i} > 0$ are droop coefficients.

In low-voltage applications with predominantly resistive lines, the "$\omega - Q$" and "$V - P$" droop characteristics are employed [109, 110]. However, in the case of resistive-inductive line conditions and in the presence of conductances, the classical droop control laws cannot achieve an efficient power sharing due to the coupled active and reactive power characteristics of the power systems [111]. Although a large amount of research in the area of droop control has focused on the microgrids with pure inductive and/or pure resistive line impedances, only two main approaches have addressed the realistic case of complex line impedances in the droop-based control. The first approach given in [112] decouples the voltage and frequency droop controls through an orthogonal linear rotational transformation which depends on the line reactance-to-resistance ratios. The second approach presented in [113] is based on the concept of virtual impedance loop which improves the decoupling of active and reactive power. The first approach is sensitive to the nature of the line impedance and restricted to networks with constant resistance-to-reactance ratios, whereas in the second strategy the large virtual impedance causes the output voltage of the inverter to drop severely [114]. Therefore, the development of a novel control strategy for the case of complex and general line conditions is still a challenging problem.

Droop-controlled inverter-interfaced microgrids have recently been under some rigorous nonlinear analyses. The first stability analysis of "$\omega - P$" droop-controlled inverter-interfaced microgrids with parallel topologies has been provided by Simpson-Porco *et al* in [115]. They have shown that a microgrid system under "$\omega - P$" droop control can be described as a Kuramoto model of phase-coupled oscillators, which have extensively been studied. Then, by applying the results of theory of coupled oscillators, a necessary and sufficient condition for frequency synchronization and a proportional active power sharing has been proposed [115]. The results addressed in [115] are devoted to acyclic network topologies; in consequence, they are not applicable to meshed microgrids with cycles. In [13], a nonlinear stability analysis of "$\omega - P$" droop-controlled inverter-interfaced microgrids with meshed topologies has been provided. They have proposed sufficient conditions on the droop coefficients and setpoints to guarantee the frequency stability and a desired active power sharing in droop-based microgrids with general structures.

An issue that has not been addressed in these recent works is a rigorous nonlinear analysis of "$V - Q$" droop-controlled microgrids. The existing voltage droop control approaches do,

in general, not guarantee a desired reactive power sharing [116]. However, this problem is difficult and still an open problem because as opposed to frequency, voltage is not fixed along the microgrid. Another important issue which has not been fully studied yet in the technical literature is a rigorous transient stability analysis of the droop-controlled inverter-interfaced microgrids due to load changes, nonlinear loads, faults, transition from the grid-connected to the islanded mode, and vice versa.

The primary droop control methods lead to an inherent trade-off between power sharing and voltage and frequency regulation. While obtaining a successful power sharing among DGs, the voltage and frequency deviate from their nominal values [99, 104, 108]. In this case, secondary control is employed to compensate the voltage and frequency deviations in the steady state. Conventional secondary controllers exploit a centralized architecture which is unreliable in case of a single point of failure [11]. Moreover, due to the distributed nature of microgrids, any kind of centralized control strategies is almost impossible [117]. For these reasons, recently several advanced distributed control strategies merging the primary and secondary levels have been developed, e.g. [12, 96, 117–120]. The proposed methods are based on continuous time averaging with all-to-all or nearest-neighbour communication. A review of the most existing distributed secondary control approaches for the microgrids can be found in [11].

Tertiary control layer that considers the economical concerns in the optimal operation of the microgrids can be formulated as an optimization problem by minimizing an economic dispatch problem subject to nonlinear constraints caused by AC injections [121]. In [117, 121], it has been shown that the optimization problem in the tertiary level can be minimized via droop control.

In addition to the droop-based control strategies in the primary level of the hierarchy, non-droop-based approaches for voltage and frequency control of the islanded microgrids have been also developed, e.g. [122–131]. The proposed methods regulate the voltage of a single-DG [122–124, 127, 128] and/or a multi-DG microgrid [126, 129–131]. In these methods, the frequency of each DG unit is controlled through an internal oscillator in an open-loop manner with $\omega_0 = 2\pi f_0$, where f_0 is nominal system frequency. All oscillators are synchronized by a common time reference signal according to a global positioning system (GPS) [129].

Although extensive research has been carried out on the development of non-droop-based control of micorgrids, there still exist several challenges to be addressed: (1) robustness to parametric uncertainties, (2) a need for advanced control design strategies with decentralized structure, (3) plug-and-play (PnP) functionality, and (4) low-complex voltage controllers.

1.3   Research Objectives

The main objectives of this dissertation are twofold: one mainly focuses on the development of LMI-based fixed-structure control approaches satisfying several performance specifications and second, the applications of the proposed control strategies to the inverter-interfaced

microgrids.

The first objective is stated as follows: Given an uncertain plant, denoted by G, and a fixed-structure controller K, find an appropriate setting for the controller (the controller parameters and/or the control structure) such that the closed-loop system, denoted by $[G,K]$, satisfies the following performance specification:

$$\phi([G,K]) < \mu \tag{1.3}$$

where ϕ is a control performance criterion such as spectral abscissa (decay rate), H_2, and H_∞ performance. The mentioned problem is formulated as follows:

$$\begin{aligned} &\min_{\mu,K} && \mu \\ &\text{subject to} && \phi([G,K]) < \mu \end{aligned} \tag{1.4}$$

To solve the above optimization problem, the following issues should be determined:

- **Uncertain plant G**

  Among all kind of structured and unstructured uncertainties, this dissertation focuses on polytopic-type uncertainty due to its simplicity, generality, and easy handling, mainly in the context of the Lyapunov-based methods. To this end, consider a linear time-invariant (LTI) plant subject to the polytopic uncertainty as follows:

  $$\begin{aligned} G(\lambda) &= \left[\begin{array}{c|c} A_g(\lambda) & B_g(\lambda) \\ \hline C_g(\lambda) & D_g(\lambda) \end{array} \right] \\ &= \sum_{i=1}^{q} \lambda_i \left[\begin{array}{c|c} A_{g_i} & B_{g_i} \\ \hline C_{g_i} & D_{g_i} \end{array} \right] \end{aligned} \tag{1.5}$$

  where $\lambda = [\lambda_1, \ldots, \lambda_q]$ is in the following unit simplex Λ_q:

  $$\Lambda_q = \left\{ \lambda_1, \ldots, \lambda_q \;\middle|\; \sum_{i=1}^{q} \lambda_i = 1, \quad \lambda_i \geq 0 \right\} \tag{1.6}$$

  q is the number of vertices of the polytopic system and $\left(A_{g_i}, B_{g_i}, C_{g_i}, D_{g_i} \right)$ is the i-th vertex of the polytopic system. It should be noted that the dissertation can also take the unmodeled dynamics into account.

- **Fixed-structure controller K**

  The controllers are limited to LTI systems subject to some constraints on their structure. The constraints include a fixed order (e.g. low-order controllers and static output feedback) and a given fixed structure (e.g. PIDs, lead-lag compensators, decentralized/distributed controllers, etc.).

- **Performance specification ϕ**

  A fundamental requirement of the closed-loop system $[G(\lambda), K]$ is robust stability for all family of systems in $G(\lambda)$, $\lambda \in \Lambda_q$. Additional performance specifications can also be considered; for instance, disturbance rejection, spectral abscissa, time-domain specifications, and H_∞ performance.

- **Appropriate algorithms/tools**

  The fixed-structure controller design which ensures the robust stability of the closed-loop system $[G, K]$ while satisfying the robust performance specifications is an important issue in the robust control theory and has attracted a remarkable attention. However, the problem even in a nominal case, i.e. systems without uncertainty, is a nonconvex and nonsmooth optimization problem [4]. To deal with these difficulties, inner convex approximations of fixed-structure control problems are developed in this dissertation. The main feature of the proposed convex optimization-based approaches in this dissertation is that they rely on the concept of strictly positive realness (SPRness) of some transfer functions [132].

The second part of the dissertation is dedicated to the control of inverter-interfaced microgrids addressing various challenges associated with robustness to parametric uncertainty and load variations, low complexity of the controller, plug-and-play operation of DGs, and mixed line microgrids with resistive-inductive line conditions. To achieve these objectives, innovative high-performance MIMO robust (decentralized) fixed-structure control strategies are developed based on an LTI model of a microgrid in a synchronous reference frame (dq-frame). The proposed control techniques are able to overcome the limitations of existing droop-based controllers which are only appropriate for microgrids with dominantly inductive and/or resistive power lines. Furthermore, opposed to most non-droop-based control methods, e.g. [122–131], the present approaches guarantee the robust stability and robust performance against the load parameter changes. Moreover, the proposed controller is robust to PnP functionality of DGs; therefore, the plug-in and/or plug-out operation of DGs do not affect the stability of the microgrid system. Simulation studies in MATLAB/SimPowerSystems toolbox and experimental results using real-time hardware-in-the-loop (HIL) environment demonstrate the effectiveness of the designed controllers.

1.4 Contributions

The salient contributions of this dissertation are as follows:

- It derives necessary and sufficient conditions in terms of bilinear matrix inequalities (BMIs) for fixed-structure H_∞ control of continuous-time LTI polytopic systems with two vertices by means of polynomially parameter-dependent Lyapunov matrices. The conditions are built upon the celebrated (D, G) scaling [133–135]. The extension of the results to a polytope with more than two vertices leads to only sufficient conditions.

- It presents a linear matrix inequality (LMI) framework to design fixed-structure stabilizing (H_∞) controllers for linear time-invariant systems subject to polytpoic uncertainty. The framework relies on the strictly positive realness (SPRness) of a transfer function depending on two slack matrices. The slack matrices are determined by a set of fixed-structure controllers designed for each vertex or all vertices of the polytope. Continuous-time and discrete-time controller design are treated in a completely unique manner.

- It proposes necessary and sufficient conditions for fixed-order controller design of LTI continuous-time and discrete-time polytopic systems via homogeneous polynomially parameter-dependent Lyapunov matrices. The proposed method is based on the concept of SPRness of a transfer function depending on a parameter-dependent gain. To convert the problem to a set of LMI conditions, the parameter-dependent gain is determined *a priori* by means of a parameter-dependent state feedback controller. It is theoretically and numerically demonstrated that the proposed approach allows fixed-order stabilizing (H_∞) controller synthesis which potentially use less decision variables than some existing approaches, e.g. [46, 49, 54, 56].

- It develops a convex optimization-based technique for sensor and actuator placement in LTI polytopic systems. The proposed approach is successfully applied to the challenging problem of phasor measurement unit (PMU) placements in IEEE 14-bus test system.

- It addresses the fixed-structure control design of LTI interconnected systems affected by polytopic uncertainty. Different from the existing approaches, where the structure of the controller is fixed *a priori*, the control structure and the controller parameters are simultaneously designed through the minimization of a weighted ℓ_1 norm of a pattern matrix subject to a guaranteed level of H_∞ performance.

The dissertation also

- proposes a robust fixed-structure decentralized/distributed H_∞ voltage controller for islanded inverter-interfaced microgrids consisting of DGs under load parameter uncertainty.

- presents a decentralized voltage control scheme for islanded inverter-interfaced microgrids with general structure enabling the plug-and-play functionality of DGs.

- develops a current controller for grid-connected voltage-source converter with L/LCL filter ensuring robust stability and robust H_∞ performance to grid inductance parameter uncertainty.

1.5 Dissertation Layout

The dissertation breaks into two main parts: The significant portion, Chapter 2-Chapter5, are devoted to fixed-order and fixed-structure control of LTI polytopic systems. The remaining chapters focus on the control of inverter-interfaced microgrids. In the following, we briefly outline the contents of each chapter.

Fixed-structure Control Strategy

Chapter 2: Fixed-structure Control: A BMI Problem

Chapter 2 deals with the problem of fixed-structure controller synthesis of LTI polytopic systems ensuring the H_∞ performance of the closed-loop system via polynomially parameter-dependent (PPD) Lyapunov matrices. In the case of a polytopic system with two vertices, the celebrated (D, G) scaling [133–135] enables us to derive necessary and sufficient conditions in terms of bilinear matrix inequalities (BMIs) in a nonconservative way. However, for the case of a polytope with more than two vertices, only sufficient conditions are developed. The set of BMI conditions are solved using existing developed approaches. The efficacy of the proposed BMI-based approach is illustrated by means of numerical comparisons with existing fixed-order controller design approaches.

Chapter 3: Fixed-structure Control of Systems with Polytopic Uncertainty via LPD Lyapunov Matrices

Chapter 3 presents how a fixed-structure control design of linear time-invariant (LTI) polytopic systems can be formulated as a convex optimization problem. To this end, inner convex approximations of fixed-structure stabilizing (H_∞) controllers are introduced. The proposed approaches rely on the concept of strictly positive realness (SPRness) of a transfer function depending on two slack matrices via linearly parameter-dependent (LPD) Lyapunov matrices. The slack matrices are determined and iteratively updated through a convex optimization problem and a set of initial fixed-structure controllers designed for each vertex of the polytope. The performance of the proposed LMI-based approaches are evaluated in detail through several numerical examples.

Chapter 4: Fixed-order Controller Synthesis of Systems with Polytopic Uncertainty via HPPD Lyapunov Matrices

Chapter 4 is concerned with the design of static output feedback stabilizing (H_∞) controllers for uncertain linear time-invariant (LTI) systems. The time-invariant uncertainty is in the form of a polytopic and affects all the system matrices. Although we mainly focus on the problem of static output feedback (SOF) controller design, it is not restrictive because a dynamic output-feedback controller can be reformulated as SOF for an augmented plant. Necessary

and sufficient conditions based upon the SPRness of a transfer function depending on a parameter-dependent gain are developed. To convert the problem to a convex optimization, the parameter-dependent gain is determined *a priori* by means of a parameter-dependent state feedback controller. The robust stability and robust H_∞ performance of the closed-loop polytopic systems are ensured via homogeneous polynomially parameter-dependent (HPPD) Lyapunov matrices.

Chapter 5: Control Structure Design for LTI Interconnected Systems subject to Polytopic Uncertainty

Chapter 5 copes with two important issues of LTI interconnected systems affected by polytopic uncertainty: sensor and actuator placement and control configuration design. To this end, the control problems are formulated as non-convex optimization problems by minimizing the cardinality of some pattern matrices, while satisfying a guaranteed level of H_∞ performance. For the resulting combinatorial optimization problem, computationally tractable convex relaxations are provided. More specifically, using the convex inner approximation of H_∞ controller synthesis in Chapter 3 and a weighted ℓ_1 norm relaxation, several iterative algorithms are proposed. The main characteristic of the proposed approaches is that the control structure and the control parameters are simultaneously designed. Simulation results confirm the effectiveness of the proposed approaches in this chapter.

Applications to Control of Inverter-interfaced Microgrids

Chapter 6: Grid-connected Voltage-Source Converters

In Chapter 6, an LMI-based method for robust decoupled *dq* current control, in the discrete-time domain, of a grid-connected voltage-source converter with L/LCL filters under the grid inductance uncertainty is presented. In fact, the robustness of the controller to the grid inductance uncertainties and the decoupling of *dq* current axes are two key features considered in this approach. The desired performance specifications including fast speed, small overshoot, high closed-loop bandwidth as well as *dq*-axes decoupling are formulated in terms of some H_∞ criteria. The MIMO controller is obtained through a solution of a convex optimization problem developed in Chapter 3. The controller guarantees the robust stability and the robust performance for all values of the grid inductance assumed to be in a given interval. The controller provides a high bandwidth; moreover, it is associated with an integral action to track all step reference current signals with zero steady state error. The simulation studies are conducted in SimPowerSystem environment of MATLAB under several case studies, e.g. *dq* reference current signal tracking and robustness to the grid inductance. The simulation results demonstrate the effectiveness of the designed current controller.

Chapter 7: Islanded Inverter-interfaced Microgrids

Chapter 7 investigates the autonomous (islanded) operation of inverter-interfaced microgrids under load parameter uncertainty. The control objective is to regulate the voltage of DGs at point of common couplings (PCCs) to achieve a prespecified load sharing among the DGs. To this end, a power management system (PMS) specifies voltage set points of each DG according to a classical power flow. The set points are sent to local robust decentralized controllers which are designed, in *dq*-frame, using the developed approach in Chapter 5, based on an LTI mathematical model of the microgrid system with polytopic-type uncertainty. To control the frequency of the microgrid, DGs are equipped with internal oscillators, synchronized based on a time-reference signal received from a global positioning system (GPS). Analysis of the microgrid dynamics, simulations case studies in MATLAB, and experimental results based on hardware-in-the-loop (HIL) test platform demonstrate the desired performance of the proposed control strategy.

Chapter 8: Voltage Control of Islanded Microgrids with General Topology

Chapter 8 considers the challenging problem of plug-and-play (PnP) functionality of DGs in an inverter-interfaced microgrid. To this end, a decentralized voltage controller for the islanded inverter-interfaced microgrids with general topology is designed. The proposed control scheme relies on Quasi-Stationary Line (QSL) approximate model of microgrid and the concept of neutral interactions. The main feature of the proposed controller is that it is robust to PnP functionality of DGs; therefore, the plug in and/or plug out operation of DGs do not have any impact on the stability of the microgrid system. The controller performance in terms of voltage tracking, microgrid topology change, and plug-and-play capability features is successfully verified through simulations case studies of a microgrid system consisting of 11 DGs.

Chapter 9: Conclusions and Future Directions

This chapter summarizes the work, draws some general conclusions, and discusses the possible future directions.

Fixed-structure Control Strategy

2 Fixed-structure Control: A BMI Problem

2.1 Introduction

This chapter addresses the problem of fixed-structure control of continuous-time linear time-invariant systems affected by polytopic uncertainty by means of polynomially parameter-dependent Lyapunov matrices. We show that such a problem is equivalent to feasibility of infinite number of bilinear matrix inequality (BMI) conditions. However, the celebrated (D, G) scaling [133–135] enables us to derive necessary and sufficient conditions in terms of finite number of BMIs in a nonconservative way in the case of a polytopic system with two vertices. For a polytope with more than two vertices, only sufficient BMI conditions are developed. Various comparisons with existing fixed-order controller design approaches illustrate the potential of the proposed framework of necessary and sufficient BMIs.

The organization of this chapter is as follows: Section 2.2 and Section 2.3 respectively present problem statement for systems without and with polytopic-type uncertainty. Sections 2.4 and 2.5 are devoted to main results. Simulation examples are given in Section 2.6. The chapter ends with concluding remarks in Section 2.7.

The notation used in this chapter is standard. In particular, I_n and $0_{n\times1}$ are the $n \times n$ identity matrix and the zero vector of dimension n, respectively. The symbols $\otimes$, $\star$, and $A(i : j,:)$ denote the Kronecker product, the symmetric blocks, and the extraction of the ith through the jth row of matrix A, respectively. The symbol $\text{He}\{A\}$ is a notation for $A + A^T$.

2.2 Fixed-structure Control

2.2.1 System Dynamics

Consider a continuous-time linear time-invariant (LTI) system described by the following state space equations:

$$
\begin{aligned}
\dot{x}_g(t) &= A_g x_g(t) + B_g u(t) + B_w w(t) \\
z(t) &= C_z x_g(t) + D_{zu} u(t) \\
y(t) &= C_g x_g(t)
\end{aligned}
\tag{2.1}
$$

where $x_g \in \mathbb{R}^n$, $u \in \mathbb{R}^{n_i}$, $w \in \mathbb{R}^r$, $y \in \mathbb{R}^{n_o}$, and $z \in \mathbb{R}^s$ are the state, the control input, the exogenous input, the measured output, and the controlled output, respectively. The state space matrices A_g, B_g, B_w, C_z, D_{zu}, and C_g are of appropriate dimensions.

2.2.2 Control Structure

The main objective is to design a fixed-structure output feedback controller $K(s)$ of order m ($0 \le m < n$) with the following state space representation:

$$
\begin{aligned}
\dot{x}_c(t) &= A_c x_c(t) + B_c y(t) \\
u(t) &= C_c x_c(t) + D_c y(t)
\end{aligned}
\tag{2.2}
$$

where $A_c \in \mathbb{R}^{m \times m}$, $B_c \in \mathbb{R}^{m \times n_o}$, $C_c \in \mathbb{R}^{n_i \times m}$, and $D_c \in \mathbb{R}^{n_i \times n_o}$.

2.2.3 Closed-loop System

The closed-loop system H_{zw}, transfer function from w to z, is obtained by augmenting the states of the system $x_g \in \mathbb{R}^n$ and the states of the controller $x_c \in \mathbb{R}^m$, yielding

$$
\begin{aligned}
\dot{x}(t) &= A x(t) + B w(t) \\
z(t) &= C x(t)
\end{aligned}
\tag{2.3}
$$

where $x(t) = \begin{bmatrix} x_g^T(t) & x_c^T(t) \end{bmatrix}^T$ and

$$
A = \begin{bmatrix} A_g + B_g D_c C_g & B_g C_c \\ B_c C_g & A_c \end{bmatrix}, \quad B = \begin{bmatrix} B_w \\ 0 \end{bmatrix}
$$
$$
C = \begin{bmatrix} C_z + D_{zu} D_c C_g & D_{zu} C_c \end{bmatrix}
\tag{2.4}
$$

The fixed-structure dynamic output feedback controller $K(s)$ stabilizes the system if and only if there exists a Lyapunov matrix $P > 0$ such that the following Lyapunov inequality is satisfied:

$$A^T P + PA < 0 \tag{2.5}$$

The main difficulty associated with fixed-structure controller design is that the stability condition in (2.5) is not convex in unknown parameters. In fact, the inequality given in (2.5) is a BMI problem which is generally NP-hard [136]. The well-known BMI solvers such as the commercial software package PENBMI [137, 138] and the free open-source MATLAB toolbox PENLAB [139] locally solve optimization problems with BMI and LMI constraints. However, the BMI solvers most often fail to provide a solution for the Lyapunov inequality in (2.5). Moreover, the choice of an initial guess is very crucial in these solvers. In the next section, we show that the problem of fixed-structure control of polytopic systems leads to infinite number of BMI conditions.

2.3 Fixed-structure Control of Systems with Polytopic Uncertainty: A Parameter-dependent BMI

Consider a continuous-time LTI polytopic system with $q = 2^l$ vertices described by:

$$\begin{aligned}
\dot{x}_g(t) &= A_g(\lambda) x_g(t) + B_g(\lambda) u(t) + B_w(\lambda) w(t) \\
z(t) &= C_z(\lambda) x_g(t) + D_{zu}(\lambda) u(t) \\
y(t) &= C_g(\lambda) x_g(t)
\end{aligned} \tag{2.6}$$

where $x_g \in \mathbb{R}^n$, $u \in \mathbb{R}^{n_i}$, $w \in \mathbb{R}^r$, $y \in \mathbb{R}^{n_o}$, and $z \in \mathbb{R}^s$ are the state, the control input, the exogenous input, the measured output, and the controlled output, respectively. The uncertain matrices belong to a polytopic domain given by:

$$\begin{aligned}
\Omega_1 &= \left\{ \left(A_g(\lambda), B_g(\lambda), C_g(\lambda), B_w(\lambda), C_z(\lambda), D_{zu}(\lambda) \right) \right. \\
&= \left. \sum_{i=1}^{q} \lambda_i \left(A_{g_i}, B_{g_i}, C_{g_i}, B_{w_i}, C_{z_i}, D_{zu_i} \right) \right\}
\end{aligned} \tag{2.7}$$

where $\lambda = [\lambda_1, \ldots, \lambda_q]$ is in the following unit simplex Λ_q:

$$\Lambda_q = \left\{ \lambda_1, \ldots, \lambda_q \, \middle| \, \sum_{i=1}^{q} \lambda_i = 1, \quad \lambda_i \geq 0 \right\}, \tag{2.8}$$

q is the number of vertices of the polytopic system and the matrices A_{g_i}, B_{g_i}, C_{g_i}, B_{w_i}, C_{z_i}, and D_{zu_i} build the i-th vertex of the polytope. To keep the linear dependency of the closed-loop matrices on the vector λ, only one of matrices B_g or C_g can have the polytopic uncertainty. In what follows, we assume that B_g belongs to the polytopic uncertainty domain Ω_1.

The polytopic model in (2.6) can be equivalently converted into an affine parameter-dependent

system as follows:

$$\dot{x}_g(t) = A'_g(\theta)x_g(t) + B'_g(\theta)u(t) + B'_w(\theta)w(t)$$
$$z(t) = C'_z(\theta)x_g(t) + D'_{zu}(\theta)u(t) \tag{2.9}$$
$$y(t) = C'_g x_g(t)$$

where the matrices $A'_g(\theta)$, $B'_g(\theta)$, C'_g, $B'_w(\theta)$, $C'_z(\theta)$, and $D'_{zu}(\theta)$ belong to the following uncertainty domain:

$$A'_g(\theta) = A'_{g_0} + \sum_{i=1}^{l} \theta_i A'_{g_i}, \quad B'_g(\theta) = B'_{g_0} + \sum_{i=1}^{l} \theta_i B'_{g_i}$$

$$B'_w(\theta) = B'_{w_0} + \sum_{i=1}^{l} \theta_i B'_{w_i}, \quad C'_g = C_g \tag{2.10}$$

$$C'_z(\theta) = C'_{z_0} + \sum_{i=1}^{l} \theta_i C'_{z_i}, \quad D'_{zu}(\theta) = D'_{zu_0} + \sum_{i=1}^{l} \theta_i D'_{zu_i}$$

where $\theta_i \in [-1, 1]$; $i = 1, \ldots, l$.

The problem addressed in this chapter is the design of a robust fixed-structure controller $K(s)$ with the state space representation given in (2.2). The closed-loop system $H_{zw}(\theta)$ is described as follows:

$$\dot{x}(t) = A(\theta)x(t) + B(\theta)w(t)$$
$$z(t) = C(\theta)x(t) \tag{2.11}$$

where $x(t) = \begin{bmatrix} x_g^T(t) & x_c^T(t) \end{bmatrix}^T$ and

$$A(\theta) = \begin{bmatrix} A'_g(\theta) + B'_g(\theta)D_cC'_g & B'_g(\theta)C_c \\ B_cC'_g & A_c \end{bmatrix}, \quad B(\theta) = \begin{bmatrix} B'_w(\theta) \\ 0 \end{bmatrix}$$
$$C(\theta) = \begin{bmatrix} C'_z(\theta) + D'_{zu}(\theta)D_cC'_g & D'_{zu}(\theta)C_c \end{bmatrix} \tag{2.12}$$

The triplet $\big(A(\theta), B(\theta), C(\theta)\big)$ belongs to the following domain:

$$A(\theta) = A_0 + \sum_{i=1}^{l} \theta_i A_i$$

$$B(\theta) = B_0 + \sum_{i=1}^{l} \theta_i B_i \tag{2.13}$$

$$C(\theta) = C_0 + \sum_{i=1}^{l} \theta_i C_i$$

where $\theta_i \in [-1, 1]$ and

$$
A_0 = \begin{bmatrix} A'_{g_0} + B'_{g_0} D_c C'_g & B'_{g_0} C_c \\ B_c C'_g & A_c \end{bmatrix}, \quad B_0 = \begin{bmatrix} B'_{w_0} \\ 0 \end{bmatrix}, \quad C_0 = \begin{bmatrix} C'_{z_0} + D'_{zu_0} D_c C'_g & D'_{zu_0} C_c \end{bmatrix}
$$

$$
A_i = \begin{bmatrix} A'_{g_i} + B'_{g_i} D_c C'_g & B'_{g_i} C_c \\ 0 & 0 \end{bmatrix}, \quad B_i = \begin{bmatrix} B'_{w_i} \\ 0 \end{bmatrix}, \quad C_i = \begin{bmatrix} C'_{z_i} + D'_{zu_i} D_c C'_g & D'_{zu_i} C_c \end{bmatrix}
$$

$$(2.14)$$

for $i = 1, \dots, l$.

The closed-loop system in (2.11) is stable via a positive polynomially parameter-dependent Lyapunov matrix of degree N ($P(\theta)$) if and only if the following constraint is satisfied:

$$
A^T(\theta) P(\theta) + P(\theta) A(\theta) < 0 \tag{2.15}
$$

for all $\theta_i \in [-1, 1]$. The above conditions are an infinite set of BMIs with respect to unknown controller matrices appearing in the closed-loop matrix $A(\theta)$ and the Lyapunov matrix $P(\theta)$. To convert the BMI conditions depending on an uncertain parameter, being hence a feasibility problem of infinite dimension, to finite-dimensional BMIs, we use (D, G) scaling [133–135] and multi-parameter (D, G) scaling approach [140, 141].

Theorem 1. $\left((D, G) \text{ Scaling [135]} \right)$ *Let* $\Phi \in \mathbb{R}^{n(k+1) \times n(k+1)}$. *Then, the following matrix inequality*

$$
\left(\theta^{[k]} \otimes I_n \right)^T \Phi \left(\theta^{[k]} \otimes I_n \right) < 0 \tag{2.16}
$$

where $\theta^{[k]} = \begin{bmatrix} 1 & \theta & \theta^2 & \cdots & \theta^k \end{bmatrix}^T$, *holds for all* $\theta \in [-1, 1]$ *if and only if there exist a positive-definite matrix* $D \in \mathbb{R}^{nk \times nk}$ *and a real skew-symmetric matrix* $G \in \mathbb{R}^{nk \times nk}$ *such that*

$$
\Phi + \Delta_k^n(D, G) < 0 \tag{2.17}
$$

where $\Delta_k^n(D, G) \in \mathbb{R}^{n(k+1) \times n(k+1)}$ *is defined as follows:*

$$
\Delta_k^n(D, G) = \begin{bmatrix} \bar{I}_k^n \\ \tilde{I}_k^n \end{bmatrix}^T \begin{bmatrix} D & G \\ G^T & -D \end{bmatrix} \begin{bmatrix} \bar{I}_k^n \\ \tilde{I}_k^n \end{bmatrix}; \quad k \neq 0 \tag{2.18}
$$

where

$$
\bar{I}_k^n = \begin{bmatrix} I_k & 0_{k \times 1} \end{bmatrix} \otimes I_n
$$

$$
\tilde{I}_k^n = \begin{bmatrix} 0_{k \times 1} & I_k \end{bmatrix} \otimes I_n
$$

$$(2.19)$$

and $\Delta_0^n(D, G) = 0$. *The inequality in (2.17) is an LMI with respect to the matrices* Φ, D, *and* G.

Theorem 2. $\left(\text{Multi-parameter } (D, G) \text{ Scaling [140]} \right)$ *Consider a symmetric matrix* $\Phi \in \mathbb{R}^{n(l+1) \times n(l+1)}$.

Then, the following matrix inequality holds

$$\left(\theta^{[l]} \otimes I_n\right)^T \Phi\left(\theta^{[l]} \otimes I_n\right) < 0 \tag{2.20}$$

where $\theta^{[l]} = \begin{bmatrix} 1 & \theta_1 & \theta_2 & \cdots & \theta_l \end{bmatrix}^T$ *and* $\theta_i \in [-1,1]$, *if there exist positive definite matrices* $D_1, D_2, \ldots, D_l$ *and skew-symmetric matrices* $G_{i,j}$, $(i = 0, \ldots, l-1, j = 1, \ldots, l)$ *of appropriate dimensions such that*

$$\Phi + \begin{bmatrix} D & G_{0,1} & \cdots & \cdots & G_{0,l} \\ G_{0,1}^T & -D_1 & G_{1,2} & \cdots & G_{1,l} \\ \vdots & \vdots & \vdots & \cdots & \vdots \\ G_{0,l-1}^T & G_{1,l-1}^T & \cdots & \cdots & G_{l-1,l} \\ G_{0,l}^T & G_{1,l}^T & \cdots & G_{l-1,l}^T & -D_l \end{bmatrix} < 0 \tag{2.21}$$

where $D = \sum\limits_{i=1}^{l} D_i$.

2.4 Fixed-structure Control of Affine Single Parameter-dependent Systems

In this section, necessary and sufficient conditions for the existence of a fixed-structure H_∞ controller for affine single parameter-dependent systems via polynomially parameter-dependent Lyapunov matrices are presented. The main idea behind of these conditions is the (D, G) scaling approach used to convert the parameter-dependent BMI condition in (2.15) to the feasibility problem of a set of inequalities independent on θ.

2.4.1 Fixed-structure H_∞ Controller Design via Linearly Parameter-dependent Lyapunov Matrices

In this part, the problem of fixed-structure H_∞ controller design of affine single parameter-dependent systems via linearly parameter-dependent Lyapunov matrices is proposed and the results are given in the following theorem:

Theorem 3. *There exists a fixed-structure controller that stabilizes the affine single parameter-dependent systems in (2.9)-(2.10) with $l = 1$ and ensures $\|H_{zw}(\theta)\|_\infty < \gamma$ with a linearly parameter-dependent Lyapunov matrix $P(\theta) = P_0 + \theta P_1$ if and only if there exist symmetric matrices P_0 and P_1, a positive-definite matrix $D > 0$, and a real skew-symmetric matrix G of appropriate dimensions such that*

$$\begin{aligned} P_0 + P_1 &> 0 \\ P_0 - P_1 &> 0 \end{aligned} \tag{2.22}$$

$$\begin{bmatrix} W_{1,1} + \Delta_2^{n+m}(D,G) & Y_{1,1}^T \\ Y_{1,1} & -\gamma I \end{bmatrix} < 0 \tag{2.23}$$

where

$$W_{1,1} = He\left\{ \begin{bmatrix} P_0 \\ P_1 \\ 0 \end{bmatrix} \begin{bmatrix} A_0 & A_1 & 0 \end{bmatrix} \right\} \tag{2.24}$$

$$Y_{1,1} = \begin{bmatrix} B_0^T P_0 & B_1^T P_0 + B_0^T P_1 & B_1^T P_1 \\ C_0 & C_1 & 0 \end{bmatrix} \tag{2.25}$$

and $\Delta_2^{n+m}(D,G)$ is given in (2.18) with $k = 2$.

Proof. First, the inequalities given in (2.22) imply that the Lyapunov matrix $P(\theta) = P_0 + \theta P_1$ is positive definite. Then, applying the Schur complement lemma on (2.23) leads to the following inequality:

$$W_{1,1} + \gamma^{-1} Y_{1,1}^T Y_{1,1} + \Delta_2^{n+m}(D,G) < 0 \tag{2.26}$$

According to the (D,G) scaling, the above inequality is equivalent to

$$\begin{bmatrix} I_{n+m} \\ \theta I_{n+m} \\ \theta^2 I_{n+m} \end{bmatrix}^T \Phi_\infty \begin{bmatrix} I_{n+m} \\ \theta I_{n+m} \\ \theta^2 I_{n+m} \end{bmatrix} < 0 \tag{2.27}$$

where

$$\Phi_\infty = He\left\{ \begin{bmatrix} P_0 \\ P_1 \\ 0 \end{bmatrix} \begin{bmatrix} A_0 & A_1 & 0 \end{bmatrix} \right\} + \gamma^{-1} \begin{bmatrix} C_0^T \\ C_1^T \\ 0 \end{bmatrix} \begin{bmatrix} C_0 & C_1 & 0 \end{bmatrix}$$
$$+ \gamma^{-1} \begin{bmatrix} P_0 B_0 \\ P_0 B_1 + P_1 B_0 \\ P_1 B_1 \end{bmatrix} \begin{bmatrix} P_0 B_0 \\ P_0 B_1 + P_1 B_0 \\ P_1 B_1 \end{bmatrix}^T \tag{2.28}$$

The inequality in (2.27) can be rewritten as follows:

$$A^T(\theta) P(\theta) + P(\theta) A(\theta) + \gamma^{-1} C^T(\theta) C(\theta) + \gamma^{-1} P(\theta) B(\theta) B^T(\theta) P(\theta) < 0 \tag{2.29}$$

Therefore, $\|H_{zw}(\theta)\|_\infty < \gamma$ and the proof is complete. □

2.4.2   Extension to Polynomially Parameter-dependent Lyapunov Matrices

In this subsection, we are interested in the extension of the previous results to polynomially parameter-dependent Lyapunov matrices of degree N, i.e. $P_N(\theta) = \sum_{i=0}^{N} \theta^i P_i$. The results are summarized in the following theorem. As the degree of the polynomial $P(\theta)$ increases, the results converge to the optimal ones [142]. Finally, necessary and sufficient conditions for the existence of a fixed-structure H_∞ controller for an affine single parameter-dependent system are derived.

Theorem 4. *For an affine single parameter-dependent system described by (2.9)-(2.10) with $l = 1$, there exists a fixed-structure controller which guarantees the robust stability and robust performance $\|H_{zw}(\theta)\|_\infty < \gamma$ via a polynomially parameter-dependent Lyapunov matrix $P_N(\theta) = \sum_{i=0}^{N} \theta^i P_i$ if and only if there exist symmetric matrices P_i for $i = 0, 1, \dots, N$, positive definite matrices D and L, and real skew-symmetric matrices G and K such that*

$$-\frac{1}{2} \begin{bmatrix} 2P_0 & P_1 & \cdots & P_{j-1} & P_j \\ P_1 & 0 & \cdots & 0 & P_{j+1} \\ \vdots & \vdots & \vdots & \ddots & \vdots \\ P_{j-1} & 0 & \cdots & 0 & P_{2j-1} \\ P_j & P_{j+1} & \cdots & P_{2j-1} & 2P_{2j} \end{bmatrix} + \Delta_j^{n+m}(L, K) < 0 \tag{2.30}$$

$$\begin{bmatrix} W_{1,N} + \Delta_{N+1}^{n+m}(D, G) & Y_{1,N}^T \\ Y_{1,N} & -\gamma I \end{bmatrix} < 0 \tag{2.31}$$

where $\Delta_{N+1}^{n+m}(D, G)$ is defined in (2.18) with $k = N + 1$ and

$$j = \begin{cases} \frac{N}{2} & \text{if } N \text{ is even} \\[2ex] \frac{N+1}{2} & \text{if } N \text{ is odd} \end{cases} \tag{2.32}$$

$$W_{1,N} = He \left\{ \begin{bmatrix} P_0 \\ P_1 \\ \vdots \\ P_N \\ 0 \end{bmatrix} \begin{bmatrix} A_0 & A_1 & 0 & \cdots & 0 \end{bmatrix} \right\} \tag{2.33}$$

$$Y_{1,N} = \begin{bmatrix} B_0^T P_0 & B_1^T P_0 + B_0^T P_1 & B_1^T P_1 + B_0^T P_2 & \cdots & B_1^T P_{N-1} + B_0^T P_N & B_1^T P_N \\ C_0 & C_1 & 0 & \cdots & 0 & 0 \end{bmatrix} \tag{2.34}$$

Note that if N is an odd number, $2j = N + 1$, therefore, P_{2j} in (2.30) is replaced with 0.

Proof. The inequality given in (2.30) directly expresses the positivity of matrix $P_N(\theta)$ based on the (D, G) scaling approach in two cases where N is either even or odd. The rest of the poof is similar to that of Theorem 3. □

Remark. The proposed conditions in Theorem 3 and Theorem 4 are necessary and sufficient for fixed-structure H_∞ controller design of polytopic systems with two vertices via linearly and polynomially parameter-dependent Lyapunov matrices of order N, respectively. The conditions are expressed by an optimization problem subject to two sets of BMI and LMI constraints. To solve the optimization problems involving BMI constraints, several local and global approaches have been developed in the literature, e.g. [137, 143–145].

2.5 Fixed-structure Control of Affine Multi Parameter-dependent Systems

In the previous section, necessary and sufficient conditions for fixed-structure H_∞ output feedback controller design of affine single parameter-dependent systems in terms of LMIs and BMIs have been developed. The results can be extended to the robust fixed-structure controller synthesis of affine multi parameter-dependent systems according to the multi parameter (D, G) scaling approach.

Theorem 5. *The fixed-structure controller given in (2.2) stabilizes the affine multi parameter-dependent systems in (2.9)-(2.10) and ensures $\| H_{zw}(\theta) \|_\infty < \gamma$ via a linearly parameter-dependent Lyapunov matrix $P(\theta) = P_0 + \sum_{i=1}^{l} \theta_i P_i$ if there exist symmetric matrices P_i $(i = 0, 1, \ldots, l)$, positive-definite matrices D_i $(i = 1, \ldots, l)$, and real skew-symmetric matrices $G_{i,j}$ $(i = 0, 1, \ldots, l - 1, j = i + 1, \ldots, l)$ of appropriate dimensions such that*

$$P_0 \pm P_1 \pm \cdots \pm P_l > 0 \tag{2.35}$$

$$\begin{bmatrix} W_{l,1} + \Delta(D, G) & Y_{l,1}^T \\ Y_{l,1} & -\gamma I \end{bmatrix} < 0 \tag{2.36}$$

where

$$W_{l,1} = He \left\{ \begin{bmatrix} P_0 \\ P_1 \\ \vdots \\ P_l \end{bmatrix} \begin{bmatrix} A_0 & A_1 & \cdots & A_l \end{bmatrix} \right\} \tag{2.37}$$

$$Y_{l,1} = \begin{bmatrix} B_0^T P_0 & B_1^T P_0 + B_0^T P_1 & \cdots & B_l^T P_l \\ C_0 & C_1 & \cdots & C_l \end{bmatrix} \tag{2.38}$$

$$\Delta(D,G) = \begin{bmatrix} D & G_{0,1} & \cdots & \cdots & G_{0,l} \\ G_{0,1}^T & -D_1 & G_{1,2} & \cdots & G_{1,l} \\ \vdots & \vdots & \vdots & \cdots & \vdots \\ G_{0,l-1}^T & G_{1,l-1}^T & \cdots & \cdots & G_{l-1,l} \\ G_{0,l}^T & G_{1,l}^T & \cdots & G_{l-1,l}^T & -D_l \end{bmatrix} \qquad (2.39)$$

where $D = \sum_{i=1}^{l} D_i$.

Proof. The set of inequalities in (2.35) indicates that $P(\theta) = P_0 + \sum_{i=1}^{l} \theta_i P_i > 0$. The following inequality results from applying the Schur complement lemma to (2.36):

$$W_{l,1} + \gamma^{-1} Y_{l,1}^T Y_{l,1} + \Delta(D,G) < 0 \qquad (2.40)$$

The remains of the proof are straightforward thanks to the multi-parameter (D,G) scaling presented in Theorem 2.

$\square$

2.6 Simulation Results

To demonstrate the effectiveness of the proposed BMI-based conditions for fixed-structure H_∞ control, they are applied to two numerical examples and compared with existing fixed-order controller design methods. The BMI constraints are implemented and solved in MATLAB using the available software packages, e.g. YALMIP [146] and PENBMI [137].

Example 1. Consider a continuous-time polytopic system with two vertices given in [57]. The system can be easily converted to an affine single parameter-dependent system in (2.9) with $l = 1$, where

$$A_g'(\theta) = \begin{bmatrix} -1.346 & 34.065 & 179.82 \\ 0.2424 & -1.135 & -21.69 \\ 0 & 0 & -30 \end{bmatrix} + \theta \begin{bmatrix} 0.356 & -16.65 & -83.67 \\ 0.0223 & 0.2834 & 10.3 \\ 0 & 0 & 0 \end{bmatrix}$$

$$B_g' = \begin{bmatrix} -91.435 \\ 0 \\ 30 \end{bmatrix} + \theta \begin{bmatrix} -6.345 \\ 0 \\ 0 \end{bmatrix}, \quad B_w' = \begin{bmatrix} 0 \\ 1 \\ 1 \end{bmatrix}$$

$$C_g' = \begin{bmatrix} 1 & 0 & 0 \\ 0 & 1 & 0 \end{bmatrix}, \quad C_z' = \begin{bmatrix} 1 & 0 & 0 \\ 0 & 1 & 0 \\ 0 & 0 & 1 \end{bmatrix}$$

$$D_{zu}' = \begin{bmatrix} 0 & 0 & 0 \end{bmatrix} \qquad (2.41)$$

Table 2.1: Upper bound of $\|H_{zw}(\theta)\|_\infty$ in Example 1

Method	γ	K
[47]	9.7315	$\begin{bmatrix} 0.5558 & 5.0823 \end{bmatrix}$
[48] (Theorem 4)	6.8028	$\begin{bmatrix} 0.0536 & 0.6384 \end{bmatrix}$
[57] (Theorem 13)	2.3267	$\begin{bmatrix} 0.4474 & 4.1860 \end{bmatrix}$
[147]	1.7947	$\begin{bmatrix} 77.1587 & 608.8698 \end{bmatrix}$
Proposed method with $N = 1$	1.6602	$\begin{bmatrix} 130.3463 & 939.3718 \end{bmatrix}$
Proposed method with $N = 2$	1.6446	$\begin{bmatrix} 0.1702e3 & 1.2234e3 \end{bmatrix}$

where $\theta \in [-1, 1]$.

The objective here is to design a static output feedback H_∞ controller with polynomially parameter-dependent Lyapunov matrices. To this end, an optimization problem, which is the minimization of γ subject to the LMI and BMI constraints respectively given in (2.30) and (2.31), is considered. The problem is solved by PENBMI (version 2.1) [137] with an initial controller $K_{c_0} = \begin{bmatrix} 0 & 0 \end{bmatrix}$ after 138 iterations in the case of $N = 1$ and after 66 iterations in the case of $N = 2$. Resulting static output feedback controllers are given in Table 2.1. The CPU times for both cases $N = 1$ and $N = 2$ are $14.20s$ and $16.27s$, respectively, on a 3.4 GHz Intel Core i7 with Mac OS X. It should be noted that PENBMI fails to provide any solution for the case of $N \geq 3$.

The results are compared with the LMI-based methods in [47, 48, 57, 147]. It can be observed from Table 2.1 that the proposed BMI-based method in this chapter with polynomially parameter-dependent Lyapunov matrices of order two leads to the best results among the others.

Example 2. Consider the model of a two-mass-spring system in [147]. The system can be represented by:

$$
\begin{aligned}
A_g'(\theta) &= \begin{bmatrix} 0 & 0 & 1 & 0 \\ 0 & 0 & 0 & 1 \\ -a_0 & a_0 & 0 & 0 \\ a_0 & -a_0 & 0 & 0 \end{bmatrix} + \theta \begin{bmatrix} 0 & 0 & 0 & 0 \\ 0 & 0 & 0 & 0 \\ -a_1 & a_1 & 0 & 0 \\ a_1 & -a_1 & 0 & 0 \end{bmatrix} \\
B_g' &= \begin{bmatrix} 0 \\ 0 \\ 1 \\ 0 \end{bmatrix}, \quad B_w' = \begin{bmatrix} 0 \\ 0 \\ -0.75 \\ 0.75 \end{bmatrix}, \quad D_{zu}' = 0 \\
C_g' &= \begin{bmatrix} 0 & 1 & 0 & 0 \end{bmatrix}, \quad C_z' = \begin{bmatrix} 1 & -1 & 0 & 0 \end{bmatrix}
\end{aligned}
\tag{2.42}
$$

where $\theta \in [-1, 1]$, $a_0 = \frac{k_l + k_u}{2}$, $a_1 = \frac{k_l - k_u}{2}$, $k_l = 1.15$, and $k_u = 2$.

The goal is the design of a second-order H_∞ controller. To this end, an optimization problem,

which is the minimization of γ subject to the LMI and BMI constraints in (2.30)-(2.31), is solved.

To solve the optimization problem, the local optimization-based method in [145] is used. In this way, the BMI constraint in (2.31) is reformulated as a difference of two positive semidefinite convex mappings. Then, the concave part is linearized at each iteration and a convex subproblem involving a set of LMIs is obtained. Finally, the resultant LMI-based optimization problem is solved using YALMIP [146] as the interface and MOSEK[1] as the solver. The termination criteria are the same as ones mentioned in [145]. The maximum iteration number is set to $h_{max} = 100$ and $\rho_i = 0.001$ for $i = 1, 2, \ldots, N + 2$. The final second-order controllers for both case $N = 1$ and $N = 2$ are respectively given by:

$$K_1 = \left[\begin{array}{c|c} A_{c_1} & B_{c_1} \\ \hline C_{c_1} & D_{c_1} \end{array} \right] \tag{2.43}$$

where

$$A_{c_1} = \left[\begin{array}{cc} -3.4963 & -2.8297 \\ 2.1438 & 0.3006 \end{array} \right], \quad B_{c_1} = \left[\begin{array}{c} 5.7701 \\ -0.6.3582 \end{array} \right]$$
$$C_{c_1} = \left[\begin{array}{cc} -5.2792 & -4.2469 \end{array} \right], \quad D_{c_1} = 8.6595 \tag{2.44}$$

$$K_2 = \left[\begin{array}{c|c} A_{c_2} & B_{c_2} \\ \hline C_{c_2} & D_{c_2} \end{array} \right] \tag{2.45}$$

where

$$A_{c_2} = \left[\begin{array}{cc} -3.6053 & -2.8822 \\ 2.2776 & 0.4338 \end{array} \right], \quad B_{c_2} = \left[\begin{array}{c} 5.8797 \\ -0.9089 \end{array} \right]$$
$$C_{c_2} = \left[\begin{array}{cc} -5.4472 & -4.3289 \end{array} \right], \quad D_{c_2} = 8.8309 \tag{2.46}$$

It should be mentioned that the resulting controller with $N = 1$ (K_1) is used as an initial guess for the case $N = 2$.

The results of the proposed method and HIFOO [31] are reported in Table 2.2, where both methods are initialized by the same controller $K^{[0]}$ designed in [147]. Note that the best results of HIFOO during three sequences with 30 iterations have been mentioned in Table 2.2.

Since HIFOO does not guarantee the stability conditions and H_∞ performance for the whole polytope, the upper bound of $\|H_{zw}(\theta)\|_\infty$, obtained by HIFOO, is not determined in Table 2.2.

It is observed that the proposed method in this chapter with $N = 2$ leads to the better results

---

[1]Available online in http://www.mosek.com

Table 2.2: Upper bound of $\|H_{zw}(\theta)\|_{\infty}$ in Example 2

Method	$\|H_{zw}(\theta)\|_{\infty}$	$\|H_{zw}(-1)\|_{\infty}$	$\|H_{zw}(1)\|_{\infty}$	Iteration Number	Time (s)
HIFOO	—	0.747	0.748	30	403.85
Proposed method with $N = 1$	0.761	0.753	0.652	81	86.17
Proposed method with $N = 2$	0.747	0.741	0.604	7	10.8

than HIFOO's. Furthermore, HIFOO needs considerable computational time to find a controller. However, the linearized convex-concave decomposition approach needs a feasible initial condition which is not easy to find.

2.7 Conclusion

In this chapter, the problem of fixed-structure H_{∞} controller synthesis of continuous-time LTI polytopic systems by means of polynomially parameter-dependent Lyapunov matrices is considered. Particular emphasis is laid upon the polytopic systems with two vertices in which necessary and sufficient conditions for the existence of a fixed-structure H_{∞} controller in terms of BMIs and LMIs are derived. The fundamental idea of this approach is based on the use of the (D, G) scaling which can convert inequality conditions depending on an uncertain parameter to a finite set of inequalities. The extension of the results to the robust fixed-structure controller synthesis of the polytopic systems with more than two vertices via linearly (polynomialy) parameter-dependent Lyapunov matrices leads to only sufficient conditions. The BMI conditions can be solved using available BMI solvers and existing approaches in the literature. However, the BMI solvers most often fail to provide a solution for the BMI problems. Moreover, the choice of an initial guess for most existing methods is very crucial and affects the feasibility of the BMI problem. In Chapter 3 and Chapter 4, we propose another set of BMIs for fixed-structure control of polytopic systems which relies on the concept of strictly positive realness (SPRness) of transfer functions and use of slack matrices. To solve the BMI conditions, several heuristic approaches for the design of the slack variables are developed.

3 Fixed-structure Control of Systems with Polytopic Uncertainty via LPD Lyapunov Matrices

3.1 Introduction

This chapter aims to develop a fixed-structure control strategy for linear time-invariant dynamical systems subject to polytopic uncertainty. The proposed approach is based on the use of slack matrices which convexify the problem of fixed-structure controller design by decoupling unknown matrices. The problem is formulated as a convex optimization problem with a set of LMI constraints. Although the presented design approach can apply to any kind of structured controllers, the main focus is on fixed-order control. The effectiveness of the proposed control techniques is illustrated using several simulation examples.

The organization of this chapter is as follows: Problem formulation and preliminaries are respectively given in Section 3.2 and Section 3.3. A new parameterization of fixed-structure stabilizing controllers is presented in Section 3.4. Two algorithms for fixed-structure stabilizing controller design are developed in Section 3.5. Section 3.6 is devoted to fixed-structure H_∞ control synthesis. The case of polytopic uncertainty in all state space matrices is considered in Section 3.7. Numerical examples are provided in Section 3.8. Section 3.9 concludes the chapter.

Throughout this chapter, matrices I and 0 are the identity matrix and the zero matrix of appropriate dimensions, respectively. The symbols T and $\star$ denote the matrix transpose and symmetric blocks, respectively. The symbol $\text{He}\{A\}$ is a notation for $A + A^T$. For symmetric matrices, $P > 0$ ($P < 0$) indicates the positive-definiteness (the negative-definiteness).

3.2 Problem Formulation

3.2.1 System Dynamics

Consider a linear time-invariant (LTI) dynamical system described by:

$$\delta[x_g(t)] = A_g x_g(t) + B_g u(t)$$
$$y(t) = C_g x_g(t)$$

(3.1)

where $x_g \in \mathbb{R}^n$ is the state, $u \in \mathbb{R}^{n_i}$ in the input, and $y \in \mathbb{R}^{n_o}$ is the output of the system. Symbol $\delta[\cdot]$ presents the derivative term for continuous-time $\left(\delta[x_g(t)] = \dot{x}_g(t)\right)$ and the forward operator for discrete-time systems $\left(\delta[x_g(t)] = x_g(t+1)\right)$. The state space matrices A_g, B_g, and C_g are of appropriate dimensions. It is assumed that the matrices A_g and B_g belong to the following polytopic uncertainty domain:

$$\Omega_2 = \left\{ \left(A_g(\lambda), B_g(\lambda)\right) = \sum_{i=1}^{q} \lambda_i \left(A_{g_i}, B_{g_i}\right) \right\}; \quad \lambda \in \Lambda_q$$

(3.2)

where $\left(A_{g_i}, B_{g_i}, C_g, 0\right)$ is the i-th vertex of the polytope. To keep the linear dependence of the closed-loop matrices on the vector λ, we assume that B_g belongs to the polytopic-type uncertainty domain Ω_2 and C_g does not contain any uncertainty.

3.2.2 Control Structure

The problem addressed in this chapter is to present a set of LMI conditions for fixed-structure controller design of the polytopic system in (3.1) and (3.2). The controller K is given by:

$$\delta[x_c(t)] = A_c x_c(t) + B_c y(t)$$
$$u(t) = C_c x_c(t) + D_c y(t)$$

(3.3)

where $A_c \in \mathbb{R}^{m \times m}$, $B_c \in \mathbb{R}^{m \times n_o}$, $C_c \in \mathbb{R}^{n_i \times m}$, and $D_c \in \mathbb{R}^{n_i \times n_o}$. The controller K can be also described as follows:

$$K = \left[\begin{array}{c|c} A_c & B_c \\ \hline C_c & D_c \end{array} \right]$$

(3.4)

It is assumed that specific structural constraints on the controller matrices can be set by designers to reflect some control design requirements/objectives. The constraints can be in the form of:

- Static output feedback ($m = 0$)

- Fixed-, low-order dynamic output feedback ($m < n$)

- Strictly proper controller ($D_c = 0$)

- PID control, e.g. the state space realization of a continuous-time SISO PID controller is given by [4]:

$$
\begin{aligned}
K(s) &= K_P + K_I \frac{1}{s} + K_D \frac{s}{1 + \tau s} \\
&= \left[\begin{array}{cc|c}
0 & 0 & K_I \\
0 & -\frac{1}{\tau} & -\frac{1}{\tau^2} K_D \\
\hline
1 & 1 & K_P + \frac{1}{\tau} K_D
\end{array}\right]
\end{aligned}
\tag{3.5}
$$

- Decentralized control with block diagonal controller structure

- Distributed control with non-block diagonal/overlapping controller structure

As an example, consider an interconnected system consisting of two subsystems with following state space realization:

$$
A_g = \left[\begin{array}{c|c}
A_{g_{11}} & A_{g_{12}} \\
\hline
A_{g_{21}} & A_{g_{22}}
\end{array}\right], \quad B_g = \mathrm{diag}\left(B_{g_1}, B_{g_1}\right), \quad C_g = \mathrm{diag}\left(C_{g_1}, C_{g_2}\right)
\tag{3.6}
$$

There exists one sub-controller for each subsystem. It is assumed that the sub-controller 1 has access to the measurements of its own subsystem as well as the measurement of the subsystem 2 while the sub-controller 2 uses only the measurements of the subsystem 2. In this case, the controller structure is expressed as follows:

$$
\begin{aligned}
A_c &= \left[\begin{array}{c|c}
A_{c_{11}} & 0 \\
\hline
0 & A_{c_{22}}
\end{array}\right], \quad
B_c = \left[\begin{array}{c|c}
B_{c_{11}} & B_{c_{12}} \\
\hline
0 & B_{c_{22}}
\end{array}\right] \\
C_c &= \left[\begin{array}{c|c}
C_{c_{11}} & 0 \\
\hline
0 & C_{c_{22}}
\end{array}\right], \quad
D_c = \left[\begin{array}{c|c}
D_{c_{11}} & D_{c_{12}} \\
\hline
0 & D_{c_{22}}
\end{array}\right]
\end{aligned}
\tag{3.7}
$$

Other specific structural constraints, such as fixed-order, on each sub-controller can be also imposed. The design problem is then to find the parameters of the structured controller, i.e the state space matrices $\left(A_c, B_c, C_c, D_c\right)$, so that the resulting closed-loop system meets the design requirements.

3.2.3 Closed-loop State Matrix

The interconnection of the controller K defined by (3.3) and the polytopic system in (3.1)-(3.2) leads to the following closed-loop state matrix $A(\lambda)$:

$$
A(\lambda) = \left[\begin{array}{cc}
A_g(\lambda) + B_g(\lambda) D_c C_g & B_g(\lambda) C_c \\
B_c C_g & A_c
\end{array}\right]
\tag{3.8}
$$

where

$$A(\lambda) = \sum_{i=1}^{q} \lambda_i A_i; \quad \lambda_i \in \Lambda_q \tag{3.9}$$

and

$$A_i = \begin{bmatrix} A_{g_i} + B_{g_i} D_c C_g & B_{g_i} C_c \\ B_c C_g & A_c \end{bmatrix} \tag{3.10}$$

The closed-loop state matrix $A(\lambda)$ is robustly stable if all its eigenvalues are located inside the unit circle for all $\lambda \in \Lambda_q$ (discrete-time case)/if all its eigenvalues have strictly negative real part for all $\lambda \in \Lambda_q$ (continuous-time case).

3.3 Preliminaries

This section provides the basic lemmas which are used throughout this chapter.

Lemma 1. ($Kalman$-$Yakubovich$-$Popov$ (KYP) $Lemma$ $[148]$) *A square transfer function $H = \left[\begin{array}{c|c} A & B \\ \hline C & D \end{array} \right]$ is strictly positive real (SPR) if and only if there exists a Lyapunov matrix $P > 0$ such that*

For continuous-time systems:

$$\begin{bmatrix} A^T P + PA & PB - C^T \\ B^T P - C & -D - D^T \end{bmatrix} < 0 \tag{3.11}$$

For discrete-time systems:

$$\begin{bmatrix} A^T PA - P & A^T PB - C^T \\ B^T PA - C & B^T PB - D - D^T \end{bmatrix} < 0 \tag{3.12}$$

Lemma 2. *The following statements are equivalent:*

1. *A square continuous-time transfer function $H(s) = \left[\begin{array}{c|c} A & B \\ \hline C & I \end{array} \right]$ is SPR with a Lyapunov matrix $P > 0$.*

2. *$H^{-1}(s) = \left[\begin{array}{c|c} A - BC & B \\ \hline -C & I \end{array} \right]$ is SPR with a Lyapunov matrix $P > 0$.*

Proof. According to the KYP lemma, Statement 1 is equivalent to the existence of a Lyapunov

matrix $P = P^T > 0$ such that

$$\begin{bmatrix} A^T P + PA & PB - C^T \\ B^T P - C & -2I \end{bmatrix} < 0 \tag{3.13}$$

Using the Schur complement lemma [149], the above inequality can be written as follows:

$$A^T P + PA + \frac{1}{2}(PB - C^T)(B^T P - C) < 0 \tag{3.14}$$

This inequality can be rearranged to

$$(A - BC)^T P + P(A - BC) + \frac{1}{2}(PB + C^T)(B^T P + C) < 0 \tag{3.15}$$

which is equivalent to

$$\begin{bmatrix} (A - BC)^T P + P(A - BC) & PB + C^T \\ B^T P + C & -2I \end{bmatrix} < 0 \tag{3.16}$$

Therefore, Statement 2 follows. $\qquad\square$

Lemma 3. *An SPR discrete-time transfer function* $H(z) = \left[\begin{array}{c|c} A & B \\ \hline C & I \end{array}\right]$ *and its inverse* $H^{-1}(z) = \left[\begin{array}{c|c} A - BC & B \\ \hline -C & I \end{array}\right]$ *satisfy the KYP lemma with a common Lyapunov matrix* $P > 0$.

Proof. The SPRness of $H(z)$ is equivalent to the existence of a Lyapunov matrix $P > 0$ such that

$$\begin{bmatrix} A^T PA - P & A^T PB - C^T \\ B^T PA - C & B^T PB - 2I \end{bmatrix} < 0 \tag{3.17}$$

Pre- and post-multiplication of (3.17) by U_1^T and U_1

$$U_1 = \begin{bmatrix} I & 0 \\ -C & I \end{bmatrix} \tag{3.18}$$

lead to the following inequality:

$$\begin{bmatrix} (A - BC)^T P(A - BC) - P & (A - BC)^T PB + C^T \\ B^T P(A - BC) + C & B^T PB - 2I \end{bmatrix} < 0 \tag{3.19}$$

which is equivalent to the SPRness of $H^{-1}(z)$ with the Lyapunov matrix $P > 0$. $\qquad\square$

3.4 New Parameterization of Fixed-structure Stabilizing Controllers

3.4.1 Main Idea of the Proposed Approach

In [42] and [150], the basic idea for the synthesis of a fixed-structure controller for a SISO polytopic system with a rational transfer function representation is given as follows: Suppose that $c_i(s)$ for $i = 1, \ldots, q$ is the closed-loop characteristic polynomials at the i-th vertex, then the polytopic system is stable if $c_i(s)/d(s)$ for $i = 1, \ldots, q$ is an SPR transfer function where $d(s)$ is a given stable polynomial called the central polynomial. The choice of the central polynomial is very crucial and affects the control performance as well as the conservatism of the approach.

In this chapter, the idea of SPR transfer functions in the state space framework is used to find a convex set of fixed-structure controllers for systems affected by polytopic-type uncertainty. The idea relies on the concept of SPRness of transfer functions, the KYP lemma, Lemma 2, and Lemma 3.

3.4.2 A Convex Set of Fixed-structure Stabilizing Controllers

The following theorems propose a new convex parameterization of fixed-structure stabilizing controllers for both continuous-time and discrete-time polytopic systems given in (3.1) and (3.2).

Theorem 6. (Continuous-time Case) *Suppose that a stable matrix M and a non-singular matrix T are given. Then, the fixed-structure controller defined in (3.3) stabilizes the continuous-time polytopic system in (3.1) and (3.2) if there exist Lyapunov matrices $P_i > 0$ such that*

$$\begin{bmatrix} M^T P_i + P_i M & P_i - M^T + (T^{-1} A_i T)^T \\ P_i - M + T^{-1} A_i T & -2I \end{bmatrix} < 0; \quad i = 1, \ldots, q \tag{3.20}$$

where A_i is the closed-loop state matrix of the i-th vertex given in (3.10).

Proof. By convex combination of (3.20) for all vertices, one can obtain:

$$\begin{bmatrix} M^T P(\lambda) + P(\lambda) M & P(\lambda) - M^T + (T^{-1} A(\lambda) T)^T \\ P(\lambda) - M + T^{-1} A(\lambda) T & -2I \end{bmatrix} < 0 \tag{3.21}$$

where $A(\lambda) = \sum_{i=1}^{q} \lambda_i A_i$, $P(\lambda) = \sum_{i=1}^{q} \lambda_i P_i$, and $\lambda \in \Lambda_q$. According to the KYP lemma, the above inequality indicates that the following transfer function is SPR with the Lyapunov matrix $P(\lambda)$:

$$H(s) = \left[\begin{array}{c|c} M & I \\ \hline M - T^{-1} A(\lambda) T & I \end{array} \right] \tag{3.22}$$

As a consequence of Lemma 2, the following transfer function is also SPR with the same

Lyapunov matrix:

$$H^{-1}(s) = \left[\begin{array}{c|c} T^{-1} A(\lambda) T & I \\ \hline -M + T^{-1} A(\lambda) T & I \end{array} \right] \tag{3.23}$$

and therefore

$$\left[\begin{array}{cc} (T^{-1} A(\lambda) T)^T P(\lambda) + P(\lambda)(T^{-1} A(\lambda) T) & P(\lambda) + M^T - (T^{-1} A(\lambda) T)^T \\ P(\lambda) + M - T^{-1} A(\lambda) T & -2I \end{array} \right] < 0 \tag{3.24}$$

By the multiplication of the above inequality on the right by $\operatorname{diag}\left(T^{-1}, T^{-1}\right)$ and on the left by $\operatorname{diag}\left(T^{-T}, T^{-T}\right)$, the following inequality is obtained:

$$\left[\begin{array}{cc} A^T(\lambda) P_T(\lambda) + P_T(\lambda) A(\lambda) & P_T(\lambda) + M_T^T - A^T(\lambda) X \\ P_T(\lambda) + M_T - X A(\lambda) & -2X \end{array} \right] < 0 \tag{3.25}$$

where

$$P_T(\lambda) = T^{-T} P(\lambda) T^{-1}, \quad M_T = T^{-T} M T^{-1}, \quad X = T^{-T} T^{-1} \tag{3.26}$$

The application of the Schur complement lemma to (3.25) leads to

$$A^T(\lambda) P_T(\lambda) + P_T(\lambda) A(\lambda) < 0 \tag{3.27}$$

for $\lambda \in \Lambda_q$. As a result, the closed-loop state matrix of the polytopic system $A(\lambda)$ is stable with a linearly parameter-dependent Lyapunov matrix $P_T(\lambda)$. $\qquad\square$

Theorem 7. (Discrete-time Case) *Suppose that a stable matrix M and a non-singular matrix T are given. Then, the fixed-structure controller in (3.3) stabilizes the discrete-time polytopic system in (3.1) and (3.2) if there exist Lyapunov matrices $P_i > 0$ such that*

$$\left[\begin{array}{cc} M^T P_i M - P_i & M^T P_i - M^T + (T^{-1} A_i T)^T \\ P_i M - M + T^{-1} A_i T & P_i - 2I \end{array} \right] < 0; \quad i = 1, \ldots, q \tag{3.28}$$

where A_i is the closed-loop state matrix of the i-th vertex given in (3.10).

Proof. Similar to the proof of Theorem 6. $\qquad\square$

The convex sets of fixed-structure stabilizing controllers presented in Theorem 6 and Theorem 7 are inner convex approximations to the non-convex set of all fixed-structure stabilizing controllers for the polytopic systems.

Remarks.

1. Inequalities given in (3.20) and (3.28) are LMIs in terms of the controller matrices $\left(A_c, B_c, C_c, D_c\right)$ and symmetric positive-definite matrices P_i, $i = 1, \ldots, q$.

2. According to Lemma 2 and Lemma 3, it can be readily shown that the inequalities given in (3.20) and (3.28) are respectively equivalent to the following sets of inequalities:

$$\begin{bmatrix} A_i^T P_{T_i} + P_{T_i} A_i & P_{T_i} - A_i^T X + M_T^T \\ P_{T_i} - X A_i + M_T & -2X \end{bmatrix} < 0; \quad i = 1, \ldots, q \tag{3.29}$$

and

$$\begin{bmatrix} A_i^T P_{T_i} A_i - P_{T_i} & A_i^T P_{T_i} - A_i^T X + M_T^T \\ P_{T_i} A_i - X A_i + M_T & P_{T_i} - 2X \end{bmatrix} < 0; \quad i = 1, \ldots, q \tag{3.30}$$

where $P_{T_i} = T^{-T} P_i T^{-1}$ and M_T and X are defined in (3.26).

3. The use of the slack matrices M and T enables us to decouple the Lyapunov matrices and the controller parameters appearing in the closed-loop matrices. Taking advantage of this property, a fixed-structure controller can be designed via linearly parameter-dependent Lyapunov matrices and without employing a common Lyapunov matrix for all vertices. However, the use of linearly parameter-dependent Lyapunov matrices instead of (homogeneous) polynomially parameter-dependent ones is one of the main sources of conservatism in the proposed approach.

3.5 Algorithms for Fixed-structure Stabilizing Controller Design

The slack matrices M and T play a crucial role in the proposed approach to fixed-structure controller design. In fact, an appropriate choice of these matrices affect the quality and the conservatism of the proposed fixed-structure control technique. However, yet, there exists no strict manner in which the slack matrices can be assigned. To tackle this issue, two heuristic algorithms for the fixed-structure control design are presented.

3.5.1 Algorithm I: "Fixed-structure stabilizing controller design"

Algorithm I is based on the use of a set of initial fixed-structure stabilizing controllers designed for each vertex/all vertices of the polytopic system. The initial controller(s) may be computed through some of the existing fixed-structure controller design approaches in MATLAB such as *hinfstruct*[1] [30] and *systune* [36]. In the case of fixed-order controller design, the initial controllers may be designed using balanced controller order reduction of a full-order controller

---

[1]Available in the Robust Control Toolbox since R2010b

[1], the convex relaxation of a rank constraint in the classical full-order controller design [16], and MATLAB toolboxes, e.g. HIFOO [31, 32, 34] and FDRC [151].

Suppose that $\bar{A}_i$ is the closed-loop state matrix of the i-th vertex with its corresponding controller. Then, the slack matrices M and T can be chosen as follows:

$$
\begin{aligned}
T &= \left(chol(X)\right)^{-1} \\
M &= T^T M_T T
\end{aligned}
\tag{3.31}
$$

where *chol* denotes Cholesky factorization and (M_T, X) are a solution to the following LMI conditions:

For continuous-time systems:

$$
\begin{bmatrix}
\bar{A}_i^T P_{T_i} + P_{T_i} \bar{A}_i & P_{T_i} - \bar{A}_i^T X + M_T^T \\
P_{T_i} - X \bar{A}_i + M_T & -2X
\end{bmatrix} < 0; \quad i = 1, \dots, q
\tag{3.32}
$$

For discrete-time systems:

$$
\begin{bmatrix}
\bar{A}_i^T P_{T_i} \bar{A}_i - P_{T_i} & \bar{A}_i^T P_{T_i} - \bar{A}_i^T X + M_T^T \\
P_{T_i} \bar{A}_i - X \bar{A}_i + M_T & P_{T_i} - 2X
\end{bmatrix} < 0; \quad i = 1, \dots, q
\tag{3.33}
$$

If the above LMIs become feasible, M and T can be used in the set of LMI conditions given in (3.20)/(3.28) to design a fixed-structure stabilizing controller. In the case of infeasibility of either (3.32)/(3.33) or (3.20)/(3.28), different initial controllers or Algorithm II can be applied.

3.5.2 Algorithm II: "Stretching algorithm"

Algorithm II relies on the fixed-structure controller design for a nominal system defined as follows:

$$
A_{g_{nom}} = \frac{1}{q} \sum_{i=1}^{q} A_{g_i} \qquad B_{g_{nom}} = \frac{1}{q} \sum_{i=1}^{q} B_{g_i} \quad C_{g_{nom}} = C_g
\tag{3.34}
$$

where $(A_{g_i}, B_{g_i}, C_g, 0)$ is the state space realization of the i-th vertex of the polytopic system.

Suppose that $K^{[0]}$ is an initial fixed-structure controller for the nominal system. The next step is to obtain the slack matrices M_T and X using (3.32) for continuous-time systems and (3.33) for discrete-time systems. Note that for a single stabilizable system, feasibility of (3.32)/(3.33) or equivalently (3.20)/(3.28) is always guaranteed, as $\bar{A}$ is a stable closed-loop state matrix.

A new polytope with following vertices is built in the iteration j of an iterative algorithm as

explained in the following.

$$A_{g_i}^{[j]} = \alpha^{[j]} A_{g_i} + \frac{1 - \alpha^{[j]}}{q - 1} \sum_{\substack{k = 1 \\ k \neq i}}^{q} A_{g_k}, \quad B_{g_i}^{[j]} = \alpha^{[j]} B_{g_i} + \frac{1 - \alpha^{[j]}}{q - 1} \sum_{\substack{k = 1 \\ k \neq i}}^{q} B_{g_k}$$

$$C_{g_i}^{[j]} = C_g \tag{3.35}$$

for $i = 1, \ldots, q$, where $\alpha^{[j]} \left(\frac{1}{q} \leq \alpha^{[j-1]} \leq \alpha^{[j]} \leq 1 \right)$ is a scaling factor for the original polytope in (3.1) and (3.2). Note that $\alpha^{[j]} = \frac{1}{q}$ and $\alpha^{[j]} = 1$ reflect that the nominal model and the original polytope are covered, respectively. Moreover, it can be easily shown that the new polytopic system in the iteration j encompasses the old one (for $\alpha^{[j-1]}$).

The objective is to create a polytopic system with maximum scaling factor $\alpha \left(\frac{1}{q} \leq \alpha \leq 1 \right)$ in which the closed-loop state matrix $A(\lambda)$ for all $\lambda \in \Lambda_q$ remains stable. In the following, a procedure to design a fixed-structure stabilizing controller with the maximum polytopic uncertainty domain is presented. The procedure is generally divided into two parts. In the first part, the slack matrices and the maximum value of α are computed using the LMI conditions given in (3.32)/(3.33) and according to the stabilizing controller from the previous iteration. In the second part, a new fixed-structure controller is designed using (3.20)/(3.28).

The iterative procedure can be summarized with the following steps. To ease the presentation, the inequalities in (3.20)/(3.28) and (3.32)/(3.33) are respectively defined as follows:

$$\mathcal{H}_1^i \left(P_i, K \mid M, T \right) < 0 \tag{3.36}$$

$$\mathcal{H}_2^i \left(P_{T_i}, M_T, X, \alpha \mid K \right) < 0 \tag{3.37}$$

for $i = 1, \ldots, q$. The sign $|$ in the arguments of $\mathcal{H}_1^i$ and $\mathcal{H}_2^i$ separates the decision variables and the known parameters in the LMI conditions. Therefore, the set of LMIs in (3.36) is used to design a fixed-structure controller $K = \left(A_c, B_c, C_c, D_c \right)$ for a given pair of (M, T). In the same way, the LMI conditions in (3.37) are employed to find M_T, X, and α for a given controller K.

Step 1 (Initialization): Choose $\alpha^{[0]} = \frac{1}{q}$ and set $j = 1$ and a small tolerance for $\epsilon > 0$. Design an initial fixed-structure stabilizing controller for the nominal model in (3.34) ($K^{[0]}$).
Step 2: Compute $M_T^{[j]}$ and $X^{[j]}$ from the following optimization problem:

$$\alpha^{[j]} = \max_{P_{T_i}, M_T^{[j]}, X^{[j]}, \alpha} \alpha$$

$$\text{subject to} \quad \mathcal{H}_2^i \left(P_{T_i}, M_T^{[j]}, X^{[j]}, \alpha \mid K^{[j-1]} \right) < 0; \quad i = 1, \ldots, q \tag{3.38}$$

Then, obtain the slack matrices $M^{[j]}$ and $T^{[j]}$ using (3.31).
Step 3: According to the current value $\alpha^{[j]}$, a new polytope with the vertices given in (3.35) is

built, i.e. $\left(A_{g_i}^{[j]}, B_{g_i}^{[j]}, C_{g_i}^{[j]}, 0\right)$.

Step 4: Solve the following set of LMIs to obtain a fixed-structure stabilizing controller $K^{[j]}$ for the new polytope corresponding to $\alpha^{[j]}$:

$$\mathcal{H}_1^i\left(P_i, K^{[j]} \middle| M^{[j]}, T^{[j]}, \alpha^{[j]}\right) < 0; \quad i = 1, \ldots, q \tag{3.39}$$

Step 5 (Termination): If either $\Delta\alpha = \alpha^{[j]} - \alpha^{[j-1]} < \epsilon$ or $\alpha^{[j]} = 1$, stop. Otherwise use the obtained controller in Step 4 as an initial controller and go to Step 2 with $j \longleftarrow j + 1$.

Remark. The iterative algorithm leads to monotonic non-decreasing convergence of the scaling parameter α.

3.6   Fixed-structure H_∞ Controller Synthesis

3.6.1   Problem Statement

Consider an LTI dynamical system described by the following minimal state space realization:

$$\begin{aligned}
\delta[x_g(t)] &= A_g x_g(t) + B_g u(t) + B_w w(t) \\
z(t) &= C_z x_g(t) + D_{zu} u(t) + D_{zw} w(t) \\
y(t) &= C_g x_g(t) + D_w w(t)
\end{aligned} \tag{3.40}$$

where $x_g \in \mathbb{R}^n$, $u \in \mathbb{R}^{n_i}$, $w \in \mathbb{R}^r$, $y \in \mathbb{R}^{n_o}$, and $z \in \mathbb{R}^s$ are the state, the control input, the exogenous input, the measured output, and the controlled output, respectively. The state space matrices are of appropriate dimensions. It is assumed that the polytopic uncertainty affects the state space matrices A_g, B_g, B_w, C_z, D_{zu}, and D_{zw}, i.e.

$$\begin{aligned}
\Omega_3 &= \left\{\left(A_g(\lambda), B_g(\lambda), B_w(\lambda), C_z(\lambda), D_{zu}(\lambda), D_{zw}(\lambda)\right)\right. \\
&= \left.\sum_{i=1}^q \lambda_i \left(A_{g_i}, B_{g_i}, B_{w_i}, C_{z_i}, D_{zu_i}, D_{zw_i}\right)\right\}
\end{aligned} \tag{3.41}$$

where $\lambda \in \Lambda_q$ and $\left(A_{g_i}, B_{g_i}, C_g, B_{w_i}, C_{z_i}, D_{zu_i}, D_{zw_i}, D_w\right)$ is the i-th vertex of the polytope. To keep the linear dependence of the closed-loop matrices upon the vector λ, either pair $\left(B_g, D_{zu}\right)$ or $\left(C_g, D_w\right)$ belongs to the polytopic uncertainty domain Ω_3. In what follows, matrices C_g and D_w are assumed to be independent of the uncertain parameter λ.

The state space representation of the closed-loop system $H_{zw}(\lambda)$, transfer function from $w(t)$ to $z(t)$, with the dynamic output feedback controller in (3.3) is as follows:

$$\begin{aligned}
\delta[x(t)] &= A(\lambda) x(t) + B(\lambda) w(t) \\
z(t) &= C(\lambda) x(t) + D(\lambda) w(t)
\end{aligned} \tag{3.42}$$

where $x(t) = \begin{bmatrix} x_g^T(t) & x_c^T(t) \end{bmatrix}^T$ and

$$
A(\lambda) = \begin{bmatrix} A_g(\lambda) + B_g(\lambda)D_cC_g & B_g(\lambda)C_c \\ B_cC_g & A_c \end{bmatrix}, \quad B(\lambda) = \begin{bmatrix} B_w(\lambda) + B_g(\lambda)D_cD_w \\ B_cD_w \end{bmatrix}
$$
$$
C(\lambda) = \begin{bmatrix} C_z(\lambda) + D_{zu}(\lambda)D_cC_g & D_{zu}(\lambda)C_c \end{bmatrix}, \quad D(\lambda) = D_{zw}(\lambda) + D_{zu}(\lambda)D_cD_w
$$

(3.43)

The vertices of the closed-loop polytopic system $H_{zw}(\lambda)$ are given as follows:

$$
H_{zw_i} = \left[\begin{array}{c|c} A_i & B_i \\ \hline C_i & D_i \end{array} \right]; \quad i = 1,\dots,q
$$

(3.44)

where

$$
A_i = \begin{bmatrix} A_{g_i} + B_{g_i}D_cC_g & B_{g_i}C_c \\ B_cC_g & A_c \end{bmatrix}, \quad B_i = \begin{bmatrix} B_w + B_{g_i}D_cD_w \\ B_cD_w \end{bmatrix}
$$
$$
C_i = \begin{bmatrix} C_{z_i} + D_{zu_i}D_cC_g & D_{zu_i}C_c \end{bmatrix}, \quad D_i = D_{zw_i} + D_{zu_i}D_cD_w
$$

(3.45)

The fixed-structure H_∞ control synthesis problem to be addressed in this section is stated as follows:

Problem 1. *(Fixed-structure H_∞ control)*

Design a fixed-structure output-feedback controller with dynamic equations given in (3.3) such that $\|H_{zw}(\lambda)\|_\infty$ is minimized, i.e.

$$
\begin{aligned}
&\min && \mu \\
&\text{subject to} && \|H_{zw}(\lambda)\|_\infty^2 < \mu, \quad \forall \lambda \in \Lambda_q
\end{aligned}
$$

(3.46)

3.6.2 Inner Convex Approximation of Fixed-structure H_∞ Controllers

The following lemma determines the H_∞ norm of the transfer function $H_{zw}(\lambda)$.

Lemma 4. *(Bounded Real Lemma) Consider $H_{zw}(\lambda) = \big(A(\lambda), B(\lambda), C(\lambda), D(\lambda)\big)$. Then, $\|H_{zw}(\lambda)\|_\infty^2 < \mu$ if and only if there exists a symmetric matrix $P(\lambda) > 0$ such that*

For continuous-time systems [148]:

$$
\begin{bmatrix} A(\lambda)^TP(\lambda) + P(\lambda)A(\lambda) & P(\lambda)B(\lambda) & C^T(\lambda) \\ B^T(\lambda)P(\lambda) & -I & D^T(\lambda) \\ C(\lambda) & D(\lambda) & -\mu I \end{bmatrix} < 0, \quad \lambda \in \Lambda_q
$$

(3.47)

For discrete-time systems [152]:

$$
\begin{bmatrix}
A(\lambda)^T P(\lambda) A(\lambda) - P(\lambda) & A(\lambda)^T P(\lambda) B(\lambda) & C^T(\lambda) \\
B^T(\lambda) P(\lambda) A(\lambda) & -\mu I + B^T(\lambda) P(\lambda) B(\lambda) & D^T(\lambda) \\
C(\lambda) & D(\lambda) & -I
\end{bmatrix} < 0, \quad \lambda \in \Lambda_q \qquad (3.48)
$$

The above parameter-dependent inequalities contain the products of the Lyapunov matrix $P(\lambda)$ and the controller parameters appearing in the closed-loop matrices $A(\lambda)$, $B(\lambda)$, $C(\lambda)$, and $D(\lambda)$. In the following, an LMI representation for fixed-structure H_∞ controller synthesis of LTI systems with polytopic uncertainty is given. The results are based on the use of slack matrices which are able to decouple the product of unknown matrices.

Theorem 8. (Continuous-time Case) *Suppose that a stable matrix M and a nonsingular slack matrix T are given. Then, the fixed-structure controller in (3.3) stabilizes the polytopic system in (3.40) and (3.41) and ensures the performance criterion $\|H_{zw}(\lambda)\|_\infty^2 < \mu$ for all $\lambda \in \Lambda_q$ if there exist symmetric matrices $P_i > 0$ such that*

$$
\begin{bmatrix}
M^T P_i + P_i M & P_i - M^T + (T^{-1} A_i T)^T & 0 & T^T C_i^T \\
P_i - M + T^{-1} A_i T & -2I & T^{-1} B_i & 0 \\
0 & (T^{-1} B_i)^T & -I & D_i^T \\
C_i T & 0 & D_i & -\mu I
\end{bmatrix} < 0; \quad i = 1, 2, \ldots, q \quad (3.49)
$$

Proof. Convex combination of (3.49) for all vertices leads to the following inequality:

$$
\begin{bmatrix}
M^T P(\lambda) + P(\lambda) M & P(\lambda) - M^T + (T^{-1} A(\lambda) T)^T & 0 & T^T C^T(\lambda) \\
P(\lambda) - M + T^{-1} A(\lambda) T & -2I & T^{-1} B(\lambda) & 0 \\
0 & (T^{-1} B(\lambda))^T & -I & D^T(\lambda) \\
C(\lambda) T & 0 & D(\lambda) & -\mu I
\end{bmatrix} < 0 \quad (3.50)
$$

where $\lambda \in \Lambda_q$, $P(\lambda) = \sum_{i=1}^{q} \lambda_i P_i$, and the closed-loop matrices $\big(A(\lambda), B(\lambda), C(\lambda), D(\lambda)\big)$ are given in (3.43). Then, the multiplication of the above inequality on the right by $U_2(\lambda)$

$$
U_2(\lambda) =
\begin{bmatrix}
I & 0 & 0 \\
P(\lambda) & 0 & 0 \\
0 & I & 0 \\
0 & 0 & I
\end{bmatrix}
\qquad (3.51)
$$

and on the left by $U_2^T(\lambda)$ leads to the following inequality:

$$
\begin{bmatrix}
P(\lambda)(T^{-1} A(\lambda) T) + (T^{-1} A(\lambda) T)^T P(\lambda) & T^{-1} B(\lambda) P(\lambda) & T^T C^T(\lambda) \\
(T^{-1} B(\lambda))^T P(\lambda) & -I & D^T(\lambda) \\
C(\lambda) T & D(\lambda) & -\mu I
\end{bmatrix} < 0 \qquad (3.52)
$$

According to the bounded real lemma [148], the above inequality indicates that $\|H_{zw}(\lambda)\|_\infty^2 < \mu$.

$\square$

Theorem 9. (Discrete-time Case) *Suppose that a stable matrix M and a nonsingular slack matrix T are given. Then, the fixed-order controller of (3.3) guarantees the robust stability and the robust performance $\|H_{zw}(\lambda)\|_\infty^2 < \mu$ of the closed-loop system given in (3.42)-(3.45) if there exist Lyapunov matrices $P_i > 0$ such that*

$$
\begin{bmatrix}
-M^T P_i M + P_i & M^T P_i - M^T + (T^{-1} A_i T)^T & 0 & T^T C_i^T \\
P_i M - M + T^{-1} A_i T & -P_i + 2I & T^{-1} B_i & 0 \\
0 & (T^{-1} B_i)^T & I & D_i^T \\
C_i T & 0 & D_i & \mu I
\end{bmatrix} > 0; \quad i = 1,2,\ldots,q
$$
(3.53)

Proof. By convex combination of (3.53) for all vertices, the following inequality is obtained:

$$
\begin{bmatrix}
-M^T P(\lambda) M + P(\lambda) & M^T P(\lambda) - M^T + (T^{-1} A(\lambda) T)^T & 0 & T^T C^T(\lambda) \\
P(\lambda) M - M + T^{-1} A(\lambda) T & -P(\lambda) + 2I & T^{-1} B(\lambda) & 0 \\
0 & (T^{-1} B(\lambda))^T & I & D^T(\lambda) \\
C(\lambda) T & 0 & D(\lambda) & \mu I
\end{bmatrix} > 0
$$
(3.54)

where $\lambda \in \Lambda_q$, $P(\lambda) = \sum_{i=1}^q \lambda_i P_i$, and $\big(A(\lambda), B(\lambda), C(\lambda), D(\lambda)\big)$ are given in (3.43). Then, pre- and post-multiplication of (3.54) with matrix $U_3(\lambda)$ and $U_3^T(\lambda)$, respectively,

$$
U_3(\lambda) = \begin{bmatrix}
T^{-T} & T^{-T} M^T - A^T(\lambda) T^{-T} & 0 & -\mu^{-1} C^T(\lambda) \\
0 & B^T(\lambda) T^{-T} & -I & \mu^{-1} D^T(\lambda)
\end{bmatrix}
$$
(3.55)

yield

$$
\begin{bmatrix}
P(\lambda) - (T^{-1} A(\lambda) T)^T P(\lambda)(T^{-1} A(\lambda) T) - (C(\lambda) T)^T(C(\lambda) T) & \star \\
(T^{-1} B(\lambda))^T P(\lambda)(T^{-1} A(\lambda) T) + D(\lambda)^T(C(\lambda) T) & \mu I - (T^{-1} B(\lambda))^T P(\lambda)(T^{-1} B(\lambda)) - D^T(\lambda) D(\lambda)
\end{bmatrix} > 0
$$
(3.56)

which is equivalent to (3.48) using the Schur complement lemma. Therefore, the closed-loop performance $\|H_{zw}(\lambda)\|_\infty^2 < \mu$ is guaranteed.

$\square$

Similar to the fixed-structure stabilizing control design, in order to choose the slack matrices M and T, matrix inequalities equivalent to (3.49) and (3.53) in which M, T, and P are decoupled are presented.

Lemma 5. *The following set of inequalities is equivalent to (3.49):*

$$
\begin{bmatrix}
A_i^T P_{T_i} + P_{T_i} A_i & P_{T_i} + M_T^T - A_i^T X & -M_T^T B_i + A_i^T X B_i & C_i^T \\
P_{T_i} + M_T - X A_i & -2X & X B_i & 0 \\
-B_i^T M_T + B_i^T X A_i & B_i^T X & -I & D_i^T \\
C_i & 0 & D_i & -\mu I
\end{bmatrix} < 0; \quad i = 1,\dots,q \quad (3.57)
$$

where $P_{T_i} = T^{-T} P_i T^{-1}$ and M_T and X are defined in (3.26).

Proof. The inequalities given in (3.57) are obtained by the multiplication of (3.49) on the left by U_4 and on the right by U_4^T.

$$
U_4 =
\begin{bmatrix}
T^{-T} & -T^{-T} M^T + A_i^T T^{-T} & 0 & 0 \\
0 & T^{-T} & 0 & 0 \\
0 & 0 & I & 0 \\
0 & 0 & 0 & I
\end{bmatrix}
\tag{3.58}
$$

$\square$

Lemma 6. *The following set of inequalities is equivalent to (3.53):*

$$
\begin{bmatrix}
-A_i^T P_{T_i} A_i + P_{T_i} & A_i^T P_{T_i} + M_T^T - A_i^T X & M_T^T B_i - A_i^T X B_i & C_i^T \\
P_{T_i} A_i + M_T - X A_i & -P_{T_i} + 2X & X B_i & 0 \\
B_i^T M_T - B_i^T X A_i & B_i^T X & I & D_i^T \\
C_i & 0 & D_i & \mu I
\end{bmatrix} > 0; \quad i = 1,\dots,q \quad (3.59)
$$

where $P_{T_i} = T^{-T} P_i T^{-1}$ and M_T and X are defined in (3.26).

Proof. Multiply the inequalities given in (3.53) on the left and on the right by the following matrix U_5 and U_5^T, respectively.

$$
U_5 =
\begin{bmatrix}
T^{-T} & T^{-T} M^T - A_i^T T^{-T} & 0 & 0 \\
0 & T^{-T} & 0 & 0 \\
0 & 0 & I & 0 \\
0 & 0 & 0 & I
\end{bmatrix}
\tag{3.60}
$$

$\square$

In the following, a systematic algorithm for the problem of the fixed-structure H_∞ controller design of LTI polytopic systems is given.

3.6.3 Algorithm III: "Fixed-structure H_∞ controller design"

To ease the presentation, the inequalities in (3.49)/(3.53) and (3.57)/(3.59) are respectively defined as follows:

$$\mathscr{F}_1^i\left(P_i, K, \mu \middle| M, T\right) < 0 \tag{3.61}$$

$$\mathscr{F}_2^i\left(P_{Ti}, M_T, X, \mu \middle| K\right) < 0 \tag{3.62}$$

for $i = 1, \ldots, q$. The sign $|$ in the arguments of $\mathscr{F}_1^i$ and $\mathscr{F}_2^i$ separates the decision variables and the known parameters in the LMI conditions. The set of LMIs in (3.61) is used to design a fixed-structure H_∞ controller $K = \left(A_c, B_c, C_c, D_c\right)$ for a given pair of (M, T) whereas the LMI conditions in (3.62) are employed to find M_T and X for a given controller K.

Step 1 (Initialization): Design an initial fixed-structure (H_∞) controller for each vertex of the polytopic system $\left(K_i^{[0]}; i = 1, \ldots, q\right)$. Put the iteration number $j = 1$ and choose the maximum number of iterations h_{max} and a small tolerance for $\epsilon > 0$.

Step 2: Compute $M_T^{[j]}$ and $X^{[j]}$ from the following optimization problem:

$$\mu_2^{[j]} = \min_{P_{Ti}, M_T^{[j]}, X^{[j]}, \mu} \mu$$

$$\text{subject to} \qquad \mathscr{F}_2^i\left(P_{Ti}, M_T^{[j]}, X^{[j]}, \mu \middle| K_i^{[j-1]}\right) < 0; \tag{3.63}$$

$$i = 1, \ldots, q$$

Then, obtain the slack matrices $M^{[j]}$ and $T^{[j]}$ using (3.31) and according to the current values of $M_T^{[j]}$ and $X^{[j]}$.

Step 3: Solve the following convex optimization problem to obtain a fixed-structure H_∞ controller $K^{[j]}$:

$$\mu_1^{[j]} = \min_{P_i, K^{[j]}, \mu} \mu$$

$$\text{subject to} \qquad \mathscr{F}_1^i\left(P_i, K^{[j]}, \mu \middle| M^{[j]}, T^{[j]}\right) < 0; \tag{3.64}$$

$$i = 1, \ldots, q$$

Step 4 (Termination): If either $\mu_1^{[j-1]} - \mu_1^{[j]} < \epsilon$ or even maximum number of iterations h_{max} reaches, stop. Otherwise use the obtained controller in Step 3 as an initial controller $\left(K_i^{[j]} = K^{[j]}; i = 1, \ldots, q\right)$ and go to Step 2 with $j \longleftarrow j + 1$.

It can be easily proven that the above iterative algorithm leads to monotonic convergence of the upper bound on the H_∞ norm. The proof is based on the fact that (3.61) and (3.62) are equivalent inequalities. Therefore, for $j > 1$, $K^{[j-1]}$ and $\mu_2^{[j]}$ are always feasible solutions to the optimization problem in Step 3 which guarantees that $\mu_1^{[j]} \leq \mu_2^{[j]}$. On the other hand, $M_T^{[j]}, X^{[j]}$ and $\mu_1^{[j]}$ are always solutions to the optimization problem in Step 2 at iteration $j + 1$. Thus,

$\mu_2^{[j+1]} \le \mu_1^{[j]}$. As a result, $\mu_1^{[j+1]} \le \mu_1^{[j]}$ which shows that the upper bound μ_1 is not increasing and monotonically converges to a suboptimal solution.

3.7 Fixed-structure Controller Design in the Case of Polytopic Uncertainty in All State Space Matrices

Consider the LTI dynamical system described by (3.40) where the polytopic uncertainty affects all the state space matrices, i.e.

$$
\begin{aligned}
\Omega_4 &= \left\{ \left(A_g(\lambda), B_g(\lambda), B_w(\lambda), C_g(\lambda), C_z(\lambda), D_{zu}(\lambda), D_{zw}(\lambda), D_w(\lambda) \right) \right. \\
&= \sum_{i=1}^{q} \lambda_i \left(A_{g_i}, B_{g_i}, B_{w_i}, C_{g_i}, C_{z_i}, D_{zu_i}, D_{zw_i}, D_{w_i} \right) \right\}
\end{aligned}
\tag{3.65}
$$

where $\lambda \in \Lambda_q$ and $\left(A_{g_i}, B_{g_i}, C_{g_i}, B_{w_i}, C_{z_i}, D_{zu_i}, D_{zw_i}, D_{w_i} \right)$ is the i-th vertex of the polytope.

In the case of polytopic uncertainty in all state space matrices, the proposed conditions in Section 3.4 and Section 3.6 cannot guarantee the stability and the H_∞ performance specification of the closed-loop systems due to the product of $B_{g_i} D_c$ and C_{g_i}, $B_{g_i} D_c$ and D_{w_i}, $D_{zu_i} D_c$ and C_{g_i}, and $D_{zu_i} D_c$ and D_{w_i}. In this section, new LMI-based conditions for fixed-structure controller synthesis of polytopic systems in which the uncertainty affects all the system matrices are developed. The results rely on the use of slack matrices which are able to decouple the product of unknown matrices as well as the state space matrices.

Theorem 10. (Continuous-time Case) *Suppose that two slack matrices M and X are given. Then, the fixed-structure controller of (3.3) stabilizes the given LTI continuous-time polytopic system in (3.40) and (3.65) and ensures the robust performance $\| H_{zw}(\lambda) \|_\infty^2 < \mu$ for all $\lambda \in \Lambda_q$ if there exist matrix L and symmetric matrices $P_i > 0$ such that*

$$
\begin{bmatrix}
M \bar{A}_{g_i} + \bar{A}_{g_i}^T M^T & P_i - M + \bar{A}_{g_i}^T X & M \bar{B}_{w_i} & \bar{C}_{z_i}^T & M \bar{B}_{g_i} K \\
\star & -X - X^T & X^T \bar{B}_{w_i} & 0 & X^T \bar{B}_{g_i} K \\
\star & \star & -I_r & \bar{D}_{zw_i}^T & 0 \\
\star & \star & \star & -\mu I_s & \bar{D}_{zu_i} K \\
\star & \star & \star & \star & 0
\end{bmatrix}
+ He \left\{ \begin{bmatrix} \bar{C}_{g_i}^T \\ 0 \\ \bar{D}_{w_i}^T \\ 0 \\ -I_{m+n_o} \end{bmatrix} L \right\} < 0
\tag{3.66}
$$

for $i = 1, \dots, q$, where

$$
K = \begin{bmatrix} A_c & B_c \\ C_c & D_c \end{bmatrix}
\tag{3.67}
$$

and

$$\bar{A}_{g_i} = \begin{bmatrix} A_{g_i} & 0 \\ 0 & 0_m \end{bmatrix}, \quad \bar{B}_{g_i} = \begin{bmatrix} 0 & B_{g_i} \\ I_m & 0 \end{bmatrix}, \quad \bar{B}_{w_i} = \begin{bmatrix} B_{w_i} \\ 0 \end{bmatrix}$$

$$\bar{C}_{g_i} = \begin{bmatrix} 0 & I_m \\ C_{g_i} & 0 \end{bmatrix}, \quad \bar{C}_{z_i} = \begin{bmatrix} C_{z_i} & 0 \end{bmatrix}, \quad \bar{D}_{zu_i} = \begin{bmatrix} 0 & D_{zu_i} \end{bmatrix}$$

$$\bar{D}_{zw_i} = D_{zw_i}, \quad \bar{D}_{w_i} = \begin{bmatrix} 0 \\ D_{w_i} \end{bmatrix} \tag{3.68}$$

Proof. By convex combination of (3.66) for all vertices, the following inequality is obtained.

$$\begin{bmatrix} M\bar{A}_g(\lambda) + \bar{A}_g^T(\lambda)M^T & P(\lambda) - M + \bar{A}_g^T(\lambda)X & M\bar{B}_w(\lambda) & \bar{C}_z^T(\lambda) & M\bar{B}_g(\lambda)K \\ \star & -X - X^T & X^T\bar{B}_w(\lambda) & 0 & X^T\bar{B}_g(\lambda)K \\ \star & \star & -I_r & \bar{D}_{zw}^T(\lambda) & 0 \\ \star & \star & \star & -\mu I_s & \bar{D}_{zu}(\lambda)K \\ \star & \star & \star & \star & 0 \end{bmatrix} + \mathrm{He}\left\{ \begin{bmatrix} \bar{C}_g^T(\lambda) \\ 0 \\ \bar{D}_w^T(\lambda) \\ 0 \\ -I_{m+n_o} \end{bmatrix} L \right\} < 0 \tag{3.69}$$

where $\lambda \in \Lambda_q$, $P(\lambda) = \sum_{i=1}^{q} \lambda_i P_i$ and

$$\{(\bar{A}_g(\lambda), \bar{B}_g(\lambda), \bar{C}_g(\lambda), \bar{B}_w(\lambda), \bar{C}_z(\lambda), \bar{D}_{zu}(\lambda), \bar{D}_{zw}(\lambda), \bar{D}_w(\lambda))$$

$$= \sum_{i=1}^{q} \lambda_i (\bar{A}_{g_i}, \bar{B}_{g_i}, \bar{C}_{g_i}, \bar{B}_{w_i}, \bar{C}_{z_i}, \bar{D}_{zu_i}, \bar{D}_{zw_i}, \bar{D}_{w_i})\}; \quad \lambda_i \in \Lambda_q \tag{3.70}$$

Pre-multiplication and post-multiplication of inequality (3.69) by $V(\lambda) = \begin{bmatrix} I_{2(m+n)+r+s} & Z^T(\lambda) \end{bmatrix}$, where

$$Z(\lambda) = \begin{bmatrix} \bar{C}_g(\lambda) & 0 & \bar{D}_w(\lambda) & 0 \end{bmatrix} \tag{3.71}$$

lead to the following inequality:

$$V(\lambda) \begin{bmatrix} M\bar{A}_g(\lambda) + \bar{A}_g^T(\lambda)M^T & P(\lambda) - M + \bar{A}_g^T(\lambda)X & M\bar{B}_w(\lambda) & \bar{C}_z^T(\lambda) & M\bar{B}_g(\lambda)K \\ \star & -X - X^T & X^T\bar{B}_w(\lambda) & 0 & X^T\bar{B}_g(\lambda)K \\ \star & \star & -I_r & \bar{D}_{zw}^T(\lambda) & 0 \\ \star & \star & \star & -\mu I_s & \bar{D}_{zu}(\lambda)K \\ \star & \star & \star & \star & 0 \end{bmatrix} V^T(\lambda) < 0 \tag{3.72}$$

Note that

$$V(\lambda)\mathrm{He}\left\{ \begin{bmatrix} \bar{C}_g^T(\lambda) \\ 0 \\ \bar{D}_w^T(\lambda) \\ 0 \\ -I_{m+n_o} \end{bmatrix} L \right\} V^T(\lambda) = 0 \tag{3.73}$$

Inequality (3.72) can be rewritten as follows:

$$
\begin{bmatrix}
M\bar{A}_g(\lambda) + \bar{A}_g^T(\lambda)M^T & P(\lambda) - M + \bar{A}_g^T(\lambda)X & M\bar{B}_w(\lambda) & \bar{C}_z^T(\lambda) \\
\star & -X - X^T & X^T\bar{B}_w(\lambda) & 0 \\
\star & \star & -I_r & \bar{D}_{zw}^T(\lambda) \\
\star & \star & \star & -\mu I_s
\end{bmatrix}
$$
$$
+ \text{He}\left\{ \begin{bmatrix} M\bar{B}_g(\lambda)K \\ X^T\bar{B}_g(\lambda)K \\ 0 \\ \bar{D}_{zu}(\lambda)K \end{bmatrix} Z(\lambda) \right\} < 0
\tag{3.74}
$$

By multiplying the inequality (3.74) by $U_6(\lambda)$ on the left

$$
U_6(\lambda) = \begin{bmatrix}
I & \bar{A}_g^T(\lambda) + \bar{C}_g^T(\lambda)K^T\bar{B}_g^T(\lambda) & 0 & 0 \\
0 & \bar{B}_w^T(\lambda) + \bar{D}_w^T(\lambda)K^T\bar{B}_g^T(\lambda) & I & 0 \\
0 & 0 & 0 & I
\end{bmatrix}
\tag{3.75}
$$

and $U_6^T(\lambda)$ on the right, the inequality (3.47) is obtained with linearly parameter-dependent Lyapunov matrix $P(\lambda)$. Thus, the proof is complete. □

Theorem 11. (Discrete-time Case) *Suppose that two slack matrices M and X are given. Then, the fixed-structure H_∞ controller of (3.3) stabilizes the given LTI discrete-time polytopic system in (3.40) and (3.65) and provides the robust performance $\| H_{zw}(\lambda)\|_\infty^2 < \mu$ for all $\lambda \in \Lambda_q$ if there exist matrix L and symmetric matrices $P_i > 0$ such that*

$$
\begin{bmatrix}
P_i - \bar{A}_{g_i}^T M^T - M\bar{A}_{g_i} & -M + \bar{A}_{g_i}^T X & -M\bar{B}_{w_i} & \bar{C}_{z_i}^T & -M\bar{B}_{g_i}K \\
\star & X + X^T + P_i & X^T\bar{B}_{w_i} & 0 & X^T\bar{B}_{g_i}K \\
\star & \star & I_r & \bar{D}_{zw_i}^T & 0 \\
\star & \star & \star & \mu I_s & \bar{D}_{zu_i}K \\
\star & \star & \star & \star & 0
\end{bmatrix}
+ \text{He}\left\{ \begin{bmatrix} \bar{C}_{g_i}^T \\ 0 \\ \bar{D}_{w_i}^T \\ 0 \\ -I_{m+n_o} \end{bmatrix} L \right\} > 0
\tag{3.76}
$$

for $i = 1,\ldots,q$, where K and $\left(\bar{A}_{g_i}, \bar{B}_{g_i}, \bar{C}_{g_i}, \bar{C}_{z_i}, \bar{D}_{zu_i}, \bar{D}_{zw_i}, \bar{D}_{w_i}\right)$ are respectively given in (3.67) and (3.68).

Proof. Convex combination of the set of conditions in (3.76) leads to the following inequality:

$$
\begin{bmatrix}
P(\lambda) - \bar{A}_g^T(\lambda)M^T - M\bar{A}_g(\lambda) & -M + \bar{A}_g(\lambda)^T X & -M\bar{B}_w(\lambda) & \bar{C}_z^T(\lambda) & -M\bar{B}_g(\lambda)K \\
\star & X + X^T + P(\lambda) & X^T\bar{B}_w(\lambda) & 0 & X^T\bar{B}_g(\lambda)K \\
\star & \star & I_r & \bar{D}_{zw}^T(\lambda) & 0 \\
\star & \star & \star & \mu I_s & \bar{D}_{zu}(\lambda)K \\
\star & \star & \star & \star & 0
\end{bmatrix}
$$

$$
+ \mathrm{He} \left\{ \begin{bmatrix} \bar{C}_g^T(\lambda) \\ 0 \\ \bar{D}_w^T(\lambda) \\ 0 \\ -I_{m+n_o} \end{bmatrix} L \right\} > 0 \tag{3.77}
$$

where $\lambda \in \Lambda_q$, $P(\lambda) = \sum_{i=1}^q \lambda_i P_i$ and $\left(\bar{A}_g(\lambda), \bar{B}_g(\lambda), \bar{C}_g(\lambda), \bar{C}_z(\lambda), \bar{D}_{zu}(\lambda), \bar{D}_{zw}(\lambda), \bar{D}_w(\lambda)\right)$ are given in (3.70). Multiply the above parameter-dependent LMI by $\begin{bmatrix} I_{2(m+n)+r+s} & Z^T(\lambda) \end{bmatrix}$ on the left, Z is given in (3.71), and its transpose on the right. Then, by multiplication of the resulting inequality by $U_7(\lambda)$ on the left

$$
U_7(\lambda) = \begin{bmatrix}
I & -\bar{A}_g^T(\lambda) - \bar{C}_g^T(\lambda)K^T\bar{B}_g^T(\lambda) & 0 & -\mu(\bar{C}_z(\lambda) + \bar{D}_{zu}(\lambda)K\bar{C}_g(\lambda))^T \\
0 & \bar{B}_w^T(\lambda) + \bar{D}_w^T(\lambda)K^T\bar{B}_g^T(\lambda) & -I & -\mu(\bar{D}_{zw}(\lambda) + \bar{D}_{zu}(\lambda)K\bar{D}_w(\lambda))^T
\end{bmatrix}
\tag{3.78}
$$

and by $U_7^T(\lambda)$ on the right and finally applying the Schur complement lemma, (3.48) is obtained. $\square$

Remarks.

1. The inequalities given in (3.66) and (3.76) are LMIs in terms of K, L, μ, and P_i, $i = 1, \ldots, q$.

2. The slack matrix L decouples the product of $\bar{B}_{g_i}K$ and $\bar{C}_{g_i}$, $\bar{B}_{g_i}K$ and $\bar{D}_{w_i}$, $\bar{D}_{zu_i}K$ and $\bar{D}_{w_i}$, as well as $\bar{D}_{zu_i}K$ and $\bar{C}_{g_i}$. In the case that the polytopic uncertainty appears in neither pair $\left(\bar{B}_{g_i}, \bar{D}_{zu_i}\right)$ nor $\left(\bar{C}_{g_i}, \bar{D}_{w_i}\right)$, the slack matrix L can be easily removed and in consequence, the conservatism caused by the use of a unique slack matrix L for all vertices is eliminated.

3. Theorem 10 and Theorem 11 can be adapted to cope with fixed-structure stabilizing controllers by excluding the third and forth rows and columns in (3.66) and (3.76).

4. Theorem 10 and Theorem 11 can be used for fixed-structure H_∞ controller design of LTI system with polytopic uncertainty given in (3.40) and (3.65). To this end, similar to Algorithm III in Subsection 3.6.3, the slack matrices M and X can be chosen and
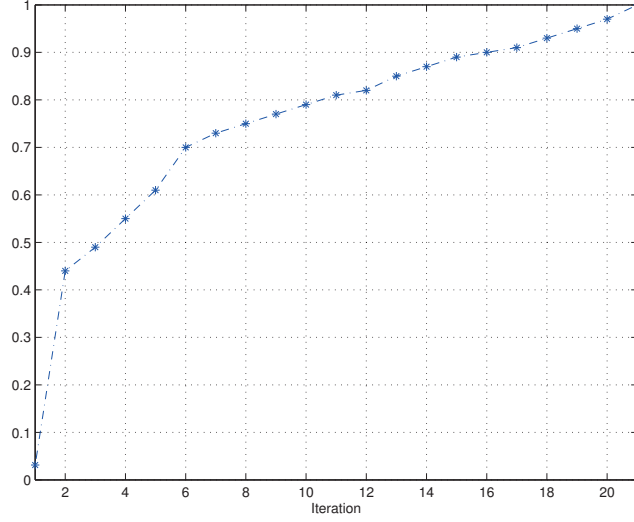
Figure 3.1: Evolution of the scaling factor α versus the iteration numbers in Example 1

iteratively updated according to a set of initial fixed-structure controllers, i.e.

$$
\begin{aligned}
&\min_{M,X,L,\mu,P_i} \quad \mu \\
&\text{s.t.} \quad (3.66)\big|_{K_i}\big((3.76)\big|_{K_i}\big) \\
&\qquad\quad P_i = P_i^T > 0; \qquad i = 1,\dots,q
\end{aligned}
\tag{3.79}
$$

3.8 Numerical Examples

In this section, three simulation examples are provided in order to demonstrate the effectiveness of the proposed methods in this chapter. The convex optimisation problems are solved by YALMIP [146] as the interface and SDPT3 [153]/SeDuMi [154] as the solver.

Example 1 (Fixed-order stabilizing control). Consider the state space model of the linearized vertical-plane dynamics of an aircraft (AC1 benchmark problem in [155]) given by:

$$
A_g = \begin{bmatrix}
0 & 0 & \rho_1 & 0 & -1 \\
0 & -0.0538 & -0.1712 & 0 & 0.0705 \\
0 & 0 & 0 & 1 & 0 \\
0 & 0.0485 & 0 & -0.8556 & -1.013 \\
0 & -0.2909 & 0 & \rho_2 & -\rho_3
\end{bmatrix}, \quad
B_g = \begin{bmatrix}
0 & 0 & 0 \\
-0.12 & 1 & 0 \\
0 & 0 & 0 \\
\rho_4 & 0 & -1.665 \\
\rho_5 & 0 & -0.0732
\end{bmatrix}
\tag{3.80}
$$

$$
C_g = \begin{bmatrix}
1 & 0 & 0 & 0 & 0 \\
0 & 1 & 0 & 0 & 0 \\
0 & 0 & 1 & 0 & 0
\end{bmatrix}
$$

where $\rho_1 = 1.132$, $\rho_2 = 1.0532$, $\rho_3 = 0.6859$, $\rho_4 = 4.419$, and $\rho_5 = 1.575$. We assume that all five parameters ρ_1, ρ_2, ρ_3, ρ_4, and ρ_5 contain the uncertainty up to $\pm 60\%$ of their nominal values. A first-order output feedback controller is sought to stabilize the resulting polytopic system with $q = 2^5$ vertices in a five-dimensional space.

According to Algorithm II in Subsection 3.5.2, a first-order output feedback stabilizing controller is designed using *hinfstruct* for the nominal system defined in (3.34) as follows:

$$A_c = -100.6193, \quad B_c = \begin{bmatrix} 7.9859 & 8.7991 & 8.8372 \end{bmatrix}$$

$$C_c = \begin{bmatrix} 9.8927 \\ 9.6167 \\ 10.1794 \end{bmatrix}, \quad D_c = \begin{bmatrix} -0.0280 & -0.7255 & -0.3759 \\ 0.4738 & -6.7940 & 1.7955 \\ 1.6036 & -1.9755 & 2.1200 \end{bmatrix} \tag{3.81}$$

This controller can be used as an initial controller for the iterative algorithm in which the scaling parameter α is maximized. Finally, after 21 iterations, α is increased up to 1. The evolution of α versus iterations is shown in Figure 3.1. The final stabilizing controller after 21 iterations is given by:

$$A_c = -183.4386, \quad B_c = \begin{bmatrix} 8.1305 & 14.6246 & 1.2300 \times 10^3 \end{bmatrix}$$

$$C_c = \begin{bmatrix} 12.7043 \\ -56.2052 \\ -3.3766 \end{bmatrix}, \quad D_c = \begin{bmatrix} -0.0302 & -0.9143 & -84.1476 \\ 0.6063 & -2.0523 & 431.3461 \\ 1.6314 & -0.9903 & 45.6236 \end{bmatrix} \tag{3.82}$$

Example 2 (Fixed-order H_∞ control). Consider the following state space model of a discrete-time system in [43] given by:

$$A_g = \begin{bmatrix} 0 & 0 & -r_1 \\ 1 & 0 & -r_2 \\ 0 & 1 & -r_3 \end{bmatrix}, \quad B_g = \begin{bmatrix} r_4 \\ 1 \\ 0 \end{bmatrix}, \quad C_g = \begin{bmatrix} 0 & 0 & 1 \end{bmatrix}$$

$$C_z = \begin{bmatrix} 0 & 0 & 1 \end{bmatrix}, \quad D_{zu} = 0, \quad D_{zw} = 1, \quad D_w = 1 \tag{3.83}$$

with $r_1 = -0.1$, $r_2 = 0.5$, $r_3 = -1.2$, and $r_4 = 0.2$. It is assumed that the parameters r_1, r_2, r_3, and r_4 contain uncertainty up to $\pm 20\%$ of their nominal values, resulting in an unstable polytope with $2^4 = 16$ vertices in a four-dimensional space. The objective is to design a second-order H_∞ controller such that the performance criterion $\|H_{zw}(\lambda)\|_\infty$ is minimized

According to Algorithm III in Subsection 3.6.3, at the first step, sixteen initial second-order controllers are designed using FDRC Toolbox [151] for each vertex of the polytope. Then, the initial controllers are utilized to determine the slack matrices M and T using the convex optimization problem given in (3.63). Finally, the iterative algorithm converges to the following
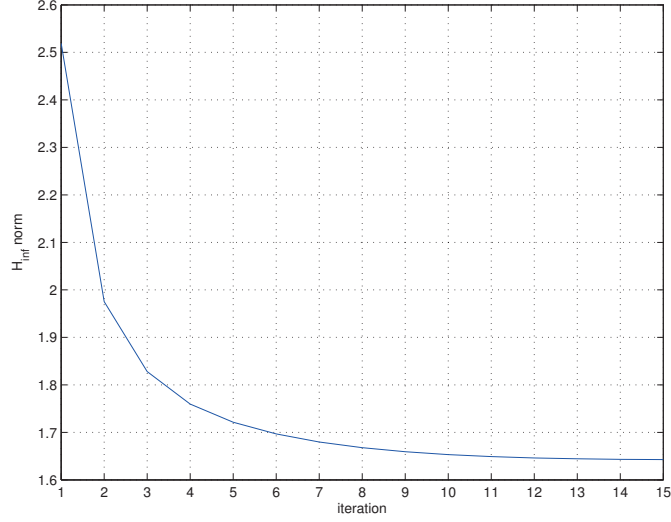
Figure 3.2: Evolution of the upper bound of the H_∞ norm versus the iteration number in Example 2

Table 3.1: Upper bound of $\|H_{zw}(\lambda)\|_\infty$ for different approaches in Example 2

Approach	[3]		[156]		[44]		Results of Theorem 9
	$d_1(z)$	$d_2(z)$	$d_1(z)$	$d_2(z)$	$d_1(z)$	$d_2(z)$	
$\gamma = \sqrt{\mu}$	2.25	1.95	2.25	1.95	1.75	1.75	1.64

controller with $\mu = 1.6428^2$ after 15 iterations:

$$A_c = \begin{bmatrix} -0.8942 & 0.0555 \\ 1.0025 & -0.1035 \end{bmatrix}, \quad B_c = \begin{bmatrix} 1.6979 \\ -0.0006 \end{bmatrix}$$
$$C_c = \begin{bmatrix} -0.4733 & 0.1292 \end{bmatrix}, \quad D_c = 0.5409 \tag{3.84}$$

Figure 3.2 shows the monotonic decreasing of the upper bound of $\|H_{zw}(\lambda)\|_\infty$ versus the iteration number. Since the state space realization of the system is in the canonical form, the polynomial-based approaches in the literature (e.g. [3, 44, 156]) which rely on the idea of SPRness are employed for the comparison purpose. The results of these approaches for two different central polynomials $d_1(z)$ and $d_2(z)$ have been reported in [44]. The results are summarised in Table 3.1. The results show that the proposed approach in this chapter obtains the best results among the others.

Example 3 (Fixed-order distributed H_∞ control). Consider a network of three intercon-nected second-order discrete-time subsystems given in [74] with following state space matri-

ces:

$$A_g = \begin{bmatrix} a_{11} & 0.1 & a_{13} & 0 & -0.3 & 0 \\ 0.1 & 0.1 & 0 & 0 & -0.3 & 0.2 \\ 0.3 & 0.1 & 0.6 & 0.1 & 0 & 0 \\ 0.2 & 0.5 & 0.1 & a_{44} & 0 & 0 \\ 0 & 0 & -0.2 & 0 & 0.4 & 0 \\ 0 & 0 & 0.4 & -0.1 & 0.2 & 0.3 \end{bmatrix}$$

$$B_g = \mathrm{diag}\left(\begin{bmatrix} -0.5 \\ 0.5 \end{bmatrix}, \begin{bmatrix} 0.2 \\ 0.4 \end{bmatrix}, \begin{bmatrix} 0.5 \\ 0.3 \end{bmatrix} \right)$$

$$B_w = \mathrm{diag}\left(\begin{bmatrix} -0.2 \\ 1.0 \end{bmatrix}, \begin{bmatrix} 0.4 \\ -0.2 \end{bmatrix}, \begin{bmatrix} 0 \\ 0.2 \end{bmatrix} \right)$$

$$C_g = \mathrm{diag}\left(\begin{bmatrix} 1 & 1 \end{bmatrix}, \begin{bmatrix} 1 & 1 \end{bmatrix}, \begin{bmatrix} 1 & 1 \end{bmatrix} \right)$$

$$C_z = \mathrm{diag}\left(\begin{bmatrix} 1.3 & 0.4 \end{bmatrix}, \begin{bmatrix} 0 & -2 \end{bmatrix}, \begin{bmatrix} -0.5 & 0 \end{bmatrix} \right)$$

$$D_{zu} = \mathrm{diag}\left(-0.3, 0.1, 0.5 \right), \quad D_{zw} = \mathrm{diag}\left(0.1, 0.5, 0 \right)$$

$$D_w = \mathrm{diag}\left(-0.3, 0, 0.5 \right)$$

(3.85)

It is assumed that the parameters a_{11}, a_{13}, and a_{44} are not precisely known, but they belong to the intervals $0 \le a_{11} \le 0.4$, $-1 \le a_{13} \le 1$, and $0 \le a_{44} \le 0.8$. The objective of this example is to design a distributed H_∞ control with the following structure for the polytope with $q = 8$ vertices:

$$A_c = \mathrm{diag}\left(A_{c_1}, A_{c_2}, A_{c_3} \right), \quad B_c = \mathrm{diag}\left(B_{c_1}, B_{c_2}, B_{c_3} \right)$$

$$C_c = \mathrm{diag}\left(C_{c_1}, C_{c_2}, C_{c_3} \right), \quad D_c = \begin{bmatrix} D_{c_{11}} & 0 & 0 \\ D_{c_{21}} & D_{c_{22}} & D_{c_{23}} \\ 0 & 0 & D_{c_{33}} \end{bmatrix}$$

(3.86)

where the order of A_{c_1}, A_{c_2}, and A_{c_3} is fixed to one.

According to Algorithm III in Subsection 3.6.3 together with *hinfstruct* for initial fixed-structure controller design, the following fixed-structure controller is obtained after 20 iterations:

$$A_c = \mathrm{diag}\left(0.2145, -0.5230, 0.2098 \right), \quad B_c = \mathrm{diag}\left(0.1262, -0.1614, 0.8826 \right)$$

$$C_c = \mathrm{diag}\left(0.8455, 1.0642, -0.6998 \right), \quad D_c = \begin{bmatrix} 1.0214 & 0 & 0 \\ -1.4114 & -0.4180 & -0.4620 \\ 0 & 0 & -0.4103 \end{bmatrix}$$

(3.87)

The results versus the iteration number are depicted in Figure 3.3, which indicates that the upper bound of the infinity norm monotonically decreases. The obtained controller achieves $\| H_{zw} \|_\infty < 1.0133$, which is 22% smaller than the results of [157] in which an H_∞ control
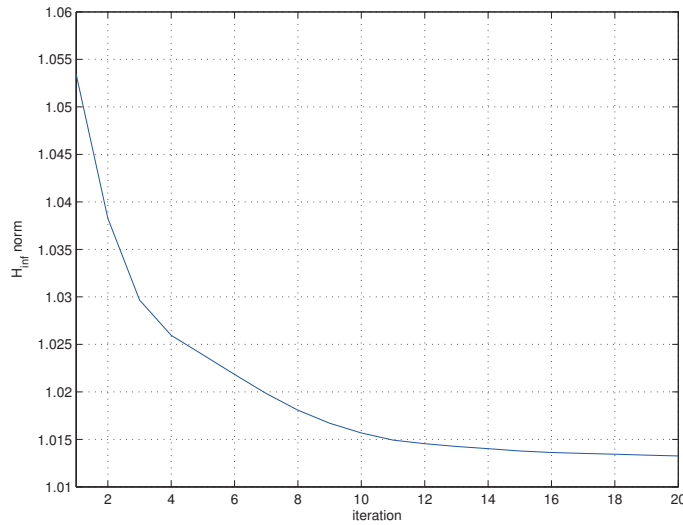
Figure 3.3: Evolution of the upper bound of the infinity norm versus the iteration number in Example 3

with the same structure given in (3.86) has been designed for the system in (3.85) without uncertainty.

3.9 Conclusion

This chapter presents LMI-based approaches to fixed-structure control of continuous-time and discrete-time LTI systems subject to polytopic uncertainty. The proposed approaches rely on the concept of strictly positive realness (SPRness) of transfer functions depending on several slack matrices. The slack matrices are utilized as a key tool to convexify the stability conditions as well as the H_∞ performance specifications. They are determined through a convex optimization problem and a set of initial fixed-structure controllers designed for each vertex of the polytopic system. To design fixed-structure stabilizing (H_∞) controllers for the polytopic systems, several systematic iterative algorithms are developed. Moreover, it is shown that the proposed approaches monotonically converge to a suboptimal solution by iterative update on the slack matrices according to the controller in the previous iteration. The simulation examples from the literature demonstrate the efficiency of the proposed methods.

In the next chapter, a slack variable-based approach for the problem of fixed-order control of polytopic systems is developed. Similar to the proposed approach in this chapter, it is based on the SPRness of a transfer function in which the slack matrices are designed using a state feedback controller.

4 Fixed-order Controller Synthesis of Systems with Polytopic Uncertainty via HPPD Lyapunov Matrices

4.1 Introduction

This chapter addresses the problem of fixed-order controller design of linear time-invariant polytopic systems via homogeneous polynomially parameter-dependent Lyapunov matrices. The proposed approach relies upon the concept of Strictly Positive Realness (SPRness) of a transfer function depending on a parameter-dependent gain. Continuous-time and discrete-time controller design are treated in a unified fashion. It is theoretically and numerically demonstrated that the proposed approach allows fixed-order stabilizing (H_∞) controller synthesis and uses less decision variables than some existing LMI-based approaches. Numerical examples show the efficacy of the proposed conditions compared with existing fixed-order control strategies.

The organization of this chapter is as follows. The problem formulation is given in Section 4.2. Section 4.3 presents necessary and sufficient parameter-dependent conditions for fixed-order stabilizing control. The relation between the proposed conditions and the existing methods is given in Section 4.4. Fixed-order H_∞ controller design strategy is proposed in Section 4.5. Section 4.6 is devoted to simulation results. Section 4.7 concludes the chapter.

The notation used throughout the paper is standard. In particular, $\mathbb{Z}_+$ is the set of nonnegative integers.

4.2 Problem Formulation

4.2.1 System Dynamics

Consider a linear time-invariant (LTI) system subject to polytopic uncertainty given by:

$$
\begin{aligned}
\delta[x_g(t)] &= A_g(\lambda)x_g(t) + B_g(\lambda)u(t) + B_w(\lambda)w(t) \\
z(t) &= C_z(\lambda)x_g(t) + D_{zu}(\lambda)u(t) + D_{zw}(\lambda)w(t) \\
y(t) &= C_g(\lambda)x_g(t)
\end{aligned}
\tag{4.1}
$$

where $x_g \in \mathbb{R}^n$, $u \in \mathbb{R}^{n_i}$, $w \in \mathbb{R}^r$, $y \in \mathbb{R}^{n_o}$, and $z \in \mathbb{R}^s$ are the state, the control input, the exogenous input, the measured output, and the controlled output, respectively. The uncertain matrices $A_g(\lambda)$, $B_g(\lambda)$, $B_w(\lambda)$, $C_z(\lambda)$, $C_g(\lambda)$, $D_{zu}(\lambda)$, and $D_{zw}(\lambda)$ belong to the following set:

$$
\begin{aligned}
\Omega_5 &= \Big\{ \big(A_g(\lambda), B_g(\lambda), B_w(\lambda), C_z(\lambda), C_g(\lambda), D_{zu}(\lambda), D_{zw}(\lambda) \big) \\
&= \sum_{i=1}^{q} \lambda_i \big(A_{g_i}, B_{g_i}, B_{w_i}, C_{z_i}, C_{g_i}, D_{zu_i}, D_{zw_i} \big) \Big\}; \quad \lambda \in \Lambda_q
\end{aligned}
\tag{4.2}
$$

where the matrices A_{g_i}, B_{g_i}, B_{w_i}, C_{z_i}, C_{g_i}, D_{zu_i}, and D_{zw_i} build the i-th vertex of the polytope.

4.2.2 Controller Dynamics

The main objective of this chapter is to design a robust fixed-order controller of order m ($0 \leq m < n$) with dynamical equations given in (3.3) that stabilizes the polytopic system of (4.1)-(4.2) and meets various closed-loop performance specifications.

The problem of dynamic output-feedback controller synthesis can be equivalently transformed to static output feedback by introducing an augmented plant as follows [15]:

$$
\begin{aligned}
\delta[\bar{x}_g(t)] &= \bar{A}_g(\lambda)\bar{x}_g(t) + \bar{B}_g(\lambda)u(t) + \bar{B}_w(\lambda)w(t) \\
z(t) &= \bar{C}_z(\lambda)\bar{x}_g(t) + \bar{D}_{zu}(\lambda)u(t) + \bar{D}_{zw}(\lambda)w(t) \\
y(t) &= \bar{C}_g(\lambda)\bar{x}_g(t)
\end{aligned}
\tag{4.3}
$$

where

$$
\begin{aligned}
\bar{A}_g(\lambda) &= \begin{bmatrix} A_g(\lambda) & 0 \\ 0 & 0_m \end{bmatrix}, \quad \bar{B}_g(\lambda) = \begin{bmatrix} 0 & B_g(\lambda) \\ I_m & 0 \end{bmatrix} \\
\bar{B}_w(\lambda &= \begin{bmatrix} B_w(\lambda) \\ 0 \end{bmatrix}, \quad \bar{C}_g(\lambda) = \begin{bmatrix} 0 & I_m \\ C_g(\lambda) & 0 \end{bmatrix} \\
\bar{C}_z(\lambda) &= \begin{bmatrix} C_z(\lambda) & 0 \end{bmatrix}, \quad \bar{D}_{zu}(\lambda) = \begin{bmatrix} 0 & D_{zu}(\lambda) \end{bmatrix} \\
\bar{D}_{zw}(\lambda) &= D_{zw}(\lambda)
\end{aligned}
\tag{4.4}
$$

4.2.3 Closed-loop System Dynamics

The closed-loop system $H_{zw}(\lambda)$, transfer function from $w(t)$ to $z(t)$, is described as follows:

$$\begin{aligned}
\delta[x(t)] &= A(\lambda)x(t) + B(\lambda)w(t) \\
z(t) &= C(\lambda)x(t) + D(\lambda)w(t)
\end{aligned} \tag{4.5}$$

where $x(t) = \begin{bmatrix} x_g^T(t) & x_c^T(t) \end{bmatrix}^T$ and

$$\begin{aligned}
A(\lambda) &= \bar{A}_g(\lambda) + \bar{B}_g(\lambda)K\bar{C}_g(\lambda), \quad B(\lambda) = \bar{B}_w(\lambda) \\
C(\lambda) &= \bar{C}_z(\lambda) + \bar{D}_{zu}(\lambda)K\bar{C}_g(\lambda), \quad D(\lambda) = \bar{D}_{zw}(\lambda)
\end{aligned} \tag{4.6}$$

where

$$K = \begin{bmatrix} A_c & B_c \\ C_c & D_c \end{bmatrix} \tag{4.7}$$

4.3 Fixed-order Stabilizing Controller Design

The following theorems present necessary and sufficient conditions for the existence of a stabilizing static output feedback controller for the augmented polytopic systems described by (4.3) and (4.4).

Theorem 12. (Continuous-time Case) *There exists a static output feedback controller K which stabilizes the augmented continuous-time polytopic system in (4.3) and (4.4) if and only if there exist a parameter-dependent gain $K_s(\lambda)$, a Lyapunov matrix $P(\lambda) > 0$, and two matrices X and L such that*

$$\begin{bmatrix} M^T(\lambda)P(\lambda) + P(\lambda)M(\lambda) & P(\lambda)\bar{B}_g(\lambda) - N^T(\lambda) \\ \bar{B}_g^T(\lambda)P(\lambda) - N(\lambda) & -X - X^T \end{bmatrix} < 0 \tag{4.8}$$

for all $\lambda \in \Lambda_q$, where

$$\begin{aligned}
M(\lambda) &= \bar{A}_g(\lambda) + \bar{B}_g(\lambda)K_s(\lambda) \\
N(\lambda) &= XK_s(\lambda) - L\bar{C}_g(\lambda)
\end{aligned} \tag{4.9}$$

Moreover, the controller gain is presented as $K = X^{-1}L$.

Proof. Sufficiency: Based on the KYP lemma, inequality (4.8) indicates that the following transfer function is SPR with Lyapunov matrix $P(\lambda)$:

$$H(s) = \left[\begin{array}{c|c} M(\lambda) & \bar{B}_g(\lambda) \\ \hline X(K_s(\lambda) - K\bar{C}_g(\lambda)) & X \end{array} \right] \tag{4.10}$$

According to Lemma 1, the SPRness of $H(s)$ implies that $H^{-1}(s)$ with the following realization is also SPR with the same Lyapunov matrix $P(\lambda)$.

$$H^{-1}(s) = \left[\begin{array}{c|c} A(\lambda) & -\bar{B}_g(\lambda)X^{-1} \\ \hline K_s(\lambda) - K\bar{C}_g(\lambda) & X^{-1} \end{array} \right] \tag{4.11}$$

The SPRness of $H^{-1}(s)$ with $P(\lambda)$ leads to the stability of the closed-loop state matrix $A(\lambda)$ with the parameter-dependent Lyapunov matrix $P(\lambda) > 0$.

Necessity: Assume that K stabilizes the closed loop polytopic system in (4.5)-(4.6). Let's choose $X = I \left(X + X^T > 0 \right)$, $L = K$, and $K_s(\lambda) = K\bar{C}_g(\lambda)$. Then, the following transfer function is SPR; accordingly, (4.8) is satisfied.

$$\begin{aligned} H(s) &= \left[\begin{array}{c|c} M(\lambda) & \bar{B}_g(\lambda) \\ \hline 0 & I \end{array} \right] \\ &= 0 \times (sI - M(\lambda))^{-1} \times \bar{B}_g(\lambda) + I \\ &= I \end{aligned} \tag{4.12}$$

Thus, this completes the proof. $\qquad\square$

Theorem 13. (Discrete-time Case) *There exists a static output feedback controller K which stabilizes the augmented discrete-time polytopic system in (4.3) and (4.4) if and only if there exist a parameter-dependent gain $K_s(\lambda)$, a Lyapunov matrix $P(\lambda) > 0$, and two matrices X and L such that*

$$\begin{bmatrix} M^T(\lambda)P(\lambda)M(\lambda) - P(\lambda) & M^T(\lambda)P(\lambda)\bar{B}_g(\lambda) - N^T(\lambda) \\ \bar{B}_g^T(\lambda)P(\lambda)M(\lambda) - N(\lambda) & \bar{B}_g^T(\lambda)P(\lambda)\bar{B}_g(\lambda) - X - X^T \end{bmatrix} < 0 \tag{4.13}$$

for all $\lambda \in \Lambda_q$, where $M(\lambda)$ and $N(\lambda)$ are defined in (4.9). Moreover, the controller gain is presented as $K = X^{-1}L$.

Proof. Similar to the proof of Theorem 12. $\qquad\square$

4.4 Relation between Theorem 12/Theorem 13 and the Existing Methods

In this section, the relation between the proposed stabilizing static output feedback control approach in Theorem 12/Theorem 13 and the methods in [46, 49, 54, 56] is given. In particular, we show that the proposed approaches in [46, 49, 54, 56] can be interpreted as relying on the concept of the SPRness of a transfer function where A-matrix is fixed by a gain matrix.

Lemma 7. *Suppose that K_s is a state feedback controller for the continuous-time augmented system described by (4.3) and (4.4). Then, the following statements are equivalent:*

(*a*) *The static output feedback K stabilizes the augmented plant in (4.3) and (4.4).*

(*b*) *There exist two matrices X and L such that the following transfer function is SPR:*

$$H(s) = \left[\begin{array}{c|c} \bar{A}_g + \bar{B}_g K_s & \bar{B}_g \\ \hline X K_s - L \bar{C}_g & X \end{array} \right] \tag{4.14}$$

(*c*) *There exist a Lyapunov matrix P > 0 and matrices X and L such that*

$$\left[\begin{array}{cc} (\bar{A}_g + \bar{B}_g K_s)^T P + P(\bar{A}_g + \bar{B}_g K_s) & P \bar{B}_g - (X K_s - L \bar{C}_g)^T \\ \bar{B}_g^T P - (X K_s - L \bar{C}_g) & -X - X^T \end{array} \right] < 0 \tag{4.15}$$

(*d*) *There exist a Lyapunov matrix P > 0 and matrices F, V, X, and L such that the following inequality holds [56]:*

$$\left[\begin{array}{ccc} (\bar{A}_g + \bar{B}_g K_s)^T F^T + F(\bar{A}_g + \bar{B}_g K_s) & \star & \star \\ P - F^T + V(\bar{A}_g + \bar{B}_g K_s) & -V - V^T & \star \\ \bar{B}_g^T F^T + L \bar{C}_g - X K_s & \bar{B}_g^T V^T & -X - X^T \end{array} \right] < 0 \tag{4.16}$$

(*e*) *There exist a Lyapunov matrix P > 0 and two matrices X and L such that the following inequality is satisfied [46].*

$$\left[\begin{array}{cc} \bar{A}_g^T P + P \bar{A}_g & \star \\ \bar{B}_g P & 0 \end{array} \right] + He\left\{ \left[\begin{array}{c} K_s^T \\ -I \end{array} \right] \left[\begin{array}{cc} L \bar{C}_g & -X \end{array} \right] \right\} < 0 \tag{4.17}$$

Moreover, the static output feedback controller is presented as $K = X^{-1} L$.

Proof. The statements (*a*), (*b*), and (*c*) directly result from the KYP lemma and Theorem 12. Therefore, it is enough to show that (4.16) is equivalent to (4.15). Post-multiplying (4.16) by Q_1 and pre-multiplying by Q_1^T, the inequalities given in (4.15) is obtained.

$$Q_1 = \left[\begin{array}{cc} I & 0 \\ \bar{A}_g + \bar{B}_g K_s & \bar{B}_g \\ 0 & I \end{array} \right] \tag{4.18}$$

To prove the statement (*e*), the inequality given in (4.15) is obtained by pre- and post-multiplication of (4.17) by the following matrix:

$$Q_2 = \left[\begin{array}{cc} I & K_s^T \\ 0 & I \end{array} \right] \tag{4.19}$$

Thus, the proof is complete. □

Lemma 8. *Suppose that K_s is a state feedback controller for the discrete-time augmented system described by (4.3) and (4.4). Then, the following statements are equivalent:*

(*a*) *The static output feedback K stabilizes the augmented plant in (4.3) and (4.4).*

(*b*) *There exist two matrices X and L such that the following transfer function is SPR:*

$$H(z) = \left[\begin{array}{c|c} \bar{A}_g + \bar{B}_g K_s & \bar{B}_g \\ \hline X K_s - L \bar{C}_g & X \end{array}\right] \tag{4.20}$$

(*c*) *There exist a Lyapunov matrix P > 0 and matrices X and L such that*

$$\left[\begin{array}{cc} (\bar{A}_g + \bar{B}_g K_s)^T P (\bar{A}_g + \bar{B}_g K_s) - P & (\bar{A}_g + \bar{B}_g K_s)^T P \bar{B}_g - (X K_s - L \bar{C}_g)^T \\ \bar{B}_g^T P (\bar{A}_g + \bar{B}_g K_s) - (X K_s - L \bar{C}_g) & \bar{B}_g^T P \bar{B}_g - X - X^T \end{array}\right] < 0 \tag{4.21}$$

(*d*) *There exist a Lyapunov matrix P > 0 and matrices F, X, and L such that [54]:*

$$\left[\begin{array}{ccc} -P & \star & \star \\ F^T(\bar{A}_g + \bar{B}_g K_s) & P - F - F^T & \star \\ L\bar{C}_g - X^T K_s & \bar{B}_g^T F & -X - X^T \end{array}\right] < 0 \tag{4.22}$$

(*e*) *There exist a Lyapunov matrix P > 0 and matrices F_1, F_2, F_3, F_4, X, and L such that [49]:*

$$\left[\begin{array}{cccc} F_1(\bar{A}_g + \bar{B}_g K_s) + (\bar{A}_g + \bar{B}_g K_s)^T F_1^T - P & \star & \star & \star \\ F_2(\bar{A}_g + \bar{B}_g K_s) & -P & \star & \star \\ F_3(\bar{A}_g + \bar{B}_g K_s) + \bar{B}_g^T F_1^T + L\bar{C}_g - XK_s & \bar{B}_g^T F_2^T & F_3\bar{B}_g^T F_3^T - (X + X^T) & \star \\ F_4(\bar{A}_g + \bar{B}_g K_s) - F_1^T & P - F_2^T & F_4\bar{B}_g - F_3^T & -F_4 - F_4^T \end{array}\right] < 0 \tag{4.23}$$

Moreover, the static output feedback controller is presented as $K = X^{-1}L$.

Proof. The statements (*a*), (*b*), and (*c*) are the direct results of the KYP lemma and Theorem 13. To show (4.22) and (4.21) are equivalent, post-multiply (4.22) by Q_1 given in (4.18) and pre-multiply it by Q_1^T.

The equivalence between the inequalities in (4.21) and (4.23) is obtained by multiplication of (4.23) on the right by Q_3 and on the left by Q_3^T

$$Q_3 = \left[\begin{array}{ccc} I & 0 & 0 \\ 0 & I & 0 \\ 0 & 0 & I \\ \bar{A}_g + \bar{B}_g K_s & 0 & \bar{B}_g \end{array}\right] \tag{4.24}$$

leading to the following inequality:

$$\left[\begin{array}{ccc} -P & \star & \star \\ P(\bar{A}_g + \bar{B}_g K_s) & -P & \star \\ L\bar{C}_g - XK_s & \bar{B}_g^T P & -X - X^T \end{array}\right] < 0 \tag{4.25}$$

Then, by pre- and post-multiplication of (4.25) by the following matrix, the inequality given in (4.21) is derived.

$$Q_4 = \begin{bmatrix} I & (\bar{A}_g + \bar{B}_g K_s)^T & 0 \\ 0 & \bar{B}_g & I \end{bmatrix} \tag{4.26}$$

Thus, the proof is complete. $\qquad\qquad\qquad\qquad\qquad\qquad\qquad\qquad\qquad\qquad\qquad\square$

As a result, the slack matrices (F, V) in (4.16), F in (4.22), and (F_1, F_2, F_3, F_4) in (4.23) can be eliminated without conservatism. In fact, these matrices do not affect the final static output feedback controller; however, elimination of them leads to less computation time.

4.5 Fixed-order H_∞ Controller Design

Theorem 14. (Continuous-time Case) *There exists a static output feedback controller K which stabilizes the augmented continuous-time LTI polytopic system in (4.3)-(4.4) and satisfies* $\|H_{zw}(\lambda)\|_\infty^2 < \mu$, *for all* $\lambda \in \Lambda_q$, *if and only if there exist a parameter-dependent gain* $K_s(\lambda)$, *a Lyapunov matrix* $P(\lambda) > 0$, *and two slack matrices X and L such that*

$$\begin{bmatrix} M^T(\lambda)P(\lambda) + P(\lambda)M(\lambda) & \star & \star & \star \\ \bar{B}_g^T(\lambda)P(\lambda) - N(\lambda) & -X - X^T & \star & \star \\ \bar{B}_w^T(\lambda)P(\lambda) & 0 & -\mu I & \star \\ \bar{C}_z(\lambda) + \bar{D}_{zu}(\lambda)K_s(\lambda) & \bar{D}_{zu}(\lambda) & \bar{D}_{zw}(\lambda) & -I \end{bmatrix} < 0 \tag{4.27}$$

where $M(\lambda)$ *and* $N(\lambda)$ *are defined in (4.9). Moreover, the controller gain is presented as* $K = X^{-1}L$.

Proof. Sufficiency: By applying the Schur complement lemma to (4.27), the following inequality is obtained:

$$\begin{bmatrix} M^T(\lambda)P(\lambda) + P(\lambda)M(\lambda) & \star & \star \\ \bar{B}_g^T(\lambda)P(\lambda) - N(\lambda) & -X - X^T & \star \\ \bar{B}_w^T(\lambda)P(\lambda) & 0 & -\mu I \end{bmatrix} + \Delta < 0 \tag{4.28}$$

where

$$\Delta = \begin{bmatrix} (\bar{C}_z(\lambda) + \bar{D}_{zu}(\lambda)K_s(\lambda))^T \\ \bar{D}_{zu}^T(\lambda) \\ \bar{D}_{zw}^T(\lambda) \end{bmatrix} \begin{bmatrix} \bar{C}_z(\lambda) + \bar{D}_{zu}(\lambda)K_s(\lambda) & \bar{D}_{zu}(\lambda) & \bar{D}_{zw}(\lambda) \end{bmatrix} \tag{4.29}$$

By multiplying the inequality in (4.28) on the left by $Q_5(\lambda)$

$$Q_5(\lambda) = \begin{bmatrix} I & \bar{C}_g^T(\lambda)K^T - K_s^T(\lambda) & 0 \\ 0 & 0 & I \end{bmatrix} \tag{4.30}$$

and on the right by $Q_5^T(\lambda)$, the following inequality is obtained:

$$\begin{bmatrix} A^T(\lambda)P(\lambda) + P(\lambda)A(\lambda) & \star \\ B^T(\lambda)P(\lambda) & -\mu I \end{bmatrix} + \begin{bmatrix} C^T(\lambda) \\ D^T(\lambda) \end{bmatrix} \begin{bmatrix} C(\lambda) & D(\lambda) \end{bmatrix} < 0 \tag{4.31}$$

which is equivalent to the following inequality by application of the Schur complement lemma:

$$Q_c(\lambda) = \begin{bmatrix} A^T(\lambda)P(\lambda) + P(\lambda)A(\lambda) & \star & \star \\ B^T(\lambda)P(\lambda) & -\mu I & \star \\ C(\lambda) & D(\lambda) & -I \end{bmatrix} < 0 \tag{4.32}$$

Therefore, the static output feedback K stabilizes the closed-loop polytopic system in (4.5)-(4.6) and ensures that $\|H_{zw}(\lambda)\|_\infty^2 < \mu$, for all $\lambda \in \Lambda_q$.

Necessity: Assume that K is an H_∞ controller for the augmented polytopic system in (4.3) and (4.4) which guarantees $\|H_{zw}(\lambda)\|_\infty^2 < \mu$, for all $\lambda \in \Lambda_q$. Therefore, based on the bounded real lemma, there always exists a Lyapunov matrix $P(\lambda) > 0$ such that the inequality (4.32) is satisfied, i.e. $Q_c(\lambda) < 0$. Let's choose $K_s(\lambda) = K\bar{C}_g(\lambda)$ and X such that

$$X + X^T > 0$$

$$X + X^T > - \begin{bmatrix} \bar{B}_g^T(\lambda)P(\lambda) - N(\lambda) & 0 & \bar{D}_{zu}^T(\lambda) \end{bmatrix} Q_c^{-1}(\lambda) \begin{bmatrix} P(\lambda)\bar{B}_g(\lambda) - N^T(\lambda) \\ 0 \\ \bar{D}_{zu}(\lambda) \end{bmatrix} \tag{4.33}$$

Then, set $L = XK$. Applying the Schur complement lemma to (4.33), the following inequality is obtained:

$$\begin{bmatrix} A^T(\lambda)P(\lambda) + P(\lambda)A(\lambda) & \star & \star & \star \\ \bar{B}_g^T(\lambda)P(\lambda) - N(\lambda) & -X - X^T & \star & \star \\ \bar{B}_w^T(\lambda)P(\lambda) & 0 & -\mu I & \star \\ C(\lambda) & \bar{D}_{zu}(\lambda) & \bar{D}_{zw}(\lambda) & -I \end{bmatrix} < 0 \tag{4.34}$$

Since $K_s(\lambda) = K\bar{C}_g(\lambda)$, we have:

$$N(\lambda) = 0, \quad M(\lambda) = A(\lambda), \quad C(\lambda) = \bar{C}_z(\lambda) + \bar{D}_{zu}(\lambda)K_s(\lambda)$$

Therefore, the parameter-dependent inequality given in (4.27) holds.

$$\square$$

Theorem 15. (Discrete-time Case) *There exists a static output feedback controller K which stabilizes the augmented discrete-time LTI polytopic system in (4.3)-(4.4) and guarantees* $\|H_{zw}(\lambda)\|_\infty^2 < \mu$, *for all $\lambda \in \Lambda_q$, if and only if there exist a parameter-dependent gain $K_s(\lambda)$, a Lyapunov matrix $P(\lambda) > 0$, and two slack matrices X and L such that*

$$
\begin{bmatrix}
M^T(\lambda)P(\lambda)M(\lambda) - P(\lambda) & \star & \star & \star \\
\bar{B}_g^T(\lambda)P(\lambda)M(\lambda) - N(\lambda) & \bar{B}_g^T(\lambda)P(\lambda)\bar{B}_g(\lambda) - X - X^T & \star & \star \\
\bar{B}_w^T(\lambda)P(\lambda)M(\lambda) & \bar{B}_w^T(\lambda)P(\lambda)\bar{B}_g(\lambda) & -\mu I + \bar{B}_w^T(\lambda)P(\lambda)\bar{B}_w(\lambda) & \star \\
\bar{C}_z(\lambda) + \bar{D}_{zu}(\lambda)K_s(\lambda) & \bar{D}_{zu}(\lambda) & \bar{D}_{zw}(\lambda) & -I
\end{bmatrix} < 0
$$

(4.35)

where $M(\lambda)$ and $N(\lambda)$ are defined in (4.9). Moreover, the controller gain is presented as $K = X^{-1}L$.

Proof. Similar to the proof of Theorem 14. □

Remarks.

1. If the parameter-dependent gain $K_s(\lambda)$ is given *a priori* and $P(\lambda)$ is considered as a homogeneous polynomial w.r.t. λ, the parameter dependent conditions in Theorem 12-Theorem 15 can be handled by a sequence of LMI relaxations. Parameter-dependent LMIs with parameters in the unit simplex always have homogenous polynomially parameter-dependent solutions of sufficiently high degree [158]. Moreover, they can be solved with no conservatism by a set of LMI relaxations.

2. A homogeneous polynomially parameter-dependent Lyapunov matrix $P(\lambda)$ of order d_p is defined as follows [158]:

$$
P(\lambda) = \sum_{k \in K(d_P)} \lambda_1^{k_1} \cdots \lambda_q^{k_q} P_k, \quad k = k_1 k_2 \cdots k_q
$$

(4.36)

where $\lambda_1^{k_1} \ldots \lambda_q^{k_q}$, $\lambda_i \in \Lambda_q$, $k_i \in \mathbb{Z}_+$, $i = 1, \ldots q$ are the monomials, and $P_k \in \mathbb{R}^{(n+m) \times (n+m)}$, $k \in K(d_P)$ are matrix-valued coefficients. $K(d_P)$ is obtained as all possible combinations of nonnegative integers k_i, $i = 1, \ldots, q$ such that $k_1 + k_2 + \cdots + k_q = d_p$.

4.5.1 Parameter-dependent Gain $K_s(\lambda)$

An appropriate choice of the parameter-dependent gain $K_s(\lambda)$ can affect the quality of the proposed fixed-order control strategy. Matrix $K_s(\lambda)$ must stabilize $M(\lambda)$ defined in (4.9), i.e. the eigenvalues of $M(\lambda)$ are located inside the unit circle for all $\lambda \in \Lambda_q$ (discrete-time case) or they have strictly negative real part (continuous-time case). In this subsection, two approaches for the design of $K_s(\lambda)$ are given.

Method 1: Matrix $K_s(\lambda)$ can be determined using a parameter-dependent state feedback controller for the augmented polytopic system in (4.3) and (4.4). The parameter-dependent state feedback controllers are designed through the following theorems.

Theorem 16. (Continuous-time Case) *The parameter-dependent state feedback controller $K_s(\lambda)$ stabilizes the augmented polytopic systems in (4.3)-(4.4) and guarantees the desired performance $\|H_{zw}(\lambda)\|_\infty^2 < \mu$, for all $\lambda \in \Lambda_q$, if and only if there exist a parameter-dependent Lyapunov matrix $P(\lambda) > 0$, matrices $F(\lambda)$, $Z(\lambda)$, and a positive scalar $\delta > 0$ such that*

$$
\begin{bmatrix}
\bar{A}_g(\lambda)F(\lambda) + F^T(\lambda)\bar{A}_g^T(\lambda) + \bar{B}_g(\lambda)Z(\lambda) + Z^T(\lambda)\bar{B}_g^T(\lambda) & \star & \star & \star \\
P(\lambda) - F(\lambda) + \delta(F^T(\lambda)\bar{A}_g^T(\lambda) + Z^T(\lambda)\bar{B}_g^T(\lambda)) & -\delta(F(\lambda) + F^T(\lambda)) & \star & \star \\
\bar{C}_w(\lambda)F(\lambda) + \bar{D}_{zu}(\lambda)Z(\lambda) & \delta(\bar{C}_w(\lambda)F(\lambda) + \bar{D}_{zu}(\lambda)Z(\lambda)) & -\mu I & \star \\
\bar{B}_w^T(\lambda) & 0 & \bar{D}_{zw} & -I
\end{bmatrix} < 0
$$

(4.37)

for all $\lambda \in \Lambda_q$. Moreover, the parameter-dependent state feedback is presented as $K_s(\lambda) = Z(\lambda)F^{-1}(\lambda)$.

Proof. Sufficiency: Multiply (4.37) by Q_6 on the left and Q_6^T on the right.

$$
Q_6 = \begin{bmatrix}
I & A_1(\lambda) & 0 & 0 \\
0 & C_1(\lambda) & I & 0 \\
0 & 0 & 0 & I
\end{bmatrix}
$$

(4.38)

where

$$
\begin{aligned}
A_1(\lambda) &= \bar{A}_g(\lambda) + \bar{B}_g(\lambda)Z(\lambda)F^{-1}(\lambda), \quad B_1(\lambda) = \bar{B}_w(\lambda) \\
C_1(\lambda) &= \bar{C}_w(\lambda) + \bar{D}_{zu}(\lambda)Z(\lambda)F^{-1}(\lambda), \quad D_1(\lambda) = \bar{D}_{zw}(\lambda)
\end{aligned}
$$

(4.39)

Necessity: Assume that there exists a parameter-dependent state feedback controller $K_s(\lambda)$ which ensures $\|H_{zw}(\lambda)\|_\infty^2 < \mu$, for all $\lambda \in \Lambda_q$. Therefore, according to the bounded real lemma, there exists a Lyapunov matrix $P(\lambda) > 0$ such that

$$
\begin{bmatrix}
A_1(\lambda)P(\lambda) + P(\lambda)A_1^T(\lambda) & \star & \star \\
C_1(\lambda)P(\lambda) & -\mu I & \star \\
B_1^T(\lambda) & D_1^T(\lambda) & -I
\end{bmatrix} < 0
$$

(4.40)

Then, we consider $F(\lambda) = P(\lambda)$ and $Z(\lambda) = K_s(\lambda)P(\lambda)$. Moreover, there always exists a scalar $\delta > 0$ such that

$$
\begin{aligned}
&\begin{bmatrix}
A_1(\lambda)P(\lambda) + P(\lambda)A_1^T(\lambda) & \star & \star \\
C_1(\lambda)P(\lambda) & -\mu I & \star \\
B_1^T(\lambda) & D_1^T(\lambda) & -I
\end{bmatrix} \\
&+ \delta \begin{bmatrix}
A_1(\lambda)F(\lambda) \\
C_1(\lambda)F(\lambda) \\
0
\end{bmatrix} (F(\lambda) + F^T(\lambda))^{-1} \begin{bmatrix} F^T(\lambda)A_1^T(\lambda) & F^T(\lambda)C_1^T(\lambda) & 0 \end{bmatrix} < 0
\end{aligned}
$$

(4.41)

Applying the Schur complement lemma on (4.41) and considering $F(\lambda) = P(\lambda)$, the inequality given in (4.37) holds. Thus, the proof is complete. $\square$

Theorem 17. (Discrete-time Case) *The parameter-dependent state feedback controller $K_s(\lambda)$ stabilizes the augmented polytopic systems in (4.3)-(4.4) and guarantees $\|H_{zw}(\lambda)\|_\infty^2 < \mu$, for all $\lambda \in \Lambda_q$, if and only if there exist a parameter-dependent Lyapunov matrix $P(\lambda) > 0$, matrices $F(\lambda)$, $Z(\lambda)$, and a positive scalar $\delta > 0$ such that*

$$\begin{bmatrix} P(\lambda) & \star & \star & \star \\ F^T(\lambda)\bar{A}_g^T(\lambda) + Z^T(\lambda)\bar{B}_g^T(\lambda) & F(\lambda) + F^T(\lambda) - P(\lambda) & \star & \star \\ 0 & \bar{C}_w(\lambda)F(\lambda) + \bar{D}_{zu}(\lambda)Z(\lambda) & I & \star \\ \bar{B}_w^T(\lambda) & 0 & \bar{D}_{zw}(\lambda) & \mu I \end{bmatrix} > 0 \quad (4.42)$$

for all $\lambda \in \Lambda_q$. Moreover, the parameter-dependent state feedback is presented as $K_s(\lambda) = Z(\lambda)F^{-1}(\lambda)$.

Proof. Sufficiency: Multiply the inequality given in (4.42) by Q_7 on the left and Q_7^T on the right.

$$Q_7 = \begin{bmatrix} I & -A_1(\lambda) & 0 & -\mu B_1(\lambda) \\ 0 & C_1(\lambda) & -I & \mu D_1(\lambda) \end{bmatrix} \quad (4.43)$$

where $A_1(\lambda)$, $B_1(\lambda)$, $C_1(\lambda)$, and $D_1(\lambda)$ are defined in (4.39).

Necessity: We assume that there exists a parameter dependent state feedback controller $K_s(\lambda)$ guaranteeing $\|H_{zw}(\lambda)\|_\infty^2 < \mu$, for all $\lambda \in \Lambda_q$. Therefore, based on the application of the bounded real lemma, there always exists a Lyapunov matrix $P(\lambda) > 0$ such that

$$\begin{bmatrix} P(\lambda) - A_1(\lambda)P(\lambda)A_1^T(\lambda) & \star & \star \\ C_1(\lambda)P(\lambda)A_1^T(\lambda) & -C_1(\lambda)P(\lambda)C_1^T(\lambda) + I & \star \\ B_1^T(\lambda) & D_1(\lambda) & \mu I \end{bmatrix} > 0 \quad (4.44)$$

The above inequality is equivalent to:

$$\begin{bmatrix} P(\lambda) & \star & \star & \star \\ P(\lambda)A_1^T(\lambda) & P(\lambda) & \star & \star \\ 0 & C_1(\lambda)P(\lambda) & I & \star \\ B_1^T(\lambda) & 0 & D_1(\lambda) & \mu I \end{bmatrix} > 0 \quad (4.45)$$

In fact, by applying the Schur complement on the $(2,2)$ submatrix of the above inequality, inequality of (4.44) results. By considering $F(\lambda) = P(\lambda)$ and $Z(\lambda) = K_s(\lambda)P(\lambda)$, the inequality given in (4.42) is obtained. Thus, the proof is complete. $\square$

Method 2: Parameter-dependent gain matrix $K_s(\lambda)$ can be obtained by a set of parameter-dependent output feedback controllers $K(\lambda) = \begin{bmatrix} A_c(\lambda) & B_c(\lambda) \\ C_c(\lambda) & D_c(\lambda) \end{bmatrix}$, provided that matrix $\bar{A}_g(\lambda) + \bar{B}_g(\lambda)K(\lambda)\bar{C}_g(\lambda)$ is stable. In this case, $K_s(\lambda) = K(\lambda)\bar{C}_g(\lambda)$.

Remarks.

1. Theorem 16 and Theorem 17 can be used for the design of stabilizing parameter-dependent state feedback controllers for the augmented system in (4.3) and (4.4) by removing the third and forth rows and columns of (4.37)/(4.42).

2. It should be mentioned that the set of LMI constraints from parameter-dependent LMIs in Theorem 12-Theorem 17 with parameters in the unit simplex can be constructed using ROLMIP (Robust LMI Parser)[159]. ROLMIP is a computational MATLAB package which provides an interface for the users to construct a finite set of LMIs from parameter-dependent LMIs with parameters in the unit simplex according to Pólya relaxation hierarchy [159] .

4.5.2   Algorithm I: "Fixed-order controller design procedure"

The robust fixed-order H_∞ controller design procedure includes the following steps:

Step 1: Choose the order of controller (m) and construct the augmented system in (4.3) and (4.4).

Step 2: Set the iteration number $j = 1$ and choose the maximum number of iterations h_{max} and a small tolerance for $\epsilon > 0$.

Step 3: Design the parameter-dependent gain $K_s^{[1]}(\lambda)$ for the augmented system using either Method 1 or Method 2.

Step 4: Update matrix $M(\lambda)$:

$$M(\lambda) = \bar{A}_g(\lambda) + \bar{B}_g(\lambda)K_s^{[j]}(\lambda) \tag{4.46}$$

Step 5: Choose the degree of the homogenous Lyapunov matrix $P(\lambda)$ in (4.27) (for continuous-time case) or in (4.35) (for discrete-time case) and solve the convex optimization problem proposed in Theorem 14 or Theorem 15 by constructing the LMI constraints in (4.27) or (4.35) (using e.g. ROLMIP) to obtain the static output feedback controller $K^{[j]}$.

Step 6: If $\mu^{[j-1]} - \mu^{[j]} > \epsilon$ and $j < h_{max}$, update the parameter-dependent gain $K_s(\lambda)$, $K_s^{[j+1]}(\lambda) = K^{[j]}\bar{C}_g(\lambda)$, and go to Step 4 with $j \longleftarrow j + 1$, else stop.

Theorem 18. *The iterative algorithm leads to monotonic convergence of the upper bound on the H_∞ norm.*

Proof. The proof stems from the fact that if controller $K^{[j-1]}$ is an H_∞ controller guaranteeing $\|H_{zw}(\lambda)\|_\infty^2 < \mu^{[j-1]}$, there always exist $X^{[j-1]}$, $L^{[j-1]}$, and $K_s^{[j-1]}(\lambda) = K^{[j-1]}\bar{C}_g(\lambda)$ such that (4.27)/(4.35) is satisfied. Now, suppose that we fix $K_s^{[j]}(\lambda) = K^{[j-1]}\bar{C}_g(\lambda)$ and a new controller $K^{[j]}$ is sought. Since $\left(K^{[j-1]}, \mu^{[j-1]}\right)$ is a feasible solution to the optimization problem in (4.27)/(4.35), it is guaranteed that $\mu^{[j]} \le \mu^{[j-1]}$. Therefore, the upper bound of the H_∞ norm in the proposed iterative algorithm is not increasing and monotonically converges to a suboptimal solution. $\qquad\square$

4.6   Simulation Examples

In this section, several examples from the literature are given to evaluate the effectiveness of the proposed approaches in this chapter. A comparison with the recent existing methods in the literature is made. It should be noted that in all tables, the set $\{d_Z, d_F, d_{P_{sf}}, d_P\}$ respectively denotes the degrees of the homogeneous polynomials $Z(\lambda)$, $F(\lambda)$, $P(\lambda)$ in Theorem 16 and Theorem 17, and the degree of homogeneous polynomially parameter-dependent Lyapunov matrix $P(\lambda)$ in Theorem 12-Theorem 15[1].

To solve the LMI problems in MATLAB, YALMIP [146] as the interface and SeDuMi [154] and MOSEK as the solvers are used.

Example 1. Consider a third-order continuous-time polytopic system, borrowed from [57], with the following vertices:

$$
\begin{aligned}
A_{g_1} &= \begin{bmatrix} -1 & 4 & 0 \\ 0 & 0 & 1 \\ a & 6 & -1 \end{bmatrix}, \quad
A_{g_2} = \begin{bmatrix} -1 & 1 & 0 \\ 0 & -5 & 1 \\ 10 & 1 & -1 \end{bmatrix} \\
B_{g_1} &= \begin{bmatrix} 0 \\ 0 \\ 1 \end{bmatrix}, \quad
B_{g_2} = \begin{bmatrix} 0 \\ 0 \\ 1 \end{bmatrix} \\
C_{g_1} &= \begin{bmatrix} 1 & 1 & 0 \\ 0 & 1 & 0 \end{bmatrix}, \quad
C_{g_2} = \begin{bmatrix} 1 & 1 & 0 \\ 0 & 0 & 0 \end{bmatrix}
\end{aligned}
\tag{4.47}
$$

The main objective is to design a stabilizing static output feedback controller which leads to the larger interval of parameter a. Therefore, the system can be modeled as a polytope with three vertices, i.e. $A_{g_1}\big|_{a=a_{min}}$, $A_{g_1}\big|_{a=a_{max}}$, and A_{g_2}. The minimum and maximum values of a can be determined by a bisection algorithm. The results of Theorem 12 are compared with ones of [56, 57, 160, 161] in Table 4.1. The proposed methods in Theorem 12 and [56] are both initialized with the same parameter-dependent state feedback $K_s(\lambda)$.

As it has been reported in [57], since matrix $C_g(\lambda)$ is not full row rank, the approaches of [160, 161] are not applicable. Results given in Table 4.1 indicate that the proposed methods in

---

[1]The degree of the other slack variables of [56] is considered equal to one.

Table 4.1: Maximum Interval of Parameter a in Example 1

Method	$\{d_Z, d_F, d_{P_{sf}}, d_P\}$	a
Theorem 12	$\{1, 0, 1, 1\}$	$\begin{bmatrix} -17.8 & 122.2 \end{bmatrix}$
[56]	$\{1, 0, 1, 1\}$	$\begin{bmatrix} -17.8 & 122.2 \end{bmatrix}$
[57]	$\{-, -, -, 1\}$	$\begin{bmatrix} 3.6 & 82.2 \end{bmatrix}$
[160]	—	Non-applicable
[161]	—	Non-applicable

Table 4.2: Upper bound of $\|H_{zw}(\lambda)\|_\infty$ in Example 2

Method	Iterations	$\gamma = \sqrt{\mu}$	K
[47]	1	9.73	$\begin{bmatrix} 0.56 & 5.08 \end{bmatrix}$
[48]	1	6.80	$\begin{bmatrix} 0.054 & 0.64 \end{bmatrix}$
[57]	1	2.33	$\begin{bmatrix} 0.45 & 4.19 \end{bmatrix}$
[147]	5	1.79	$\begin{bmatrix} 77.16 & 608.87 \end{bmatrix}$
[162]	30	1.66	$\begin{bmatrix} 130.35 & 939.37 \end{bmatrix}$
Theorem 14	5	1.78	$\begin{bmatrix} 9.36 & 69.57 \end{bmatrix}$

this chapter and [56] lead to the best results among the others.

Example 2. Consider the following continuous-time polytopic system with two vertices in [57]:

$$
A_{g_1} = \begin{bmatrix} -0.9896 & 17.41 & 96.15 \\ 0.2648 & -0.8512 & -11.39 \\ 0 & 0 & -30 \end{bmatrix}, \quad A_{g_2} = \begin{bmatrix} -1.702 & 50.72 & 263.5 \\ 0.2201 & -1.418 & -31.99 \\ 0 & 0 & -30 \end{bmatrix},
$$

$$
B_{g_1} = \begin{bmatrix} -97.78 \\ 0 \\ 30 \end{bmatrix}, \quad B_{g_2} = \begin{bmatrix} -85.09 \\ 0 \\ 30 \end{bmatrix}, \quad B_w = \begin{bmatrix} 0 \\ 1 \\ 1 \end{bmatrix} \tag{4.48}
$$

$$
C_g = \begin{bmatrix} 1 & 0 & 0 \\ 0 & 1 & 0 \end{bmatrix}, \quad C_w = \begin{bmatrix} 1 & 0 & 0 \\ 0 & 1 & 0 \\ 0 & 0 & 1 \end{bmatrix}, \quad D_{zu} = \begin{bmatrix} 0 \\ 0 \\ 0 \end{bmatrix}
$$

The objective here is to design a static output feedback H_∞ controller with linearly parameter-dependent Lyapunov matrices. To this end, an optimization problem, which is the minimization of μ subject to a sequence of LMI constraints is solved. Resulting static output feedback initialized by a parameter-dependent state feedback controller with $d_Z = 1$, $d_F = 0$, and $d_{P_{sf}} = 2$ is given in Table 4.2. The results are compared with the LMI-based methods in [47, 48, 57, 147] and the BMI-based method in [162]. For all cases, the degree of Lyapunov matrix P is one. As it is observed from Table 4.2, the proposed approach in this chapter provides the best results among the other LMI-based methods.

Table 4.3: Parameters of four operating points in Example 3

Operating points	1	2	3	4
Mach number	0.5	0.9	0.85	1.5
Altitude(ft)	5000	35000	5000	35000
a_{11}	-0.9896	-0.6607	-1.0702	-0.5162
a_{12}	17.41	18.11	50.72	29.96
a_{13}	96.15	84.34	263.5	178.9
a_{21}	0.2648	0.08201	0.2201	-0.6896
a_{22}	-0.8512	-0.6587	-1.418	-1.225
a_{23}	-11.39	-10.81	-31.99	-30.38
b_1	-97.78	-272.2	-85.09	-175.6

Example 3. As the third example, consider the modified version of the pitch control of F4E, given in [53], described by the following state space matrices:

$$
A_g = \begin{bmatrix} a_{11} & a_{12} & a_{13} & b_1 \\ a_{21} & a_{22} & a_{23} & 0 \\ 0 & 0 & -30 & 30 \\ 0 & 0 & 0 & -10^4 \end{bmatrix}, \quad B_g = \begin{bmatrix} 0 \\ 0 \\ 0 \\ 10^4 \end{bmatrix}, \quad C_g = \begin{bmatrix} c & 0 & 0 & 0 \\ 0 & c & 0 & 0 \end{bmatrix}
$$

$$
B_w = \begin{bmatrix} 1 & 0 & 0 \\ 0 & 1 & 0 \\ 0 & 0 & 1 \\ 0 & 0 & 0 \end{bmatrix}, \quad C_w = \begin{bmatrix} 1 & 0 & 0 & 0 \\ 0 & 1 & 0 & 0 \\ 0 & 0 & 1 & 0 \end{bmatrix}, \quad D_{zu} = \begin{bmatrix} 0 \\ 0 \\ 1 \end{bmatrix}
$$

(4.49)

where $0.5 \le c \le 1$ and parameters a_{ij}, $i = 1,2$; $j = 1,2,3$, and b_1 for four operating points are given in Table 4.3.

The uncertainty of the system in (4.49) is in the form of a polytope with $q = 8$ vertices. The proposed approach in [53] as well as the full-order controller design method of [51] are employed for the comparison purposes. It should be noted since the main assumption of [57] is that $C_w^T D_{zu} = 0$, it cannot be applied to Example 3.

Theorem 15 is initialized by two different parameter-dependent gain $K_s(\lambda)$. In the first case, initial parameter-dependent state feedback controllers are designed using Theorem 17 with $d_Z = 0$, $d_F = 0$, and $d_{P_{sf}} = 1$. In the second case, $K_s(\lambda) = K_0^m C_g(\lambda)$ is considered, where K_0^m is a simultaneously stabilizing controller of order m designed by HIFOO [31]. The results of both cases are then summarized in Table 4.4.

Theorem 15 initialized by the parameter-dependent state feedback $K_s(\lambda)$ resulted from Theo-

Table 4.4: Upper bound of $\|H_{zw}(\lambda)\|_\infty$ in Example 3

Initialization	Theorem 17		HIFOO	
controller order	$m=0$	$m=1$	$m=0$	$m=1$
degree of P (d_P)	1	1	1	2
Iterations	4	2	30	30
$\gamma = \sqrt{\mu}$	3.0780	3.1026	3.3378	2.2818

rem 17 leads to the following reduced-order H_∞ controllers:

$$K^{m=0} = \begin{bmatrix} 1.9407 & 12.3911 \end{bmatrix}$$

$$K^{m=1} = \left[\begin{array}{c|cc} -4.3979 & 0 & 0 \\ \hline 0 & 2.2321 & 14.3543 \end{array} \right] \tag{4.50}$$

For the second case, the following HIFOO controllers are used to initialize $K_s(\lambda)$:

$$K_0^{m=0} = \begin{bmatrix} 0.0958 & 0.7670 \end{bmatrix}$$

$$K_0^{m=1} = \left[\begin{array}{c|cc} -1.1754 & 0.2729 & -1.8780 \\ \hline 0.6998 & 0.3876 & 0.24434 \end{array} \right] \tag{4.51}$$

Theorem 15 initialized by $K_s(\lambda)$ obtained by HIFOO controllers in (4.51) leads to the following reduced-order H_∞ controllers:

$$K^{m=0} = \begin{bmatrix} 0.0965 & 0.8012 \end{bmatrix}$$

$$K^{m=1} = \left[\begin{array}{c|cc} -1.8044 & 0.1048 & -3.1589 \\ \hline 0.9039 & 0.3921 & 3.1998 \end{array} \right] \tag{4.52}$$

As mentioned in [56], the proposed approach of [53] leads to the lowest H_∞ upper bound 37.20 for $m = 0, 1$ and the full-order control design method in [51] does not find any feasible solution.

4.7   Conclusion

This chapter deals with the problem of fixed-order H_∞ controller design of LTI continuous-time and discrete-time polytopic systems. Necessary and sufficient conditions based on the concept of strictly positive realness (SPRness) of a transfer function depending on a parameter-dependent gain are developed. To convert the problem to a set of LMI conditions, the parameter-dependent gain is determined *a priori* by means of a parameter-dependent state feedback controller. The robust stability and robust H_∞ performance of the closed-loop polytopic systems are ensured via homogeneous polynomially parameter-dependent Lyapunov matrices. Simulation results and comparison with recent existing methods demonstrate

the effectiveness of the proposed approach.

In the next chapter, the problem of fixed-structure H_∞ control of LTI interconnected systems subject to polytopic-type uncertainty is considered. The problem is formulated as an optimization problem which is the minimization of the cardinality of a pattern matrix subject to an H_∞ performance constraint. Due to intrinsical non-convexity of the problem, a convex optimization-based design procedure for the control structure design and the controller synthesis is proposed in Chapter 5.

5 Control Structure Design for LTI Interconnected Systems subject to Polytopic Uncertainty

5.1 Introduction

Control of interconnected systems has attracted considerable attention in recent years due to their numerous applications such as power systems, urban traffic control systems, water distribution, digital communication networks, etc. Most available strategies for the control of interconnected systems assume that a control structure is specified *a priori*. However, it is not generally easy to determine an appropriate structure for the controller in advance, especially in the control of large-scale interconnected systems. Furthermore, it is possible that the assumed control structure is not the best one which can be taken into consideration. In general, the control structure design is an important step toward the control of complex systems. The problem of control structure selection consists of the following tasks [69]:

1. Controlled input selection (actuator placement problem)

2. Selection of outputs (sensor placement problem)

3. Control configuration selection (a structure interconnecting the measurements and the control inputs)

4. Control type selection (control law specification, e.g. PID, fixed-order controller, etc.)

The problem of actuator/sensor placement is to choose a minimal set of actuators/sensors (k) from a possible set of g actuators/sensors provided that a good performance of the system is obtained. The problem has been attracted remarkable attention due to its application in large-scale systems, e.g. power grids [59], target-tracking [60], transportation networks [61], and buildings [62]. Number of actuators/sensors as well as actuator/sensor locations affect the performance of the system. The objective is to minimize the number of expensive sensors/actuators while the best possible performance for a given number of sensors/actuators is achieved. The exact solution for the problem of actuator/sensor placement is to evaluate the system performance for all $\frac{g!}{k!(g-k)!}$ possible choices of actuators/sensors. However, this approach is not practical for the large values of k and g.

Chapter 5. Control Structure Design for LTI Interconnected Systems subject to Polytopic Uncertainty

The problem of the control configuration design refers to the restrictions imposed on the overall controller by its decomposition into a set of local controllers with their communication links [69]. In this case, the question usually arises is that what is the best control configuration, in terms of the connections between the subsystems and their local controllers, to satisfy given control objectives?

The main objective of this chapter is to describe the main issues involved in control structure design and to develop some convex optimization-based approaches to fixed-structure control of polytopic interconnected systems. Different from the existing approaches, where the control structure is fixed *a priori*, the structure of the controller is part of the optimization problems. As a result, the control structure and the control parameters are simultaneously designed.

The organization of the chapter is as follows: A convex optimization-based solution to the problem of sensor and actuator placement in LTI polytopic systems is presented in Section 5.2. Convex set of fixed-structure decentralized/distributed control of polytopic systems with guaranteed H_∞ performance is provided in Section 5.3. Section 5.4 concludes the chapter.

5.2 Sensor and Actuator Placement

5.2.1 Problem Formulation

Consider a linear time-invariant dynamical system subject to polytopic uncertainty described by

$$
\begin{aligned}
\delta[x_g(t)] &= A_g(\lambda)x_g(t) + B_g(\lambda)u(t) + B_w(\lambda)w(t) \\
z(t) &= C_z(\lambda)x_g(t) + D_{zu}(\lambda)u(t) + D_{zw}(\lambda)w(t) \\
y(t) &= C_g(\lambda)x_g(t) + D_w(\lambda)w(t)
\end{aligned}
\tag{5.1}
$$

where $x_g \in \mathbb{R}^n$, $u \in \mathbb{R}^{n_i}$, $w \in \mathbb{R}^r$, $y \in \mathbb{R}^{n_o}$, and $z \in \mathbb{R}^s$ are the state, the control input, the exogenous input, the measured output, and the controlled output, respectively. The uncertain state space matrices belong to the following set:

$$
\begin{aligned}
\Omega_6 &= \Big\{ \big(A_g(\lambda), B_g(\lambda), B_w(\lambda), C_g(\lambda), C_z(\lambda), D_{zu}(\lambda), D_{zw}(\lambda), D_w(\lambda) \big) \\
&= \sum_{i=1}^{q} \lambda_i \big(A_{g_i}, B_{g_i}, B_{w_i}, C_{g_i}, C_{z_i}, D_{zu_i}, D_{zw_i}, D_{w_i} \big) \Big\}
\end{aligned}
\tag{5.2}
$$

where $\lambda \in \Lambda_q$ and $\big(A_{g_i}, B_{g_i}, C_{g_i}, B_{w_i}, C_{z_i}, D_{zu_i}, D_{zw_i}, D_{w_i} \big)$ is the i-th vertex of the polytope. The main objective is to minimize the number of actuators/sensors while ensuring the robust stability and a satisfactory robust H_∞ performance of the closed-loop system with the following dynamic output-feedback controller:

$$
\begin{aligned}
\delta[x_c(t)] &= A_c x_c(t) + B_c y(t) \\
u(t) &= C_c x_c(t) + D_c y(t)
\end{aligned}
\tag{5.3}
$$

where $A_c \in \mathbb{R}^{m \times m}$, $B_c \in \mathbb{R}^{m \times n_o}$, $C_c \in \mathbb{R}^{n_i \times m}$, and $D_c \in \mathbb{R}^{n_i \times n_o}$.

The basic idea of the problem of sensor placement relies on the fact that the ith sensor is not employed in the dynamic output feedback controller if the ith column of the matrix $\begin{bmatrix} B_c \\ D_c \end{bmatrix}$ has only zero entries. In other words, the number of sensors can be minimized by minimizing the number of nonzero columns of matrix $\begin{bmatrix} B_c \\ D_c \end{bmatrix}$. In the same manner, the number of actuators can be minimized by minimizing the number of nonzero rows of the matrix $\begin{bmatrix} C_c & D_c \end{bmatrix}$.

To minimize the number of the non-zero columns of $\begin{bmatrix} B_c \\ D_c \end{bmatrix}$ and non-zero rows of $\begin{bmatrix} C_c & D_c \end{bmatrix}$, the following pattern matrices are respectively defined:

$$\mathcal{Z}_1 = \begin{bmatrix} card\left(\begin{bmatrix} B_c(:,1) \\ D_c(:,1) \end{bmatrix} \right) & \cdots & card\left(\begin{bmatrix} B_c(:,n_o) \\ D_c(:,n_o) \end{bmatrix} \right) \end{bmatrix} \tag{5.4}$$

$$\mathcal{Z}_2 = \begin{bmatrix} card\left(\begin{bmatrix} C_c(1,:) & D_c(1,:) \end{bmatrix} \right) & \cdots & card\left(\begin{bmatrix} C_c(n_i,:) & D_c(n_i,:) \end{bmatrix} \right) \end{bmatrix} \tag{5.5}$$

where $card(\cdot)$ is the cardinality operator defined as the number of non-zero elements of $(\cdot)$. Note that $B_c(:,i)$, $D_c(:,i)$, $C_c(j,:)$, and $D_c(j,:)$ respectively present the i-th column of the matrices B_c and D_c and the j-th row of C_c and D_c. It is obvious that the i-th element of $\mathcal{Z}_1$ (z_{1_i}) is equal to zero if and only if $\begin{bmatrix} B_c(:,i) \\ D_c(:,i) \end{bmatrix} = 0$ or equivalently, the i-th sensor is not used. In a similar way, the j-th actuator is not utlized in the controller if and only if the j-th element of $\mathcal{Z}_2$ is equal to zero. Therefore, to find a minimum number of the sensors (actuators), matrix $\mathcal{Z}_1$ ($\mathcal{Z}_2$) should be as sparse as possible. The sparsity of $\mathcal{Z}_1$ and $\mathcal{Z}_2$ are presented by their cardinality.

The sensor and actuator placement problems to be addressed in this chapter are stated as follows:

Problem 2. *(Sensor placement)*

Given a linear dynamical system subject to polytopic uncertainty, determine a set of sensors and design a fixed-structure dynamic output feedback controller such that

1. *Closed-loop system is robustly stable.*

2. *A trade-off between the performance $\|H_{zw}(\lambda)\|_\infty^2 < \mu$ and the number of sensors is obtained.*

The aforementioned conditions can be formulated as the following optimization problem:

$$\min_{K} \quad \mu + \alpha_1 \times card\left(\mathcal{Z}_1\right)$$
$$\text{subject to} \quad \|H_{zw}(\lambda)\|_\infty^2 < \mu$$

$$(5.6)$$

where α_1 determines a trade-off between two objectives. A larger α_1 leads to a sparser $\mathcal{Z}_1$ whereas $\alpha_1 = 0$ renders the fixed-structure H_∞ controller design problem.

Problem 3. *(Actuator placement)*

Given an LTI polytopic system, select a set of actuators and design a fixed-structure dynamic output feedback controller such that

1. *Closed-loop system is robustly stable.*

2. *A trade-off between the performance $\|H_{zw}(\lambda)\|_\infty^2 < \mu$ and the number of actuators is obtained.*

The aforementioned conditions can be formulated as the following optimization problem:

$$\min_{K} \quad \mu + \alpha_2 \times card\left(\mathcal{Z}_2\right)$$
$$\text{subject to} \quad \|H_{zw}(\lambda)\|_\infty^2 < \mu$$

$$(5.7)$$

where α_2 determines a trade-off between two objectives.

The above-mentioned problems are non-convex due to the noncovexity of the cardinality operator and the non-convex fixed-structure H_∞ dynamic output feedback controller synthesis problem. In the next section, a convex relaxation of the cardinality is presented.

5.2.2 Sensor and Actuator Placement via Convex Optimization

The non-convex cardinality minimization can be relaxed via the convex weighted ℓ_1 norm as follows [163]:

$$J_1 = \|W_1 * \mathcal{Z}_1\|_1$$
$$= \sum_{i=1}^{n_o} w_{1_i} \left\| \begin{bmatrix} B_c(:,i) \\ D_c(:,i) \end{bmatrix} \right\|_1$$

$$(5.8)$$

$$J_2 = \|W_2 * \mathcal{Z}_2\|_1$$
$$= \sum_{i=1}^{n_i} w_{2_i} \left\| \begin{bmatrix} C_c(i,:) & D_c(i,:) \end{bmatrix}^T \right\|_1$$

$$(5.9)$$

where w_{1_i} and w_{2_i} respectively are the ith entry of the weighting vectors W_1 and W_2. If w_{1_i} and w_{2_i} are respectively chosen to be inversely proportional to $F_i = \left\| \begin{bmatrix} B_c(:,i) \\ D_c(:,i) \end{bmatrix} \right\|_1$ and $H_i = \left\| \begin{bmatrix} C_c(i,:) & D_c(i,:) \end{bmatrix}^T \right\|_1$, i.e.

$$
\begin{aligned}
w_{1_i} &= \begin{cases} 1/F_i, & \text{if } F_i \neq 0 \\ \infty, & \text{if } F_i = 0 \end{cases} \\
w_{2_i} &= \begin{cases} 1/H_i, & \text{if } H_i \neq 0 \\ \infty, & \text{if } H_i = 0 \end{cases}
\end{aligned} \tag{5.10}
$$

then the weighted ℓ_1 norm and the cardinality operator coincide. However, since the weights depend on the unknown controller parameters, the above strategy cannot be implemented. In [163], an iterative algorithm for choosing the vectors $W_1 = [w_{1_i}]$ and $W_2 = [w_{2_i}]$ has been developed.

An inner convex approximation of fixed-structure H_∞ controllers is presented in Chapter 3. Therefore, the problem of sensor and actuator placement of linear time-invariant polytopic systems can be respectively solved by the following convex optimization problems:

$$
\begin{aligned}
\min_{A_c,B_c,C_c,D_c,\mu,(L),P_i} \quad & \mu + \alpha_1 \sum_{j=1}^{n_o} w_{1_j} \left\| \begin{bmatrix} B_c(:,j) \\ D_c(:,j) \end{bmatrix} \right\|_1 \\
\text{s.t.} \quad & (3.66)/(3.76) \\
& P_i = P_i^T > 0; \qquad i = 1,\dots,q
\end{aligned} \tag{5.11}
$$

$$
\begin{aligned}
\min_{A_c,B_c,C_c,D_c,\mu,(L),P_i} \quad & \mu + \alpha_2 \sum_{j=1}^{n_i} w_{2_j} \left\| \begin{bmatrix} C_c(j,:) & D_c(j,:) \end{bmatrix}^T \right\|_1 \\
\text{s.t.} \quad & (3.66)/(3.76) \\
& P_i = P_i^T > 0; \qquad i = 1,\dots,q
\end{aligned} \tag{5.12}
$$

Remark. In the case of polytopic uncertainty only in the state space matrices A_g, B_g, B_w, C_z, D_{zu}, and D_{zw}, the slack matrix L can be removed and the set of inequalities in (3.66)/(3.76) is replaced with (3.49)/(3.53).

In the following, a systematic iterative algorithm for the problem of sensor and actuator placement is given.

5.2.3 Algorithm I: "Sensor and actuator placement in LTI polytopic systems"

The algorithm for sensor and actuator placement in linear dynamical systems subject to polytopic-type uncertainty described by (5.1)-(5.2) is summarized with the following steps:

Step 1: Design some initial controllers for each vertex of the polytope $\left(K_i^{[0]}\right)$. Put the iteration number $h = 1$, $w_{1_j}^{[1]} = 1$; $j = 1,\ldots,n_o$, and $w_{2_j}^{[1]} = 1$; $j = 1,\ldots,n_i$. choose a small tolerance for $\epsilon_1 > 0$ and $\epsilon_2 > 0$, and maximum number of iteration h_{max}.

Step 2: For given $K_i^{[h-1]}$, solve the convex optimization problem given in (3.79) and determine $M^{[h]}$ and $X^{[h]}$.

Step 3: Solve the following convex optimization problem to obtain a fixed-structure H_∞ controller $K^{[h]}$ which simultaneously minimize the number of sensors and actuators.

$$
\min_{A_c,B_c,C_c,D_c,\mu,(L),P_i} \quad \mu + \alpha_1 \sum_{j=1}^{n_o} w_{1_j}^{[h]} \left\| \begin{bmatrix} B_c(:, j) \\ D_c(:, j) \end{bmatrix} \right\|_1 + \alpha_2 \sum_{j=1}^{n_i} w_{2_j}^{[h]} \left\| \begin{bmatrix} C_c(j,:) & D_c(j,:) \end{bmatrix}^T \right\|_1
$$

$$
\text{s.t.} \qquad (3.66)/(3.76)
$$

$$
P_i = P_i^T > 0; \qquad i = 1,\ldots,q
$$

(5.13)

Step 4: Update $F_j^{[h]} = \left\| \begin{bmatrix} B_c^{[h]}(:, j) \\ D_c^{[h]}(:, j) \end{bmatrix} \right\|_1$ and $H_j^{[h]} = \left\| \begin{bmatrix} C_c^{[h]}(j,:) & D_c^{[h]}(j,:) \end{bmatrix}^T \right\|_1$ according to the current controller $K^{[h]}$.

Step 5: Update the weighting vectors $W_1^{[h+1]}$ and $W_2^{[h+1]}$ as follows:

$$
w_{1_j}^{[h+1]} = \frac{1}{F_j^{[h]} + \epsilon_1}; \quad j = 1,\ldots,n_o
$$

$$
w_{2_j}^{[h+1]} = \frac{1}{H_j^{[h]} + \epsilon_2}; \quad j = 1,\ldots,n_i
$$

(5.14)

Step 6: Terminate the algorithm if it converges or if maximum number of iterations h_{max} reaches. Otherwise, use the obtained controller in Step 3 as an initial controller $\left(K_i^{[h]} \leftarrow K^{[h]}; i = 1,\ldots,q\right)$ and go to Step 2 with $h \leftarrow h + 1$.

Remark. Algorithm I can be used for the problem of sensor placement if we consider $\alpha_2 = 0$ in the cost function given in (5.13). In the similar way, we can apply Algorithm I to place the actuators if $\alpha_1 = 0$ is set in (5.13).

5.2.4 Simulation Examples

In this section, the effectiveness of the proposed algorithm is evaluated through some simulation examples. The LMI-based optimization problems are solved by YALMIP [146] and SDPT3 [153]/SeDuMi [154] as the interface and the solvers, respectively.

Example 1 (PMU placement in IEEE 14-bus test system). In this example, the problem of phasor measurement units (PMUs) placement in IEEE 14-bus test system shown in Figure 5.1
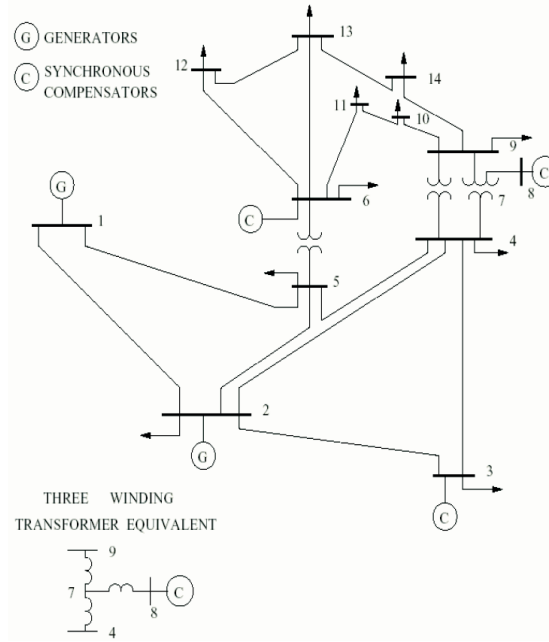
Figure 5.1: IEEE 14-bus test system

is considered.

The IEEE 14-bus system consists of 14 buses with 2 generators and 3 synchronous compensators. The synchronous compensators in the grid are replaced with some generators resulting in five buses with generators and nine load buses. The phase dynamics of the grid can be modeled using electromechanical swing equations [107] as follows:

$$J_i\ddot{\theta} + D_i\dot{\theta} = P_i - \sum_{i=1, j\neq i}^{n_g} \frac{E_i E_j}{X_{ij}} sin(\theta_i - \theta_j) \tag{5.15}$$

where J_i is the moment of inertia of the generator, D_i is the damping coefficient, E_i is the q-axis voltage at node i, P_i is the power injection at node i, and $X_{ij} = X_{ji}$ is the reactance of the line between node i and j. Then, the nonlinear swing equations are linearized by first-order Taylor approximation method around the operating points θ_i^*. Finally, the system is described by the following state space representation:

$$\begin{aligned} \dot{x}_g(t) &= A_g x_g(t) + B_g u(t) + B_w w(t) \\ y(t) &= C_g x_g(t) \end{aligned} \tag{5.16}$$

where x_g contains the phase angle θ_i; $i = 1,\ldots,14$ and the phase velocity (frequency) $\dot{\theta}_j$; $j = 1, 2, 3, 6, 8$. The inputs and outputs of the system are P_j; $j = 1, 2, 3, 6, 8$ and θ_i; $i = 1,\ldots,14$, respectively. Moreover, the disturbance signal w is a sudden change in the mechanical power or in the load demand. More details about the state space matrices and the parameters of the
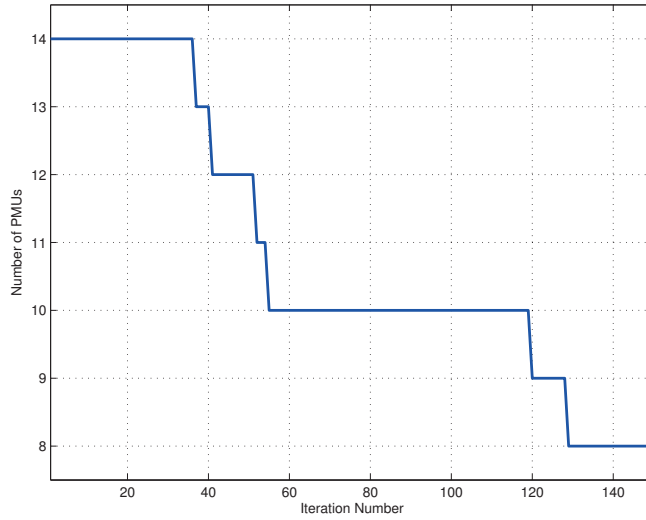
Figure 5.2: Number of PMUs versus iteration number in Example 1

system can be found in [164] and [65].

We assume that there exists a group of N generators at bus 1 and 2. In this case, to model the dynamical behaviour of each bus, the aggregated swing equation can be applied. In the aggregated swing equation, the moment of inertia J_i in (5.15) is replaced with the aggregated inertia of N generators [165]. In conventional power systems, the assumption is that the (aggregated) inertia is fixed. However, nowadays with the high depth of penetration of distributed generation (DG) units, e.g. wind turbines and photovoltaics (PV), in power grids, this assumption is not valid. In fact, wind and PV units significantly decrease the inertia of the system. A case study on German power system shows that the aggregated inertia is changing from its nominal value, in the case of conventional generators, to half of the nominal value when wind turbines and photovoltaics are deployed [165]. Therefore, the moment of inertia J_1 and J_2 are not precisely known and it is reasonable to assume that they are uncertain up to 50% of their nominal values leading to a polytope with $q = 2^2$ vertices.

The objective is to place the minimum number of PMUs, which measure the phase angles at certain buses, such that the effect of the disturbance on the outputs is minimized. To this end, PMUs should be placed on the buses which provide a satisfactory H_∞ closed-loop performance with a static output feedback controller.

The parameters $\epsilon_1 = 10^{-5}$, $\alpha_1 = 1$, and $\alpha_2 = 0$ are set. Using Algorithm I in Subsection 5.2.3 and after 150 iterations, minimum $g = 8$ PMUs in the buses $1, 2, 3, 4, 9, 12, 13$, and 14 are placed. Figure 5.2 depicts the number of PMUs versus the iteration number. The worst case upper bound of $\|H_{zw}(\lambda)\|_\infty$ versus the number of PMUs is shown in Figure 5.3. The obtained results indicate that as the number of PMUs decreases, the upper bound of $\|H_{zw}(\lambda)\|_\infty$ increases. It
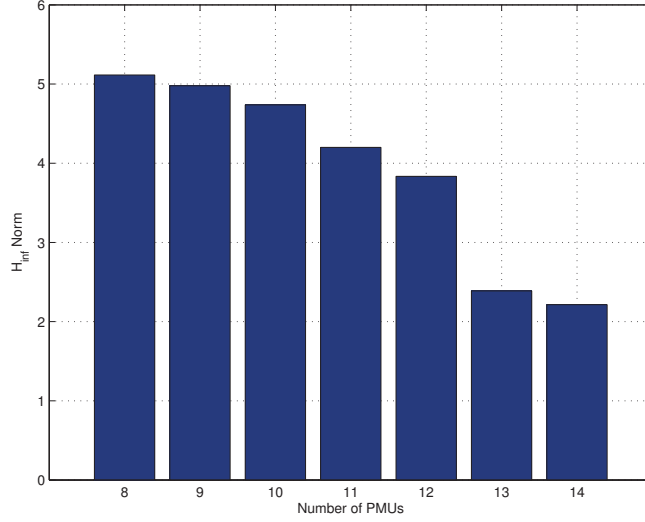
Figure 5.3: Worst case upper bound of $\|H_{zw}(\lambda)\|_\infty$ versus the number of PMUs

should be mentioned that the proposed algorithm could not find any subsets of less than 8 PMUs for $h_{max} = 150$ iterations.

Example 2. Consider a discrete-time interconnected system of five SISO subsystems, borrowed from [70], with the following state space matrices:

$$
A_g = \left[\begin{array}{cc|cc|cc|cc|cc}
0.30 & -0.29 & 0 & 0 & -0.24 & 0.21 & -0.16 & 0.03 & 0 & 0 \\
-0.29 & 0.32 & 0 & 0 & -0.18 & 0 & -0.28 & -0.32 & 0 & 0 \\
\hline
0 & 0 & 0.50 & 0.04 & 0 & 0 & 0 & 0 & 0 & 0 \\
0 & 0 & 0.18 & 0.59 & 0 & 0 & 0 & 0 & 0 & 0 \\
\hline
0 & 0 & -0.08 & -0.51 & 0.36 & -0.10 & 0 & 0 & -0.28 & 0.15 \\
0 & 0 & -0.13 & 0.04 & -0.24 & 0.69 & 0 & 0 & -0.29 & -0.20 \\
\hline
-0.38 & -0.20 & 0 & 0 & 0.47 & 0.07 & -0.10 & 0.11 & 0 & 0 \\
0.06 & -0.34 & 0 & 0 & -0.01 & -0.22 & -0.09 & 0.18 & 0 & 0 \\
\hline
0 & 0 & 0.04 & -0.01 & 0 & 0 & a_1 & -0.01 & a_2 & 0.15 \\
0 & 0 & 0.03 & 0.13 & 0 & 0 & 0.05 & 0.34 & 0.15 & 0.25
\end{array}\right]
\tag{5.17}
$$

$$
B_g = \mathrm{diag}\left(\left[\begin{array}{c} -0.2 \\ -1 \end{array}\right], \left[\begin{array}{c} 0 \\ -0.8 \end{array}\right], \left[\begin{array}{c} 0 \\ -0.4 \end{array}\right], \left[\begin{array}{c} 1.9 \\ 1.6 \end{array}\right], \left[\begin{array}{c} -0.4 \\ b_1 \end{array}\right]\right)
$$

$$
B_w = \mathrm{diag}\left(\left[\begin{array}{c} -0.5 \\ 0 \end{array}\right], \left[\begin{array}{c} 0 \\ 0.8 \end{array}\right], \left[\begin{array}{c} 0 \\ 1.3 \end{array}\right], \left[\begin{array}{c} -1.1 \\ 0 \end{array}\right], \left[\begin{array}{c} -0.6 \\ -1 \end{array}\right]\right)
$$

$$
C_g = \mathrm{diag}\left(\left[\begin{array}{cc} 1.8 & 0 \end{array}\right], \left[\begin{array}{cc} 0 & -0.2 \end{array}\right], \left[\begin{array}{cc} -1.5 & 0 \end{array}\right], \left[\begin{array}{cc} -0.3 & 0 \end{array}\right], \left[\begin{array}{cc} 0 & 0.2 \end{array}\right]\right)
$$

$$
C_z = \mathrm{diag}\left(\left[\begin{array}{cc} 1.3 & 0.4 \end{array}\right], \left[\begin{array}{cc} 0 & -2 \end{array}\right], \left[\begin{array}{cc} -0.5 & 0 \end{array}\right], \left[\begin{array}{cc} -1.3 & -0.2 \end{array}\right], \left[\begin{array}{cc} 0 & 0.2 \end{array}\right]\right)
$$

$$
D_{zu} = 0, \quad D_{zw} = 0, \quad D_w = 0
$$

where $0.378 \le a_1 \le 0.702$, $-0.182 \le a_2 \le -0.098$, and $-0.52 \le b_1 \le -0.28$. The objective of this example
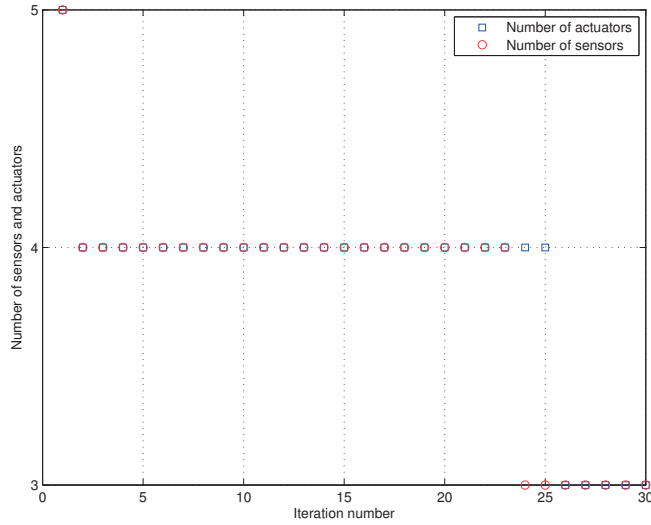
Figure 5.4: Number of sensors and actuators versus iteration number in Example 2

Table 5.1: Upper bound of $\|H_{zw}(\lambda)\|_\infty$ for different number of sensors and actuators in Example 2

$\gamma = \sqrt{\mu}$	1.6234	1.9534	1.9966	2.002
No. of sensors	5	4	3	3
No. of actuators	5	4	4	3
Performance gap	0 %	20.32 %	22.99 %	23.32 %

is to design a static output feedback H_∞ controller for the polytope of eight vertices with the minimum number of sensors and actuators.

In Algorithm I in Subsection 5.2.3, the parameters $\epsilon = 10^{-5}$, $\alpha_1 = 0.5$, $\alpha_2 = 0.5$, and $h_{max} = 30$ are considered. Figure 5.4 shows the number of sensors and actuators versus the iteration numbers. As it can be observed from this figure, the minimum number of sensors and actuators is 3. The upper bound of $\|H_{zw}(\lambda)\|_\infty$ (γ) for different number of sensors and actuators is shown in Table 5.1. By decreasing the number of sensors and actuators, the upper bound of $\|H_{zw}(\lambda)\|_\infty$ is increasing. Table 5.1 shows the H_∞ performance gap of 20.32% and 23.32% for the case of $g = 4$ and $g = 3$ sensors and actuators compared to the best performance obtained for $k = 5$ sensors.

5.3 Control Configuration Design

This section is devoted to the problem of control configuration design for a given interconnected system subject to polytopic-type uncertainty. We assume that the measurements and the control inputs are determined *a priori*.

5.3.1 Problem Formulation

System Dynamics

Consider a linear time-invariant interconnected system consisting of N subsystems described by the following state space equations:

$$\delta[x_g^j(t)] = A_g^{jj} x_g^j(t) + \sum_{k=1(k \neq j)}^{N} A_g^{jk} x_g^k(t) + \sum_{k=1}^{N} B_w^{jk} w^k(t) + B_g^j u^j(t)$$

$$z^j(t) = \sum_{k=1}^{N} C_z^{jk} x_g^k(t) + \sum_{k=1}^{N} D_{zw}^{jk} w^k(t) + D_{zu}^j u^j(t) \tag{5.18}$$

$$y^j(t) = C_g^j x_g^j(t) + \sum_{k=1}^{N} D_w^{jk} w^k(t); \quad j = 1, \dots, N$$

where $x_g^j \in \mathbb{R}^n$, $u^j \in \mathbb{R}^{n_i}$, $w^j \in \mathbb{R}^r$, $y^j \in \mathbb{R}^{n_o}$, and $z^j \in \mathbb{R}^s$ are the state, the control input, the exogenous input, the measured output, and the controlled output of the j-th subsystem, respectively. Symbol $\delta[\cdot]$ presents the derivative term for continuous-time $(\delta[x(t)] = \dot{x}(t))$ and the forward operator for discrete-time systems $(\delta[x(t)] = x(t+1))$. The state space matrices A_g^{jj}, A_g^{jk}, B_g^j, C_g^j, B_w^{jk}, C_z^{jk}, D_{zu}^j, D_{zw}^{jk}, and D_w^{jk} are of appropriate dimensions. Matrix $A_g^{jk} = 0$ if and only if there is no interaction between the subsystems j and k. It is assumed that the state space matrices belong to a polytopic uncertainty region as follows:

$$\Omega_7 = \{ \left(A_g^{jk}(\lambda), B_g^j(\lambda), B_w^{jk}(\lambda), C_g^j(\lambda), C_z^{jk}(\lambda), D_{zu}^j(\lambda), D_{zw}^{jk}(\lambda), D_w^{jk}(\lambda) \right)$$

$$= \sum_{i=1}^{q} \lambda_i \left(A_{g_i}^{jk}, B_{g_i}^j, B_{w_i}^{jk}, C_{g_i}^j, C_{z_i}^{jk}, D_{zu_i}^j, D_{zw_i}^{jk}, D_{w_i}^{jk} \right) \}, \quad j, k = 1, \dots, N \tag{5.19}$$

where $\lambda \in \Lambda_q$ defined in (2.8) and $\left(A_{g_i}^{jk}, B_{g_i}^j, B_{w_i}^{jk}, C_{g_i}^j, C_{z_i}^{jk}, D_{zu_i}^j, D_{zw_i}^{jk}, D_{w_i}^{jk} \right)$ is the i-th vertex of the subsystem j.

The whole network of N subsystems is presented by the following equations:

$$\delta[x_g(t)] = A_g(\lambda) x_g(t) + B_g(\lambda) u(t) + B_w(\lambda) w(t)$$

$$z(t) = C_z(\lambda) x_g(t) + D_{zu}(\lambda) u(t) + D_{zw}(\lambda) w(t) \tag{5.20}$$

$$y(t) = C_g(\lambda) x_g(t) + D_w(\lambda) w(t)$$

where

$$x_g(t) = \left[x_g^{1T}, \dots, x_g^{NT} \right]^T,$$

$$u(t) = \left[u^{1T}, \dots, u^{NT} \right]^T, \quad w(t) = \left[w^{1T}, \dots, w^{NT} \right]^T \tag{5.21}$$

$$y(t) = \left[y^{1T}, \dots, y^{NT} \right]^T, \quad z(t) = \left[z^{1T}, \dots, z^{NT} \right]^T$$

and the state space matrices are given as follows:

$$
A_g(\lambda) = \begin{bmatrix} A_g^{11}(\lambda) & \cdots & A_g^{1N}(\lambda) \\ \vdots & \ddots & \vdots \\ A_g^{\bar{N}1}(\lambda) & \cdots & A_g^{NN}(\lambda) \end{bmatrix}, \quad B_w(\lambda) = \begin{bmatrix} B_w^{11}(\lambda) & \cdots & B_w^{1N}(\lambda) \\ \vdots & \ddots & \vdots \\ B_w^{\bar{N}1}(\lambda) & \cdots & B_w^{NN}(\lambda) \end{bmatrix},
$$

$$
C_z(\lambda) = \begin{bmatrix} C_z^{11}(\lambda) & \cdots & C_z^{1N}(\lambda) \\ \vdots & \ddots & \vdots \\ C_z^{\bar{N}1}(\lambda) & \cdots & C_z^{NN}(\lambda) \end{bmatrix}, \quad D_{zw}(\lambda) = \begin{bmatrix} D_{zw}^{11}(\lambda) & \cdots & D_{zw}^{1N}(\lambda) \\ \vdots & \ddots & \vdots \\ D_{zw}^{\bar{N}1}(\lambda) & \cdots & D_{zw}^{NN}(\lambda) \end{bmatrix} \quad (5.22)
$$

$$
D_w(\lambda) = \begin{bmatrix} D_w^{11}(\lambda) & \cdots & D_w^{1N}(\lambda) \\ \vdots & \ddots & \vdots \\ D_w^{\bar{N}1}(\lambda) & \cdots & D_w^{NN}(\lambda) \end{bmatrix}
$$

and

$$
\begin{aligned}
B_g(\lambda) &= \mathrm{diag}\left(B_g^1(\lambda), \ldots, B_g^N(\lambda)\right) \\
C_g(\lambda) &= \mathrm{diag}\left(C_g^1(\lambda), \ldots, C_g^N(\lambda)\right) \\
D_{zu}(\lambda) &= \mathrm{diag}\left(D_{zu}^1(\lambda), \ldots, D_{zu}^N(\lambda)\right)
\end{aligned} \quad (5.23)
$$

Dynamic Output Feedback Controllers

It is assumed that there is one local controller corresponding to each subsystem described by:

$$
\begin{aligned}
\delta[x_c^j(t)] &= \sum_{k=1}^{N} A_c^{jk} x_c^k(t) + \sum_{k=1}^{N} B_c^{jk} y^k(t) \\
u^j(t) &= \sum_{k=1}^{N} C_c^{jk} x_c^k(t) + \sum_{k=1}^{N} D_c^{jk} y^k(t); \quad j = 1, \ldots, N
\end{aligned} \quad (5.24)
$$

where $x_c^j \in \mathbb{R}^m$ is the state vector of the j-th local controller. The controller matrices A_c^{jk}, B_c^{jk}, C_c^{jk}, and D_c^{jk} are of appropriate dimensions. According to this structure, each local controller uses the outputs of its own subsystem and other subsystems as well as the states of other local controllers (centralized control strategy). The centralized controller K with this structure is given by:

$$
\begin{aligned}
\delta[x_c(t)] &= A_c x_c(t) + B_c y(t) \\
u(t) &= C_c x_c(t) + D_c y(t)
\end{aligned} \quad (5.25)
$$

where

$$
x_c(t) = \left[x_c^{1^T}, \ldots, x_c^{N^T} \right]^T \quad (5.26)
$$

$$A_c = \begin{bmatrix} A_c^{11} & \cdots & A_c^{1N} \\ \vdots & \ddots & \vdots \\ A_c^{\bar{N}1} & \cdots & A_c^{\bar{N}\bar{N}} \end{bmatrix}, \quad B_c = \begin{bmatrix} B_c^{11} & \cdots & B_c^{1N} \\ \vdots & \ddots & \vdots \\ B_c^{\bar{N}1} & \cdots & B_c^{\bar{N}\bar{N}} \end{bmatrix},$$
$$C_c = \begin{bmatrix} C_c^{11} & \cdots & C_c^{1N} \\ \vdots & \ddots & \vdots \\ C_c^{\bar{N}1} & \cdots & C_c^{\bar{N}\bar{N}} \end{bmatrix}, \quad D_c = \begin{bmatrix} D_c^{11} & \cdots & D_c^{1N} \\ \vdots & \ddots & \vdots \\ D_c^{\bar{N}1} & \cdots & D_c^{\bar{N}\bar{N}} \end{bmatrix}$$

(5.27)

To select an appropriate control configuration, it is important to determine whether there exists any link between the local controller j and the subsystem k as well as the local controller h. In other words, the outputs of the subsystem k do not contribute to the construction of the control inputs j if and only if both $B_c^{jk} = 0$ and $D_c^{jk} = 0$. Moreover, the states of the local controllers h are not employed in the construction of $x_c^j(t)$ and $u^j(t)$ if and only if both $A_c^{jh} = 0$ and $C_c^{jh} = 0$.

The main objective is to design a controller such that each local controller uses a minimum amount of information exchange between the subsystems and the local controllers. In order to design such controller, the following pattern matrix $\mathscr{Z}(K) = [z_{jk}]$ is defined:

$$\mathscr{Z}(K) = \begin{bmatrix} card\left(\begin{bmatrix} A_c^{11} & B_c^{11} \\ C_c^{11} & D_c^{11} \end{bmatrix} \right) & \cdots & card\left(\begin{bmatrix} A_c^{1N} & B_c^{1N} \\ C_c^{1N} & D_c^{1N} \end{bmatrix} \right) \\ \vdots & \ddots & \vdots \\ card\left(\begin{bmatrix} A_c^{N1} & B_c^{N1} \\ C_c^{N1} & D_c^{N1} \end{bmatrix} \right) & \cdots & card\left(\begin{bmatrix} A_c^{NN} & B_c^{NN} \\ C_c^{NN} & D_c^{NN} \end{bmatrix} \right) \end{bmatrix}$$

(5.28)

Element z_{jk} of $\mathscr{Z}(K)$ represents the communication links between the local controller j and the subsystem and the local controller k. The number of the non-zero elements of $\mathscr{Z}(K)$ is equal to the number of the communication links of the controller. Note that $z_{jk} = 0$ if and only if $\begin{bmatrix} A_c^{jk} & B_c^{jk} \\ C_c^{jk} & D_c^{jk} \end{bmatrix} = 0$, i.e. there exists no link between the local controller j and the subsystem k with its corresponding controller. The control configuration is represented by a binary information flow matrix $\mathscr{I}(K) = [I_{jk}]$ determined as follows:

$$I_{jk} = sgn(z_{jk})$$

(5.29)

where *sgn* is the signum function. When all entries of matrix $\mathscr{I}(K)$ are equal to 1, the corresponding controller is centralized and when $\mathscr{I}(K)$ is diagonal, the corresponding controller is decentralized. Any case between the centralized and decentralized control strategy is a distributed controller.

To find a controller configuration with minimum communication links between the subsys-

tems and the local controllers, the cardinality of $\mathscr{Z}(K)$ should be minimized. The problem of fixed-structure decentralized/distributed control of LTI interconnected systems subject to polytopic uncertainty described by (5.18)-(5.19) is summarized as:

Problem 4. *(Control Configuration Design in Interconnected Systems)*

Given a linear dynamical interconnected system consists of N subsystems subject to polytopic uncertainty, design a fixed-structure dynamic output feedback controller K such that

1. *The cardinality of $\mathscr{Z}(K)$ is minimized (Control Configuration Selection).*

2. *Closed-loop system is robustly stable and performance criterion $\|H_{zw}(\lambda)\|_\infty^2 < \mu$ is guaranteed (Controller Parameter Design).*

The aforementioned conditions can be formulated as the following non convex optimization problem:

$$\min_{K} \quad \mu + \alpha \times card\big(\mathscr{Z}(K)\big)$$
$$subject\ to \quad \|H_{zw}(\lambda)\|_\infty^2 < \mu \tag{5.30}$$

where α determines a trade-off between the sparsity of the controller and the H_∞ performance criterion.

5.3.2 An LMI-based Approach to Control Configuration Selection

To reduce the amount of information exchange between the subsystems and the local controllers in an interconnected system, matrix $\mathscr{Z}(K)$ in (5.28) should be sparse. The sparsity requirements are expressed in terms of the cardinality which is non-convex. The non-convex cardinality minimization can be relaxed by the convex one-norm (ℓ_1) minimization [163]. In fact, one-norm is the convex envelope of the cardinality [166].

To have a better approximation of the cardinality, the weighted ℓ_1 norm is used [163]. Therefore, the objective function in (5.30) can be written as:

$$J = \mu + \alpha \|W * \mathscr{Z}(K)\|_1 \tag{5.31}$$

where $W = [w_{jk}]$ is the matrix of weights. The cost function J is written as follows:

$$J = \mu + \alpha \sum_{j=1}^{N} \sum_{k=1}^{N} w_{jk} \|k_{jk}\|_1 \tag{5.32}$$

where $k_{jk} = \begin{bmatrix} A_c^{jk} & B_c^{jk} \\ C_c^{jk} & D_c^{jk} \end{bmatrix}$ and $w_{jk} \geq 0$ is the jk-th entry of W which is inversely proportional

to $\left\| k_{jk} \right\|_1$, i.e.

$$w_{jk} = \frac{1}{\epsilon + \left\| k_{jk} \right\|_1} \tag{5.33}$$

where ϵ is a small positive number used to ensure that the weights are well-defined when $\left\| k_{jk} \right\|_1 = 0$. In this case, for almost zero-valued k_{jk}, a very high weight is assigned. Since the weights depend on the unknown local controllers, the above weight matrix design strategy cannot be implemented. In [163], an iterative algorithm for choosing the weights has been given.

A convex set of fixed-structure controllers based on the use of slack matrices has been given in Chapter 3. Therefore, the problem of fixed-structure decentralized/distributed H_∞ control of LTI interconnected systems subject to polytopic uncertainty can be solved by the following convex optimization problem:

$$
\begin{aligned}
&\min_{A_c, B_c, C_c, D_c, P_i, \mu} && \mu + \alpha \| W * \mathcal{Z}(K) \|_1 \\
&\text{s.t.} && (3.66)/(3.76) \\
& && P_i > 0; \qquad i = 1, \ldots, q
\end{aligned} \tag{5.34}
$$

where α determines a trade-off between the number of communication links in the distributed controller and the H_∞ performance criterion. In the following, a systematic algorithm for the problem of fixed-structure decentralized/distributed H_∞ controller design of LTI polytopic systems is given.

5.3.3 Algorithm II: "Fixed-structure decentralized/distributed H_∞ controller design"

In this subsection, an iterative LMI-based algorithm for the problem of fixed-structure sparse H_∞ controller design of LTI interconnected system affected by polytopic uncertainty in (5.18)-(5.19) is presented. The iterative procedure can be summarized by the following steps:

Step 1 (Initialization): Design some initial controllers for each vertex of the polytope $\left(K_i^{[0]} \right)$. Put the iteration number $h = 1$, a small tolerance for $\epsilon > 0$, maximum iteration number h_{max}, and $w_{jk}^{[1]} = 1$, $j, k = 1, \ldots, N$. Determine α based on the desired H_∞ performance and the sparsity of the controller.

Step 2: Solve the convex optimization problem given in (3.79) for a given controller and determine $M^{[h]}$ and $X^{[h]}$.

Step 3: Solve the convex optimization problem given in (5.34) to obtain a sparse fixed-structure H_∞ controller $K^{[h]}$.

Step 4: Find $\left\| k_{jk} \right\|_1^{[h]}$ for $j, k = 1, \ldots, N$ based on the current controller $K^{[h]}$.

Step 5: Update the jk-th elements of the weighting matrix $W^{[h+1]}$:

$$w^{[h+1]}_{jk} = \begin{cases} \dfrac{1}{\|k_{jk}\|^{[h]}_1 + \epsilon}, & j \neq k \\[2ex] 0, & j = k \end{cases} \tag{5.35}$$

for $j, k = 1, ..., N$.

Step 6: Terminate on convergence or when maximum number of iterations h_{max} reaches. Otherwise, use the obtained controller in Step 3 as an initial controller $\left(K^{[h+1]}_i \leftarrow K^{[h]}; i = 1, \ldots, q\right)$ and go to Step 2 with $h \leftarrow h+1$.

Step 7 (Polishing): Design a fixed-structure H_∞ controller by solving the optimization problem in (5.34), where $\alpha = 0$ is considered.

5.3.4   Simulation Examples

Example 3 (Fixed-order distributed control). Consider a network of three interconnected second-order subsystems subject to polytopic uncertainty given in (3.85). The objective of this example is to design a first-order sparse H_∞ controller. To this end, according to Algorithm II in Subsection 5.3.3 with the parameters $\epsilon = 10^{-5}$ and $\alpha = 0.5$, at the first step, eight initial first-order centralized controllers are designed by using the command *hinfstruct* in MATLAB for each vertex of the polytope. The initial controllers are transformed to discrete-time ones by using the bilinear (Tustin) approximation with the sampling time $T_s = 0.1s$. Then, these controllers are utilized to obtain the slack matrices M and T using LMIs in (3.63). The next step is to determine the sparse controller by solving the convex optimization problem in (5.34). These steps are iteratively repeated and finally after $h_{max} = 60$ iterations, some control structures are obtained. The computational time is about $187s$, on a 3.4 GHz Intel Core i7 with Mac OS X. Figure 5.5 shows the number of communication links versus the iteration numbers.

For each obtained control structure, an H_∞ controller is iteratively designed where the structure of the controller is fixed *a priori*. For instance, in the case of four communication links, the following distributed H_∞ controller with $\|H_{zw}(\lambda)\|_\infty < 0.9673$ is obtained:

$$\begin{aligned} A_c &= \begin{bmatrix} 0.0074 & 0 & 0 \\ -0.3107 & 0.6538 & 0 \\ 0 & 0 & 0.1519 \end{bmatrix}, & B_c &= \begin{bmatrix} 0.0945 & 0 & 0 \\ 0.0430 & 0.0013 & 0 \\ 0 & 0 & 0.0662 \end{bmatrix} \\[2ex] C_c &= \begin{bmatrix} 2.6502 & 0 & 0 \\ -3.8635 & 0.4953 & 0 \\ 0 & 0 & -3.2312 \end{bmatrix}, & D_c &= \begin{bmatrix} 1.2327 & 0 & 0 \\ -1.4132 & -0.8750 & 0 \\ 0 & 0 & 0.4798 \end{bmatrix} \end{aligned} \tag{5.36}$$

The above controller guarantees the stability as well as the H_∞ performance of the whole polytope. Figure 5.6 shows the upper bound of $\|H_{zw}(\lambda)\|_\infty$ versus the number of communication
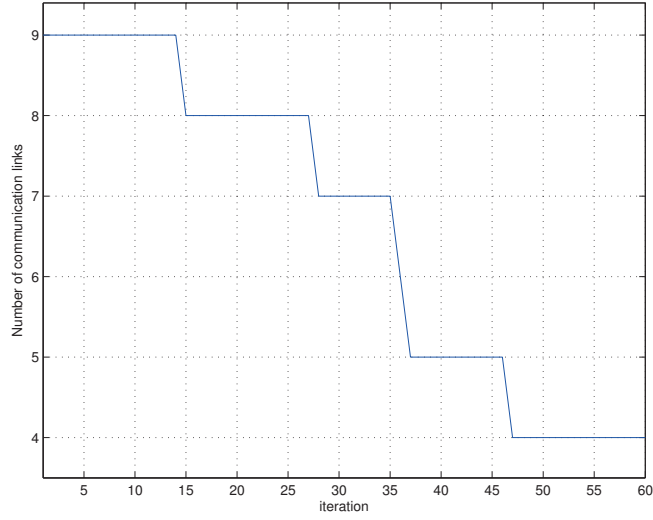
Figure 5.5: Candidates for the control structure in Example 3

links. It is observed that by increasing the sparsity of the controller structure, a decrease in the H_∞ performance is achieved. For example, the closed-loop system with a centralized controller (with 9 communication links) has an H_∞ upper bound of $\|H_{zw}(\lambda)\|_\infty < 0.8962$ whereas the distributed controller given in (5.36) with 4 communication links leads to $\|H_{zw}(\lambda)\|_\infty < 0.9673$.

Example 4 (Distributed static output feedback control). Consider the discrete-time interconnected polytopic system of five SISO subsystems given in (5.17). The objective is to design a distributed or decentralized (if possible) static output feedback controller which minimizes the H_∞ norm of the closed-loop system $H_{zw}(\lambda)$ for the whole polytope of $q = 2^3$ vertices. To this end, the iterative algorithm given in Subsection 5.3.3 is used. First, $\epsilon = 10^{-5}$ and $\alpha = 0.5$ are set. Since a static output feedback is sought, eight static output feedbacks are designed via *hinfstruct* as initial controllers for the vertices. After 30 iterations, some candidates for the control configuration are obtained. Then, $\|H_{zw}(\lambda)\|_\infty$ is iteratively minimized using LMI conditions in (3.53) and subject to the structural constraints determined by the candidates.

The upper bound of $\|H_{zw}(\lambda)\|_\infty$ versus the number of communication links is plotted in Fig. 5.7. It is observed that by decreasing the sparsity of the controller structure, the H_∞ performance is improved. For example, the closed-loop system corresponding to a centralized controller (with 25 communication links) has an H_∞ upper bound of $\|H_{zw}(\lambda)\|_\infty < 1.62$ whereas the distributed controller with 8 communication links leads to $\|H_{zw}(\lambda)\|_\infty < 1.745$.

The distributed static output-feedback controller corresponding to 8 communication links is
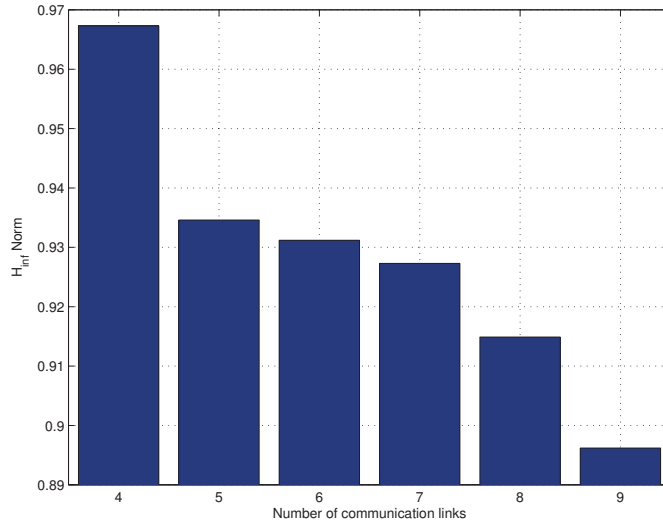
Figure 5.6: Upper bound of $\|H_{zw}(\lambda)\|_\infty$ versus the number of communication links in Example 3

given as follows:

$$D_c = \begin{bmatrix} 0.1113 & 0 & 0 & 0.7823 & 0 \\ 0 & -3.7119 & 0 & 0 & 0 \\ 0.5719 & 0 & 0.5807 & 0 & 0 \\ 0 & 0 & 0.2012 & -0.0380 & 0 \\ 0 & 0 & 0 & 0 & 6.3590 \end{bmatrix} \tag{5.37}$$

The sparse controller guarantees the robust stability as well as the H_∞ performance of the whole polytope.

5.4 Conclusion

This chapter centres around addressing two important issues in the control structure design of LTI interconnected systems subject to polytopic uncertainty: sensor and actuator placement and control configuration design. The control problems are formulated as optimization problems by minimizing the cardinality of some pattern matrices, while satisfying a guaranteed level of H_∞ performance. For the resulting combinatorial optimization problem, computationally tractable convex relaxations are provided. More specifically, using the convex inner approximation of fixed-structure H_∞ control design proposed in Chapter 3 and a weighted ℓ_1 norm relaxation, several iterative algorithms are developed. The main feature of the proposed approaches is that the control structure and the control parameters are simultaneously designed.
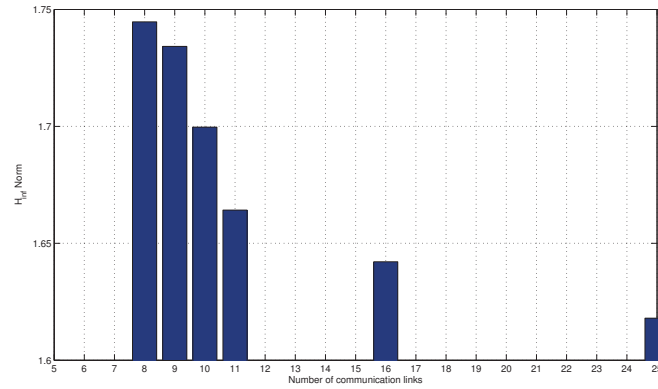
Figure 5.7: Upper bound of $\|H_{zw}(\lambda)\|_\infty$ versus the number of communication links in Example 4

As compared to the existing approaches for control structure design, the proposed LMI-based strategy is advantageous since (i) the control structure and the control parameters are simultaneously designed. (ii) the controller structure is designed for a family of models which belongs to a polytopic-type uncertainty domain (iii) the communication links between the subsystems and the local controllers as well as the communication among the local controllers are minimized.

Applications to Control of Inverter-interfaced Microgrids

6 Grid-connected Voltage-Source Converters

6.1 Introduction

This chapter studies the problem of dq-based current control of a grid-connected voltage-source converter with L/LCL filters under grid inductance uncertainties. The current controller must be able to provide desired performance specifications including current reference tracking, high closed-loop bandwidth as well as dq-axes decoupling. The control objectives are encoded into an optimization problem subject to H_∞ constraints. The problem is then overcome and a robust fixed-structure MIMO current controller is designed through the developed algorithms in Chapter 3.

The controller ensures robust stability and robust performance against grid inductance parameter uncertainty. In addition, the proposed MIMO controller decouples the d and q components of the current signal. The simulation studies conducted in MATLAB/SimPowerSystems show the effectiveness of the proposed controller in terms of current reference tracking and robustness to the grid inductance parameter uncertainty.

The organization of this chapter is as follows. The system description is given in Section 6.2. Section 6.3 presents controller design method. The robust dq-based current controllers are given in Section 6.4. Section 6.5 is devoted to simulation results. Section 6.6 concludes the chapter.

6.2 System Description

Consider the configuration of an electronically-interfaced distributed generation (DG) unit in grid-connected mode, as shown in Fig. 6.1. The DG unit is connected to the grid via a voltage-source converter (VSC) and an L/LCL-type filter at the point of common coupling (PCC). In this figure, Phase-Locked Loop (PLL), which is used for the synchronization, estimates the phase angle $\theta(t)$ at the PCC [167]. The abc/dq and dq/abc blocks convert the signals from stationary reference to the rotating reference frame and vice versa, according to Park's
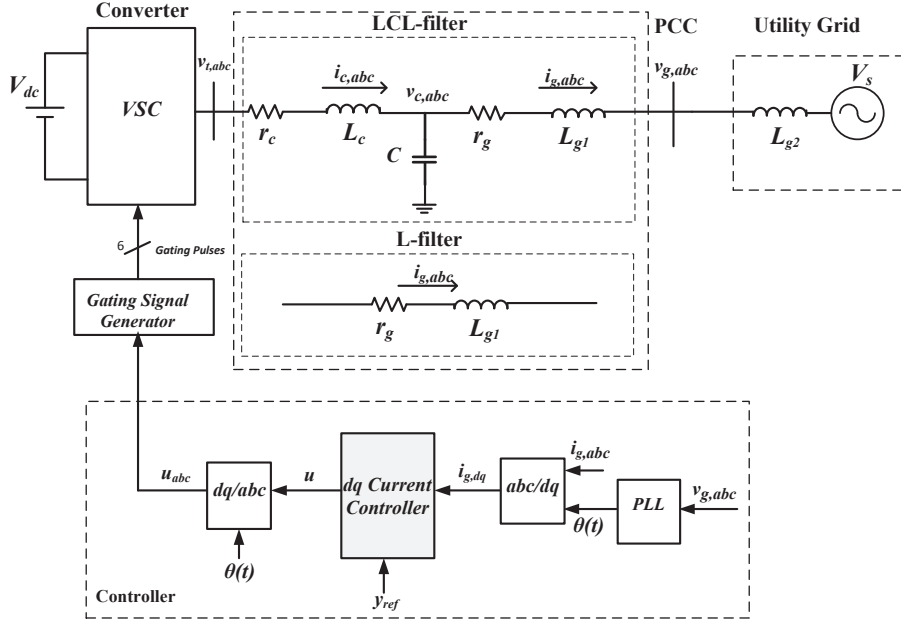
Figure 6.1: Configuration of a grid-connected voltage-source converter under study and its *dq*-based current controller

transformation [107]. The values and definitions of the system parameters are given in Table 6.1.

Remark: It would be better to connect the PLL to a stiff source, i.e. V_s, to avoid disturbances imposed to PLL input. However, it may need a communication link.

6.2.1 Grid-connected VSC with an L-type Filter

In this subsection, the mathematical model of the three-phase grid-connected VSC system with an L-type filter in Fig. 6.1 is derived. The dynamics of the system are described as follows:

$$L_g \frac{di_{g,abc}}{dt} = v_{t,abc}(t) - r_g i_{g,abc}(t) - V_s(t) \tag{6.1}$$

where $i_{g,abc}$, $v_{t,abc}$, and V_s are the grid current, the VSC terminal voltage, and the grid voltage, respectively. $L_g = L_{g_1} + L_{g_2}$ presents the total inductance.

Assuming that the three-phase system of Fig. 6.1 is balanced, the mathematical model in *abc*-frame is first transformed to $\alpha\beta$-frame using $x_{\alpha\beta} = x_a + x_b e^{-j(2\pi/3)} + x_c e^{j(2\pi/3)}$. Then, it is transformed to the *dq*-frame using $x_{dq} = \sqrt{2/3} x_{\alpha\beta} e^{j\theta}$, where θ is the transformation angle (phase angle of $v_{g,abc}$ at the PCC is considered as the reference). The system equations in

Table 6.1: Parameters of VSC in Fig. 6.1

$L_c = 1.5mH$	Converter-side inductor of the LCL filter
$r_c = 0.1\Omega$	Series resistance of L_c
$L_{g_1} = 1mH$	Grid-side inductor of the LCL filter
$r_g = 0.1\Omega$	Series resistance of L_{g_1}
$C = 15\mu F$	Capacitance of the LCL filter
$L_{g_1} = 5mH$	Inductance of the L filter
$r_g = 0.3\Omega$	Resistance of the L filter
$L_{g_2} \in \left[L_{g_{2min}}\; L_{g_{2max}}\right]$	Grid inductance
$V_s = 220V$	Grid voltage (phase-to-phase rms voltage)
$V_{dc} = 440V$	DC bus voltage
$f_0 = 60Hz$	System nominal frequency ($\omega_0 = 2\pi f_0$)
$f_s = 10020Hz$	Sampling frequency
$f_{PWM} = 5010Hz$	PWM carrier frequency

dq-frame are given as follows:

$$\dot{x}_g(t) = A_g x_g(t) + B_g v_t(t) + B_v v_s(t)$$
$$y(t) = C_g x_g(t) \tag{6.2}$$

where $x_g(t) = \begin{bmatrix} i_{g,d} & i_{g,q} \end{bmatrix}^T$ is the state, $v_t(t) = \begin{bmatrix} v_{t,d} & v_{t,q} \end{bmatrix}^T$ is the input, $v_s(t) = \begin{bmatrix} V_{s_d} & V_{s_q} \end{bmatrix}^T$ is the disturbance, and $y(t) = \begin{bmatrix} i_{g,d} & i_{g,q} \end{bmatrix}^T$ is the output signals. The dq-subscripts indicate the dq components of the corresponding signals. The state space matrices are as follows:

$$A_g = \begin{bmatrix} -\frac{r_g}{L_g} & \omega_0 \\ -\omega_0 & -\frac{r_g}{L_g} \end{bmatrix}, \quad B_g = \begin{bmatrix} \frac{1}{L_g} & 0 \\ 0 & \frac{1}{L_g} \end{bmatrix}$$
$$B_v = \begin{bmatrix} -\frac{1}{L_g} & 0 \\ 0 & -\frac{1}{L_g} \end{bmatrix}, \quad C_g = \begin{bmatrix} 1 & 0 \\ 0 & 1 \end{bmatrix} \tag{6.3}$$

Due to the *abc-dq* transformation, coupling terms $\omega_0 L_g i_{g,q}$ and $\omega_0 L_g i_{g,d}$ appear between the direct and quadrature current axes. To remove the cross coupling terms and decouple these axes, feedback and feedforward controllers are designed such that the coupling terms are encapsulated in control laws (conventional dq current control)[168].

$$v_{t,d} = V_{s_d} - \omega_0 L_g i_{g,q} + u_d$$
$$v_{t,q} = V_{s_q} + \omega_0 L_g i_{g,d} + u_q \tag{6.4}$$

where u_d and u_q are the feedback control signals of the direct and quadrature axes. The feedback controller is a conventional PI controller with the following structure:

$$K_{PI}(s) = \frac{1 + sT_n}{sT_i} \tag{6.5}$$

The controller time constant T_n is usually chosen qual to the dominant time constant of the system, i.e. $T_n = L_g / r_g$. The parameter T_i is equal to τ / r_g, where τ is normally between $0.5ms$ and $5ms$ [169].

According to (6.4), the use of the feedforward terms theoretically results in fully decoupled control loops. Nevertheless, in practice due to measurement errors and grid parameter uncertainties, it is almost impossible to precisely determine the values of ω_0, L_g, $i_{g,d}$, and $i_{g,q}$. Therefore, exact coupling term cancellation is not possible and a full axis-decoupling cannot be achieved [170].

To improve the axes decoupling, a modified multivariable-PI controller has been developed in [170], where the control laws are written as follows:

$$
\begin{aligned}
v_{t,d} &= V_{s_d} - \frac{\omega_0 T_n}{s T_i} \left(i_{g,q_{ref}} - i_{g,q} \right) + u_d \\
v_{t,q} &= V_{s_q} + \frac{\omega_0 T_n}{s T_i} \left(i_{g,d_{ref}} - i_{g,d} \right) + u_q
\end{aligned}
\tag{6.6}
$$

where

$$
\begin{aligned}
u_d &= \frac{1 + s T_n}{s T_i} \left(i_{g,d_{ref}} - i_{g,d} \right) \\
u_q &= \frac{1 + s T_n}{s T_i} \left(i_{g,q_{ref}} - i_{g,q} \right)
\end{aligned}
\tag{6.7}
$$

$i_{g,d_{ref}}$ and $i_{g,q_{ref}}$ respectively are the direct and quadrature reference current signals. Although the integral terms in (6.6) reduce the effect of axes coupling, parameter uncertainties in the system can still degrade an ideal axis-decoupling. For instance, in the case of grid inductance parameter uncertainty, the feedback and feedforward control terms are fixed and it may result in a poor operation of the current controllers.

6.2.2 Grid-connected VSC with an LCL-type Filter

Consider the voltage-source converter in Fig. 6.1 connected to the utility grid through an LCL-type filter. The resonance frequency of the LCL filter is determined as follows:

$$
f_{res} = \frac{1}{2\pi} \sqrt{\frac{L_g + L_c}{L_c L_g C}}
\tag{6.8}
$$

The resonance frequency varies depending on the grid inductance values. Inductive grids lead to a decrease of the resonance frequency.

The dynamical equations of the system in the *abc*-frame are as follows:

$$L_c \frac{di_{c,abc}}{dt} = -r_c i_{c,abc}(t) - v_{c,abc}(t) + v_{t,abc}(t)$$

$$C \frac{dv_{c,abc}}{dt} = i_{c,abc}(t) - i_{g,abc}(t) \tag{6.9}$$

$$L_g \frac{di_{g,abc}}{dt} = v_{c,abc}(t) - r_g i_{g,abc}(t) - V_s(t)$$

where $i_{c,abc}$, $i_{g,abc}$, $v_{c,abc}$, $v_{t,abc}$, and V_s are the converter-side current, the grid-side current, the voltage of the filter capacitance, the VSC terminal voltage, and the grid voltage, respectively. The dynamical equations can be described by the following state space representation:

$$\dot{x}_{g,abc}(t) = A_{g,abc} x_{g,abc}(t) + B_{g,abc} v_{t,abc}(t) + B_{v,abc} V_s(t)$$

$$y_{abc}(t) = C_{g,abc} x_{g,abc}(t) \tag{6.10}$$

where $x_{g,abc}(t) = \begin{bmatrix} i_{c,abc} & v_{c,abc} & i_{g,abc} \end{bmatrix}^T$ and $y_{abc}(t) = i_{g,abc}$. The state space matrices are given by:

$$A_{g,abc} = \begin{bmatrix} -\frac{r_c}{L_c} & -\frac{1}{L_c} & 0 \\ \frac{1}{C} & 0 & -\frac{1}{C} \\ 0 & \frac{1}{L_g} & -\frac{r_g}{L_g} \end{bmatrix}$$

$$B_{g,abc} = \begin{bmatrix} \frac{1}{L_c} \\ 0 \\ 0 \end{bmatrix}, \quad B_{v,abc} = \begin{bmatrix} 0 \\ 0 \\ -\frac{1}{L_g} \end{bmatrix} \tag{6.11}$$

$$C_{g,abc} = \begin{bmatrix} 0 & 0 & 1 \end{bmatrix}$$

Under balanced conditions, the dynamical equations in *abc*-frame are transformed to *dq*-frame and expressed by (6.2), where the state, input, disturbance, and output signals respectively are $x_g(t) = \begin{bmatrix} i_{c,d} & i_{c,q} & v_{c,d} & v_{c,q} & i_{g,d} & i_{g,q} \end{bmatrix}^T$, $v_t(t) = \begin{bmatrix} v_{t,d} & v_{t,q} \end{bmatrix}^T$, $v_s(t) = \begin{bmatrix} V_{s_d} & V_{s_q} \end{bmatrix}^T$, $y(t) = \begin{bmatrix} i_{g,d} & i_{g,q} \end{bmatrix}^T$, and

$$A_g = \begin{bmatrix} -\frac{r_c}{L_c} & \omega_0 & -\frac{1}{L_c} & 0 & 0 & 0 \\ -\omega_0 & -\frac{r_c}{L_c} & 0 & -\frac{1}{L_c} & 0 & 0 \\ \frac{1}{C} & 0 & 0 & \omega_0 & -\frac{1}{C} & 0 \\ 0 & \frac{1}{C} & -\omega_0 & 0 & 0 & -\frac{1}{C} \\ 0 & 0 & \frac{1}{L_g} & 0 & -\frac{r_g}{L_g} & \omega_0 \\ 0 & 0 & 0 & \frac{1}{L_g} & -\omega_0 & -\frac{r_g}{L_g} \end{bmatrix}, \quad B_g = \begin{bmatrix} \frac{1}{L_c} & 0 \\ 0 & \frac{1}{L_c} \\ 0 & 0 \\ 0 & 0 \\ 0 & 0 \\ 0 & 0 \end{bmatrix}, \quad B_v = \begin{bmatrix} 0 & 0 \\ 0 & 0 \\ 0 & 0 \\ 0 & 0 \\ -\frac{1}{L_g} & 0 \\ 0 & -\frac{1}{L_g} \end{bmatrix} \tag{6.12}$$

$$C_g = \begin{bmatrix} 0 & 0 & 0 & 0 & 1 & 0 \\ 0 & 0 & 0 & 0 & 0 & 1 \end{bmatrix}$$

6.2.3 Grid Parameter Uncertainty

It is assumed that the grid inductance value is not precisely known and it belongs to a given interval, $L_{g_2} \in \begin{bmatrix} L_{g_2 min} & L_{g_2 max} \end{bmatrix}$. Therefore, the state space matrices A_g, B_v, and B_g (in the case of L-type filter) represent a polytopic uncertainty with $q = 2$ vertices as follows:

$$
\begin{aligned}
A_g(\lambda) &= \lambda A_{g_1} + (1 - \lambda) A_{g_2} \\
B_v(\lambda) &= \lambda B_{v_1} + (1 - \lambda) B_{v_2} \\
B_g(\lambda) &= \lambda B_{g_1} + (1 - \lambda) B_{g_2}
\end{aligned}
\tag{6.13}
$$

where $0 \le \lambda \le 1$. Vetrices A_{g_1}, A_{g_2}, B_{v_1}, B_{v_2}, and B_{g_1}, B_{g_2} are obtained based on the maximum and the minimum values of the grid inductance L_{g_2}. For instance, matrices A_{g_1} and A_{g_2} for the system with L-type filter are as follows:

$$
\begin{aligned}
A_{g_1} &= \begin{bmatrix} -\frac{r_g}{L_{g_1} + L_{g_2 min}} & \omega_0 \\ -\omega_0 & -\frac{r_g}{L_{g_1} + L_{g_2 min}} \end{bmatrix} \\
A_{g_2} &= \begin{bmatrix} -\frac{r_g}{L_{g_1} + L_{g_2 max}} & \omega_0 \\ -\omega_0 & -\frac{r_g}{L_{g_1} + L_{g_2 max}} \end{bmatrix}
\end{aligned}
\tag{6.14}
$$

The state space model given in (6.2) is transformed to the following discrete-time system with the sampling time $T_s = \frac{1}{f_s}$

$$
\begin{aligned}
x_g(k + 1) &= A_{g_d}(\lambda) x_g(k) + B_{g_d}(\lambda) v_t(k) + B_{v_d}(\lambda) v_s(k) \\
y(k) &= C_{g_d} x_g(k)
\end{aligned}
\tag{6.15}
$$

according to the following approximations, based on the first-order Taylor series, assuming that the sampling time T_s is small enough.

$$
\begin{aligned}
A_{g_d} &= e^{A_g T_s} \approx I + T_s A_g \\
B_{g_d} &= \int_0^{T_s} e^{A_g \tau} B_g \, d\tau \approx T_s B_g \\
B_{v_d} &= \int_0^{T_s} e^{A_g \tau} B_v \, d\tau \approx T_s B_v \\
C_{g_d} &= C_g
\end{aligned}
\tag{6.16}
$$

It is assumed that there exists one sample delay between the converter voltage command $u(k)$ and the VSC terminal voltage $v_t(k)$, i.e. $v_t(k) = u(k - 1)$ [84]. Therefore, by considering the delay, the following augmented model G is derived.

$$
\begin{aligned}
x_{g_{aug}}(k + 1) &= A_{g_{aug}}(\lambda) x_{g_{aug}}(k) + B_{g_{aug}} u(k) + B_{v_{aug}}(\lambda) v_s(k) \\
y(k) &= C_{g_{aug}} x_{g_{aug}}(k)
\end{aligned}
\tag{6.17}
$$

where $x_{g_{aug}}(k) = \begin{bmatrix} x_g^T(k) & v_t^T(k) \end{bmatrix}^T$ and

$$A_{g_{aug}}(\lambda) = \begin{bmatrix} A_{g_d}(\lambda) & B_{g_d}(\lambda) \\ 0 & 0 \end{bmatrix}$$

$$B_{g_{aug}} = \begin{bmatrix} 0 \\ I \end{bmatrix}, \quad B_{v_{aug}}(\lambda) = \begin{bmatrix} B_{v_d}(\lambda) \\ 0 \end{bmatrix} \tag{6.18}$$

$$C_{g_{aug}} = \begin{bmatrix} C_{g_d} & 0 \end{bmatrix}$$

6.3 Controller Design Method

In this section, a robust fixed-structure MIMO control strategy for the current controller design of the grid-connected voltage-source converter in Fig. 6.1 is proposed.

6.3.1 Controller Design Requirements

A current controller for the grid-connected voltage-source converter described by (6.17)-(6.18) with grid inductance uncertainty is sought to meet the following performance criteria:

- The closed-loop system must be asymptotically stable for all values of L_{g_2} in the given interval.

- The closed-loop polytopic system should be able to track all step current reference signals (y_{ref}) with zero steady state error.

- The closed-loop response to step current reference signals should have small rise time (within about one cycle of $f_0 = 60$ Hz) and overshoot for all values of the grid inductance within the pre-specified uncertainty interval.

- The closed-loop system should eliminate the impact of the disturbance signal v_s.

- The coupling between the d and q output channels should be small.

6.3.2 Structure of the Proposed Current Controllers

To satisfy all the aforementioned criteria, a current controller K with the following structure is proposed.

$$\begin{aligned} x_c(k+1) &= A_c x_c(k) + B_c\big(y_{ref}(k) - y(k)\big) \\ u(k) &= C_c x_c(k) + D_c\big(y_{ref}(k) - y(k)\big) \end{aligned} \tag{6.19}$$

where $A_c \in \mathbb{R}^{m \times m}$ and B_c, C_c, and D_c are of appropriate dimensions. The above controller is a solution of the following optimization problem:

$$
\begin{aligned}
\min_{K(z)} \quad & \alpha_1 \mu_1 + \alpha_2 \mu_2 \\
\text{subject to} \quad & \|WS(\lambda)\|_\infty^2 < \mu_1 \\
& \|T(\lambda) - T_d\|_\infty^2 < \mu_2
\end{aligned}
\tag{6.20}
$$

where $S = (I + GK)^{-1}$, $T = GK(I + GK)^{-1}$, W, and T_d are the sensitivity function, the complementary sensitivity function, the weighting filter, and the desired closed-loop model, respectively. The positive scalars α_1 and α_2 characterize the emphasis on the H_∞ norm of the weighted sensitivity transfer function and the model matching problem $\|T(\lambda) - T_d\|_\infty$.

The weighting filter W is responsible to shape the sensitivity function S. In fact, the minimization of $\|WS(\lambda)\|_\infty$ provides the desired performance characteristics of the closed-loop system while the minimization of $\|T(\lambda) - T_d\|_\infty$ leads to a decoupling between two output channels for a desired diagonal T_d. The signals z_1 and z_2 are defined as follows:

$$
\begin{aligned}
z_1(k) &= W\big(y_{ref}(k) - y(k)\big) \\
z_2(k) &= y(k) - T_d y_{ref}(k)
\end{aligned}
\tag{6.21}
$$

A common choice for W [69] and T_d in continuous-time case is given as follows:

$$
W(s) = \begin{bmatrix} \frac{\frac{s}{M_w} + \omega_B^*}{s + \omega_B^* \epsilon} & 0 \\ 0 & \frac{\frac{s}{M_w} + \omega_B^*}{s + \omega_B^* \epsilon} \end{bmatrix}
\tag{6.22}
$$

$$
T_d(s) = \begin{bmatrix} \frac{\omega_B^*}{s + \omega_B^*} & 0 \\ 0 & \frac{\omega_B^*}{s + \omega_B^*} \end{bmatrix}
\tag{6.23}
$$

where ω_B^* is the desired closed-loop bandwidth, ϵ is the maximum tracking steady state error, and $M_w \geq 1$ is the maximum peak value of the magnitude of S. Weighting filter W and the model reference T_d are discretized using the ZOH method. We assume that the state space equations of these transfer functions are given by:

$$
\begin{aligned}
x_w(k+1) &= A_w x_w(k) + B_w\big(y_{ref}(k) - y(k)\big) \\
z_1(k) &= C_w x_w(k) + D_w\big(y_{ref}(k) - y(k)\big)
\end{aligned}
\tag{6.24}
$$

$$
\begin{aligned}
x_d(k+1) &= A_d x_d(k) + B_d y_{ref}(k) \\
y_r(k) &= C_d x_d(k) + D_d y_{ref}(k)
\end{aligned}
\tag{6.25}
$$

To obtain the state space representation of WS, first the dynamical equations of the plant

given in (6.17)-(6.18) and the weighting filter W are augmented as follows:

$$\hat{x}_g(k+1) = \hat{A}_g(\lambda)\hat{x}_g(k) + \hat{B}_g(\lambda)u(k) + \hat{B}_v(\lambda)v_s(k) + \hat{B}_w w(k)$$
$$\hat{y}(k) = \hat{C}_g \hat{x}_g(k) + \hat{D}_w w(k) \tag{6.26}$$
$$z_1(k) = \hat{C}_z \hat{x}_g(k) + \hat{D}_{zw} w(k)$$

where $\hat{x}_g(k) = \begin{bmatrix} x_{g_{aug}}^T(k) & x_w^T(k) \end{bmatrix}^T$, $w(k) = y_{ref}(k)$, $\hat{y}(k) = y_{ref}(k) - y(k)$, and

$$\hat{A}_g(\lambda) = \begin{bmatrix} A_{g_{aug}}(\lambda) & 0 \\ -B_w C_{g_{aug}} & A_w \end{bmatrix}$$

$$\hat{B}_g = \begin{bmatrix} B_{g_{aug}} \\ 0 \end{bmatrix}, \quad \hat{B}_v(\lambda) = \begin{bmatrix} B_{v_{aug}}(\lambda) \\ 0 \end{bmatrix}, \quad \hat{B}_w = \begin{bmatrix} 0 \\ B_w \end{bmatrix}$$

$$\hat{C}_g = \begin{bmatrix} -C_{g_{aug}} & 0 \end{bmatrix}, \quad \hat{D}_w = I \tag{6.27}$$

$$\hat{C}_z = \begin{bmatrix} -D_w C_{g_{aug}} & C_w \end{bmatrix}, \quad \hat{D}_{zw} = D_w$$

Then, by augmenting the dynamical equations of the augmented plant in (6.26)-(6.27) and the controller in (6.19), the state space representation of WS is obtained as follows:

$$x_1(k+1) = A_1(\lambda)x_1(k) + B_1 y_{ref}(k)$$
$$z_1(k) = C_1 x_1(k) + D_1 y_{ref}(k) \tag{6.28}$$

where $x_1(k) = \begin{bmatrix} \hat{x}_g^T(k) & x_c^T(k) \end{bmatrix}^T$ and

$$A_1(\lambda) = \begin{bmatrix} \hat{A}_g(\lambda) + \hat{B}_g D_c \hat{C}_g & \hat{B}_g C_c \\ B_c \hat{C}_g & A_c \end{bmatrix}, \quad B_1 = \begin{bmatrix} \hat{B}_g D_c \hat{D}_w + \hat{B}_w \\ B_k \hat{D}_w \end{bmatrix}$$

$$C_1 = \begin{bmatrix} \hat{C}_g & 0 \end{bmatrix}, \quad D_1 = \hat{D}_{zw} \tag{6.29}$$

In a similar way, the dynamical equations of the system $T - T_d$ are given by:

$$x_2(k+1) = A_2(\lambda)x_2(k) + B_2 y_{ref}(k)$$
$$z_2(k) = C_2 x_2(k) + D_2 y_{ref}(k) \tag{6.30}$$

where $x_2(k) = \begin{bmatrix} x_{g_{aug}}^T(k) & x_c^T(k) & x_d^T(k) \end{bmatrix}^T$, $z_2(k) = y(k) - y_r(k)$, and

$$A_2(\lambda) = \begin{bmatrix} A_{g_{aug}}(\lambda) - B_{g_{aug}} D_c C_{g_{aug}} & B_{g_{aug}} C_c & 0 \\ -B_c C_{g_{aug}} & A_c & 0 \\ 0 & 0 & A_d \end{bmatrix}, \quad B_2 = \begin{bmatrix} B_{g_{aug}} D_c \\ B_c \\ B_d \end{bmatrix}$$

$$C_2 = \begin{bmatrix} C_{g_{aug}} & 0 & -C_d \end{bmatrix}, \quad D_2 = -D_d \tag{6.31}$$

We assume that specific structural constraints on the controller matrices can be imposed. These constraints can be in the form of:

- Fixed-order dynamic output feedback

  The order of the controller is independent of the plant order and it is fixed *a priori.*

- Fixed-structure matrix A_c

  To track step current reference signals and reject the disturbance signal v_s, the controller $K(z)$ must contain integrators. To this end, matrix A_c must have two poles at $z = 1$.

- PI control design (for the case of L-filter)

  For the case of L-type filter, the objective is to design a simple PI controller to satisfy all the required criteria.

Remark: The control design method can also consider the impact of high frequency dynamics due to PWM switching.

6.3.3 Controller Design Method

All the aforementioned control design requirements for grid-connected VSCs with L/LCL-type filter described by (6.17)-(6.18) can be ensured by the set of LMI-based conditions, given in Theorem 9 in Chapter 3.

6.4 Robust dq-frame Current Controllers

In order to design a fixed-structure controller for the voltage-source converter of Fig. 6.1 with an L/LCL-type filter, the weighting filter W and desired closed-loop transfer function T_d are chosen as follows:

$$W(s) = \begin{bmatrix} \frac{\frac{s}{3}+1000}{s+0.01} & 0 \\ 0 & \frac{\frac{s}{3}+1000}{s+0.01} \end{bmatrix} \tag{6.32}$$

$$T_d(s) = \begin{bmatrix} \frac{1000}{s+1000} & 0 \\ 0 & \frac{1000}{s+1000} \end{bmatrix} \tag{6.33}$$

We also set $\alpha_1 = 0.2$ and $\alpha_2 = 1$ in the optimization problem given in (6.20).

6.4.1 dq-frame Current Controller for the VSC with an L-type Filter

In this part, a dq-based PI current controller for a VSC with an L-type filter with the parameters given in Table 6.1 is designed. It is assumed that the grid inductance L_{g_2} belongs to $[0, 1mH]$.

According to Algorithm III in Subsection 3.6.3, the following H_∞ PI controller is obtained after 20 iterations:

$$A_c = \begin{bmatrix} 1 & 0 \\ 0 & 1 \end{bmatrix}, \quad B_c = \begin{bmatrix} 0.506 & 0.0021 \\ -0.0021 & 0.5061 \end{bmatrix}$$
$$C_c = \begin{bmatrix} 0.0602 & -0.3999 \\ 0.3988 & 0.0605 \end{bmatrix}, \quad D_c = \begin{bmatrix} 5.2880 & -0.1361 \\ 0.1425 & 5.2900 \end{bmatrix} \tag{6.34}$$

The designed PI controller guarantees the robust stability and the robust performance criteria $\|WS(\lambda)\|_\infty < 1.1235$ and $\|T(\lambda) - T_d\|_\infty < 0.1102$ for all values of the uncertain parameter $L_{g_2} \in [0, 1mH]$.

6.4.2 *dq*-frame Current Controller for the VSC with an *LCL*-type Filter

The objective is to design a robust *dq*-based current controller for a VSC with an *LCL* filter described by (6.17)-(6.18). We assume that the grid inductance L_{g_2} belongs to $[0, 0.5mH]$. Following the control design procedure in Algorithm III and the stretching approach in Algorithm II respectively given in Subsection 3.6.3 and Subsection 3.5.2, the final H_∞ current controller is obtained after 5 iterations as follows:

$$A_c = \begin{bmatrix} 1 & 0 & -0.058 & 0.046 & -0.020 & -0.005 & -0.011 & 0.016 \\ 0 & 1 & -0.028 & 0.046 & -0.023 & -0.150 & 0.173 & -0.088 \\ 0 & 0 & 0.008 & 0.493 & 0.003 & 0.002 & 0.0004 & -0.002 \\ 0 & 0 & 0.024 & -0.018 & 0.507 & 0.0003 & 0.004 & -0.005 \\ 0 & 0 & 0.036 & -0.029 & 0.012 & 0.003 & 0.007 & -0.011 \\ 0 & 0 & 0.003 & -0.005 & 0.002 & 0.014 & 0.482 & 0.009 \\ 0 & 0 & 0.009 & -0.013 & 0.005 & 0.035 & -0.038 & 0.519 \\ 0 & 0 & 0.011 & -0.02 & 0.01 & 0.062 & -0.073 & 0.037 \end{bmatrix}$$

$$B_c = \begin{bmatrix} 3.045 & -0.001 \\ 0.003 & 4.614 \\ -0.5 & 0.0002 \\ -1.002 & 0.001 \\ -2.006 & 0.0004 \\ -0.0011 & -0.5 \\ -0.0014 & -1.0005 \\ -0.0017 & -2.002 \end{bmatrix}, \quad C_c = \begin{bmatrix} 0.005 & 0.025 \\ -0.016 & 0.004 \\ 2.204 & -0.218 \\ -5.347 & 0.352 \\ 4.254 & -0.119 \\ 0.197 & 2.163 \\ -0.337 & -5.274 \\ 0.124 & 4.212 \end{bmatrix}^T \tag{6.35}$$

$$D_c = \begin{bmatrix} 3.1729 & -0.1467 \\ 0.1488 & 3.1662 \end{bmatrix}$$

The resulting controller ensures the robust stability as well as the robust performance criteria $\|WS(\lambda)\|_\infty < 1.4532$ and $\|T(\lambda) - T_d\|_\infty < 1.5068$ for the whole range of the uncertain parameter L_{g_2}.

Remark. The LMI-based optimization problems are solved using YALMIP [146] and SDPT3

[153] as the interface and the solver, respectively.

6.5   Performance Evaluation

In this section, the performance of the designed controllers in (6.34) and (6.35) is evaluated by means of simulation results carried out in MATALB/SimPowerSystems under several scenarios: 1) current tracking and 2) robustness to the grid inductance uncertainty.

In the tracking test scenario, the performance of the proposed controllers in the step dq-current reference tracking is assessed. The second scenario is conducted to demonstrate the robustness of the controllers against the interval uncertainty in the grid inductance. In the simulation case studies, a realistic model of the VSC (nonlinear switching model) is used.

6.5.1   VSC with an L-type Filter

The values of the parameters of the VSC with an L filter in Fig. 6.1 are set according to Table 6.1. We study the dynamical responses of the system for two case: $L_{g_2} = 0$ and $L_{g_2} = 1 mH$. In both case studies, the d and q components of the current signal are initially set at 0.686 pu and 0.5145 pu, respectively, by the PI controller in (6.34). The d component is stepped up to 0.8575 pu at $t = 0.1s$. The d component is suddenly stepped down to 0.1715 pu at $t = 0.3s$. Fig. 6.2 and Fig. 6.3 show the dynamical responses of the system to these changes.

6.5.2   Comparison with Conventional and Multivariable-PI Current Control Methods

In this subsection, the performance of the proposed robust PI controller for the VSC with an L-type filter is compared to the conventional [168] and the multivariable-PI current controllers [170]. To this end, the parameters of the the conventional and the multivariable-PI controller (T_i, T_n) are properly tuned assuming that $L_{g_2} = 0$.

To show the transient behavior of the controllers, two step changes in the direct and quadrature current axes are applied. The d component of the current signal changes from 0.686 pu to 0.8575 pu at $t = 0.1s$ whereas q component is stepped down to 0.1715 pu at $t = 0.3s$.

Fig. 6.4 shows the dynamical response of $i_{g,dq}$ for three PI current controllers to those step changes in the case of $L_{g_2} = 0$. It is observed that the proposed robust PI controller in (6.34) provides better transient response in terms of rise time and dq-channels decoupling. The conventional and multivariable-PI controller are slower than the proposed PI controller. Moreover, the conventional controller is not able to completely decouple the direct and quadrature axes.

In the second case study, a test scenario similar to the pervious case is carried out to verify the

110

Figure 6.2: Dynamical responses of the grid-connected VSC with an L-type filter- Case 1) Current tracking with $L_{g_2} = 0$ (a) dq-components of the the grid current $i_{g,dq}$, (b) control inputs u, (c) real and reactive power components of DG, and (d) instantaneous grid currents $i_{g,abc}$
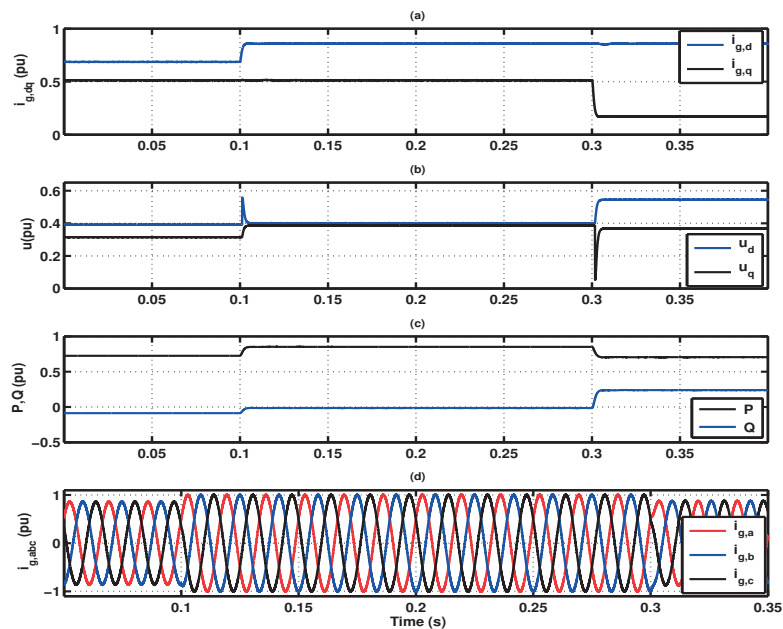
Figure 6.3: Dynamical responses of the grid-connected VSC with an L-type filter- Case 1) Current tracking with $L_{g_2} = 1mH$ (a) dq-components of the the grid current $i_{g,dq}$, (b) control inputs u, (c) real and reactive power components of DG, and (d) instantaneous grid currents $i_{g,abc}$

111
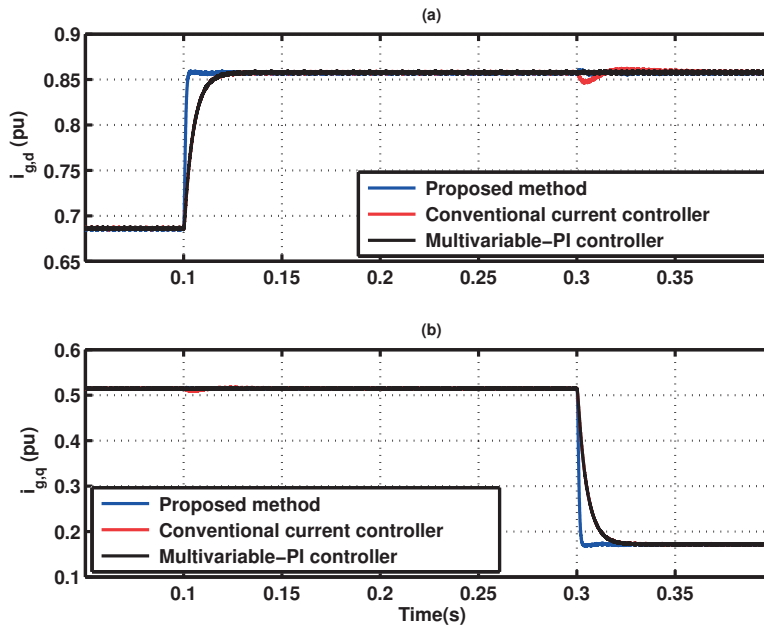
Figure 6.4: Transient response of the proposed, conventional, and multivariable-PI controllers to step changes in the direct and quadrature axis reference current- Case 1) Current tracking with $L_{g_2} = 0$ (a) d-component of the the grid current $i_{g,dq}$ and (b) q-component of the the grid current $i_{g,dq}$.
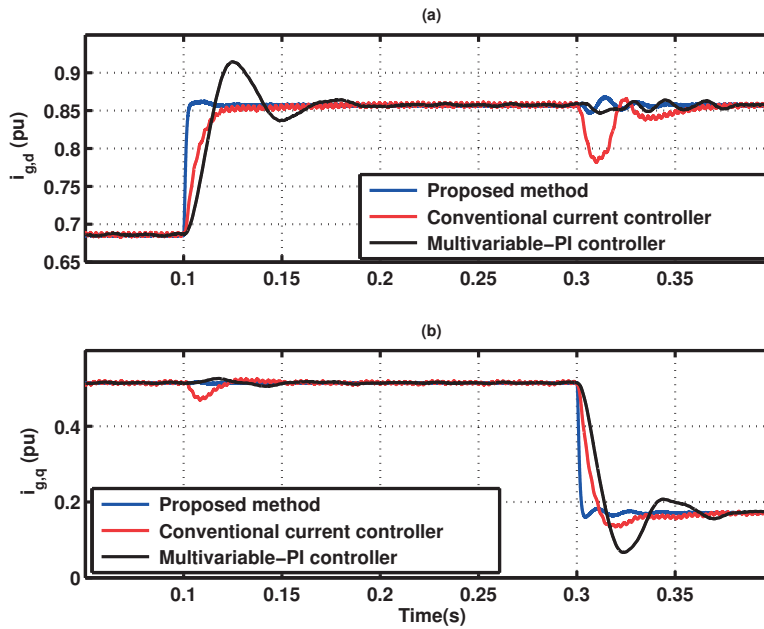
Figure 6.5: Transient response of the proposed, conventional, and multivariable-PI controllers to step changes in the direct and quadrature axis defence current- Case 1) Current tracking with $L_{g_2} = 1mH$ (a) d-component of the the grid current $i_{g,dq}$ and (b) q-component of the the grid current $i_{g,dq}$.
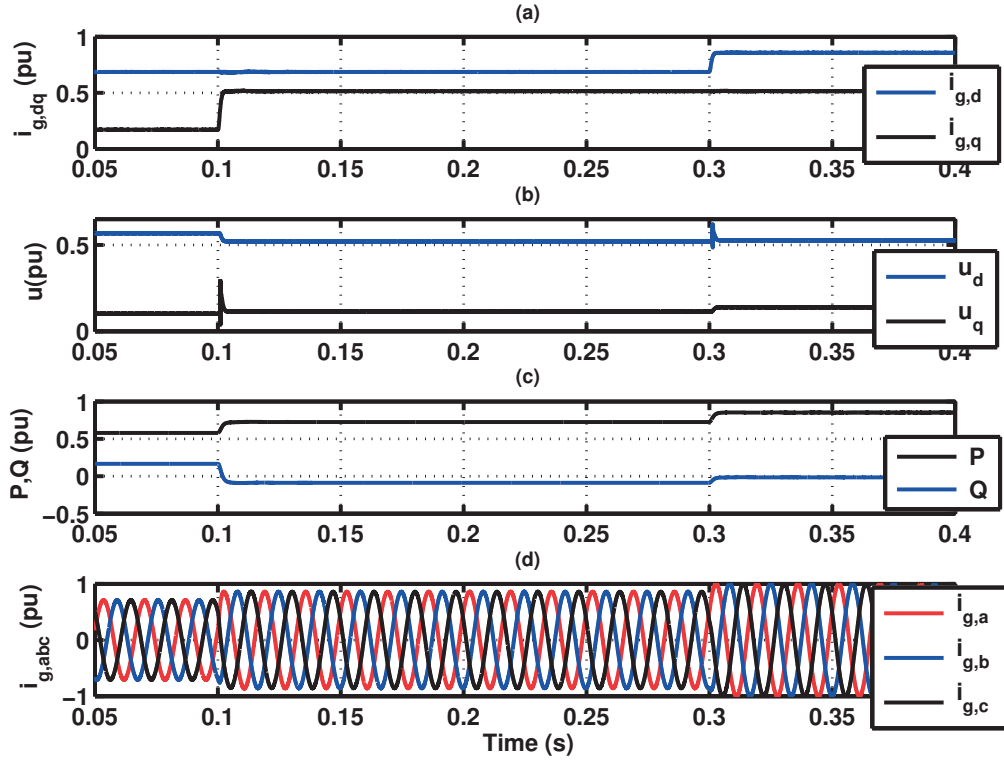
Figure 6.6: Dynamical responses of the grid-connected VSC with an *LCL* filter- Case 1) Current tracking with $L_{g_2} = 0$ (a) dq-components of the the grid current $i_{g,dq}$, (b) control inputs u, (c) real and reactive power components of DG, and (d) instantaneous grid currents $i_{g,abc}$

performance of the controllers in spite of the grid inductance uncertainty. It is assumed that real value of the grid inductance is $L_{g_2} = 1mH$. Dynamical responses of the controllers to the step changes in $i_{g,dq}$ are depicted in Fig. 6.5. As it is observed from Fig. 6.5, the convention and the multivariable-PI controllers are really sensitive to the system parameter uncertainties.

6.5.3 VSC with an *LCL*-type Filter

1) Current Tracking: The values of the parameters of the system in Fig. 6.1 with an *LCL* filter are considered according to Table 6.1. First, we assume that $L_{g_2} = 0$. Initially, the d and q components of the reference current signals are respectively set at 0.686 pu and 0.1715 pu. Then, the q component of the reference current is stepped up to 0.5145 pu at $t = 0.1s$. Finally, there is a step change in d component of the reference current to 0.8575 pu at $t = 0.3s$. The dq components of the grid current $i_{g,dq}$, the controller signals u, the real and reactive power components of DG, and the instantaneous grid currents $i_{g,abc}$ are illustrated in Fig. 6.6.

Next, we consider that the grid inductance value is $L_{g_2} = 0.5mH$. The d and q components of
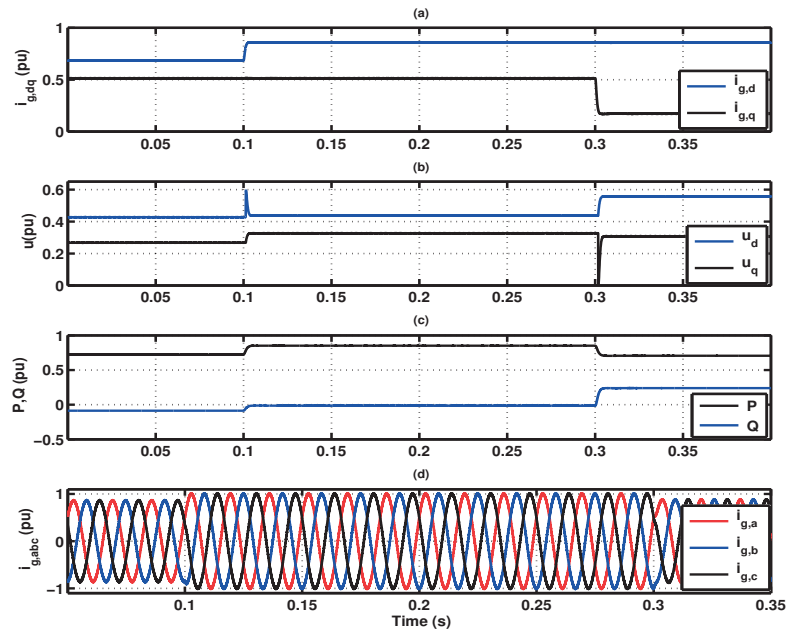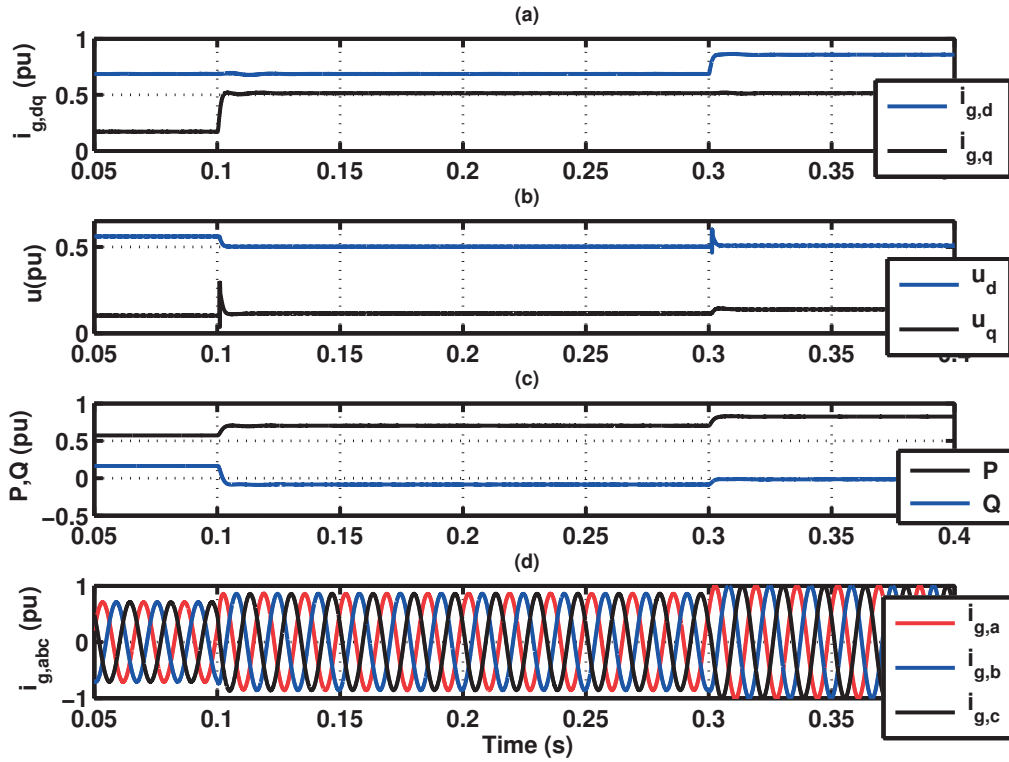
Figure 6.7: Dynamical responses of the grid-connected VSC with an *LCL*-type filter- Case 1) Current tracking with $L_{g_2} = 0.5mH$ (a) dq-components of the the grid current $i_{g,dq}$, (b) control inputs u, (c) real and reactive power components of DG, and (d) instantaneous grid currents $i_{g,abc}$

the reference current signals are initially regulated at 0.6708 pu and 0.4472 pu, respectively. Then, a step change in the *d* component of the reference signal from 0.6708 pu to 0.8944 pu is made at $t = 20ms$ while the reference value of *d* component is fixed. The dynamical responses of the system are shown in Fig. 6.7.

2) Sudden Change in Grid Inductance: To evaluate the robustness of the the designed controller in (6.35) to the grid inductance uncertainty, the grid inductance L_{g_2} is suddenly changed from $0.5mH$ to 0 at $t = 0.2s$. Fig. 6.8 shows the transient behaviour of the system under the grid inductance uncertainty. The results verify that the designed controller is robust with respect to the uncertainty in the grid inductance.

Remark. It should be noted that the grid inductance value is uncertain and it does not change in step; however, the step variations in this parameter leads to the worst-case transient response of the system. Therefore, it can be a good index for the evaluation of the robustness of the designed controller to the grid inductance uncertainty.
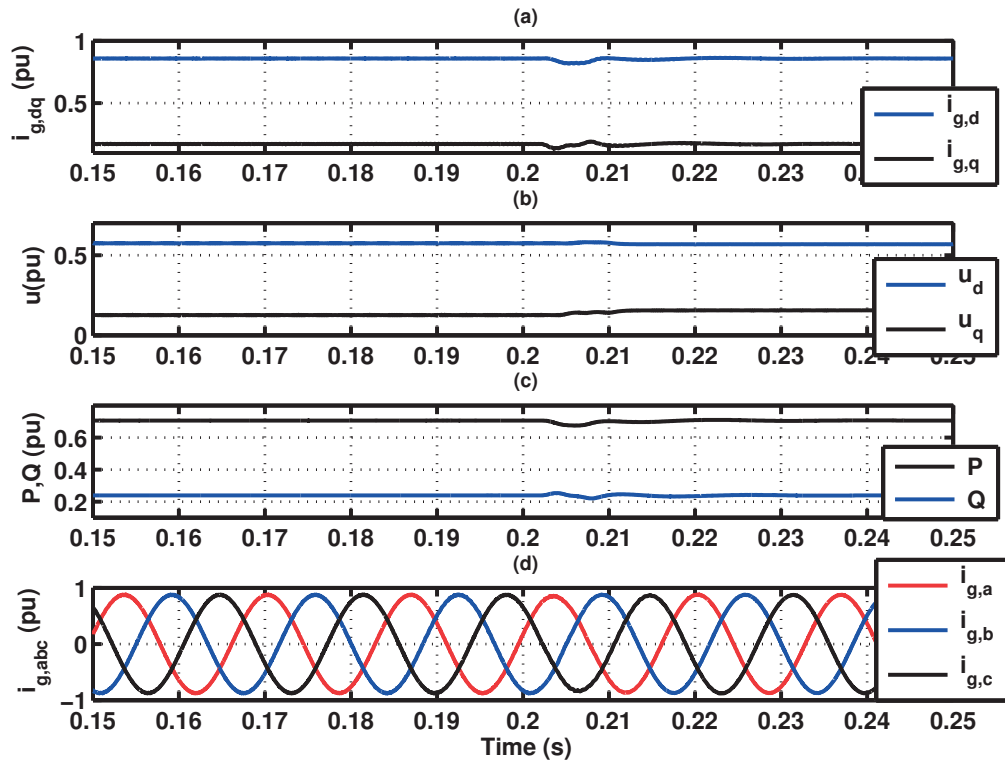
Figure 6.8: Dynamical responses of the grid-connected VSC with an *LCL*-type filter- Case 2) Sudden change in the grid inductance (a) dq-components of the the grid current $i_{g,dq}$, (b) control inputs u, (c) real and reactive power components of DG, and (d) instantaneous grid currents $i_{g,abc}$

6.6 Conclusion

In this chapter, dq-based current controllers for grid-connected voltage-source converters (VSC) with L/LCL-type filters under polytopic uncertainty are designed. The uncertainty is imposed by the grid inductance which is assumed to belong to a given interval. The current controllers assigned with integrators result from a convex optimization problem developed in Chapter 3. The proposed controllers guarantee the robust stability and robust performance of the system against the grid inductance uncertainty.

In summary, as compared to the existing grid-connected VSCs control methods, the proposed current controllers have the following main advantages:

1. The controllers require to measure only the current signal; therefore, in contrast to multi-loop control strategies, only one sensor is necessary.

2. The controllers provide dq axes-decoupling between the direct (d) and the quadrature (q) components of the current signal by means of the minimization of an H_∞ norm

constraint.

3. The MIMO controllers fulfil the requirements of stability, fast rise-time, small overshoot, attenuated resonance damping, and robustness to a pre-specified range of the grid inductance.

4. The controller design procedure is straightforward and equally applicable to VSC-based energy conversion applications.

To verify the performance of the proposed controllers, several case studies are conducted in MATLAB/SimPowerSystems. The simulation results confirm that the designed controllers are robust to the grid inductance uncertainty and they are able to track step current reference current signals with fast rise-time and small overshoot.

7 Islanded Inverter-interfaced Micro-grids

7.1   Introduction

This chapter focuses on the development of a robust fixed-structure control strategy for autonomous inverter-interfaced microgrids consisting of DGs. The special emphasis is given to decentralized control technique where there is not any communication link and information exchange among the local controllers of DGs. The control strategy is composed of (i) a power management system (PMS) which specifies voltage setpoints for each voltage-controlled bus based on a power flow analysis, (ii) local voltage controllers of DGs which provide tracking of the voltage setpoints with fast rise time and smooth non-peaking transient responses and robustness to load parameter uncertainties, and (iii) an open-loop frequency control and synchronization scheme maintaining system frequency.

The robustness and the decentralized features of the local voltage controllers are important for a microgrid system because

- centralized controllers are uneconomical due to the complexity and cost of the required high-bandwidth communication infrastructure, and they are unreliable in case of a single point of failure. Moreover, due to the distributed nature of microgrids, any kind of centralized control strategies is almost impossible [117].

- robust controllers are able to overcome the uncertainty issues of the microgrid parameters/structure.

The emphasis of this chapter is on local voltage controllers of DGs which are designed based on the developed algorithms in Chapter 3 and Chapter 5. To study different performance aspects of the proposed voltage controllers, they are applied to a single-DG and a three-DG microgrid and a set of comprehensive simulation case studies in MATLAB and experimental results validate the desired performance of the proposed controllers.

The organization of Chapter 7 is as follows: Section 7.2 presents the dynamical model of

an islanded inverter-interfaced multi-DG microgrid. Sections 7.3 is devoted to the islanded microgrid control system. The *dq*-frame robust fixed-structure voltage controllers are given in Section 7.4. Simulation and experimental results are presented in Section 7.5. Chapter 7 ends with concluding remarks in Section 7.6.
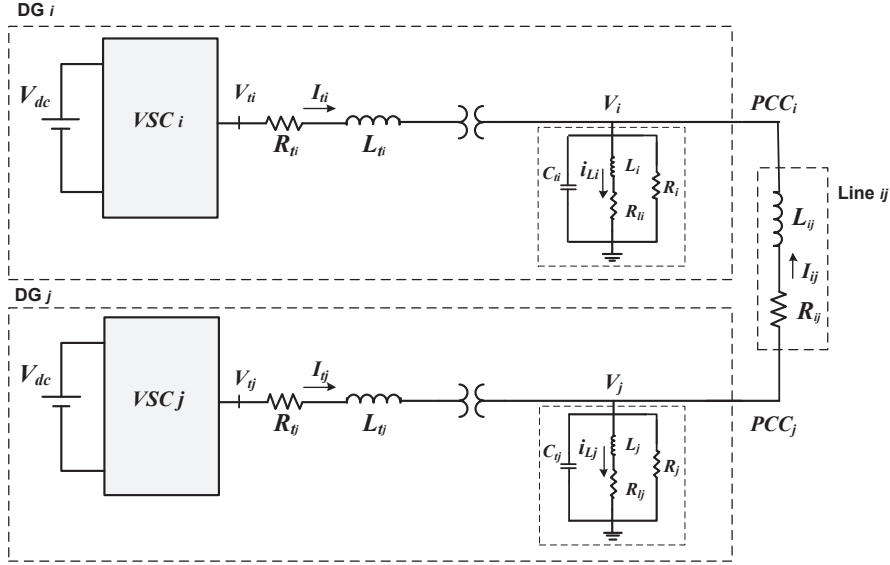
Figure 7.1: Configuration of two DGs connected via line ij

7.2   Dynamical Model of Islanded Inverter-interfaced Microgrids

Consider an islanded inverter-interfaced microgrid consisting of N DGs. Each DG is modeled by a DC voltage source, a voltage-source converter (VSC), a series RL filter, a step-up transformer with transformation ratio k, and a local load modeled by a three-phase parallel RLC network. For the sake of simplicity, first we consider the configuration of a microgrid system with two DGs as shown in Fig. 7.1. However, the proposed voltage control method in this chapter is general and can be applied to the microgrids composed of N DGs with radial configuration. The system is described by the following dynamical equations in *dq*-frame:

$$
\text{DG } i
\begin{cases}
\frac{dV_{i,dq}}{dt} + j\omega_0 V_{i,dq} = -\frac{1}{R_i C_{ti}} V_{i,dq} + \frac{k_i}{C_{ti}} I_{ti,dq} - \frac{1}{C_{ti}} i_{L_i,dq} + \frac{1}{C_{ti}} I_{ij,dq} \\
\frac{dI_{ti,dq}}{dt} + j\omega_0 I_{ti,dq} = -\frac{k_i}{L_{ti}} V_{i,dq} - \frac{R_{ti}}{L_{ti}} I_{ti,dq} + \frac{1}{L_{ti}} V_{ti,dq} \\
\frac{di_{L_i,dq}}{dt} + j\omega_0 i_{L_i,dq} = \frac{1}{L_i} V_{i,dq} - \frac{R_{li}}{L_i} i_{L_i,dq}
\end{cases}
\tag{7.1}
$$

$$\text{DG } j \begin{cases} \frac{dV_{j,dq}}{dt} + j\omega_0 V_{j,dq} = -\frac{1}{R_j C_{tj}} V_{j,dq} + \frac{k_j}{C_{tj}} I_{tj,dq} - \frac{1}{C_{tj}} i_{L_j,dq} - \frac{1}{C_{tj}} I_{ij,dq} \\ \frac{dI_{tj,dq}}{dt} + j\omega_0 I_{tj,dq} = -\frac{k_j}{L_{tj}} V_{j,dq} - \frac{R_{tj}}{L_{tj}} I_{tj,dq} + \frac{1}{L_{tj}} V_{tj,dq} \\ \frac{di_{L_j,dq}}{dt} + j\omega_0 i_{L_j,dq} = \frac{1}{L_j} V_{j,dq} - \frac{R_{lj}}{L_j} i_{L_j,dq} \end{cases} \tag{7.2}$$

$$\text{Line } ij: \quad \frac{dI_{ij,dq}}{dt} + j\omega_0 I_{ij,dq} = -\frac{R_{ij}}{L_{ij}} I_{ij,dq} + \frac{1}{L_{ij}} V_{j,dq} - \frac{1}{L_{ij}} V_{i,dq} \tag{7.3}$$

where $(V_{i,dq}, V_{j,dq})$, $(I_{ti,dq}, I_{tj,dq})$, $(i_{L_i,dq}, i_{L_j,dq})$, $(V_{ti,dq}, V_{tj,dq})$, and $I_{ij,dq}$ respectively are the dq components of the load voltage at PCCs, the current filters, the load inductance currents, the VSC terminal voltages, and the transmission line current. It should be noted that the dc-side of VSC is modeled by an ideal voltage source.

The microgrid system in Fig. 7.1 can be presented as a linear time-invariant system by the following state space equations:

$$\begin{bmatrix} \dot{x}_i(t) \\ \dot{x}_{l_{ij}}(t) \\ \dot{x}_j(t) \end{bmatrix} = \begin{bmatrix} A_i & A_{lij} & 0 \\ -A_{lj,ij} & A_{l,ij} & A_{lj,ij} \\ 0 & -A_{lji} & A_j \end{bmatrix} \begin{bmatrix} x_i(t) \\ x_{l_{ij}}(t) \\ x_j(t) \end{bmatrix} + \begin{bmatrix} B_i & 0 \\ 0 & 0 \\ 0 & B_j \end{bmatrix} \begin{bmatrix} u_i(t) \\ u_j(t) \end{bmatrix}$$

$$\begin{bmatrix} y_i(t) \\ y_j(t) \end{bmatrix} = \begin{bmatrix} C_i & 0 & 0 \\ 0 & 0 & C_j \end{bmatrix} \begin{bmatrix} x_i(t) \\ x_{l_{ij}}(t) \\ x_j(t) \end{bmatrix} \tag{7.4}$$

where

$$x_i = \begin{bmatrix} V_{i,d} & V_{i,q} & I_{ti,d} & I_{ti,q} & i_{L_i,d} & i_{L_i,q} \end{bmatrix}^T$$

$$x_j = \begin{bmatrix} V_{j,d} & V_{j,q} & I_{tj,d} & I_{tj,q} & i_{L_j,d} & i_{L_j,q} \end{bmatrix}^T, \quad x_{l_{ij}} = \begin{bmatrix} I_{ij,q} & I_{ij,q} \end{bmatrix}^T$$

$$u_i = \begin{bmatrix} V_{ti,d} & V_{ti,q} \end{bmatrix}^T, \quad u_j = \begin{bmatrix} V_{tj,d} & V_{tj,q} \end{bmatrix}^T \tag{7.5}$$

$$y_i = \begin{bmatrix} V_{i,d} & V_{i,q} \end{bmatrix}^T, \quad y_j = \begin{bmatrix} V_{j,d} & V_{j,q} \end{bmatrix}^T$$

and

$$A_i = \begin{bmatrix} -\frac{1}{R_i C_{ti}} & \omega_0 & \frac{k}{C_{ti}} & 0 & -\frac{1}{C_{ti}} & 0 \\ -\omega_0 & -\frac{1}{R_i C_{ti}} & 0 & \frac{k}{C_{ti}} & 0 & -\frac{1}{C_{ti}} \\ -\frac{k}{L_{ti}} & 0 & -\frac{R_{ti}}{L_{ti}} & \omega_0 & 0 & 0 \\ 0 & -\frac{k}{L_{ti}} & -\omega_0 & -\frac{R_{ti}}{L_{ti}} & 0 & 0 \\ \frac{1}{L_i} & 0 & 0 & 0 & -\frac{R_{li}}{L_i} & \omega_0 \\ 0 & \frac{1}{L_i} & 0 & 0 & -\omega_0 & -\frac{R_{li}}{L_i} \end{bmatrix}, \quad A_{lij} = \begin{bmatrix} \frac{1}{C_{ti}} & 0 \\ 0 & \frac{1}{C_{ti}} \\ 0 & 0 \\ 0 & 0 \\ 0 & 0 \\ 0 & 0 \end{bmatrix} \tag{7.6}$$

119

$$
A_j = \begin{bmatrix} -\frac{1}{R_j C_{tj}} & \omega_0 & \frac{k}{C_{tj}} & 0 & -\frac{1}{C_{tj}} & 0 \\ -\omega_0 & -\frac{1}{R_j C_{tj}} & 0 & \frac{k}{C_{tj}} & 0 & -\frac{1}{C_{tj}} \\ -\frac{k}{L_{tj}} & 0 & -\frac{R_{tj}}{L_{tj}} & \omega_0 & 0 & 0 \\ 0 & -\frac{k}{L_{tj}} & -\omega_0 & -\frac{R_{tj}}{L_{tj}} & 0 & 0 \\ \frac{1}{L_j} & 0 & 0 & 0 & -\frac{R_{lj}}{L_j} & \omega_0 \\ 0 & \frac{1}{L_j} & 0 & 0 & -\omega_0 & -\frac{R_{lj}}{L_j} \end{bmatrix}, \quad A_{lji} = \begin{bmatrix} \frac{1}{C_{tj}} & 0 \\ 0 & \frac{1}{C_{tj}} \\ 0 & 0 \\ 0 & 0 \\ 0 & 0 \\ 0 & 0 \end{bmatrix} \tag{7.7}
$$

$$
A_{l,ij} = \begin{bmatrix} -\frac{R_{ij}}{L_{ij}} & \omega_0 \\ -\omega_0 & -\frac{R_{ij}}{L_{ij}} \end{bmatrix}, \quad A_{lj,ij} = \begin{bmatrix} \frac{1}{L_{ij}} & 0 & 0 & 0 & 0 & 0 \\ 0 & \frac{1}{L_{ij}} & 0 & 0 & 0 & 0 \end{bmatrix} \tag{7.8}
$$

$$
B_i = \begin{bmatrix} 0 & 0 \\ 0 & 0 \\ \frac{1}{L_{ti}} & 0 \\ 0 & \frac{1}{L_{ti}} \\ 0 & 0 \\ 0 & 0 \end{bmatrix}, \quad B_j = \begin{bmatrix} 0 & 0 \\ 0 & 0 \\ \frac{1}{L_{tj}} & 0 \\ 0 & \frac{1}{L_{tj}} \\ 0 & 0 \\ 0 & 0 \end{bmatrix} \tag{7.9}
$$

$$
C_i = C_j = \begin{bmatrix} 1 & 0 & 0 & 0 & 0 & 0 \\ 0 & 1 & 0 & 0 & 0 & 0 \end{bmatrix} \tag{7.10}
$$

7.2.1 Islanded Microgrids with N DGs

The state space model in (7.4) can be extended to the islanded microgrids composed of N DGs with a radial topology. The overall microgrid system $G(s)$ is described as follows:

$$
\begin{aligned} \dot{x}_g(t) &= A_g x_g(t) + B_g u(t) \\ y(t) &= C_g x_g(t) \end{aligned} \tag{7.11}
$$

where

$$
\begin{aligned} x_g &= \begin{bmatrix} x_1^T & x_{l_{12}}^T & x_2^T & x_{l_{23}}^T & \dots & x_N^T \end{bmatrix}^T \\ u &= \begin{bmatrix} u_1^T & \dots & u_N^T \end{bmatrix}^T \\ y &= \begin{bmatrix} y_1^T & \dots & y_N^T \end{bmatrix}^T \end{aligned} \tag{7.12}
$$

and the state space matrices are given:

$$
A_g = \begin{bmatrix}
A_1 & A_{l12} & 0 & 0 & 0 & \ldots & 0 \\
-A_{l2,12} & A_{l,12} & A_{l2,12} & 0 & 0 & \ldots & 0 \\
0 & -A_{l21} & A_2 & A_{l23} & 0 & \ldots & 0 \\
0 & 0 & -A_{l3,23} & A_{l,23} & A_{l3,23} & \ldots & 0 \\
\vdots & \vdots & \vdots & \vdots & \vdots & \ddots & \vdots \\
0 & 0 & 0 & 0 & 0 & \ldots & A_N
\end{bmatrix}
$$

$$
B_g = \begin{bmatrix}
B_1 & 0 & 0 & \ldots & 0 \\
0 & 0 & 0 & \ldots & 0 \\
0 & B_2 & 0 & \ldots & 0 \\
0 & 0 & 0 & \ldots & 0 \\
0 & 0 & B_3 & \ldots & 0 \\
\vdots & \vdots & \vdots & \ddots & \vdots \\
0 & 0 & 0 & \ldots & B_N
\end{bmatrix}, \quad
C_g = \begin{bmatrix}
C_1 & 0 & 0 & 0 & 0 & \ldots & 0 \\
0 & 0 & C_2 & 0 & 0 & \ldots & 0 \\
0 & 0 & 0 & 0 & C_3 & \ldots & 0 \\
\vdots & \vdots & \vdots & \vdots & \vdots & \ddots & \vdots \\
0 & 0 & 0 & 0 & 0 & \ldots & C_N
\end{bmatrix}
$$

(7.13)

where A_i, A_{lij}, $A_{lj,ij}$, $A_{l,ij}$, B_i, and C_i are define in (7.6)-(7.10) for $i, j = 1, \ldots, N$.

7.2.2 Islanded Microgrids with Polytopic-type Uncertainty

The parametric uncertainty of the microgrid system in Fig. 7.1 arises from the fact that the RLC load parameters of DG i can vary based on consumers' demands. For the sake of simplicity, the following definitions are used.

$$
\theta_i^1 = \frac{1}{R_i}, \quad \theta_i^2 = \frac{1}{L_i}, \quad \theta_i^3 = \frac{1}{C_{ti}}
$$

It is also assumed that the RLC load parameters are bounded within the maximum and minimum values as $R_{i_{min}} \leq R_i \leq R_{i_{max}}$, $L_{i_{min}} \leq L_i \leq L_{i_{max}}$, and $C_{i_{min}} \leq C_{ti} \leq C_{i_{max}}$ which represents a cube in which the load parameters are allowed to change. In the general case of N DGs, it is a hyper-cube with $q = 2^{n_\theta}$ vertices, where n_θ is the number of uncertain load parameters. It can be shown that the image of this hyper-cube in the space of the elements of matrix A_g is inside a polytope of $q = 2^{n_\theta}$ vertices. This polytope covers the whole uncertainty in the RLC load parameters and is defined as the convex combination of the vertices A_g^l, $l = 1, \ldots, q$ [148]:

$$
A_g(\lambda) = \sum_{l=1}^{q} \lambda_l A_g^l, \quad \lambda_l \in \Lambda_q \tag{7.14}
$$

where Λ_q is defined in (2.8) and vertices A_g^l are obtained based on the maximum and minimum values of the RLC load parameters.
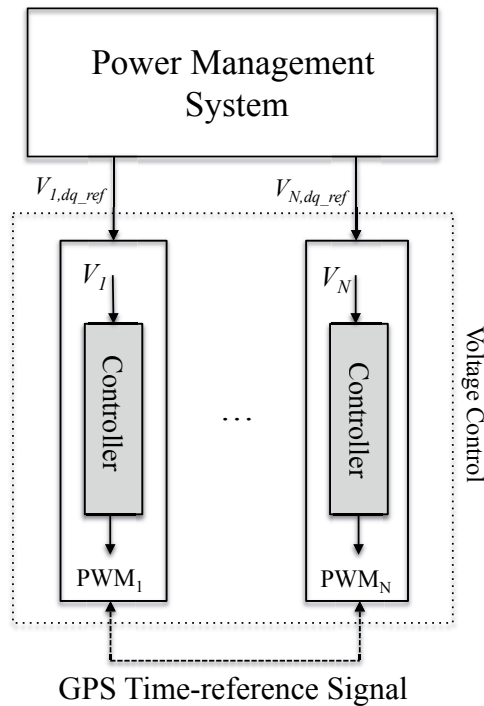
Figure 7.2: Block diagram of the proposed control strategy

7.3   Islanded Microgrid Control System

Consider a schematic diagram of the microgrid control strategy composed of a power management system (PMS), local voltage controllers of DGs, and a frequency control scheme in Fig. 7.2.

7.3.1   Power Management System

A power management strategy is required for reliable and efficient operation of a microgrid system with multiple DGs, particularly in the islanded mode of operation [171]. The main function of PMS is to maintain an optimal operating point for the microgrid. PMS assigns the active and reactive power setpoints for the DGs to (i) properly share the real and reactive power among the DGs based on a cost function associated with each DG, a market signal [126], power rate of DGs, etc., (ii) appropriately respond to the microgrid disturbances and major changes [172], (iii) balance the microgrid power, and (iv) provide the resynchronization of the microgrid system with the main grid, if required [172]. The setpoints are then transmitted to the local controllers of the DGs. The local controllers measure the voltage at their corresponding PCC or the active/reactive output power of their own DG and then enable the voltage tracking according to the received reference setpoints [129].

7.3.2 Frequency Control

The frequency of the microgrid system is controlled in open-loop. To this end, each DG includes an oscillator which generates $\theta(t) = \int_0^t \omega_0 d\tau$, where $\omega_0 = 2\pi f_0$ and f_0 is the nominal frequency of the microgrid. All DGs are then synchronized by a global synchronization signal that is communicated to the oscillators of DGs through a global positioning system (GPS) [126]. The global phase-angle is employed for *dq/abc* (*abc/dq*) transformations.

7.3.3 Voltage Control

The voltage setpoints are communicated from PMS to the local controllers of the DGs and transformed to the *dq*-frame based on the phase-angle signal $\theta(t)$ generated by their internal oscillator. The main objective is to develop a robust voltage controller for the islanded operation of the inverter-interfaced microgrids with load parameter uncertainties given in (7.14).

7.4 Robust Fixed-structure Voltage Control

A fixed-structure voltage controller for the islanded microgrid system whose dynamical equations are given in (7.11)-(7.13) with polytopic-type uncertainty in (7.14) is sought to satisfy the following performance criteria:

- The closed-loop system must be asymptotically stable for the whole polytope.

- The closed-loop polytopic system should be able to asymptotically track all step voltage reference signals $(y_{ref}(t))$.

- The closed-loop response to step voltage reference signals should be fast within about two/three cycles of $f_0 = 60$ Hz with small overshoot for all values of the load parameters within the prespecified uncertainty.

- Each local controller uses the minimum information exchange and communication among DGs and their local controllers.

- The local controllers are structurally simple (low-order control design).

- The coupling among the output channels should be small.

To achieve all above mentioned conditions, in following, a fixed-order Two-Degree-of-Freedom (2DOF) sparse controller with integral action is designed. The dynamics of the controller $K(s)$

are given by:

$$\dot{x}_c(t) = A_c x_c(t) + \begin{bmatrix} B_{c_1} & B_{c_2} \end{bmatrix} \begin{bmatrix} y(t) \\ y_{ref}(t) \end{bmatrix}$$

$$u(t) = C_c x_c(t) + \begin{bmatrix} D_{c_1} & D_{c_2} \end{bmatrix} \begin{bmatrix} y(t) \\ y_{ref}(t) \end{bmatrix}$$

(7.15)

where $x_c(t)$ is the states of the controller and matrices A_c, B_{c_1}, B_{c_2}, C_c, D_{c_1}, and D_{c_2} are of appropriate dimensions. The transfer functions of the feedback and feedforward controllers $K_{fb}(s)$ and $K_{ff}(s)$ are respectively given by:

$$K_{fb}(s) = C_c (sI - A_c)^{-1} B_{c_1} + D_{c_1}$$

$$K_{ff}(s) = C_c (sI - A_c)^{-1} B_{c_2} + D_{c_2}$$

(7.16)

The 2DOF controller is a solution of the following optimization problem:

$$\min_{A_c, B_{c_1}, B_{c_2}, C_c, D_{c_1}, D_{c_2}} \quad \mu + \alpha \|W * \mathcal{Z}(K)\|_1$$

$$\text{subject to} \quad \|W_s S(\lambda)\|_\infty^2 < \mu$$

(7.17)

where $\mathcal{Z}(K)$ is defined in (5.28). Transfer functions $S(\lambda) = (I + G(\lambda)K)^{-1}$ and W_s are sensitivity function and a weighting filter designed based on the desired time-domain performance [1]. The positive scalar α characterizes the emphasis on the tracking dynamics and the sparsity of the controller architecture.

The weighting filter W_s is responsible to shape the sensitivity function S and provides the desired performance characteristics of the closed-loop system. A common choice of W_s is given as follows [1, 69]:

$$W_s(s) = \text{diag}\left(\begin{bmatrix} \frac{\frac{s}{M_{s_i}} + \omega_{B_i}^*}{s + \omega_{B_i}^* \epsilon_i} & 0 \\ 0 & \frac{\frac{s}{M_{s_i}} + \omega_{B_i}^*}{s + \omega_{B_i}^* \epsilon_i} \end{bmatrix} \right)$$

(7.18)

where $\omega_{B_i}^*$ is approximately the desired closed-loop bandwidth, ϵ_i is the maximum tracking steady state error, and $M_{s_i} \geq 1$ is the maximum peak value of S. The choice of $\epsilon_i << 1$ ensures approximate integral action $S(0) \approx 0$ [69]. A large value of $\omega_{B_i}^*$ leads to a faster response for output i. However, there always exists a trade-off between the speed of the closed-loop system response and the sensitivity of the closed-loop system with respect to the measurement noise. Therefore, to have an acceptable dynamic response of the microgrid system in terms of step signal tracking and robustness to the measurement noise, the parameters of the weighting filter $W_s(s)$ are selected as follows:

$$\omega_{B_i}^* = 30, \quad M_{s_i} = 1.5, \quad \epsilon_i = 3.33e - 4$$

(7.19)
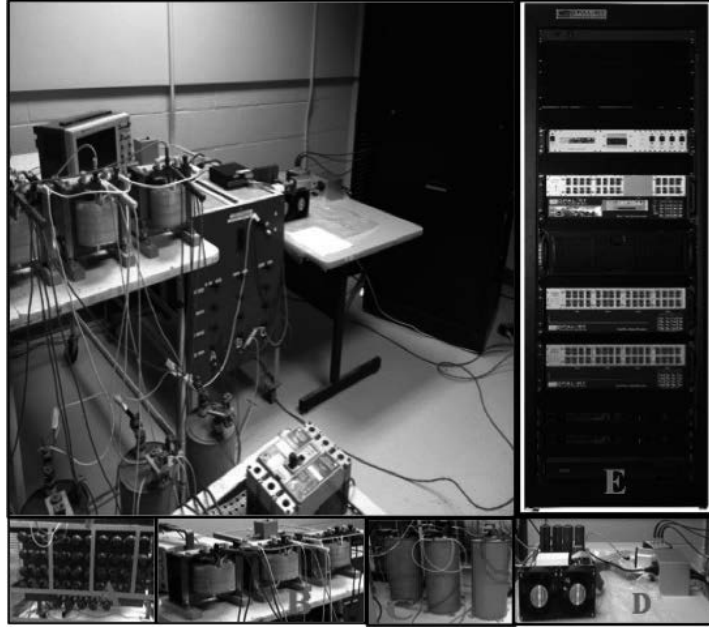
Figure 7.3: Experimental setup: (A) load resistance, (B) load inductance, (C) load capacitance, (D) three-phase converter and gating signal generator, and (E) OPAL-RT.

$\omega_{B_i}^* = 30$ is chosen to have a rise-time of about $t_r \approx 30$ ms (two cycles of f_0) which is one of the controller design requirements, $M_{s_i} = 1.5$ is chosen to have a damping ratio of $\xi \approx 0.48$ (equal to an overshoot of $M_p = 18\%$), and $\epsilon_i = 3.33e - 4$ is chosen to obtain $\omega_{B_i}^* \epsilon_i \approx 0.01$ which indicates that the pole of the low-pass filter $W_s(s)$ which should be much less than the closed-loop bandwidth.

7.5 Simulation and Experimental Results

In this section, the proposed fixed-structure control design techniques in Chapter 3 and Chapter 5 are utilized to design a robust voltage controller for the islanded inverter-interfaced microgrid in Fig. 7.1. The performance of the designed controllers is then verified by a set of comprehensive simulation studies and is validated by means of experiments.

7.5.1 Scenario 1: Single-DG Microgrid

For the sake of simplicity, first we consider a single-DG microgrid system which supplies a three-phase parallel RLC network whose parameters are given in Table 7.1. It is assumed that the load resistance R_1 can vary within $\pm 80\%$ of its nominal value (R_{nom}). Moreover, the load parameters L_1 and C_{t1} are assumed to be bounded in the intervals $[0.5, 1.5] \times L_{nom}$ and $[0.5, 1.5] \times C_{nom}$, respectively, where L_{nom} and C_{nom} are their nominal values. Therefore, the RLC load parameter uncertainties build a polytope with $q = 2^3$ vertices.

Table 7.1: Parameters of islanded single-DG microgrid

Filter parameters	$R_t = 37.7m\Omega, \quad L_t = 5mH$
DC bus voltage	$V_{dc} = 340V$
VSC rated power	$S_{VSC} = 10KVA$
PWM carrier frequency	$f_{sw} = 10KHz$
Load nominal resistance	$R_{nom} = 23\Omega$
Load nominal inductance	$L_{nom} = 5mH$
Load nominal capacitance	$C_{nom} = 850\mu F$
Inductor quality factor	$q_l = 120$
System nominal frequency	$f_0 = 60Hz \ (\omega_0 = 2\pi f_0)$

The frequency of the islanded microgrid is controlled through an internal oscillator in the open-loop manner with $\omega_0 = 2\pi f_0$. To design the 2DOF voltage controller, we impose a restriction that the feedback part of the controller $(K_{fb}(s))$ is first designed to guarantee the robust stability while the feedforward controller $K_{ff}(s)$ is then designed for the robust performance of the closed-loop system in the presence of load parameter uncertainties.

According to the fixed-structure stabilizing controller design procedure given in Algorithm I in Subsection 3.5.1, first, eight initial sixth-order controllers with integrators are designed using FDRC Toolbox [151] for eight vertices of the polytope. Then, using the initial controllers and the set of LMIs in (3.32), the slack matrices M and T are determined. In the next step, the feedback controller is determined by solving the set of LMIs given in (3.20). The parameters of the resulting robust sixth-order feedback controller are as follows:

$$
\begin{aligned}
A_c &= \begin{bmatrix}
0 & 114.187 & 200.576 & 0 & -3.384e3 & 2.687e3 \\
0 & -1.281e4 & 8.110e3 & 0 & -7.561e3 & 5.674e3 \\
0 & 964.293 & -1.227e4 & 0 & -2.328e3 & 1.779e3 \\
0 & 1.495e3 & -1.003e3 & 0 & 560.633 & -321.734 \\
0 & -1.581e3 & 2.471e3 & 0 & -3.086e4 & 2.430e4 \\
0 & -6.624e3 & 4.181e3 & 0 & -4.259e3 & -7.559e3
\end{bmatrix} \\[2mm]
B_{c_1} &= \begin{bmatrix}
-3.96 & -10.813 \\
-190.697 & -7.335 \\
-1.278e3 & -23.570 \\
20.591 & -15.528 \\
46.662 & -92.329 \\
-55.562 & -1.354e3
\end{bmatrix}, \quad
C_c = \begin{bmatrix}
14.552 & 25.395 \\
-1.387e3 & 53.608 \\
957.818 & 154.008 \\
-22.352 & 17.363 \\
-1.119e3 & -2.948e3 \\
793.861 & 2.359e3
\end{bmatrix}^T \\[2mm]
D_{c_1} &= \begin{bmatrix}
-20.298 & -4.549 \\
7.979 & -11.005
\end{bmatrix}
\end{aligned}
\tag{7.20}
$$

The parameters of feedforward controller (B_{c_2}, D_{c_2}) are determined by solving the following

convex optimization problem and fixing the matrices A_i, $i = 1,\ldots,q$, C, and D.

$$
\min_{P_i,B_{c_2},D_{c_2},M,X,\mu} \quad \mu
$$

$$
\text{subject to} \quad
\begin{bmatrix}
P_i A_i^T + A_i P_i & P_i + M - A_i X & B & P_i C^T \\
P_i + M^T - X A_i^T & -2X & 0 & 0 \\
B^T & 0 & -I & D^T \\
C P_i & 0 & D & -\mu I
\end{bmatrix} < 0
\tag{7.21}
$$

$$
P_i = P_i^T > 0; \quad i = 1,\ldots,q
$$

where

$$
A_i = \begin{bmatrix} A_g^i + B_g D_{c_1} C_g & B_g C_c \\ B_{c_1} C_g & A_c \end{bmatrix}, \quad
B = \begin{bmatrix} B_g D_{c_2} \\ B_{c_2} \end{bmatrix}
\tag{7.22}
$$

$$
C = \begin{bmatrix} C_g & 0 \end{bmatrix}, \quad D = 0
$$

The resulting feedforward controller is:

$$
B_{c_2} = \begin{bmatrix}
20.817 & 3.304 \\
48.723 & -34.250 \\
28.047 & 2.704 \\
-11.663 & 29.727 \\
-24.629 & 1.592 \\
13.016 & 51.422
\end{bmatrix}, \quad
D_{c_2} = \begin{bmatrix}
6.238 & -5.233 \\
-1.149 & 1.927
\end{bmatrix}
\tag{7.23}
$$

The designed 2DOF voltage controller guarantees the robust stability as well as the robust performance criterion $\|W_s S(\lambda)\|_\infty < 1.087$ in spite of the prespecified load parameter uncertainties. Moreover, the controller provides the asymptotic tracking of all step voltage reference signals.

Experimental Results: The performance of the designed robust H_∞ voltage controller in (7.20) and (7.23) is validated by means of an experimental test system with the parameters given in Table 7.1. The experiment has been carried out at the Electrical Engineering Department, Ecole Polytechnique de Montreal, Montreal, QC, Canada and implemented in the RT-LAB real-time platform of OPAL-RT Technologies[1].

A photo of the laboratory experimental setup is shown in Fig. 7.3 which includes OPAL-RT, three-phase two-level converter, and three-phase RLC load. The performance of the control system is validated using several tests including voltage tracking and sudden changes in the load parameters. In all case studies, the system is assumed balanced and operates in the islanded mode.

The first test demonstrates the capability of the designed controller in voltage reference signal

---

[1]www.opal-rt.com
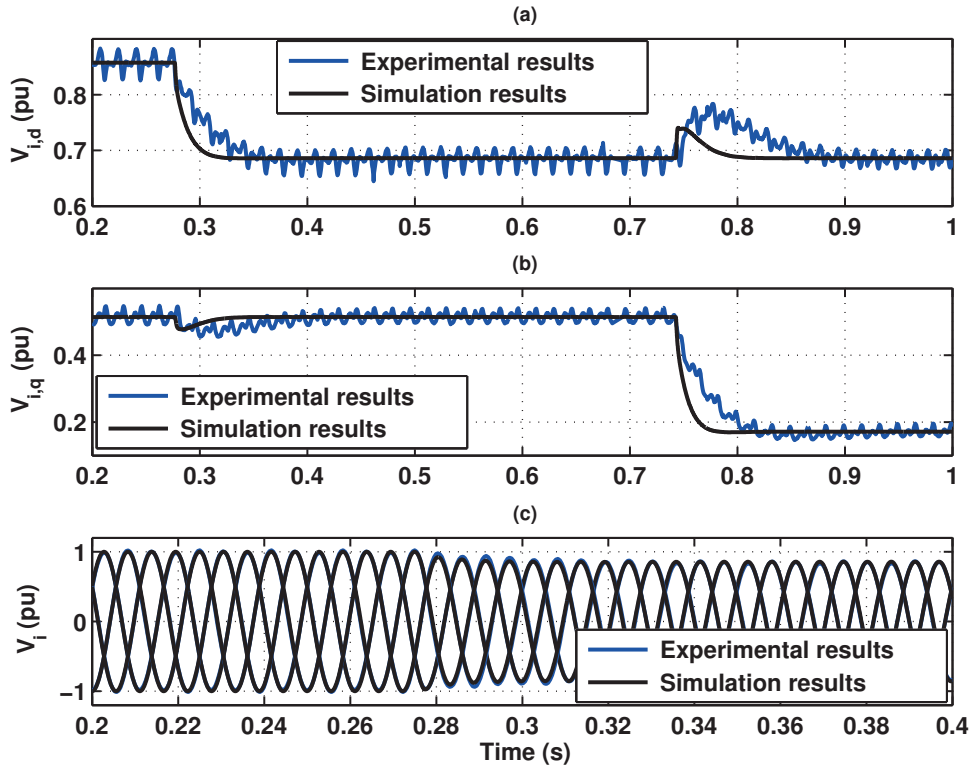
Figure 7.4: Experimental and simulation results of the islanded microgrid in voltage tracking (a) d-component of the load voltage, (b) q-component of the load voltage, and (c) instantaneous load voltages

tracking. The d-component of the voltage reference is stepped down to 0.686 pu at $t = 0.28s$ and then the q-component of the reference voltage is suddenly changed from 0.5145 pu to 0.1715 pu at $t = 0.743s$. The experimental and simulation results of the islanded microgrid system due to these step changes in the load reference signals are shown in Fig. 7.4. The results demonstrate that the proposed controller can regulate the load voltages with good tracking performance. Moreover, Fig. 7.4 shows that the simulation results are very close to the experimental data. However, in the experimental results some ripples and delays are observed in the load voltages due to non-idealities of the DC source and the dynamics and switching harmonics of the PWM-based voltage-source converter. The differences between the simulation and experimental results arise from the fact that the dynamics of the PWM-based voltage-source converter have not been considered in the simulations. However, note that the amount of ripples in the experimental results is acceptable according to IEEE standards [173]. Moreover, the effects of the ripples are negligible in the instantaneous load voltages at PCC (Fig. 7.4, part (c)).

In the second test, the proposed voltage controller regulates the d and q components of the load voltages at 0.8 pu and 0.6 pu, respectively. The load inductance and load capacitance
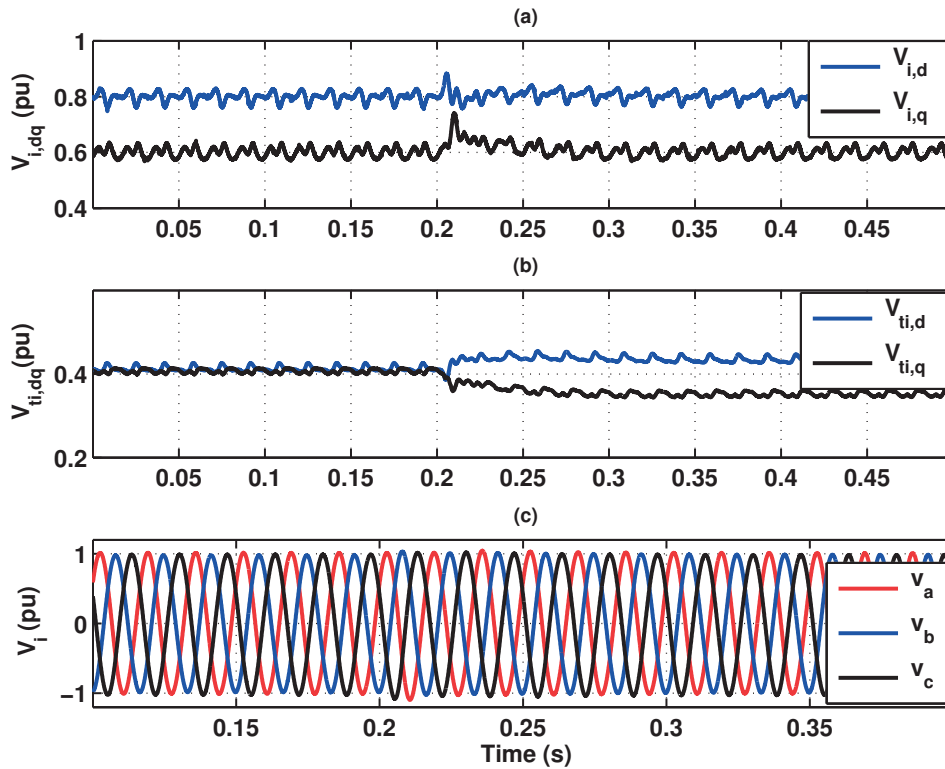
Figure 7.5: Dynamic responses of the experimental test system due to a resistive load change (a) dq-components of the load voltage, (b) control inputs, and (c) instantaneous load voltages

are also fixed at their nominal values, as given in Table 7.1. The load resistances in the three phases are equally stepped down from 5 lamps to no lamp (Δ configuration) at about $t = 200ms$. Fig. 7.5 shows the dynamical response of the test system due to this resistive load change.

In the third test, the d and q components of the load voltages are set at 0.93 pu and 0.37 pu, respectively. While the load resistances and the load capacitances are fixed at their nominal values, the load inductances in the three phases are suddenly stepped up from $5mH$ to $25mH$. Then, they suddenly decrease to $5mH$ at about $t = 0.5s$. The dynamic response of the system for the second load inductance change is shown in Fig. 7.6.

In the last test, a change in the load capacitance is considered. To this end, the load capacitances in the three-phases are suddenly changed from the nominal value $850\mu F$ to $1700\mu F$ at about $t = 1.1s$, while the load resistances and the load inductances are set based on the values given in Table 7.1. The dynamic response of the test system is depicted in Fig. 7.7.

Fig. 7.5 and Fig. 7.6 demonstrate that in spite of the large variations in the load resistance and the load inductance, the controller successfully regulates the load voltage with small transients

Table 7.2: Parameters of the islanded microgrid system with three DGs

Parameters of RL filter 1	$R_{t1} = 1m\Omega, \quad L_{t1} = 137.271\mu H$
Parameters of RL filter 2	$R_{t2} = 1.4m\Omega, \quad L_{t2} = 183.028\mu H$
Parameters of RL filter 3	$R_{t3} = 2.1m\Omega, \quad L_{t3} = 274.542\mu H$
DC bus voltages	$V_{dc} = 1500V$
VSC terminal voltage (line-line)	$V_{VSC} = 600V$
Transformer parameters	$X_T = 8\%$
Transformer voltage ratio	$k = 0.6/13.8KV(\Delta/Y)$
Parameters of RLC load 1	$R_1 = 350\Omega, \quad C_{t1} = 60\mu F$
(nominal values)	$L_1 = 0.11H, \quad R_{l_1} = 2\Omega$
Parameters of RLC load 2	$R_2 = 375\Omega, \quad C_{t2} = 65\mu F$
(nominal values)	$L_2 = 0.1mH, \quad R_{l_2} = 2\Omega$
Parameters of RLC load 3	$R_3 = 400\Omega, \quad C_{t3} = 55\mu F$
(nominal values)	$L_3 = 0.12mH, \quad R_{l_3} = 2\Omega$
System nominal frequency	$f_0 = 60Hz$
Parameters of line 1	$R_{12} = 3.35\Omega, \quad L_{12} = 2.97mH$
Parameters of line 2	$R_{23} = 5.025\Omega, \quad L_{23} = 4.5mH$

in the responses. Fig. 7.7 also indicates that the controller adjusts the load voltages within about two cycles. Therefore, the obtained results confirm that the controller is robust with respect to the load parameter uncertainties. In addition, the coupling between the output signals is small.

The experimental results show that the proposed voltage controller provides satisfactory dynamic performance in terms of voltage tracking and robustness to load parameter variations according to IEEE standards [173].

7.5.2   Scenario 2: Three-DG Microgrid

In the second scenario, an islanded microgrid consisting of three DGs with the voltage rating of 0.6 kV and power ratings of 1.6 MVA, 1.2 MVA, and 0.8 MVA is considered. The values and the definition of the parameters are provided in Table 7.2.

It is assumed that the load resistances R_i and inductances L_i, $i = 1,2,3$ are uncertain up to $\pm 20\%$ of their nominal values given in Table 7.2. Therefore, the uncertainty in this system is in the form of a polytope built by $q = 2^6$ vertices.

The proposed fixed-structure H_∞ control method with minimum communication links in Chapter 5 is used to design a controller for the islanded microgrid consisting of 3 DGs. The final controller is resulted from the following hierarchy of issues:

- Initial centralized controllers are designed using FDRC Toolbox [151] for each vertex of the polytope.
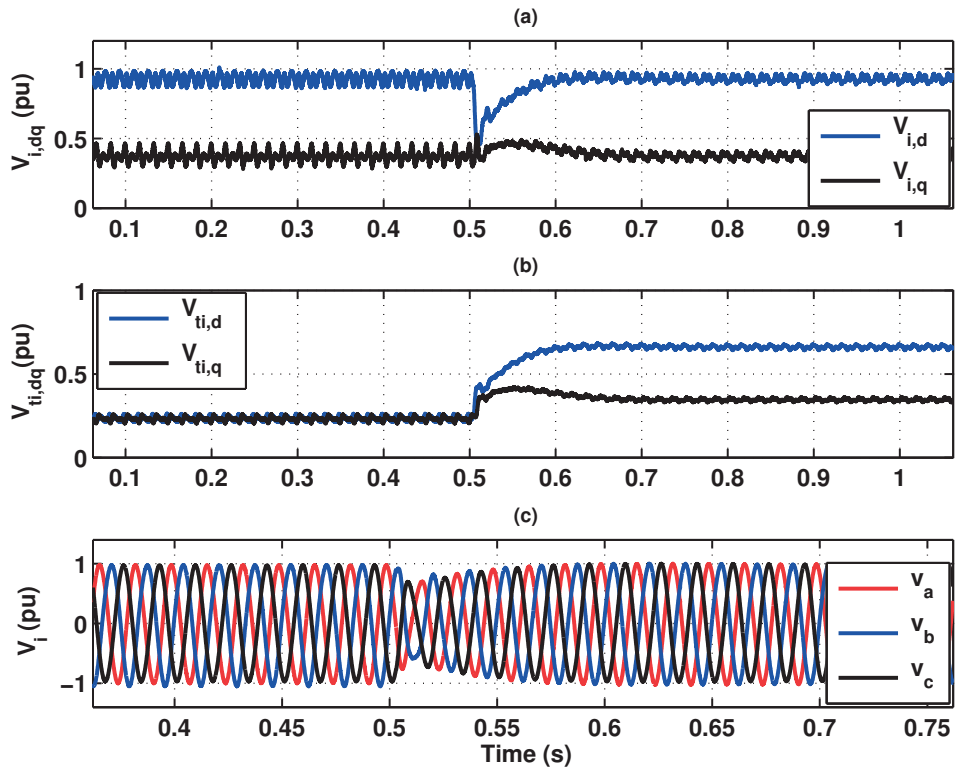
Figure 7.6: Dynamic responses of the experimental test system due to an inductive load change (a) dq-components of the load voltage, (b) control inputs, and (c) instantaneous load voltages

131
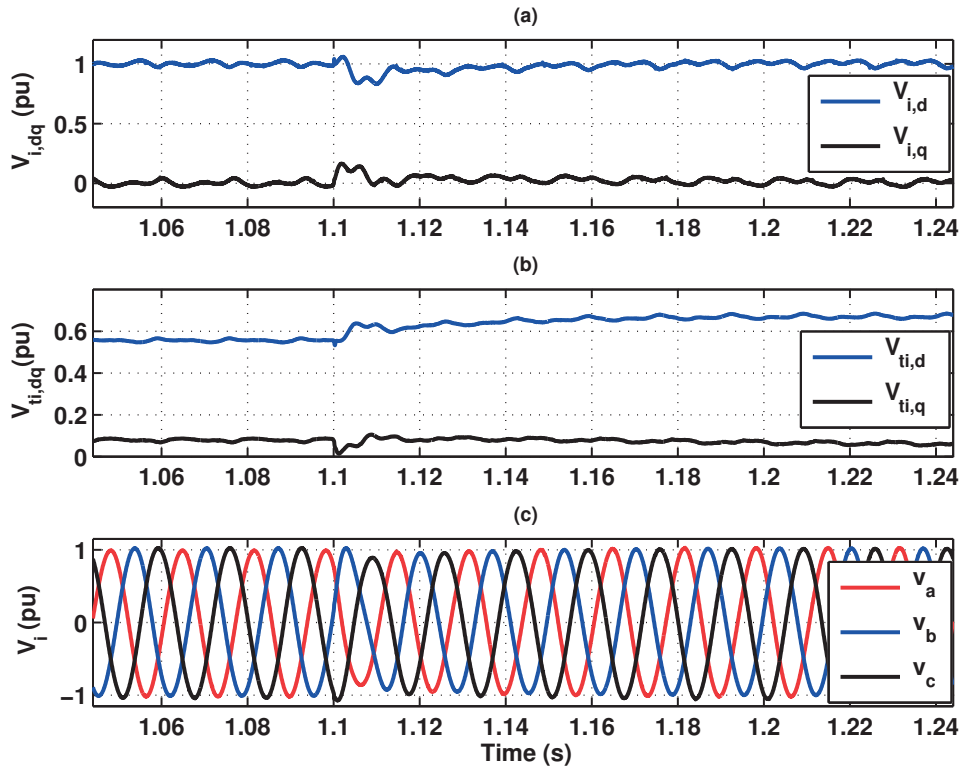
Figure 7.7: Dynamic responses of the experimental test system due to a capacitive load change (a) dq-components of the load voltage, (b) control inputs, and (c) instantaneous load voltages
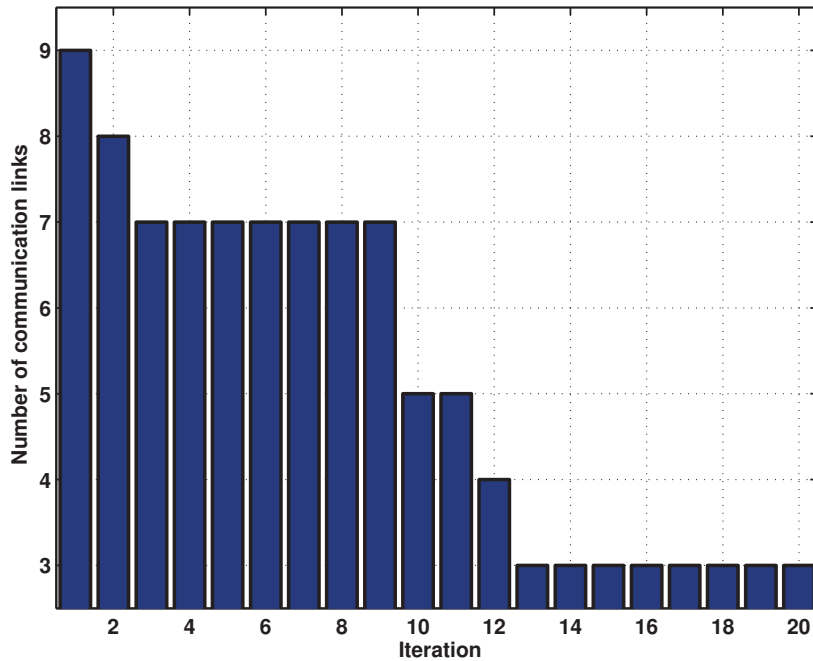
Figure 7.8: Number of communication link in the feedback controller versus the iteration number

- To ensure the integral action of the controller, the controller must have six poles at zero. Therefore, one can simply consider six columns/rows of matrix A_c to be identically equal to zero (one integrator for each output loop).

- The feedback term of the controller is first designed such that the closed-loop system is robustly stable and its spectral abscissa (β) is minimized.

- The feedforward term of the controller is then designed such that $\|W_s S(\lambda)\|_\infty$ is minimized.

- The parameters of Algorithm IV given in Subsection 5.3.3 are set as follows: $\epsilon = 1e-10$ and $\alpha = 1$.

- LMI-based optimization problems are solved using YALMIP [146] as the interface and MOSEK as the solver.

After 20 iterations, some control structures are obtained. Fig. 7.8 shows the number of communication links of the feedback controller versus the iteration numbers. The resulting

Figure 7.9: Reference setpoint tracking of DG 1: (a) d-component of the load voltage at PCC 1, (b) q-component of the load voltage at PCC 1, (c) d-component of the control signal of DG 1, (d) q-component of the control signal of DG 1, and (e) instantaneous load voltages at PCC 1

decentralized controller in the 20th iteration is given as follows:

$$
A_c = \text{diag}\left(\begin{bmatrix} 0 & 9.08e2 & 0 & -1.07e2 \\ 0 & -1.885e4 & 0 & 1.65e3 \\ 0 & 1.068e2 & 0 & 9.079e2 \\ 0 & -1.65e3 & 0 & -1.885e4 \end{bmatrix}, \begin{bmatrix} 0 & 2.787e2 & 0 & -1.122e1 \\ 0 & -4.53e3 & 0 & 1.096e3 \\ 0 & 8.99e0 & 0 & 2.787e2 \\ 0 & -1.064e3 & 0 & -4.526e3 \end{bmatrix}, \begin{bmatrix} 0 & 9.74e2 & 0 & -1.17e2 \\ 0 & -1.84e4 & 0 & 1.012e3 \\ 0 & 1.167e2 & 0 & 9.74e2 \\ 0 & -1.0117e3 & 0 & -1.839e4 \end{bmatrix}\right)
$$

$$
B_{c_1} = \text{diag}\left(\begin{bmatrix} 3.24e2 & 3.23e1 \\ -3.217e3 & -3.6157e3 \\ -3.0583e1 & 3.227e2 \\ 3.618e3 & -3.158e3 \end{bmatrix}, \begin{bmatrix} -1.518e2 & 7.034e2 \\ 5.711e3 & -1.1076e4 \\ -7.0023e2 & -1.577e2 \\ 1.101e4 & 5.8155e3 \end{bmatrix}, \begin{bmatrix} 3.066e2 & 1.8206e2 \\ 1.206e3 & -5.15e3 \\ -1.832e2 & 3.052e2 \\ 5.16e3 & 1.2445e3 \end{bmatrix}\right)
$$

$$
C_c = \text{diag}\left(\begin{bmatrix} 4.9264 & 2.58 \\ 2.2890 & 3.926 \\ -2.5786 & 4.926 \\ -3.9323 & 2.287 \end{bmatrix}^T, \begin{bmatrix} 8.0376 & 3.368 \\ -5.73 & 6.8521 \\ -3.3725 & 8.0425 \\ -6.82 & -5.776 \end{bmatrix}^T, \begin{bmatrix} 5.532 & 4.6948 \\ -3.081 & 8.642 \\ -4.6955 & 5.516 \\ -8.6424 & -3.0794 \end{bmatrix}^T\right)
$$

$$
D_{c_1} = \text{diag}\left(\begin{bmatrix} 6.8763 & -9.899e-1 \\ 1.0153 & 6.871 \end{bmatrix}, \begin{bmatrix} 2.9976e1 & -2.243 \\ 2.3468 & 3.0213e1 \end{bmatrix}, \begin{bmatrix} 1.728e1 & -1.156 \\ 1.163 & 1.7314e1 \end{bmatrix}\right)
$$

$$(7.24)$$
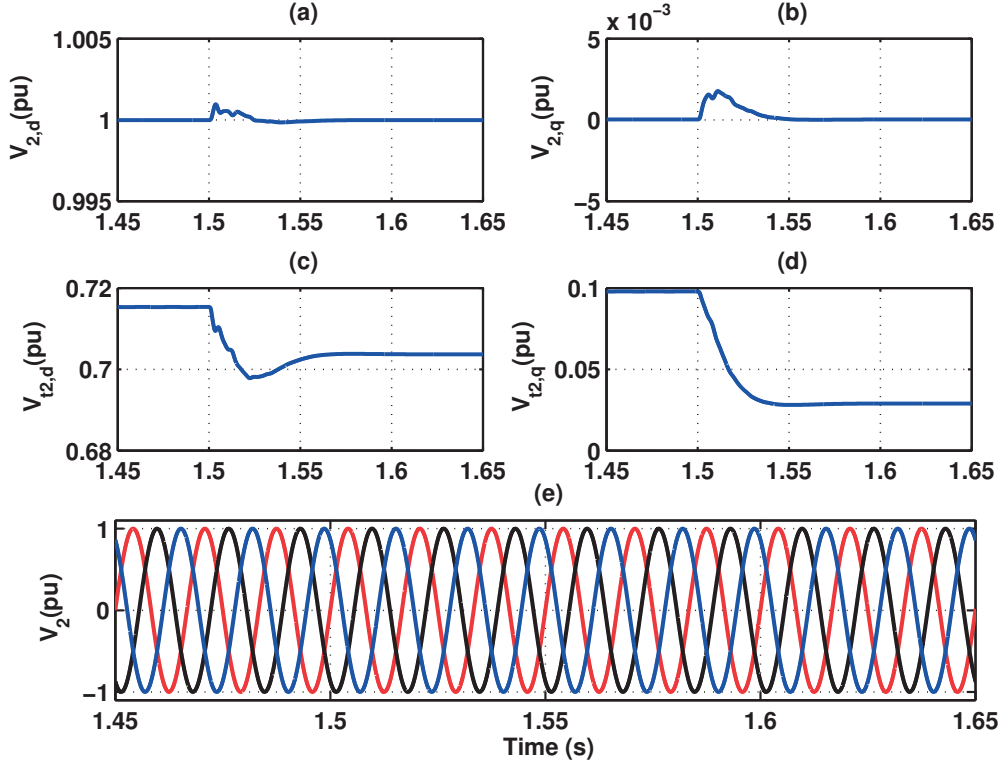
Figure 7.10: Reference setpoint tracking of DG 2: (a) d-component of the load voltage at PCC 2, (b) q-component of the load voltage at PCC 2, (c) d-component of the control signal of DG 2, (d) q-component of the control signal of DG 2, and (e) instantaneous load voltages at PCC 2

The above controller provides the spectral abscissa $\beta = -4.9219$. The decentralized feedforward term of the controller is resulted after 2 iterations:

$$
B_{c_2} = \mathrm{diag}\left(\begin{bmatrix} 162.22 & -138.43 \\ 27.298 & 15.629 \\ 140.24 & 163.68 \\ -15.459 & 27.16 \end{bmatrix}, \begin{bmatrix} 315.49 & 117.7 \\ -27.581 & 60.459 \\ -117.98 & 317.01 \\ -59.828 & -28.427 \end{bmatrix}, \begin{bmatrix} 351.9 & -96.812 \\ 18.278 & 19.767 \\ 96.12 & 352.65 \\ -19.944 & 18.106 \end{bmatrix}\right)
$$
$$
D_{c_2} = \mathrm{diag}\left(\begin{bmatrix} 0.085 & -0.014 \\ 0.013 & 0.086 \end{bmatrix}, \begin{bmatrix} 0.010 & -0.336 \\ 0.335 & 0.007 \end{bmatrix}, \begin{bmatrix} 0.367 & -0.009 \\ 0.008 & 0.369 \end{bmatrix}\right)
$$
(7.25)

The 2DOF feedback-feedforward controller guarantees the robust stability as well as the robust performance criterion $\|W_s S(\lambda)\|_\infty < 1.547$ for the whole polytope.

Simulation Results: To evaluate the performance of the designed controller, we consider the capability of the nominal system in voltage setpoint tracking of each DGs. We assume that the load voltages at PCCs are initially regulated at $1\angle 0°$. Then, the output power of DG 2 varies due to a change in its local load. Since all three DGs contribute to compensate the
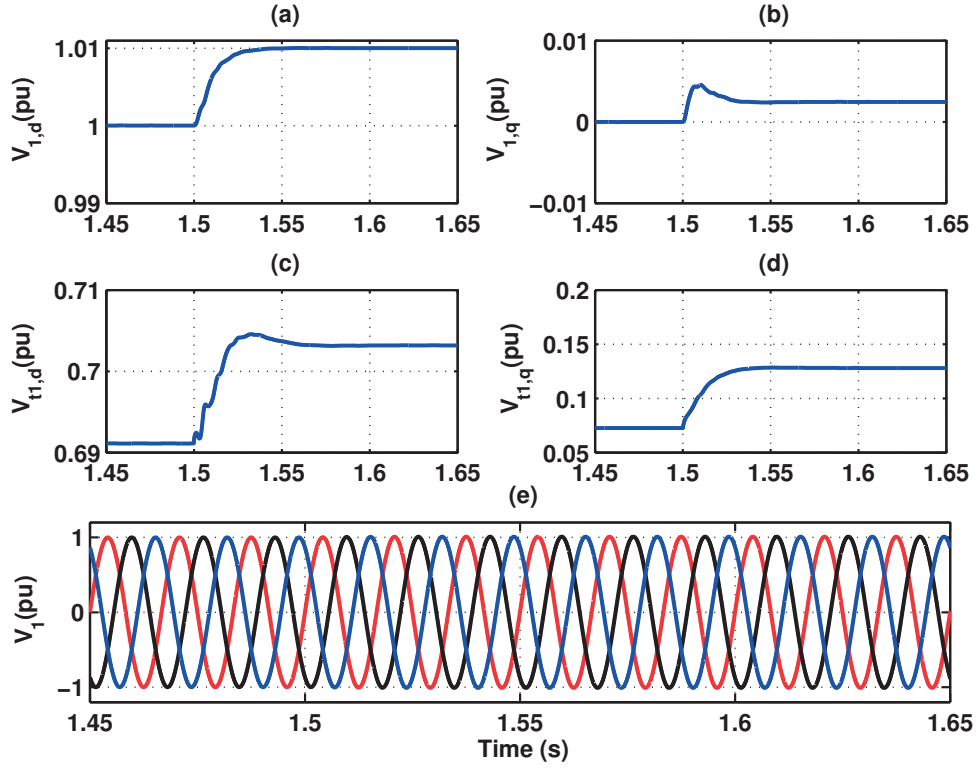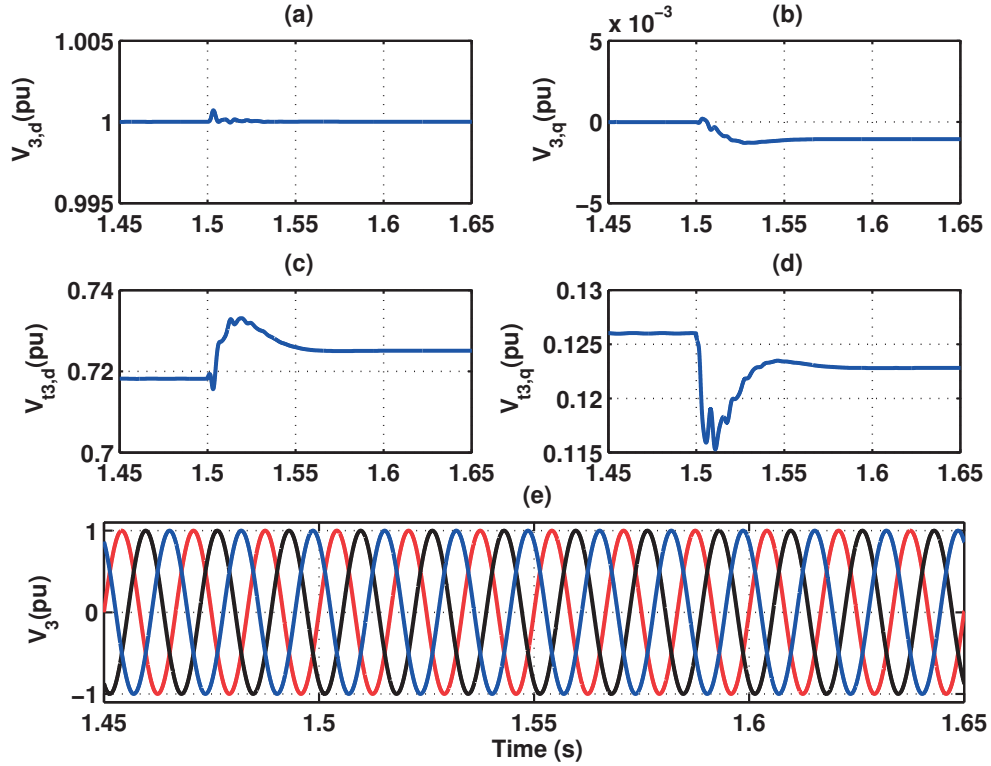
Figure 7.11: Reference setpoint tracking of DG 3: (a) d-component of the load voltage at PCC 3, (b) q-component of the load voltage at PCC 3, (c) d-component of the control signal of DG 3, (d) q-component of the control signal of DG 3, and (e) instantaneous load voltages at PCC 3

total power demand, the PMS determines the following new setpoints for each DG at $t = 1.5s$: $V_{1,dq_{ref}} = 1.01\angle 0.14°$, $V_{2,dq_{ref}} = 1\angle 0°$, and $V_{3,dq_{ref}} = 1\angle -0.06°$. Fig. 7.9, Fig. 7.10, and Fig. 7.11 show the transient response of each DG due to the setpoint change. The results demonstrate that the proposed controller provides satisfactory dynamic performance according to IEEE standards [173].

Remark. Two-stage 2DOF control design restricts the achievable performance compared to a simultaneous design [69]. However, due to the size of system and number of vertices in the microgrid case study, SDP solvers encounter numerical problems in the design of one-stage 2DOF H_∞ control through the convex optimization problem in (5.34). Therefore, the 2DOF decentralized voltage controller for the microgrid system is designed in two steps.

7.6 Conclusion

This chapter presents a control strategy for autonomous inverter-interfaced microgrids composed of distributed generation units with radial configuration. It mainly consists of three

parts: a power management system (PMS), an open-loop frequency control and a synchronization scheme, and local voltage controllers. The power management system assigns the terminal voltage setpoints for DGs according to a classical power flow analysis. Frequency of the microgrid is controlled in an open-loop manner by the use of an internal oscillator for each DG which also generates the phase-angle waveform $\theta(t)$ required for dq/abc (abc/dq) transformations. Synchronization of DGs is achieved by exploiting a GPS-based time-reference signal. The local voltage controller of each DG, which is the main focus of the chapter, is designed through the proposed results in Chapter 3 and Chapter 5.

The prominent features of the proposed control strategy are severalfold: (i) The PMS precisely controls power flow of the system and achieves a prescribed load sharing among the DGs, (ii) Local controllers provide voltage tracking with fast transient time and small overshoot, (iii) Local controllers are robust to load parameter uncertainties, (iv) Local controllers are implemented in a decentralized manner which obviates the need for a high-bandwidth communication and information exchange among the local controllers of DGs, (v) Local controllers are low-order and structurally simple, and (vi) frequency of the microgrid system is fixed and cannot deviate due to transients.

The effectiveness of the proposed control technique is evaluated through some simulation studies in MATLAB and some Hardware-In-the-Loop (HIL) verifications. The simulation and experimental results demonstrate satisfactory dynamic performance of the islanded microgrid system in terms of load voltage regulation and robustness to step changes in linear loads.

The proposed voltage control approach in this chapter cannot cope with challenging problem of plug-and-play (PnP) functionality of DGs. Under plug-in/-out operation, the proposed control strategy, which relies on the microgrid model, needs to retune the local controllers in order to guarantee the stability of the new system. In the next chapter, a decentralized voltage control technique is developed which enables PnP operations of DGs. The controller is robust with respect to PnP functionality and does not require to retune the local controllers when a DG is plugged in/out.

8 Voltage Control of Islanded Micro-grids with General Topology

8.1 Introduction

A challenging problem in the context of inverter-interfaced microgrids is plug-and-play (PnP) functionality of DGs. DGs frequently join and leave power generation systems due to availability and intermittency of renewable energies, such as solar power and wind, an increase in energy demand, faults, converter failure, maintenance, etc. Under plug-in/-out feature of DGs, the topology of the microgrid system is changed and the main objective is to preserve the stability of the new system.

The main advantage of the droop-based control strategy is the elimination of the communication links among droop controllers enabling the plug-and-play operation of DGs. Nonetheless, the droop-based approaches suffer from several drawbacks including poor transient performance, load-dependent frequency/voltage deviation, and coupled dynamics between active and reactive power. Moreover, the main assumption about the droop controllers is that the transmission lines are purely inductive or resistive [9]. Therefore, in the case of resistive-inductive line conditions (mixed lines) and in the presence of conductances, the classical droop control laws cannot achieve an efficient power sharing due to the coupled active and reactive power characteristics of the power systems [111].

Under PnP functionality of DGs, non-droop-based controllers, which rely on the system model, need to retune their local controllers in order to guarantee the stability of the new system. Recently, a decentralized control strategy has been developed in [130, 131] which is based on a Quasi-Stationary Line (QSL) approximate model of microgrids [174] and the idea of neutral interactions [175]. According to this control technique, when a DG is plugged in and/or plugged out, the other DGs which are physically connected to it have to retune their local controllers. Although the control strategy almost bridges the gap between the existing droop and non-droop-based controllers, the problem of non-droop-based control of the inverter-interfaced microgrids enabling the PnP functionality of DGs without a need for retuning their local controllers can still benefit from further research.

This chapter focuses on the design of a decentralized voltage controller for the islanded inverter-interfaced microgrids with general topology. The microgrid system consists of different local loads and several DGs. It is also expected that some of DGs can be arbitrarily plugged in or plugged out from the microgrid system. The main objective is to preserve the voltage stability at the PCCs in a decentralized manner, i.e. with no communication links among the local controllers of DGs. To this end, a decentralized voltage controller is developed. Similar to [131], the proposed method relies on the Quasi-Stationary Line (QSL) approximate model of microgrids and the concept of neutral interactions. The main contribution of this chapter is that the proposed controller is robust to PnP operation of DGs; therefore, the plug-in and/or plug-out operation of DGs do not affect the stability of the microgrid system. To this end, all possible connections and disconnections of DGs to a DG are considered as polytopic-type uncertainty. Then, a robust controller is designed for the microgrid system subject to the polytopic uncertainty.

In summary, the proposed control technique is able to overcome the limitations of existing droop-based controllers which are only appropriate for microgrids with dominantly inductive and/or resistive power lines. Furthermore, opposed to most non-droop-based control methods, e.g. [126, 129–131], the present approach does not require to retune the local controllers when a DG is plugged in/out.

The organization of the chapter is as follows: The mathematical model of the microgrid is presented in Section 8.2. The problem of decentralized voltage controller design is proposed in Section 8.3. A solution for the problem of plug-and-play operation of DGs in the microgrids is given in Section 8.4. Section 8.5 is devoted to simulation results. Section 8.6 concludes the chapter.

Throughout the chapter, matrices I and 0 are the identity matrix and the zero matrix of appropriate dimensions, respectively. The symbols T and $\star$ denote the matrix transpose and a symmetric block, respectively. Signals X_d and X_q are the d and q components of the three-phase signal X, respectively. For symmetric matrices, $P > 0$ ($P < 0$) indicates the positive-definiteness (the negative-definiteness).

8.2   Islanded Microgrid Model

Consider an islanded microgrid with general structure consisting of N DGs. Each DG is modeled as a DC voltage source, a voltage-source converter (VSC), a series RL filter, a step-up transformer with transformation ratio k_i, a shunt capacitor, and a local load whose topology and parameters are unknown. It is assumed that DG i is connected to a set of $N_i \subset \{1,\dots,N\}$ DGs. The schematic diagram of a microgrid system of two DGs i, j connected through a transmission line ij is shown in Fig. 8.1. In this figure, V_i, I_{t_i}, I_{L_i}, V_{t_i}, and I_{ij} are the load voltage at PCC i, the filter current, the load current, the VSC terminal voltage, and the transmission line current, respectively. The islanded system is described by the following dynamical equations
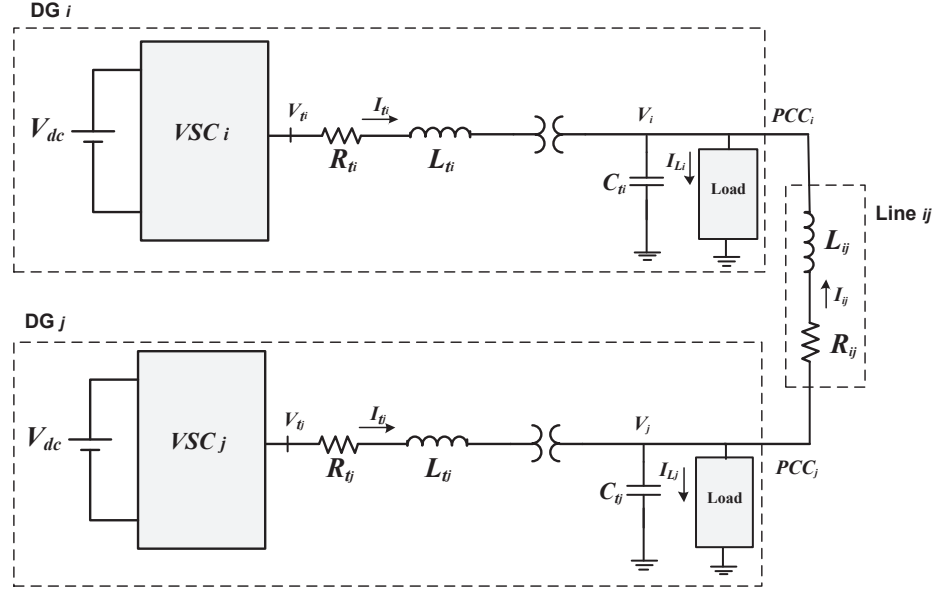
Figure 8.1: Electrical scheme of two DGs connected via line ij

in dq-frame:

$$\text{DG } i \begin{cases} \frac{dV_{i,dq}}{dt} + j\omega_0 V_{i,dq} = \frac{k_i}{C_{ti}} I_{ti,dq} - \frac{1}{C_{ti}} I_{L_i,dq} + \frac{1}{C_{ti}} I_{ij,dq} \\ \frac{dI_{ti,dq}}{dt} + j\omega_0 I_{ti,dq} = -\frac{k_i}{L_{ti}} V_{i,dq} - \frac{R_{ti}}{L_{ti}} I_{ti,dq} + \frac{1}{L_{ti}} V_{ti,dq} \end{cases} \tag{8.1}$$

$$\text{DG } j \begin{cases} \frac{dV_{j,dq}}{dt} + j\omega_0 V_{j,dq} = \frac{k_j}{C_{tj}} I_{tj,dq} - \frac{1}{C_{tj}} I_{L_j,dq} - \frac{1}{C_{tj}} I_{ij,dq} \\ \frac{dI_{tj,dq}}{dt} + j\omega_0 I_{tj,dq} = -\frac{k_j}{L_{tj}} V_{j,dq} - \frac{R_{tj}}{L_{tj}} I_{tj,dq} + \frac{1}{L_{tj}} V_{tj,dq} \end{cases} \tag{8.2}$$

$$\text{Line } ij: \quad \frac{dI_{ij,dq}}{dt} + j\omega_0 I_{ij,dq} = -\frac{R_{ij}}{L_{ij}} I_{ij,dq} + \frac{1}{L_{ij}} V_{j,dq} - \frac{1}{L_{ij}} V_{i,dq} \tag{8.3}$$

where $\left(V_{i,dq}, V_{j,dq}\right)$, $\left(I_{ti,dq}, I_{tj,dq}\right)$, $\left(I_{L_i,dq}, I_{L_j,dq}\right)$, $\left(V_{ti,dq}, V_{tj,dq}\right)$, and $I_{ij,dq}$ respectively are the dq components of the load voltages at PCCs, the current filters, the load currents, the VSC terminal voltages, and the transmission line current. It should be noted that in this study the dynamics of the renewable energy sources are not considered and they are just modeled by an ideal voltage source.

Under the assumption of the Quasi-Stationary Line (QSL) [174], i.e. $\frac{dI_{ij,dq}}{dt} = 0$, the islanded microgrid system is described in the following state space framework:

$$\begin{aligned} \dot{x}_{g_i} &= A_{g_{ii}} x_{g_i} + A_{g_{ij}} x_{g_j} + B_{g_i} u_i + B_{w_i} w_i \\ y_i &= C_{g_i} x_{g_i}; \quad i = 1,\dots,N \end{aligned} \tag{8.4}$$

139

where $x_{g_i} = \begin{bmatrix} V_{i,d} & V_{i,q} & I_{t_i,d} & I_{t_i,q} \end{bmatrix}^T$ is the state, $u_i = \begin{bmatrix} V_{t_i,d} & V_{t_i,q} \end{bmatrix}^T$ is the input, $w_i = \begin{bmatrix} I_{L_i,d} & I_{L_i,q} \end{bmatrix}^T$ is the exogenous input, and $y_i = \begin{bmatrix} V_{i,d} & V_{i,q} \end{bmatrix}^T$ is the output of DG i. The state space matrices are given as follows [131]:

$$A_{g_{ii}} = \begin{bmatrix} -\frac{1}{C_{t_i}} \sum_{j \in N_i} \frac{R_{ij}}{Z_{ij}^2} & \omega_0 - \frac{1}{C_{t_i}} \sum_{j \in N_i} \frac{X_{ij}}{Z_{ij}^2} & \frac{k_i}{C_{t_i}} & 0 \\ -\omega_0 + \frac{1}{C_{t_i}} \sum_{j \in N_i} \frac{X_{ij}}{Z_{ij}^2} & -\frac{1}{C_{t_i}} \sum_{j \in N_i} \frac{R_{ij}}{Z_{ij}^2} & 0 & \frac{k_i}{C_{t_i}} \\ -\frac{k_i}{L_{t_i}} & 0 & -\frac{R_{t_i}}{L_{t_i}} & \omega_0 \\ 0 & -\frac{k_i}{L_{t_i}} & -\omega_0 & -\frac{R_{t_i}}{L_{t_i}} \end{bmatrix}$$

$$A_{g_{ij}} = \frac{1}{C_{t_i}} \begin{bmatrix} \frac{R_{ij}}{Z_{ij}^2} & \frac{X_{ij}}{Z_{ij}^2} & 0 & 0 \\ -\frac{X_{ij}}{Z_{ij}^2} & \frac{R_{ij}}{Z_{ij}^2} & 0 & 0 \\ 0 & 0 & 0 & 0 \\ 0 & 0 & 0 & 0 \end{bmatrix},$$

$$B_{g_i} = \begin{bmatrix} 0 & 0 \\ 0 & 0 \\ \frac{1}{L_{t_i}} & 0 \\ 0 & \frac{1}{L_{t_i}} \end{bmatrix}, \quad B_{w_i} = \begin{bmatrix} -\frac{1}{C_{t_i}} & 0 \\ 0 & -\frac{1}{C_{t_i}} \\ 0 & 0 \\ 0 & 0 \end{bmatrix}$$

$$C_{g_i} = \begin{bmatrix} 1 & 0 & 0 & 0 \\ 0 & 1 & 0 & 0 \end{bmatrix}$$

(8.5)

where $\omega_0 = 2\pi f_0$ (f_0 is the nominal frequency of the microgrid), $X_{ij} = \omega_0 L_{ij}$, and $Z_{ij}^2 = R_{ij}^2 + \omega_0^2 L_{ij}^2$. The dynamics of the transmission lines are described by the following equations:

$$\dot{x}_{l,ij} = A_{ll,ij} x_{l,ij} + A_{l_i,ij} x_{g_i} + A_{l_j,ij} x_{g_j} \tag{8.6}$$

for $i = 1, 2, \dots, N$, $j \in N_i$, $i \neq j$, where

$$x_{l,ij} = \begin{bmatrix} I_{ij,d} & I_{ij,q} \end{bmatrix}^T \tag{8.7}$$

and

$$A_{l_i,ij} = \begin{bmatrix} -\frac{1}{L_{ij}} & 0 & 0 & 0 \\ 0 & -\frac{1}{L_{ij}} & 0 & 0 \end{bmatrix}$$

$$A_{l_j,ij} = \begin{bmatrix} \frac{1}{L_{ij}} & 0 & 0 & 0 \\ 0 & \frac{1}{L_{ij}} & 0 & 0 \end{bmatrix}$$

$$A_{ll,ij} = \begin{bmatrix} -\frac{R_{ij}}{L_{ij}} & \omega_0 \\ -\omega_0 & -\frac{R_{ij}}{L_{ij}} \end{bmatrix}$$

(8.8)

The overall microgrid system in Fig. 8.1. is modelled as follows:

$$
\begin{bmatrix} \dot{x}_{g_i} \\ \dot{x}_{g_j} \\ \dot{x}_{l,ij} \\ \dot{x}_{l,ji} \end{bmatrix} = \underbrace{\begin{bmatrix} A_{g_{ii}} & A_{g_{ij}} & 0 & 0 \\ A_{g_{ji}} & A_{g_{jj}} & 0 & 0 \\ A_{l_{i,ij}} & A_{l_{j,ij}} & A_{ll,ij} & 0 \\ A_{l_{i,ji}} & A_{l_{j,ji}} & 0 & A_{ll,ji} \end{bmatrix}}_{A_{ij}} \begin{bmatrix} x_{g_i} \\ x_{g_j} \\ x_{l,ij} \\ x_{l,ji} \end{bmatrix} + \begin{bmatrix} B_{g_i} & 0 \\ 0 & B_{g_j} \\ 0 & 0 \\ 0 & 0 \end{bmatrix} \begin{bmatrix} u_i \\ u_j \end{bmatrix}
$$

$$
+ \begin{bmatrix} B_{w_i} & 0 \\ 0 & B_{w_j} \\ 0 & 0 \\ 0 & 0 \end{bmatrix} \begin{bmatrix} w_i \\ w_j \end{bmatrix}
\tag{8.9}
$$

$$
\begin{bmatrix} y_i \\ y_j \end{bmatrix} = \begin{bmatrix} C_{g_i} & 0 & 0 & 0 \\ 0 & C_{g_j} & 0 & 0 \end{bmatrix} \begin{bmatrix} x_{g_i} \\ x_{g_j} \\ x_{l,ij} \\ x_{l,ji} \end{bmatrix}
$$

It should be noted that due to block triangular structure of matrix A_{ij} and stability of $A_{ll,ij} = A_{ll,ji}$, the stability of the following system leads to stability of (8.9).

$$
\begin{bmatrix} \dot{x}_{g_i} \\ \dot{x}_{g_j} \end{bmatrix} = \begin{bmatrix} A_{g_{ii}} & A_{g_{ij}} \\ A_{g_{ji}} & A_{g_{jj}} \end{bmatrix} \begin{bmatrix} x_{g_i} \\ x_{g_j} \end{bmatrix} + \begin{bmatrix} B_{g_i} & 0 \\ 0 & B_{g_j} \end{bmatrix} \begin{bmatrix} u_i \\ u_j \end{bmatrix} + \begin{bmatrix} B_{w_i} & 0 \\ 0 & B_{w_j} \end{bmatrix} \begin{bmatrix} w_i \\ w_j \end{bmatrix}
$$

$$
\begin{bmatrix} y_i \\ y_j \end{bmatrix} = \begin{bmatrix} C_{g_i} & 0 \\ 0 & C_{g_j} \end{bmatrix} \begin{bmatrix} x_{g_i} \\ x_{g_j} \end{bmatrix}
\tag{8.10}
$$

Therefore, in what follows, we consider the dynamics of DGs interconnected through the QSL model given in (8.4)-(8.5).

8.2.1 QSL-based Model of Islanded Microgrids with N DGs

In a similar way, the overall model of the islanded microgrid system of N DGs can be described in the state space framework as follows:

$$
\begin{bmatrix} \dot{x}_{g_1} \\ \dot{x}_{g_2} \\ \vdots \\ \dot{x}_{g_N} \end{bmatrix} = \begin{bmatrix} A_{g_{11}} & A_{g_{12}} & \cdots & A_{g_{1N}} \\ A_{g_{21}} & A_{g_{22}} & \cdots & A_{g_{2N}} \\ \vdots & \vdots & \ddots & \vdots \\ A_{g_{N1}} & A_{g_{N2}} & \cdots & A_{g_{NN}} \end{bmatrix} \begin{bmatrix} x_{g_1} \\ x_{g_2} \\ \vdots \\ x_{g_N} \end{bmatrix} + \begin{bmatrix} B_{g_1} & 0 & \cdots & 0 \\ 0 & B_{g_2} & \cdots & 0 \\ \vdots & \vdots & \ddots & \vdots \\ 0 & 0 & \cdots & B_{g_N} \end{bmatrix} \begin{bmatrix} u_1 \\ u_2 \\ \vdots \\ u_N \end{bmatrix}
$$

$$
+ \begin{bmatrix} B_{w_1} & 0 & \cdots & 0 \\ 0 & B_{w_2} & \cdots & 0 \\ \vdots & \vdots & \ddots & \vdots \\ 0 & 0 & \cdots & B_{w_N} \end{bmatrix} \begin{bmatrix} w_1 \\ w_2 \\ \vdots \\ w_N \end{bmatrix} \tag{8.11}
$$

$$
\begin{bmatrix} y_1 \\ y_2 \\ \vdots \\ y_N \end{bmatrix} = \begin{bmatrix} C_{g_1} & 0 & \cdots & 0 \\ 0 & C_{g_2} & \cdots & 0 \\ \vdots & \vdots & \ddots & \vdots \\ 0 & 0 & \cdots & C_{g_N} \end{bmatrix} \begin{bmatrix} x_{g_1} \\ x_{g_2} \\ \vdots \\ x_{g_N} \end{bmatrix}
$$

where matrices $A_{g_{ii}}$, $A_{g_{ij}}$, B_{g_i}, B_{w_i}, and C_{g_i} (for $i, j = 1, 2, \ldots, N$) are defined in (8.5). Matrix $A_{g_{ij}} = 0$ if and only if there exists no connection between DG i and DG j. The frequency of the microgrid system is controlled via the approach explained in Chapter 7, Section 7.3.2.

8.3 Decentralized Voltage Control of Islanded Microgrids

This section focuses on the development of a voltage control strategy for autonomous microgrids. It can be applied to the microgrids with different types of configuration. The main emphasis is given to decentralized voltage control techniques which do not use any communication links.

8.3.1 Design Requirements

A *dq*-based voltage controller for the islanded inverter-interfaced microgrid described in (8.11) is sought such that the following conditions are met:

- The controller has a fully decentralized structure.

- The closed-loop system is asymptotically stable.

- The closed-loop system asymptotically tracks all voltage reference signals y_{ref_i} with desired time-domain performance.

In the following, a decentralized voltage controller with integral action is developed in order to achieve the mentioned conditions.

8.3.2 Decentralized Voltage Controllers

One of the control requirements is that DGs must track reference voltage signals y_{ref_i}. To this end, each DG is augmented with an integrator whose dynamics are as follows:

$$\begin{aligned} \dot{v}_i &= y_{ref_i} - y_i \\ &= y_{ref_i} - C_{g_i} x_{g_i} \end{aligned} \tag{8.12}$$

Therefore, the augmented DG system is described by:

$$\begin{aligned} \dot{\hat{x}}_{g_i} &= \hat{A}_{g_{ii}} \hat{x}_{g_i} + \sum_{j \in N_i} \hat{A}_{g_{ij}} \hat{x}_{g_j} + \hat{B}_{g_i} u_i + \hat{B}_{w_i} \hat{w}_i \\ \hat{y}_i &= \hat{C}_{g_i} \hat{x}_{g_i} \end{aligned} \tag{8.13}$$

where $\hat{x}_{g_i} = \begin{bmatrix} x_{g_i}^T & v_i^T \end{bmatrix}^T$, $\hat{y}_i = \begin{bmatrix} y_i^T & v_i^T \end{bmatrix}^T$, $\hat{w}_i = \begin{bmatrix} w_i^T & y_{ref_i}^T \end{bmatrix}^T$, and

$$\begin{aligned} \hat{A}_{g_{ii}} &= \begin{bmatrix} A_{g_{ii}} & 0 \\ -C_{g_i} & 0 \end{bmatrix}, \quad \hat{A}_{g_{ij}} = \begin{bmatrix} A_{g_{ij}} & 0 \\ 0 & 0 \end{bmatrix} \\ \hat{B}_{g_i} &= \begin{bmatrix} B_{g_i} \\ 0 \end{bmatrix}, \quad \hat{B}_{w_i} = \begin{bmatrix} B_{w_i} & 0 \\ 0 & I \end{bmatrix} \\ \hat{C}_{g_i} &= \begin{bmatrix} C_{g_i} & 0 \\ 0 & I \end{bmatrix} \end{aligned} \tag{8.14}$$

The remaining of this subsection belong to the design of decentralized voltage controllers K_i with the following control laws:

$$u_i(t) = K_i \hat{x}_{g_i}(t); \quad i = 1, 2, \dots, N \tag{8.15}$$

The closed-loop dynamics of the ith augmented subsystem with the local controller K_i are described as follows:

$$\begin{aligned} \dot{\hat{x}}_{g_i}(t) &= \left(\hat{A}_{g_{ii}} + \hat{B}_{g_i} K_i \right) \hat{x}_{g_i}(t) + \sum_{j \in N_i} \hat{A}_{g_{ij}} \hat{x}_{g_j}(t) + \hat{B}_{w_i} \hat{w}_i(t) \\ \hat{y}_i(t) &= \hat{C}_{g_i} \hat{x}_{g_i}(t) \end{aligned} \tag{8.16}$$

The overall closed-loop system is presented as follows:

$$\begin{aligned} \dot{\hat{x}}(t) &= \left(\hat{A} + \hat{B} K \right) \hat{x} + \hat{B}_w \hat{w}(t) \\ \hat{y}(t) &= \hat{C} \hat{x}(t) \end{aligned} \tag{8.17}$$

where $\hat{x} = \left[\hat{x}_{g_1}^T \ldots \hat{x}_{g_N}^T\right]^T$, $\hat{w} = \left[\hat{w}_1^T \ldots \hat{w}_N^T\right]^T$, $\hat{y} = \left[\hat{y}_1^T \ldots \hat{y}_N^T\right]^T$, $\hat{z} = \left[\hat{z}_1^T \ldots \hat{z}_N^T\right]^T$, and

$$
\begin{aligned}
\hat{A} &= \begin{bmatrix}
\hat{A}_{g_{11}} & \hat{A}_{g_{12}} & \cdots & \hat{A}_{g_{1N}} \\
\hat{A}_{g_{21}} & \hat{A}_{g_{22}} & \cdots & \hat{A}_{g_{2N}} \\
\vdots & \vdots & \ddots & \vdots \\
\hat{A}_{g_{N1}} & \hat{A}_{g_{N2}} & \cdots & \hat{A}_{g_{NN}}
\end{bmatrix} \\
\hat{B} &= \operatorname{diag}\left(\hat{B}_{g_1}, \ldots, \hat{B}_{g_N}\right) \\
\hat{B}_w &= \operatorname{diag}\left(\hat{B}_{w_1}, \ldots, \hat{B}_{w_N}\right) \\
\hat{C} &= \operatorname{diag}\left(\hat{C}_{g_1}, \ldots, \hat{C}_{g_N}\right) \\
K &= \operatorname{diag}\left(K_1, \ldots, K_N\right)
\end{aligned}
\tag{8.18}
$$

The state feedback controller is designed via the following theorem which is based on the use of slack variables [176].

Theorem 19. *There exists a state feedback controller K which stabilizes an open-loop system $G(s) = \left(\hat{A}, \hat{B}, \hat{C}, 0\right)$ if and only if there exist a symmetric matrix $P = P^T > 0$, slack matrices G, Y, and a positive scalar ϵ such that the following conditions hold:*

$$
\begin{bmatrix}
\hat{A}G + G^T \hat{A}^T + \hat{B}Y + Y^T \hat{B}^T & P - G^T + \epsilon\left(G^T \hat{A}^T + Y^T \hat{B}^T\right)^T \\
P - G + \epsilon\left(G^T \hat{A}^T + Y^T \hat{B}^T\right) & -\epsilon\left(G + G^T\right)
\end{bmatrix} < 0
\tag{8.19}
$$

Moreover, the state feedback gain is presented as $K = YG^{-1}$.

If the coupling terms $\sum_{j \in N_i} \hat{A}_{g_{ij}} \hat{x}_{g_j}$ are neglected, according to Theorem 19, the augmented subsystem of each DG $\left(\hat{A}_{g_{ii}}, \hat{B}_{g_i}, \hat{C}_{g_i}, 0\right)$ with the state feedback gain K_i is stable if and only if there exist Lyapunov matrices $P_i = P_i^T > 0$ and slack variables $G_i, Y_i, \epsilon_i > 0$ such that

$$
\begin{bmatrix}
\hat{A}_{g_{ii}} G_i + G_i^T \hat{A}_{g_{ii}}^T + \hat{B}_{g_i} Y_i + Y_i^T \hat{B}_{g_i}^T & P_i - G_i^T + \epsilon_i\left(G_i^T \hat{A}_{g_{ii}}^T + Y_i^T \hat{B}_{g_i}^T\right)^T \\
P_i - G_i + \epsilon_i\left(G_i^T \hat{A}_{g_{ii}}^T + Y_i^T \hat{B}_{g_i}^T\right) & -\epsilon_i\left(G_i + G_i^T\right)
\end{bmatrix} < 0
\tag{8.20}
$$

for $i = 1, \ldots, N$. The local state feedback controllers are presented as $K_i = Y_i G_i^{-1}$; $i = 1, \ldots, N$. However, the interaction terms have significant effects on the stability of the closed-loop system and decentralized design of the local controllers cannot generally guarantee the stability of the whole system, i.e. $\hat{A}$. In the next subsection, we show that under some specific conditions, the stability conditions given in (8.20) lead to the overall closed-loop asymptotic stability.

8.3.3 Decentralized Voltage Control based on Neutral Interactions

In this subsection, a decentralized voltage controller design strategy is presented. The main objective is to design the local controllers individually without considering the interaction terms such that the asymptotic stability of the closed-loop microgrid system is guaranteed.

To this end, the idea of neutral interaction [175] is used. The interaction terms are neutral with respect to the stability criterion in (8.19) if and only if the interaction matrix $\hat{A}_c = \hat{A} - \hat{A}_d$, where $\hat{A}_d = \text{diag}\left(\hat{A}_{g_{11}}, \ldots, \hat{A}_{g_{NN}}\right)$, is factorized as follows:

$$\hat{A}_c = G^T S \tag{8.21}$$

where G is the slack matrix in (8.19) and S is a skew-symmetric matrix, i.e. $S^T = -S$.

Under the following conditions, the interaction terms in the augmented microgrid model described by (8.17)-(8.18) are neutral.

1. $C_{t_i} = C_s$ for $i = 1, \ldots, N$.

2. The local state feedback controllers K_i satisfy the stability conditions given in (8.20) with the following fixed-structure slack matrices G_i:

$$G_i = \left[\begin{array}{c|c} \eta I_{2\times 2} & 0 \\ \hline 0 & G_{22_i} \end{array} \right]; \quad i = 1, \ldots, N \tag{8.22}$$

where $\eta > 0$ is a common parameter among all G_i, $i = 1, \ldots, N$ and matrices G_{22_i} are of appropriate dimensions.

3. $\frac{\eta R_{ij}}{C_s Z_{ij}^2} \approx 0$ for $i = 1, \ldots, N$ and $j \in N_i$.

If the above mentioned conditions hold, the interaction term $\hat{A}_c G + G^T \hat{A}_c^T \approx 0$, where $G = \text{diag}\left(G_1, \ldots, G_N\right)$ because

$$\hat{A}_{g_{ij}} G_j = \left[\begin{array}{c|c} \Phi_{ij} & 0 \\ \hline 0 & 0 \end{array} \right] \tag{8.23}$$

where $\Phi_{ij} = \left[\begin{array}{cc} \frac{\eta R_{ij}}{C_s Z_{ij}^2} & \frac{\eta X_{ij}}{C_s Z_{ij}^2} \\ -\frac{\eta X_{ij}}{C_s Z_{ij}^2} & \frac{\eta R_{ij}}{C_s Z_{ij}^2} \end{array} \right] \approx \left[\begin{array}{cc} 0 & \frac{\eta X_{ij}}{C_s Z_{ij}^2} \\ -\frac{\eta X_{ij}}{C_s Z_{ij}^2} & 0 \end{array} \right].$

8.3.4 Pre-filter Design & Disturbance Rejection Strategy

Under the conditions 1-3 in Subsection 8.3.3, the decentralized state feedback controllers K_i designed by (8.20) guarantee the stability of the closed-loop microgrid system. However, to improve the performance of the system in terms of dynamics behaviour for voltage reference tracking and disturbance rejection, the local controllers are modified. The modification procedure are based on the use of a three-degree-of-freedom (3DOF) controller whose structure is shown in Fig. 8.2. The feedforward controller K_r^i is designed to improve reference tracking performance whereas K_d^i aims to attenuate the effects from the disturbance w_i on the output
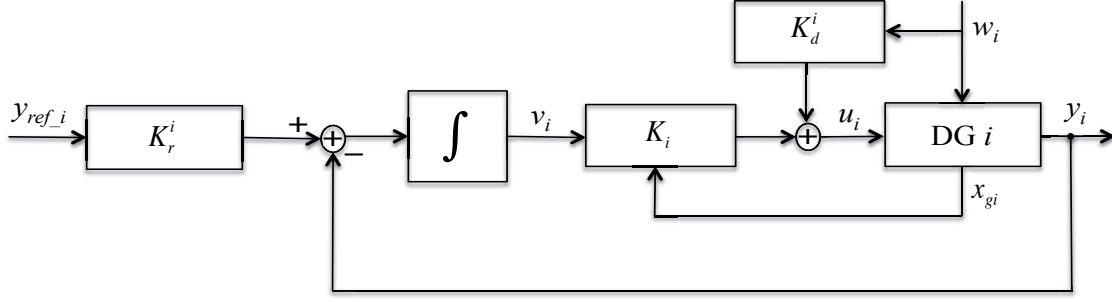
Figure 8.2: Block diagram of 3DOF controller

signals. The closed-loop system including the 3DOF controller in Fig. 8.2 is described as follows:

$$y_i = \left(T_i(s) K_r^i(s) \right) y_{ref_i} + \left(H_i(s) K_d^i(s) + H_i^d(s) \right) w_i \tag{8.24}$$

where

$$
\begin{aligned}
T_i(s) &= \hat{C}_{g_i} \left(sI - (\hat{A}_{g_{ii}} + \hat{B}_{g_i} K_i) \right)^{-1} \begin{bmatrix} 0 \\ I \end{bmatrix} \\
H_i(s) &= \hat{C}_{g_i} \left(sI - (\hat{A}_{g_{ii}} + \hat{B}_{g_i} K_i) \right)^{-1} \hat{B}_{g_i} \\
H_i^d(s) &= \hat{C}_{g_i} \left(sI - (\hat{A}_{g_{ii}} + \hat{B}_{g_i} K_i) \right)^{-1} \hat{B}_{w_i}
\end{aligned}
\tag{8.25}
$$

To achieve desired time-domain performance specifications for reference tracking and minimize the effect of load changes on the voltages at PCCs, the controllers $K_r^i(s)$ and $K_d^i(s)$ are respectively designed by means of solving the following optimization problems:

$$\min_{K_r^i} \| T_i(s) K_r^i(s) - T_{d_i}(s) \|_\infty \tag{8.26}$$

$$\min_{K_d^i} \| H_i(s) K_d^i(s) + H_i^d(s) \|_\infty \tag{8.27}$$

where $T_{d_i}(s)$ is a desired reference tracking (reference model) designed according to the desired performance of DG i . To solve the above optimization problems, the MATLAB commands *hinfstruct* and *systune* can be used.

8.4   Plug-and-Play (PnP) Functionality in Microgrids

In this section, the problem of plug-in/-out operation of DGs in the islanded inverter-interfaced microgrids is considered. The objective is to preserve the stability of the microgrid system when several DGs are plugged in and/or plugged out.

8.4.1 Robustness to PnP Functionality of DGs

A new feature is added to the proposed decentralized control strategy which is robustness to PnP functionality of DGs. By virtue of the fact that the connection/disconnection of DG j to/from DG i affects matrix $A_{g_{ii}}$, two cases for each DG are considered: first, maximum possible connections of the DGs to DG i ($N_{i_{max}} \subset \{1,\dots,N\}$) and second, only the connection j with minimum values of $\frac{R_{ij}}{Z_{ij}^2}$ and $\frac{X_{ij}}{Z_{ij}^2}$ among the other connections. Corresponding matrix $A_{g_{ii}}$ for both cases are given as follows:

$$
A_{g_{ii}}^1 = \begin{bmatrix}
-\frac{1}{C_{t_i}} \sum\limits_{j \in N_{i_{max}}} \frac{R_{ij}}{Z_{ij}^2} & \omega_0 - \frac{1}{C_{t_i}} \sum\limits_{j \in N_{i_{max}}} \frac{X_{ij}}{Z_{ij}^2} & \frac{k_i}{C_{t_i}} & 0 \\
-\omega_0 + \frac{1}{C_{t_i}} \sum\limits_{j \in N_{i_{max}}} \frac{X_{ij}}{Z_{ij}^2} & -\frac{1}{C_{t_i}} \sum\limits_{j \in N_{i_{max}}} \frac{R_{ij}}{Z_{ij}^2} & 0 & \frac{k_i}{C_{t_i}} \\
-\frac{k_i}{L_{t_i}} & 0 & -\frac{R_{t_i}}{L_{t_i}} & \omega_0 \\
0 & -\frac{k_i}{L_{t_i}} & -\omega_0 & -\frac{R_{t_i}}{L_{t_i}}
\end{bmatrix}
$$

$$
A_{g_{ii}}^2 = \begin{bmatrix}
-\frac{1}{C_{t_i}} \frac{R_{ij}}{Z_{ij}^2} & \omega_0 - \frac{1}{C_{t_i}} \frac{X_{ij}}{Z_{ij}^2} & \frac{k_i}{C_{t_i}} & 0 \\
-\omega_0 + \frac{X_{ij}}{Z_{ij}^2} & -\frac{1}{C_{t_i}} \frac{R_{ij}}{Z_{ij}^2} & 0 & \frac{k_i}{C_{t_i}} \\
-\frac{k_i}{L_{t_i}} & 0 & -\frac{R_{t_i}}{L_{t_i}} & \omega_0 \\
0 & -\frac{k_i}{L_{t_i}} & -\omega_0 & -\frac{R_{t_i}}{L_{t_i}}
\end{bmatrix}
\tag{8.28}
$$

Therefore, any possible connection/disconnection of DGs to/from DG i belongs to the following polytopic uncertainty domain:

$$
A_{g_{ii}}(\lambda) = \lambda A_{g_{ii}}^1 + (1-\lambda) A_{g_{ii}}^2 \tag{8.29}
$$

where $0 \le \lambda \le 1$. As a result, matrices $\hat{A}_{g_{ii}}$ also have the polytopic uncertainty as follows:

$$
\hat{A}_{g_{ii}}(\lambda) = \lambda \hat{A}_{g_{ii}}^1 + (1-\lambda) \hat{A}_{g_{ii}}^2 \tag{8.30}
$$

where

$$
\hat{A}_{g_{ii}}^1 = \begin{bmatrix} A_{g_{ii}}^1 & 0 \\ -C_{g_i} & 0 \end{bmatrix}, \quad \hat{A}_{g_{ii}}^2 = \begin{bmatrix} A_{g_{ii}}^2 & 0 \\ -C_{g_i} & 0 \end{bmatrix} \tag{8.31}
$$

for $i = 1,\dots,N$.

Now, we aim to design a decentralized state feedback controller for the augmented polytopic system $\left(\hat{A}_{g_{ii}}(\lambda), \hat{B}_{g_i}, \hat{C}_{g_i}, 0 \right)$ by means of the following theorem:

Theorem 20. *If there exist symmetric matrices $P_i^j > 0$, slack matrices G_i, Y_i, and a given scalar $\epsilon_i > 0$ such that the following set of LMIs holds*

$$
\begin{bmatrix}
\hat{A}_{g_{ii}}^j G_i + G_i^T (\hat{A}_{g_{ii}}^j)^T + \hat{B}_{g_i} Y_i + Y_i^T \hat{B}_{g_i}^T & P_i^j - G_i^T + \epsilon_i \left(\hat{A}_{g_{ii}}^j G_i + \hat{B}_{g_i} Y_i \right) \\
P_i^j - G_i + \epsilon_i \left(\hat{A}_{g_{ii}}^j G_i + \hat{B}_{g_i} Y_i \right)^T & -\epsilon_i \left(G_i + G_i^T \right)
\end{bmatrix} < 0
\tag{8.32}
$$

for $j = 1, 2$. Then, the state feedback controller $K_i = Y_i G_i^{-1}$ stabilizes the polytopic system $\left(\hat{A}_{g_{ii}}(\lambda), \hat{B}_{g_i}, \hat{C}_{g_i}, 0\right)$ via a linearly parameter-dependent Lyapunov matrix $P_i(\lambda) = \lambda P_i^1 + (1 - \lambda) P_i^2$, where $0 \le \lambda \le 1$.

Remark. In the case of microgrids with radial configuration, the connection/disconnection of DGs to/from DG i can be described by a multi-model uncertainty composed of three models: 1) $N_i = \{i - 1, i + 1\}$, 2) $N_i = \{i - 1\}$, and 3) $N_i = \{i + 1\}$.

8.4.2 Algorithm I: "Decentralized Control of Islanded Inverter-interfaced Microgrids"

In this subsection, a systematic algorithm for the design of the local state feedback controllers K_i for the DG i described by (8.4)-(8.5) under plug-and-play functionality of DGs is given. The algorithm consists of the following steps:

Step 1: Build two vertices $A_{g_{ii}}^1$ and $A_{g_{ii}}^2$ given in (8.28) as well as augmented matrices $\hat{A}_{g_{ii}}^1$ and $\hat{A}_{g_{ii}}^2$ in (8.31), for $i = 1, \dots, N$.

Step 2: Impose the structural constraints given in (8.22) on the slack matrix G_i in (8.32).

Step 3: Fix the scalar parameter $\epsilon_i > 0$ in (8.32) and solve the following convex optimization problem to obtain the state feedback controllers K_i:

$$
\begin{aligned}
&\min_{Y_i, P_i^j, \eta, G_{22_i}} \quad \eta \\
&\text{subject to} \quad \begin{bmatrix} \hat{A}_{g_{ii}}^j G_i + G_i^T (\hat{A}_{g_{ii}}^j)^T + \hat{B}_{g_i} Y_i + Y_i^T \hat{B}_{g_i}^T & P_i^j - G_i^T + \epsilon_i \left(\hat{A}_{g_{ii}}^j G_i + \hat{B}_{g_i} Y_i \right) \\ P_i^j - G_i + \epsilon_i \left(\hat{A}_{g_{ii}}^j G_i + \hat{B}_{g_i} Y_i \right)^T & -\epsilon_i \left(G_i + G_i^T \right) \end{bmatrix} < 0 \\
&\qquad\quad\ P_i^j = {P_i^j}^T > 0 \\
&\qquad\qquad\ i = 1, \dots, N; \quad j = 1, 2
\end{aligned}
$$

$$(8.33)$$

Set $K_i = Y_i G_i^{-1}$.

Step 4: Design pre-filters for controller performance improvement.

Step 5: Improve the local controllers to minimize the effect of disturbance (load changes) on the voltages at PCCs.

8.5 Simulation Results

To verify the performance of the proposed control approach, we consider an islanded inverter-intefaced microgrid consisting of 11 DGs with meshed topology, borrowed from [130], as graphically shown in Fig. 8.3. The parameters of each DG and the transmission lines are given
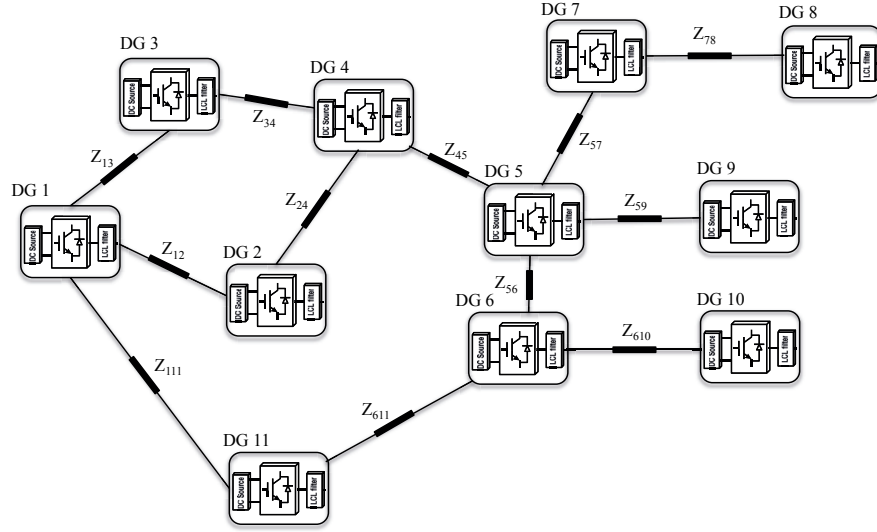
Figure 8.3: Layout of an islanded microgrid system composed of 11 DGs

in Table 8.1 and Table 8.2, respectively.

Following Algorithm I in Subsection 8.4.2, all possible connections of DGs to each DG are considered. For example, DG 1 has connections with DG 2, DG 3, and DG 11 ($N_{1_{max}} = \{2, 3, 11\}$). Moreover, for DG1, the second vertex $A_{g_{11}}^2$ is constructed through the connection with DG 11. Then, local voltage controllers are designed through the convex optimization problem given in (8.33) which is solved using YALMIP [146] as the interface and MOSEK as the solver.

The dynamic performance of the microgrid system in Fig. 8.3 with the designed controllers is validated by a set of comprehensive test cases including voltage setpoint variations, PnP operation of DGs, and major changes in the microgrid topology.

Case 1: Voltage Tracking Performance Assessment: Consider the microgrid system in Fig. 8.3 which contains 11 DGs. Each DG provides the active and reactive power for own local loads according to the information/setpoints received from Energy Management System (EMS). The *dq* components of the reference voltages for DGs are initially set according to the values listed in Table 8.1. The *d* and *q* components of the reference voltage for DG 6 respectively change from 0.6 pu and 0.8 pu to 0.8 pu and 0.6 pu at $t = 2.5s$. The dynamic responses of DG 6 due to new reference voltages are plotted in Fig. 8.4. Fig. 8.5 also shows the *dq* voltages of the other DGs connected to DG 6. The simulation results illustrate that the local voltage controller of DG 6 manages to reach the new setpoints in less than 0.5s with zero steady state error.

Case 2: Plug-and-Play Capability: The objective of this case study is to demonstrate the capability of the proposed control strategy in PnP operation of DGs. To conduct this case study, we assume that DG 11 is plugged out at $t = 1.5s$ and due to this failure all the connections attached to DG 11 are disconnected. Therefore, because of this disconnection, dynamics of
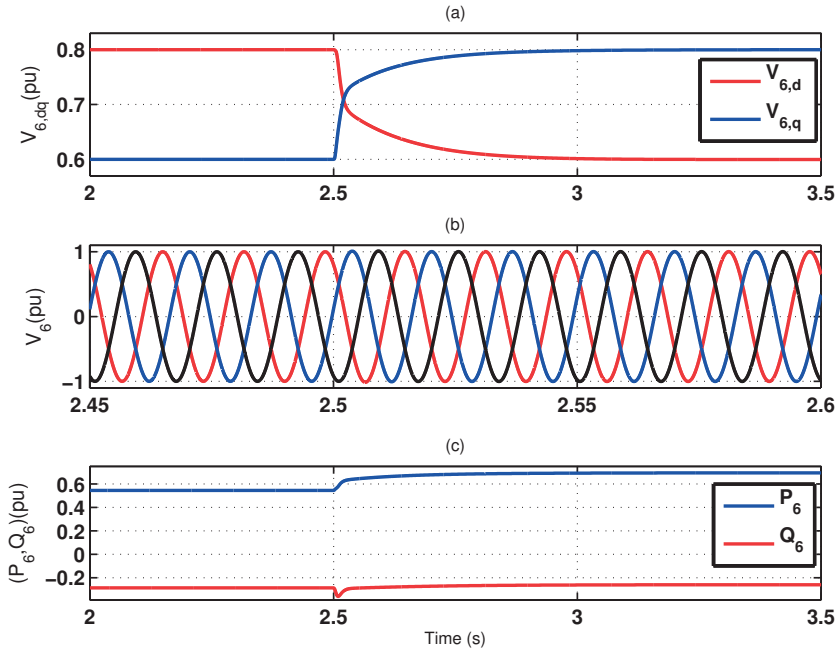
Figure 8.4: Dynamic responses of DG 6 due to new reference voltages (a) dq-components of the load voltage at PCC 6, (b) instantaneous load voltages of PCC 6, and (c) output active and reactive power of DG 6
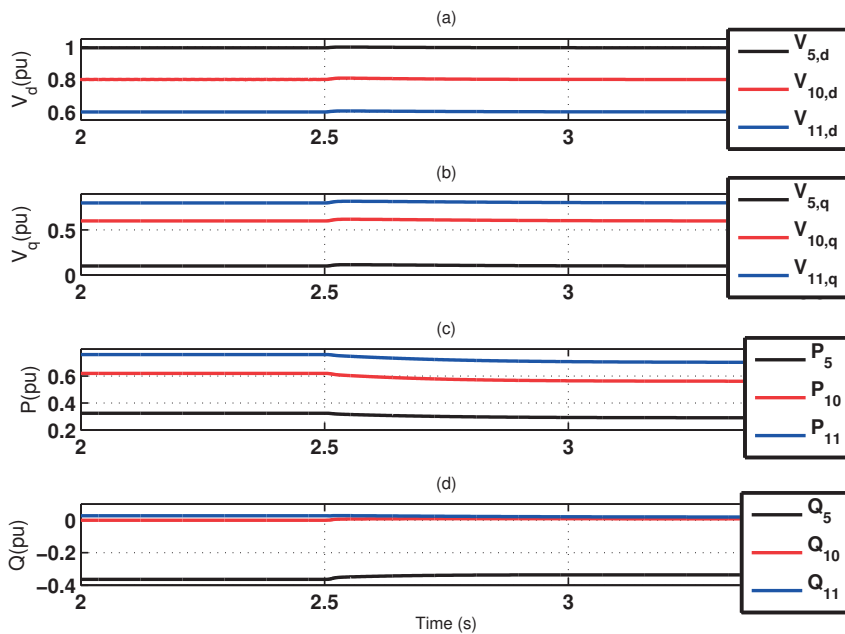
Figure 8.5: Dynamic responses of DG 5,10,11 due to step changes in $V_{dq_{ref_6}}$ (a) d-component of the load voltages at PCCs, (b) q-component of the load voltages at PCCs, (c) output active power of DGs, and (d) output reactive power of DGs
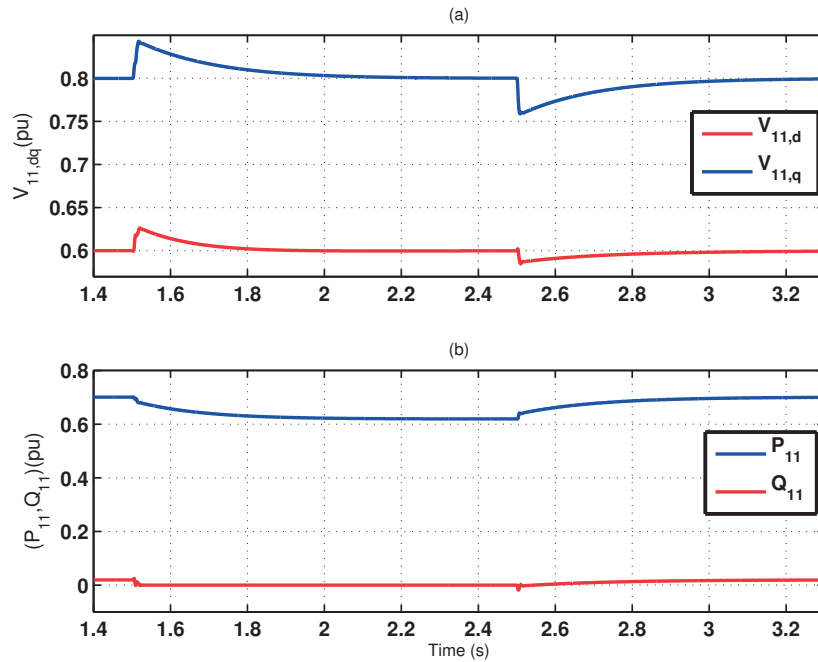
Figure 8.6: Dynamic responses of DGs due to plug-out and plug-in of DG 11 at $t = 1.5s$ and $t = 2.5s$ (a) dq-component of the load voltages at PCC 11 and (b) output active and reactive power of DG 11.
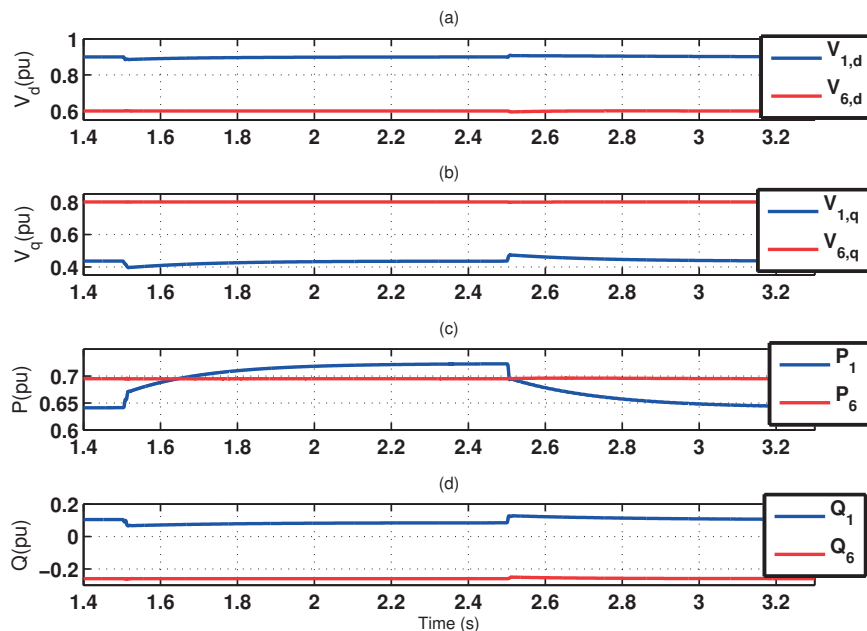
Figure 8.7: Dynamic responses of DG 1 and DG 6 due to PnP functionality of DG 11 (a) d-component of the load voltages at PCCs, (b) q-component of the load voltages at PCCs, (c) output active power of DGs, and (d) output reactive power of DGs

Table 8.1: Electrical parameters of microgrid in Fig. 8.3

DGs	Filter parameters		Shunt capacitance	Load parameters		Reference voltages	
	$R_t(m\Omega)$	$L_t(\mu H)$	$C_t(\mu F)$	$R(\Omega)$	$L(\mu H)$	$V_{d_{ref}}$ (pu)	$V_{q_{ref}}$ (pu)
DG 1	1.2	93.7	62.86	76	111.9	0.9	0.436
DG 2	1.6	94.8	62.86	85	134.3	0.9	-0.436
DG 3	1.5	107.7	62.86	93	123.1	0.8	0.6
DG 4	1.5	90.6	62.86	80	167.9	0.8	-0.6
DG 5	1.7	99.8	62.86	125	223.8	0.995	0.1
DG 6	1.6	93.4	62.86	90	156.7	0.6	0.8
DG 7	1.6	109.6	62.86	103	145.5	0.707	0.707
DG 8	1.7	104.3	62.86	150	179	0.9	0.436
DG 9	1.7	100	62.86	81	190.2	0.9	-0.436
DG 10	1.5	99.4	62.86	76	111.9	0.8	0.6
DG 11	1.5	100	62.86	76	111.9	0.6	0.8

|	
DC bus voltage	$V_{dc} = 2000V$
Power base value	$S_{base} = 8KVA$
Voltage base value	$V_{base,low} = 0.5KV, V_{base,high} = 11.5KV$
VSC terminal voltage (line-line)	$V_{VSC} = 600V$
VSC rated power	$S_{VSC} = 3MVA$
Transformer voltage ratio	$k_i = 0.6/13.8KV(\Delta/Y)$
Switching frequency	$f_{sw} = 10KHz$
System nominal frequency	$f_0 = 60Hz$

Table 8.2: Parameters of the transmission lines in Fig. 8.3

Line impedance Z_{ij}	$R_{ij}(\Omega)$	$L_{ij}(mH)$
Z_{12}	1.1	600
Z_{13}	0.9	400
Z_{34}	1	500
Z_{24}	1.2	700
Z_{45}	1	550
Z_{57}	0.7	350
Z_{56}	1.3	800
Z_{59}	1.2	650
Z_{78}	1	450
Z_{610}	1.1	600
Z_{111}	1	700
Z_{611}	1.1	600

DG1 and DG6 are affected. Then, DG 11 is plugged into the system at $t = 2.5s$. Dynamic responses of DG 11 and its neighbours due to the PnP functionality of DG 11 are depicted in Fig. 8.6 and Fig. 8.7. The results illustrate the robust performance of the proposed control technique to PnP functionality of DGs. Although the PnP operation of DG 11 changes the microgrid dynamics, the robustness of the voltage controllers guarantees stability and a desirable microgrid performance even in the case of PnP functionality of DGs.
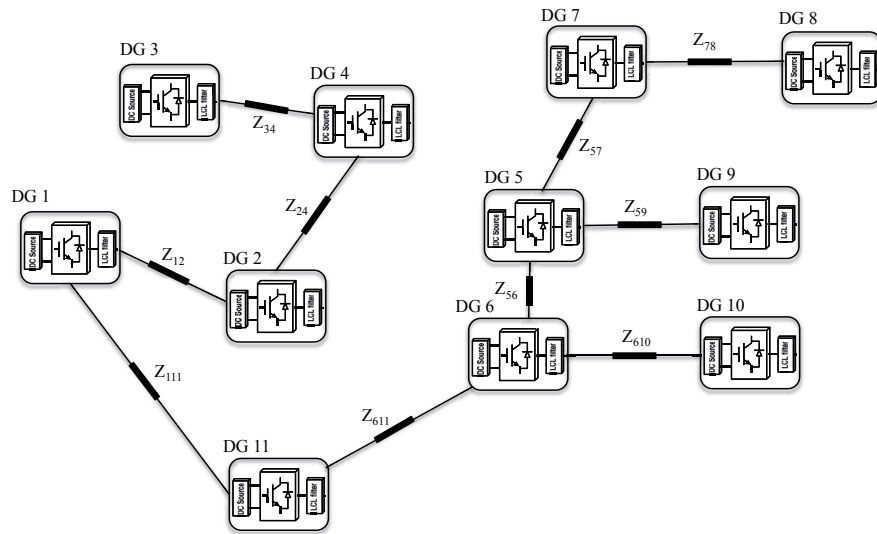
Figure 8.8: Layout of a new microgrid.
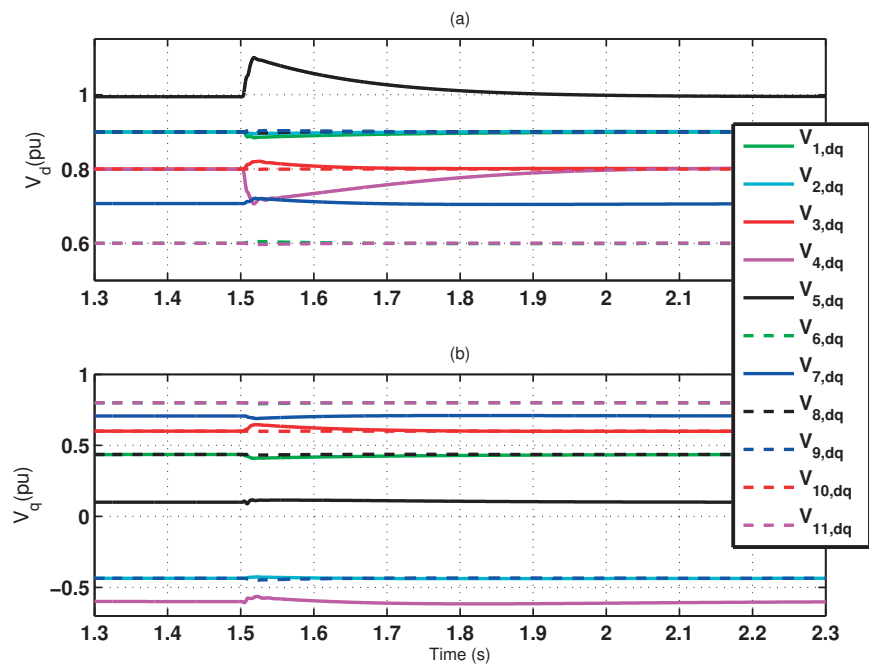
Figure 8.9: Dynamic responses of DGs due to a change in microgrid topology at $t = 1.5s$ (a) d-component of the load voltages at PCCs and (b) q-component of the load voltages at PCCs.

Case 3: Microgrid Topology Change: The objective of this case study is to assess the robust performance of the local voltage controllers to major topological uncertainties. To this end, the topology of the microgrid in Fig. 8.3 is changed to the configuration of Fig. 8.8 at $t = 1.5s$. The microgrid transients due to this topology change are illustrated in Fig. 8.9. The change in the microgrid configuration affects the system dynamics. However, simulation results reveal that the local voltage controllers are able to maintain the stability of the microgrid after a significant change in its configuration.

8.6   Conclusion

In this chapter, a voltage control technique is developed for the islanded operation of inverter-interfaced microgrids with general topology. The control structure is fully decentralized and it relies on the Quasi-Stationary Line (QSL) approximate model of microgrids. The main features of the proposed control strategy is that local controllers are robust to plug-and-play operation of DGs. As a result, the stability of the microgrid system is preserved in the case of plug-in/-out of the DGs. The performance of the proposed controller is verified under several case studies such as voltage tracking, microgrid topology change, and plug-and-play capability of DGs.

9 Conclusions and Future Directions

9.1 Conclusions

This dissertation proposes the innovative fixed-order and fixed-structure control strategies for linear time-invariant (LTI) systems affected by polytopic-type uncertainty. The developed approaches are mainly based on strictly positive realness (SPRness) of transfer functions depending on some slack matrices in the state space framework. By fixing the slack matrices in different ways, the problem of fixed-order and fixed-structure control design is converted to a convex optimization subject to a set of LMI constraints. The control design approaches are evaluated via a set of different examples and compared with the existing methods in the literature.

The dissertation also covers the main issues involved in the control of LTI interconnected systems with polytopic uncertainty, e.g. sensor and actuator placement problem, control configuration design, and robust fixed-structure control. The problems of sensor and actuator placement as well as control configuration design are formulated as optimization problems by minimizing a weighted ℓ_1 norm relaxation of the cardinality of some pattern matrices, while satisfying a guaranteed level of H_∞ performance. The solution of the optimization problems delivers a trade-off curve between the control structure and the H_∞ performance criteria.

The application part of the dissertation focuses on the control of inverter-interfaced microgrids consisting of distributed generation units (DGs). The dissertation addresses several important problems in the context of microgrids including (i) current control strategy of grid-connected voltage-source converters (ii) voltage control of islanded microgrids. Moreover, it is shown that an inverter-interfaced microgrid under plug-and-play (PnP) functionality of DGs can be cast as a polytopic system. By virtue of this novel description and use of the results from theory of robust control, the microgrid system guarantees stability and a desired performance even in the case of PnP operation of DGs. Various case studies, based on time-domain simulations in MATLAB/SimPowerSystems Toolbox and real-time hardware-in-the-loop experiments, are carried out to evaluate the performance of the proposed control strategies under different test scenarios, e.g., load change, voltage and current tracking, PnP functionality of DGs, and

microgrid topology change. The simulation and experimental results demonstrate satisfactory performance of the designed controllers.

The following main conclusions can be drawn from the work presented in this dissertation.

- The proposed LMI-based approaches in this dissertation are developed in the state space framework and are based on the use of slack variables. The size of these variables and the Lyapunov matrices grow with the order of the system and/or the number of vertices of the polytopic system. For instance, if a system of order n without uncertainty (nominal system) is considered, the control strategy introduces a Lyapunov matrix with $\frac{n^2+n}{2}$ unknown variables whereas a fixed-order controller with a comparatively small number of parameters is sought. This issue turns out to be problematic for large scale interconnected systems with large number of states, inputs, and outputs. The main problem arises from the numerical issues associated with the inapplicability of LMI solvers to large-scale problems.

- The LMI-based fixed-order/fixed-structure H_∞ controller design algorithms presented in Chapter 3 and Chapter 4 can only ensure the monotonically non-increasing convergence of the upper bound of H_∞ norm. However, there is not any guarantee that the algorithms converge to a local or global minimum.

- Non-droop-based control strategies in Chapter 7 and Chapter 8 do not take account of the dynamic behavior of renewable energy sources and model them as a constant voltage source.

9.2   Future Research Directions

Further research in the continuation of this work includes the following:

Fixed-structure Control of Polytopic Systems

- Fixed-structure control of MIMO polytopic systems in frequency domain

  The main drawback of the existing LMI-based fixed-structure control techniques is the inherent use of Lyapunov variables, whose numbers quadratically grow according to the size of the closed-loop system. This issue turns out to be highly problematic for large scale systems where the order of plant is significantly large. In this case, the existing SDP solvers may easily fail to provide a feasible solution to the underlying problem. Therefore, frequency domain-based approaches have a beneficial effect on fixed-structure control of the large-scale polytopic systems without introducing extra unknown matrices.

- Nonsoomth non-convex fixed-structure control of polytopic systems

  The recent MATLAB functions *hinfstruct* and *systune*, available in the Robust Control Toolbox, can cope with fixed-structure H_∞ control of linear time-invariant systems. These functions are based on the state-of-the-art nonsmooth non-convex optimization techniques [30, 36]. As compared to the LMI-based methods in the state space setting, *hinfstruct* and *systune* are quite fast in terms of execution time due to the absence of the Lyapunov matrix and the slack variables. For instance, given a 55×55 matrix A_g, a 55×2 matrix B_g, and a 2×55 matrix C_g, we are looking for a 2×2 stabilizing static output feedback K. The control design according to the Lyapunov inequality needs 1544 decision variables, most of them, i.e. 1540, for Lyapunov matrix P whereas the optimization problem in (1.1) requires just 4 tunable controller parameters. However, the main shortage of the existing nonsmooth non-convex optimization techniques is that they cannot deal with the polytopic systems. Therefore, development of an innovative nonsmooth non-convex optimization-based approach or the extension of the current ones to LTI polytopic systems can be an interesting research direction.

Inverter-interfaced Microgris

Generally, in the context of non-droop-based control of the inverter-interfaced microgrids, there are several areas which can still benefit from further research:

- Voltage stabilization in presence of unbalanced voltage conditions and nonlinear loads

  The voltage control systems proposed in this dissertation do not consider voltage imbalance and distortions caused by unbalanced and nonlinear loads. To ensure balanced voltages at PCCs, it is suggested that robust (decentralized) fixed-structure controllers are developed in the *abc*-frame and track sinusoidal reference signals, in consequence, eliminate the imbalance. To provide an acceptable total harmonic distortion (THD) of the voltages at PCCs, the controllers should include imaginary poles corresponding to significant harmonic frequencies.

- Improvement to non-droop-based control strategy

  The following improvements can be made to the non-droop-based control approaches:

  - Accurate modeling of DGs, e.g. incorporation of the DC-side dynamics
  - A need for advanced control design strategies with decentralized structure
  - Robustness to (non)parametric uncertainties

Bibliography

[1] K. Zhou and J. C. Doyle, *Essentials of robust control.* N.Y.: Prentice-Hall, 1998.

[2] D. Gu, P. Petkov, and M. M. Konstantinov, *Robust Control Design with MATLAB.* Springer, 2005.

[3] F. Yang, M. Gani, and D. Henrion, "Fixed-order robust H_∞ controller design with regional pole assignment," *IEEE Trans. on Automatic Control*, vol. 52, no. 10, pp. 1959–1963, 2007.

[4] R. Toscano, *Structured controllers for uncertain systems: A stochastic optimization approach.* Springer, 2013.

[5] B. A. Francis and W. M. Wonham, "The internal model principal of control theory," *Automatica*, vol. 12, no. 5, pp. 457–465, 1976.

[6] M. Fu and Z.-Q. Luo, "Computational complexity of a problem arising in fixed order output feedback design," *Systems and Control Letters*, vol. 30, no. 5, pp. 209–215, 1997.

[7] R. K. Yedavalli, *Robust control of uncertain dynamic systems in linear state space approaches.* Springer, 2013.

[8] D. E. Olivares, A. Mehrizi-Sani, A. H. Etemadi, C. A. Canizares, R. Iravani, M. Kazerani, A. H. Hajimiragha, O. Gomis-Bellmunt, M. Saeedifard, R. Palma-Behnke, G. A. Jimenez-Estevez, and N. D. Hatziargyriou, "Trends in microgrid control," *IEEE Trans. on Smart Grid*, vol. 5, no. 4, pp. 1905 – 1919, July 2014.

[9] J. M. Guerrero, M. Chandorkar, T. Lee, and P. C. Loh, "Advanced control architecture for intelligent microgrids–Part I: Decentralized and hierarchical control," *IEEE Trans. on Industrial Electronics*, vol. 60, no. 4, pp. 1254–1262, April 2013.

[10] M. Yazdanian and A. Mehrizi-Sani, "Distributed control techniques in microgrids," *IEEE Trans. on Smart Grids*, vol. 5, no. 6, pp. 2901–2909, November 2014.

[11] A. Bidram, F. L. Lewis, and A. Davoudi, "Distributed control systems for small-scale power networks: using multi agent cooperative control theory," *IEEE Control Systems Magazine*, vol. 34, no. 6, pp. 56–77, December 2014.

Bibliography

[12] G. Shafiee, J. M. Guerrero, and J. C. Vasquez, "Distributed secondary control for islanded microgrids–A novel approach," *IEEE Trans. on Power Electronics*, vol. 29, no. 2, pp. 1018–1031, February 2014.

[13] J. Schiffer, R. Ortega, A. Astolfi, J. Raisch, and T. Sezi, "Conditions for stability of droop-controlled inverter-based microgrids," *Automatica*, vol. 50, no. 10, pp. 2457–2469, October 2014.

[14] V. L. Syrmos, C. T. Abdallah, P. Dorato, and K. Grigoriadis, "Static output feedback–A survey," *Automatica*, vol. 33, no. 2, pp. 125–137, 1997.

[15] J. C. Ghaoui, F. Oustry, and M. Ait-Rami, "A cone complementarity linearisation algorithm for static output feedback and related problems," *IEEE Trans. on Automatic Control*, vol. 42, no. 8, pp. 1171–1176, 1997.

[16] K. M. Grigoriadis and R. E. Skelton, "Low order control design for LMI problems using alternating projection methods," *Automatica*, vol. 32, no. 8, pp. 1117–1125, 1996.

[17] K. M. Grigoriadis and E. B. Beran, "Alternating projection algorithms for linear matrix inequalities problems with rank constraints," *Advances in Linear Matrix Inequality Methods in Control*, pp. 251–267, SIAM, 2000.

[18] J. C. Geromel, C. C. de Souza, and R. E. Skelton, "Static output feedback controllers: Stability and convexity," *IEEE Trans. on Automatic Control*, vol. 43, no. 1, pp. 120–126, 1998.

[19] A. Hassibi, J. How, and S. Boyd, "A path-following method for solving BMI problems in control," in *American Control Conference (ACC)*, San Diego, CA, USA, 1999, pp. 1385–1389.

[20] T. Iwasaki, "The dual iteration for fixed-order control," *IEEE Trans. on Automatic Control*, vol. 44, no. 4, pp. 783–788, April 1999.

[21] T. Iwasaki and R. E. Skelton, "The XY-centring algorithm for the dual LMI problem: A new approach to fixed-order control design," *International Journal of Control*, vol. 62, no. 6, pp. 1257–1272, 1995.

[22] S.-J. Kim, Y.-H. Moon, and S. Kwon, "Solving rank-constrained LMI problems with application to reduced-order output feedback stabilization," *IEEE Trans. on Automatic Control*, vol. 52, no. 9, pp. 1737–1741, 2007.

[23] M. Fazel, H. Hindi, and S. P. Boyd, "Log-det heuristic for matrix rank minimization with applications to Hankel and Euclidean distance matrices," in *American Control Conference*, Denver, Colorado, 2003.

[24] F. Leibfritz, "An LMI-based algorithm for designing supotimal static H_2/H_∞ output feedback controllers," *SIAM Journal on Control and Optimization*, vol. 39, no. 6, pp. 1711–1735, 2001.

[25] P. Apkarian, D. Noll, and H. D. Tuan, "Fixed-order H_∞ control design via a partially augmented Lagrangian method," *International Journal of Robust and Nonlinear Control*, vol. 13, pp. 1137–1148, 2003.

[26] D. Noll, M. Torki, and P. Apkarian, "Partially augmented Lagrangian method for matrix inequality constraints," *SIAM Journal on Optimization*, vol. 15, no. 1, pp. 161–184, 2004.

[27] P. Apkarian and H. D. Tuan, "Concave programming in control theory," *Journal of Global Optimization*, vol. 15, no. 4, pp. 299–305, 1999.

[28] ——, "Robust control via concave minimization local and global algorithms," *IEEE Trans. on Automatic Control*, vol. 45, no. 2, pp. 343–370, 2000.

[29] H. D. Tuan and P. Apkarian, "Low nonconvexity-rank bilinear matrix inequalities: Alogarithms and applications in robust controller and structure designs," *IEEE Trans. on Automatic Control*, vol. 45, no. 11, pp. 2111–2117, 2000.

[30] P. Apkarian and D. Noll, "Nonsmooth H_∞ synthesis," *IEEE Trans. on Automatic Control*, vol. 51, no. 1, pp. 71–86, 2006.

[31] S. Gumussoy and M. L. Overton, "Fixed-order H_∞ controller design via HIFOO, a specialized nonsmooth optimization package," in *IEEE American Control Conference*, Seattle, USA, 2008, pp. 2750–2754.

[32] J. V. Burke, D. Henrion, and A. S. L. M. L. Overton, "HIFOO: A MATLAB package for fixed-order controller design and H_∞ optimization," in *Fifth IFAC Symposium on Robust Control Design, Toulouse*, 2006.

[33] S. Gumussoy, D. Henrion, M. Millstone, and M. L. Overton, "Multiobjective robust control with HIFOO 2.0," in *6th IFAC Symposium on Robust Control Design*, Haifa, Israel, 2009.

[34] D. Arzelier, G. Deaconu, S. Gumussoy, and D. Henrion, "H2 for HIFOO," in *Int. Conference on Control and Optimization with Industrial Applications*, Bilkent University, Ankara, Turkey, 2011.

[35] P. Apkarian, V. Bompart, and D. Noll, "Non-smooth structured control design with application to PID loop-shaping of a process," *International Journal of Robust and Nonlinear Control*, vol. 17, pp. 1320–1342, 2007.

[36] P. Apkarian, "Tuning controllers against multiple design requirements," in *American Control Conference (ACC)*, Washington, DC, USA, 2013, pp. 3888–3893.

[37] J. V. Burke, D. Henrion, A. S. Lewis, and M. L. Overton, "Satibilization via nonsmooth, nonconvex optimization," *IEEE Trans. on Automatic Control*, vol. 51, no. 11, pp. 1760–1769, 2006.

[38] J. V. Burke, A. S. Lewis, and M. L. Overton, "A robust gradient sampling algorithm for nonsmooth nonconvex optimization," *SIAM Journal on Optimization*, vol. 15, pp. 751–779, 2005.

[39] P. Gahinet and P. Apkarian, "Decentralized and fixed-structure H_∞ control in MATLAB," in *50th IEEE Conference on Decision and Control (CDC)*, Orlando, FL, USA, 2011, pp. 8205–8210.

[40] P. Apkarian, "Software (*hinfstruct, looptune, systune*)," Available: http://pierre.apkarian.free.fr/Software.html.

[41] S. Wang and J. H. Chow, "Low-order controller design for SISO systems using coprime factors and LMI," *IEEE Trans. on Automatic Control*, vol. 45, no. 6, pp. 1166–1169, June 2000.

[42] D. Henrion, M. Sebek, and V. Kucera, "Positive polynomials and robust stabilization with fixed-order controllers," *IEEE Trans. on Automatic Control*, vol. 48, no. 7, pp. 1178–1186, 2003.

[43] A. Karimi, H. Khatibi, and R. Longchamp, "Robust control of polytopic systems by convex optimization," *Automatica*, vol. 43, no. 6, pp. 1395–1402, 2007.

[44] A. Sadeghzadeh, "Fixed-order H_∞ controller design for systems with polytopic uncertainty," in *18th IFAC World Congress*, Milano, Italy, 2011, pp. 10 162–10 166.

[45] A. Sadeghzadeh, "Fixed-structure H_2 controller design: An LMI solution," in *The 7th IFAC Symposium on Robust Controller Design*, Aalborg, Denmark, 2012, pp. 325–330.

[46] D. Peaucelle and D. Arzelier, "An efficient numerical solution for H_2 static output feedback synthesis," in *European Control Conference (ECC01)*, Porto, Portugal, 2001.

[47] C. A. R. Crusius and A. Trofino, "Sufficient LMI conditions for output feedback control problems," *IEEE Trans. on Automatic Control*, vol. 44, no. 5, pp. 1053–1057, 1999.

[48] U. Shaked, "An LPD approach to robust H_2 and H_∞ static output-feedback design," *IEEE Trans. on Automatic Control*, vol. 48, no. 5, pp. 866–872, 2003.

[49] D. Mehdi, E. K. Boukas, and O. Bachelier, "Static output feedback design for uncertain linear discrete time systems," *IMA Journal of mathematical control and information*, vol. 21, pp. 1–13, 2004.

[50] K. H. Lee, J. H. Lee, and W. H. Kwon, "Sufficient LMI conditions for H_∞ output feedback stabilization of linear discrete-time systems," *IEEE Trans. on Automatic Control*, vol. 51, no. 4, pp. 675–680, 2006.

[51] J. C. Geromel, R. H. Korogui, and J. Bernussou, "H_2 and H_∞ robust output feedback control for continuous time polytopic systems," *IET Control Theory and Applications*, vol. 1, no. 5, pp. 1541–1549, September 2007.

[52] X. Du and G.-H. Yang, "LMI conditions for H_∞ static output feedback control of discrete-time systems," in *47th IEEE Conference on Decision and Control*, Cancun, Mexico, 2008, pp. 5450–5455.

[53] I. Yaesh and U. Shaked, "Robust reduced-order output-feedback H_∞ control," in *6th IFAC Sym. Robust Control Design*, Haifa, Israel, 2009, pp. 155–160.

[54] H. R. Moreira, R. C. L. F. Oliveira, and P. L. D. Peres, "Robust H_2 static output feedback design starting from a parameter-dependent state feedback controller for time-invariant discrete-time polytopic systems," *Optimal Control Applications and Methods*, vol. 32, pp. 1–13, 2011.

[55] K. Dabboussi and J. Zrida, "Sufficient dilated LMI conditions for H_∞ static output feedback robust stabilization of linear continuous-time systems," *Journal of Applied Mathematics*, vol. 2012, pp. 1–13, 2012.

[56] C. M. Agulhari, R. C. L. F. Oliveira, and P. L. D. Peres, "LMI relaxations for reduced-order robust H_∞ control of continuous-time uncertain linear systems," *IEEE Trans. on Automatic Control*, vol. 57, no. 6, pp. 1532–1537, 2012.

[57] J. Dong and G.-H. Yang, "Robust static output feedback control synthesis for linear continuous systems with polytopic uncertainties," *Automatica*, vol. 49, pp. 1821–1829, 2013.

[58] A. Sadeghzadeh, "Fixed-order H_2 controller design for state space polytopic systems," *International Journal of Control, Automation, and Systems*, vol. 12, no. 2, pp. 316–323, 2014.

[59] T. L. Baldwin, L. Mili, M. B. Boisen, and R. Adapa, "Power system observability with minimal phasor measurement placement," *IEEE Trans. on Power Systems*, vol. 8, no. 2, pp. 707–715, 1993.

[60] S. Martinez and F. Bullo, "Optimal sensor placement and motion coordination for target tracking," *Automatica*, vol. 42, no. 4, pp. 661–668, 2006.

[61] X. Ban, R. Herring, J. D. Margulici, and A. M. Bayen, "Optimal sensor placement for freeway travel time estimation," in *the 18th International Symposium on Transportation and Traffic Theory*, Hong Kong, 2009, pp. 697–721.

[62] D. G. Eliades, M. P. Michaelides, C. G. Panayiotou, and M. M. Polycarpou, "Security-oriented sensor placement in intelligent buildings," *Building and Enviroment*, vol. 63, pp. 114–121, 2013.

[63] Y. Oshman, "Optimal sensor selection strategy for discrete-time stable estimators," *IEEE Trans. on Aerospace and Electronic Systems*, vol. 30, no. 2, pp. 307–314, 1994.

Bibliography

[64] V. Gupta, T. Chung, B. Hassibi, and R. Murray, "On a stochastic sensor selection algorithm with applications in sensor scheduling and sensor coverage," *Automatica*, vol. 42, no. 2, pp. 251–260, 2006.

[65] U. Münz, M. Pfister, and P. Wolfrum, "Sensor and actuator placement for linear systems based on H_2 and H_∞ optimization," *IEEE Trans. on Automatic Control*, vol. 59, no. 11, pp. 2984–2989, 2014.

[66] S. Joshi and S. Boyd, "Sensor selection via convex optimization," *IEEE Trans. on Signal Processing*, vol. 57, no. 2, pp. 451–462, 2009.

[67] N. K. Dhingra, M. R. Jovanovic, and Z.-Q. Luo, "An ADMM algorithm for optimal sensor and actuator selection," in *53nd IEEE Conference on Decision and Control (CDC)*, Los Angeles, California, USA, 2014, pp. 4039–4044.

[68] L. Bakule, "Decentralized control: An overview," *Annual Reviews in Control*, vol. 32, no. 1, pp. 87–98, 2008.

[69] S. Skogestad and I. Postlethwaite, *Multivariable Feedback Control-Analysis and design*. Wiley, First Edition, 1996.

[70] S. Schuler, M. Gruhler, U. Münz, and F. Allgöwer, "Design of structured static output feedback controllers," in *18th IFAC World Congress*, Milano, Italy, 2011.

[71] M. Fardad, F. Lin, and M. R. Jovanovic, "Sparsity-promoting optimal control for a class of distributed systems," in *IEEE American Control Conference*, San Francisco, CA, USA, 2011.

[72] F. Lin, M. Fardad, and M. R. Jovanovic, "Design of optimal sparse feedback gains via the alternating direction method of multipliers," *IEEE Trans. on Automatic Control*, vol. 58, no. 9, pp. 2426–2431, 2013.

[73] S. Schuler, U. Münz, and F. Allgöwer, "Decentralized state feedback control for interconnected process systems," in *8th IFAC Symposium on Advanced Control of Chemical Processes*, Furama Riverfront, Singapore, 2012.

[74] S. Schuler, P. Li, J. Lam, and F. Allgöwer, "Design of structured dynamic output-feedback controllers for interconnected systems," *International Journal of Control*, vol. 84, no. 12, pp. 2081–2091, 2011.

[75] S. Schuler, U. Münz, and F. Allgöwer, "Decentralized state feedback control for interconnected systems with application to power systems," *Journal of Process Control*, vol. 24, pp. 379–388, 2014.

[76] A. I. Zecevic and D. D. Siljak, *Control of Complex Systems: Structural Constraints and Uncertainty*. Springer Verlag, 2010.

[77] S. A. Khajehoddin, M. Karimi-Ghartemani, P. K. Jain, and A. Bakhshai, "A control design approach for three-phase grid-connected renewable energy resources," *IEEE Trans. on Sustainable Energy*, vol. 2, no. 4, pp. 423–432, 2011.

[78] R. Pena-Alzola, M. Liserre, F. Blaabjerg, R. Sebastian, J. Dannehl, and F. W. Fuchs, "Analysis of the passive damping losses in LCL-filter-based grid converters," *IEEE Trans. on Power Electronics*, vol. 28, no. 6, pp. 2642–2646, 2013.

[79] E. Twining and D. Holmes, "Grid current regulation of a three-phase voltage scorch inverter with an LCL input filter," *IEEE Trans. on Power Electronics*, vol. 18, no. 3, pp. 888–895, 2003.

[80] D. N. Zmood and D. G. Holmes, "Stationary frame current regulation of PWM inverters with zero steady-state error," *IEEE Trans. on Power Electronics*, vol. 18, no. 3, pp. 814–822, 2003.

[81] M. Liserre, A. D. Aquila, and F. Blaabjerg, "Genetic algorithm-based design of the active damping for an LCL-filter three-phase active rectifier," *IEEE Trans. on Power Electronics*, vol. 19, no. 1, pp. 76–86, 2004.

[82] P. C. Loh and D. Holmes, "Analysis of multiloop control strategies for LC/CL/LCL-filtered voltage-source and current-source inverters," *IEEE Trans. on Industrial Applications*, vol. 41, no. 2, pp. 644–654, 2005.

[83] M. Liserre, R. Teodorescu, and F. Blaabjerg, "Stability of photovoltaic and wind turbine grid-connected inverters for a large set of grid impedance values," *IEEE Trans. on Power Electronics*, vol. 21, no. 1, pp. 263–272, 2006.

[84] E. Wu and P. W. Lehn, "Digital current control of a voltage source converter with active damping of LCL resonance," *IEEE Trans. on Power Electronics*, vol. 21, no. 5, pp. 1364–1373, 2006.

[85] J. Dannehl, F. W. Fuchs, and P. B. Thogersen, "PI state space current control of grid-connected PWM converters with LCL filters," *IEEE Trans. on Power Electronics*, vol. 25, no. 9, pp. 2320–2330, 2010.

[86] J. Dannehl, M. Liserre, and E. W. Funchs, "Filter-based active damping of voltage source converters with LCL filter," *IEEE Trans. on Industrial Electronics*, vol. 58, no. 8, pp. 3623–3633, 2011.

[87] B. Bahrani, M. Vasiladiotis, and A. Rufer, "High-order vector control of grid-connected voltage-source converters with LCL-filters," *IEEE Trans. on Industrial Informatics*, vol. 61, no. 6, pp. 2767 – 2775, 2014.

[88] L. A. Maccari, J. R. Massing, L. Schuch, C. Rech, H. Pinheiro, R. C. L. F. Oliveira, and V. F. Montagner, "LMI-based control for grid-connected converters with LCL filters under uncertain parameters," *IEEE Trans. on Power Electronics*, vol. 29, no. 7, pp. 3776–3785, 2014.

Bibliography

[89] W. Wu, Y. He, T. Tang, and F. Blaabjerg, "A new design method for the passive damped LCL and LLCL filter-based single-phase grid-tied inverter," *IEEE Trans. on Industrial Electronics*, vol. 60, no. 10, pp. 4339–4350, 2013.

[90] I. Gabe, M. Montagner, and H. Pinheiro, "Design and implementation of a robust current controller for VSI connected to the grid through an LCL filter," *IEEE Trans. on Power Electronics*, vol. 24, no. 6, pp. 1444–1452, 2009.

[91] M. Liserre, R. Teodorescu, F. Blaabjerg, and D. di Elettrotecnica, "Multiple harmonics control for three-phase grid converter systems with the use of PI-RES current controller in a rotating frame," *IEEE Trans. on Power Electronics*, vol. 21, no. 3, pp. 836–841, 2006.

[92] F. Blaabjerg, R. Teodorescu, M. Liserre, and A. Timbus, "Overview of control and grid synchronization for distributed power generation systems," *IEEE Trans. on Industrial Electronics*, vol. 53, no. 5, pp. 1398–1409, 2006.

[93] M. Malinowski and S. Bernet, "A simple voltage sensor less active damping scheme for three-phase PWM converters with an LCL filter," *IEEE Trans. on Industrial Electronics*, vol. 55, no. 4, pp. 1876–1880, 2008.

[94] B. Bahrani, A. Karimi, B. Rey, and A. Rufer, "Decoupled dq-current control of grid-tied voltage source converters using nonparametric models," *IEEE Trans. on Industrial Electronics*, vol. 60, no. 4, pp. 1356 – 1366, 2013.

[95] J. M. Guerrero, J. C. Vasquez, J. Matas, L. G. de Vicuna, and M. Castilla, "Hierarchical control of droop-controlled AC and DC microgrids–A general approach towards standardization," *IEEE Trans. on Industrial Electronics*, vol. 58, no. 1, pp. 158–172, January 2011.

[96] G. Shafiee, C. Stefanovic, T. Dragicevic, P. Popovski, J. C. Vasquez, and J. M. Guerrero, "Robust networked control scheme for distributed secondary control of islanded microgrids," *IEEE Trans. on Industrial Electronics*, vol. 61, no. 10, pp. 5363–5374, October 2014.

[97] A. Bidram and A. Davoudi, "Hierarchical structure of microgrids control system," *IEEE Trans. on Smart Grid*, vol. 3, no. 4, pp. 1963–1976, December 2012.

[98] P. Piagi and R. H. Lasseter, "Autonomous control of microgrids," in *IEEE power and energy society general meeting*, 2006, pp. 1–8.

[99] J. Lopes, C. Moreira, and A. Madureira, "Defining control strategies for microgrids islanded operation," *IEEE Trans. on Power Systems*, vol. 21, no. 2, pp. 916–924, May 2006.

[100] J. C. Vasquez, J. M. Guerrero, A. Luna, P. Rodriguez, and R. Teodorescu, "Adaptive droop control applied to voltage-source inverters operating in grid-connected and islanded modes," *IEEE Trans. on Industrial Electronics*, vol. 56, no. 10, pp. 4088–4096, 2009.

[101] J. C. Vasquez, R. A. Mastromauro, J. M. Guerrero, and M. Liserre, "Voltage support provided by a droop-controlled multifunctional inverter," *IEEE Trans. on Industrial Electronics*, vol. 56, no. 11, pp. 4510–4519, 2009.

[102] R. Majumder, G. Ledwich, A. Ghosh, S. Chakrabarti, and F. Zare, "Droop control of converter-interfaced micro source in rural distributed generation," *IEEE Trans. on Power Delivery*, vol. 25, no. 4, pp. 2768–2778, 2010.

[103] J. Guerrero, P. C. Loh, T. Lee, and M. Chandorkar, "Advanced control architecture for intelligent microgrids–Part II: Power quality, energy storage, and AC/DC microgrids," *IEEE Trans. on Industrial Electronics*, vol. 60, no. 4, pp. 1263–1275, 2013.

[104] J. M. Guerrero, J. C. Vasquez, J. Matas, M. Castilla, and I. G. de Vicuna, "Control strategy for flexible microgrid based on parallel line-interactive UPS systems," *IEEE Trans. on Industrial Electronics*, vol. 56, no. 3, pp. 726–736, 2009.

[105] C.-T. Lee, C.-C. Chu, and P.-T. Cheng, "A new droop control method for the autonomous operation of distributed energy resource interface converters," *IEEE Trans. on Power Electronics*, vol. 28, no. 4, pp. 1980–1993, April 2013.

[106] M. Savaghebi, A. Jalilian, J. C. Vasquez, and J. M. Guerrero, "Autonomous voltage unbalance compensation in an islanded droop-controlled microgrid," *IEEE Trans. on Industrial Electronics*, vol. 60, no. 4, pp. 1390–1402, April 2013.

[107] P. Kundur, N. J. Balu, and M. G. Lauby, *Power System Stability and Control*.   McGraw-Hill Professional, 1994.

[108] M. C. Chandorkar, D. M. Divan, and R. Adapa, "Control of parallel connected inverters in standalone AC supply systems," *IEEE Trans. on Industry Applications*, vol. 29, no. 1, pp. 136–143, 1993.

[109] J. M. Guerrero, L. G. de Vicuna, J. Matas, M. Castilla, and J. Miret, "Output impedance design of parallel-connected UPS inverters with wireless load-sharing control," *IEEE Trans. on Industrial Electronics*, vol. 52, no. 4, pp. 1126–1135, August 2005.

[110] Q.-C. Zhong, "Robust droop controller for accurate proportional load sharing among inverters operated in parallel," *IEEE Trans. on Industrial Electronics*, vol. 60, no. 4, pp. 1281–1290, April 2013.

[111] W. Yao, M. Chen, J. Matas, J. M. Guerrero, and Z.-M. Qian, "Design and analysis of the droop control method for parallel inverters considering the impact of the complex impedance on the power sharing," *IEEE Trans. on Industrial Electronics*, vol. 58, no. 2, pp. 576–588, February 2011.

[112] K. D. Brabandere, B. Bolsens, J. V. den Keybus, A. Woyte, J. Driesen, and R. Belmans, "A voltage and frequency droop control method for parallel inverters," *IEEE Trans. on Industrial Electronics*, vol. 22, no. 4, pp. 1107–1115, July 2007.

Bibliography

[113] J. M. Guerrero, J. Matas, L. G. de Vicuna, M. Castilla, and J. Miret, "Decentralized control for parallel operation of distributed generation inverters using resistive output impedance," *IEEE Trans. on Industrial Electronics*, vol. 54, no. 2, pp. 994–1004, April 2007.

[114] X. Yu, A. M. Khambadkone, H. Wang, and S. T. S. Terence, "Control of parallel-connected power converters for voltage microgrid-Part I: A hybrid control architecture," *IEEE Trans. on Power Electronics*, vol. 25, no. 12, pp. 2962–2970, December 2010.

[115] J. W. Simpson-Porco, F. Dörfler, and F. Bullo, "Synchronization and power sharing for droop-controlled inverters in islanded microgrids," *Automatica*, vol. 49, no. 9, pp. 2603–2611, September 2013.

[116] J. Schiffer, T. Seel, J. Raisch, and T. Sezi., "Voltage stability and reactive power sharing in inverter-based microgrids with consensus-based distributed voltage control," *IEEE Control Systems Technology*, 2015. [Online]. Available: http://www.control.tu-berlin.de/wiki/images/a/a4/DistributedPowerSharing_cst.pdf

[117] F. Dörfler, J. W. Simpson-Porco, and F. Bullo, "Plug-and-play control and optimization in microgrids," in *53nd IEEE Conference on Decision and Control (CDC)*, Los Angeles, California, USA, 2014, pp. 211–216.

[118] H. Bouattour, J. W. Simpson-Porco, F. Dörfler, and F. Bullo, "Further results on distributed secondary control in microgrids," in *52nd IEEE Conference on Decision and Control (CDC)*, Florence, Italy, December 2013, pp. 1514–1519.

[119] A. Bidram, A. Davoudi, F. L. Lewis, and J. M. Guerrero, "Distributed cooperative secondary control of microgrids using feedback linearization," *IEEE Trans. on Power Systems*, vol. 28, no. 3, pp. 3462–3470, August 2013.

[120] H. Liang, B. J. Choi, W. Zhuang, and X. Shen, "Stability enhancement of decentralized inverter control through wireless communications in microgrids," *IEEE Trans. on Smart Grid*, vol. 4, no. 1, pp. 321–331, March 2013.

[121] F. Dörfler, J. W. Simpson-Porco, and F. Bullo, "Breaking the hierarchy: Ddistributed control and economic optimality in microgrids," *IEEE Trans. on Control of Network Systems*, 2014 (submitted). [Online]. Available: http://arxiv.org/abs/1401.1767

[122] H. Karimi, H. Nikkhajoei, and R. Iravani, "Control of an electronically-coupled distributed resource unit subsequent to an islanding event," *IEEE Trans. on Power Delivery*, vol. 23, no. 1, pp. 493–501, 2008.

[123] H. Karimi, E. J. Davison, and R. Iravani, "Multivariable servomechanism controller for autonomous operation of a distributed generation unit: Design and performance evaluation," *IEEE Trans. on Power Systems*, vol. 25, no. 2, pp. 853–865, 2010.

[124] R. Moradi, H. Karimi, and M. Karimi-Ghartemani, "Robust decentralized control for islanded operation of two radially connected DG systems," in *IEEE International Symposium on Industrial Electronics (ISIE)*, Bari, Italy, 2010, pp. 2272–2277.

[125] H. Karimi, A. Yazdani, and R. Iravani, "Robust control of an autonomous four-wire electronically-coupled distributed generation unit," *IEEE Trans. on Power Delivery*, vol. 26, no. 1, pp. 455–466, January 2011.

[126] A. H. Etemadi, E. J. Davison, and R. Iravani, "A decentralized robust control strategy for multi-DER microgrid-Part I: Fundamental concepts," *IEEE Trans. on Power Delivery*, vol. 27, no. 4, pp. 1843–1853, 2012.

[127] B. Bahrani, M. Saeedifard, A. Karimi, and A. Rufer, "A multivariable design methodology for voltage control of a single-DG-unit microgrid," *IEEE Trans. on Industrial Informatics*, vol. 9, no. 2, pp. 589 – 599, 2013.

[128] M. Babazadeh and H. Karimi, "A robust two-degree-of-freedom control strategy for an islanded microgrid," *IEEE Trans. on Power Delivery*, vol. 28, no. 3, pp. 1339–1347, 2013.

[129] A. H. Etemadi, E. J. Davison, and R. Iravani, "A generalized decentralized robust control of islanded microgrids," *IEEE Trans. on Power Systems*, vol. 29, no. 6, pp. 3102–3113, 2014.

[130] S. Riverso, F. Sarzo, and G. Ferrari-Trecate, "Voltage and frequency control of islanded microgrids: A plug-and-play approach," in *IEEE International Conference on Smart Grid Communications*, Venice, Italy, November 2014, pp. 73–78.

[131] ——, "Plug-and-play voltage and frequency control of islanded microgrids with meshed topology," *IEEE Trans. on Smart Grid*, vol. 6, no. 3, pp. 1176–1184, 2015.

[132] I. D. Landau, R. Lozano, and M. M'Saad, *Adaptive Control*.   London: Springer-Verlag, 1997.

[133] G. Meinsma and M. Fu, "A dual formulation of mixed μ and on the losslessness of (D, G) scaling," *IEEE Trans. on Automatic Control*, vol. 42, no. 7, pp. 1032–1036, 1997.

[134] Y. Ebihara, "On the exactness proof of (D, G) scaling," *SICE Journal of Control, Measurement, and System Integration*, vol. 1, no. 6, pp. 474–478, 2008.

[135] X. Zhang, P. Tsiotras, and T. Iwasaki, "Lyapunov-based exact stability analysis and synthesis for linear single-parameter dependent systems," *Int. Journal of Control*, vol. 83, no. 9, pp. 1823–1838, 2010.

[136] O. Toker and H. Ozbay, "On the NP-hardness of solving bilinear matrix inequalities and simultaneous stabilization with static output feedback," in *IEEE American Control Conference*, Seattle, Washington, 1995, pp. 2525–2526.

[137] M. Kocvara and M. Stingl, "Available at `www.penopt.com`," *Version 2.1*, 2006.

Bibliography

[138] D. Henrion, J. Lofberg, M. Kocvara, and M. Stingl, "Solving polynomial static output feedback problems with PENBMI," in *44th IEEE Conference on Decision and Control (CDC) and the European Control Conference (ECC)*, Seville, Spain, 2005, pp. 7581–7586.

[139] J. Fiala, M. Kocvara, and M. Stingl, "PENLAB-A solver for nonlinear semidefinite programming," *Technical Report*, 2013.

[140] Y. Ebihara, Y. Onishi, and T. Hagiwara, "Robust performance analysis of uncertain LTI systems: Dual LMI approach and verifications for exactness," *IEEE Trans. on Automatic Control*, vol. 54, no. 5, pp. 938–951, 2009.

[141] X. Zhang, P. Tsiotras, and P. A. Bliman, "Multi-parameter dependent Lyapunov functions for the stability analysis of parameter-dependent LTI systems," in *13th Mediterranean Conference on Control and Automation*, Limassol, Cyprus, 2005, pp. 1263–1268.

[142] P. A. Bliman, "An existence result for polynomial solutions of parameter-dependent LMIs," *Systems and Control Letters*, vol. 51, pp. 165–169, 2004.

[143] M. G. Safonov, K. C. Goh, and J. H. Ly, "Control system synthesis via bilinear matrix inequalities," in *IEEE American Control Conference*, Baltimore. Maryland, 1994.

[144] S. Kanev, C. Scherer, M. Verhaegen, and B. D. Schutter, "Robust output feedback controller design via local BMI optimization," *Automatica*, vol. 40, no. 7, pp. 1115–1127, July 2004.

[145] Q. T. Dinh, S. Gumussoy, W. Michiels, and M. Diehl, "Combining convex-concave decompositions and linearization approaches for solving BMIs, with application to static output feedback," *IEEE Trans. on Automatic Control*, vol. 57, no. 6, pp. 1377–1390, 2012.

[146] J. Löfberg, "YALMIP: A toolbox for modeling and optimization in MATLAB," in *CACSD Conference*, 2004. [Online]. Available: http://control.ee.ethz.ch/~joloef/yalmip.php

[147] M. S. Sadabadi and A. Karimi, "Fixed-order H_∞ and H_2 controller design for continuous-time polytopic systems: An LMI-based approach," in *European Control Conference (ECC13)*, Zurich, Switzerland, 2013, pp. 1132–1137.

[148] S. Boyd, L. E. Ghaoui, E. Feron, and V. Balakrishnan, *Linear Matrix Inequalities in System and Control Theory*. Philadelphia: SIAM, 1994.

[149] A. Albert, "Conditions for positive and nonnegative definiteness in terms of pseudoinverses," *SIAM Journal on Applied Mathematics*, vol. 17, no. 2, pp. 434–440, 1969.

[150] H. Khatibi, A. Karimi, and R. Longchamp, "Fixed-order controller design for systems with polytopic uncertainty using LMIs," *IEEE Trans. on Automatic Control*, vol. 53, no. 1, pp. 428–434, 2008.

[151] A. Karimi, "Frequency-domain robust control toolbox," in *52nd IEEE Conference in Decision and Control*, Florence, Italy, 2013, pp. 3744 – 3749.

[152] P. P. Vaidyanathan, "The discrete-time bounded-real lemma in digital filters," *IEEE Trans. on Circuits and Systems*, vol. 32, no. 9, pp. 918–924, 1985.

[153] K. C. Toh, M. J. Todd, and R. H. Tutuncu, "SDPT3: A MATLAB software package for semidefinite programming," *Optimization Methods and Software*, vol. 11, pp. 545–581, 1999.

[154] J. F. Sturm, "Using SeDuMi 1.02, A Matlab toolbox for optimization over symmetric cones," *Optimization Methods and Software*, vol. 11, pp. 625–653, 1999.

[155] F. Leibfritz and W. Lipinski, "Description of the benchmark examples in $COMPl_eib$ 1.0," University of Trier, Germany, Tech. Rep., 2003.

[156] H. Khatibi and A. Karimi, "H_∞ controller design using an alternative to Youla parameterization," *IEEE Trans. on Automatic Control*, vol. 55, no. 9, pp. 2119–2123, 2010.

[157] M. C. de Oliveira, J. C. Geromel, and J. Bernussou, "Extended H_2 and H_∞ norm characterizations and controller parameterizations for discrete-time systems," *Int. Journal of Control*, vol. 75, no. 9, pp. 666–679, 2002.

[158] R. C. L. F. Oliveira and P. L. D. Peres, "Parameter-dependent LMIs in robust analysis: Characterisation of homogeneous polynomially parameter-dependent solutions via LMI relaxations," *IEEE Trans. on Automatic Control*, vol. 52, no. 7, pp. 1334–1340, 2007.

[159] C. M. Agulhari, R. C. L. F. de Oliveira, and P. L. D. Peres, "Robust LMI Parser: A computational package to construct LMI conditions for uncertain systems," in *XIX Brazilian Conference on Automation (CBA 2012)*, Campina Grande, PB, Brazil, 2012, pp. 2298–2305.

[160] J. Dong and G.-H. Yang, "Static output feedback control synthesis for linear systems with time-invariant parametric uncertainties," *IEEE Trans. on Automatic Control*, vol. 52, no. 10, pp. 1930–1936, 2007.

[161] D. Arzelier, E. N. Gryazina, D. Peaucelle, and B. T. Polyak, "Mixed LMI/randomized methods for static output feedback control design," in *American Control Conference (ACC10)*, Baltimore, MD, USA, 2010, pp. 4683–4688.

[162] M. S. Sadabadi and A. Karimi, "Robust performance analysis of single parameter-dependent systems with polynomially parameter-dependent Lyapunov matrices," in *19th IFAC World Congress (IFAC WC 2014)*, Cape Town, South Africa, 2014, pp. 6141–6146.

[163] E. J. Candes, M. B. Wakin, and S. P. Boyd, "Enhancing sparsity by reweighted ℓ_1 minimization," *Journal of Fourier Analysis and Applications*, vol. 14, pp. 877–905, 2008.

[164] M. Pfister, "Optimal sensor placement for linear systems," Bachelor Thesis, University of Bayreuth, 2012.

Bibliography

[165] A. Ulbig, T. S. Borsche, and G. Andersson, "Impact of low rotational inertia on power system stability and operation," in *19th IFAC World Congress (IFAC WC 2014)*, Cape Town, South Africa, 2014.

[166] M. Fazel, "Matrix rank minimization with applications," Ph.D. dissertation, Department of Electrical Engineering, Stanford University, Stanford, USA, 2002.

[167] H. Karimi, A. Yazdani, and R. Iravani, "Negative-sequence current injection for fast islanding detection of a distributed resource unit," *IEEE Trans. on Power Electronics*, vol. 23, no. 1, pp. 298–307, 2008.

[168] C. Schauder and H. Mehta, "Vector analysis and control of advanced static VAR compensators," in *IEE Proceedings C, Generation, Transmission and Distribution*, vol. 140, no. 4, 1993, pp. 299–306.

[169] P. P. Khargonekar, I. R. Peterson, and K. Zhou, "Internal model-based current control of the RL filter-based voltage-sourced converter," *IEEE Trans. on Energy Conversion*, vol. 29, no. 4, pp. 873–881, 2014.

[170] B. Bahrani, S. Kenzelmann, and A. Rufer, "Multivariable-PI-based *dq* current control of voltage source converters with superior axes decoupling capability," *IEEE Trans. on Industrial Electronics*, vol. 58, no. 7, pp. 3016–3026, 2011.

[171] F. Katiraei and M. R. Iravani, "Power management strategies for a microgrid with multiple distributed generation units," *IEEE Trans. on Power Systems*, vol. 21, no. 4, pp. 1821–1831, 2006.

[172] F. Katiraei, M. R. Iravani, N. Hatziargyriou, and A. Dimeas, "Microgrids management," *IEEE Power & Energy Magazine*, vol. 6, no. 3, pp. 54–65, 2008.

[173] "IEEE recommended practice for monitoring electric power quality, IEEE standard 1159," 2009.

[174] V. Venkatasubramanian, H. Schattler, and J. Zaborszky, "Fast time-varying phasor analysis in the balanced three-phase large electric power system," *IEEE Trans. on Automatic Control*, vol. 40, no. 11, pp. 1975–1982, 1995.

[175] J. Lunze, *Feedback Control of Large Scale Systems*.   NJ, USA: Prentice Hall, 1992.

[176] R. C. L. F. Oliveira, M. C. de Oliveira, and P. L. D. Peres, "Robust state feedback LMI methods for continuous-time linear systems: Discussions, extensions and numerical comparisons," in *IEEE International Symposium on Computer-Aided Control System Design (CACSD)*, Denver, CO, USA, 2011, pp. 1038–1043.

172

Mahdieh S. Sad Abadi

Address   Ave. de Longemalle 16,
                   1020 Renens, VD, Switzeralnd   **Phone**   +41 (0) 78 658 9086
Date of Birth 23/07/1982   **Email**   sadabadi.mahdieh@gmail.com

Education

01/2011 – 09/2015   **Ph.D. in Systems and Control Theory**
                      Ecole Polytechnique Federale de Lausanne (EPFL),
                      Lausanne, Switzerland

09/2004 – 07/2007   **M.Sc. in Systems and Control Theory** (First class honours)
                      Amirkabir University of Technology (Tehran Polytechnic),
                      Tehran, Iran

09/2000 – 07/2004   **B.Sc. in Electronics** (First class honours)
                      Amirkabir University of Technology (Tehran Polytechnic),
                      Tehran, Iran

Teaching and Research Experience

01/2011 – 09/2015   Teaching and research duties at the Automatic Control Laboratory, EPFL
                      – Supervision of more than 10 semester projects in systems and control theory
                      – Teaching assistant for various courses

04/2015   Visting scholar at LAAS-CNRS, Toulouse, France

04/2014 – 06/2014   Visting scholar at Departement de Genie Electrique,
                      Ecole Polytechnique de Montreal, Montreal, Canada

09/2004 – 07/2007   Electrical Engineering Department, Tehran Polytechnic
                      – Graduate research assistant
                      – Teaching assistant for various courses

Research Interests

- **Fixed-structure Control**
- **Distributed Generations and Microgrid Control**
- **Robust Control**
- **Multidimensional Systems**

Publications

Journal Papers

[6] M. S. Sadabadi, A. Karimi, and H. Karimi, "Fixed-order Decentralized/Distributed Control of Islanded Inverter-interfaced Microgrids", Control Engineering Practice, Vol. 45, pp. 174-193, 2015.

[5] M. S. Sadabadi, M. Shafiee, and M. Karrari, "Two-Dimensional ARMA Model Order Determination", ISA Transactions, Vol. 48, No. 3, pp. 247-253, 2009.

[4] M. S. Sadabadi and M. Shafiee, "AR Order Determination of 3-D ARMA Model Based on the Minimum Eigenvalue (MEV) Criterion and Instrumental Variable Method", Journal of Control, Vol. 3, No. 2, pp. 25-32, 2009.

[3] M. S. Sadabadi, M. Shafiee, and M. Karrari, "Experimental Modeling of Two-Dimensional systems with ARMA Structure", Iranian Journal of Electrical and Computer Engineering (IJECE), Vol. 7, No. 1, pp. 76-83, 2009 (in Farsi).

[2] M. S. Sadabadi, M. Shafiee, and M. Karrari, "System Identification of Two-Dimensional Continuous-Time Systems Using Wavelets as Modulating Functions", ISA Transactions, Vol. 47, No. 3, pp. 256-266, 2008.

[1] M. S. Sadabadi, M. Shafiee, and M. Karrari, "A New Technique for Order Determination of Two-Dimensional ARMA Models", Systems Science, Vol. 34, No. 2, pp. 49-53, 2008.

Conference Papers

[20] M. S. Sadabadi and A. Karimi, "Sensor Placement in LTI Systems with Polytopic Uncertainty via Convex Optimization", 8th IFAC Symposium on Robust Control Design (ROCOND), Bratislava, Slovakia, July 2015.

[19] M. S. Sadabadi and A. Karimi, "Fixed-order Control of LTI Systems subject to Polytopic Uncertainties via the Concept of Strictly Positive Realness", American Control Conference (ACC), Chicago, IL, July 2015.

[18] M. S. Sadabadi and A. Karimi, "Fixed-structure Sparse Control of Interconnected Systems with Polytopic Uncertainty", 19th IFAC World Congress, Cape Town, South Africa, August 2014.

[17] M. S. Sadabadi and A. Karimi, "Robust Performance Analysis of Single Parameter-dependent Systems with Polynomially Parameter-dependent Lyapunov Matrices", 19th IFAC World Congress, Cape Town, South Africa, August 2014.

[16] M. S. Sadabadi and A. Karimi, "An LMI Formulation of Fixed-order H-infinity and H-2 Controller Design for Discrete-time Systems with Polytopic Uncertainty", Proceedings of the 52nd Conference in Decision and Control (CDC), Florence, Italy, December 2013.

[15] M. S. Sadabadi and A. Karimi, "Fixed-order H-infinity and H2 Controller Design for Continuous-time Polytopic Systems: An LMI-based Approach", Proceedings of European Control Conference (ECC), Zurich, Switzerland, July 2013.

[14] A. Karimi and M. S. Sadabadi, "Fixed-order Controller Design for State Space Polytopic Systems by Convex Optimization", Proceedings of IFAC Joint Conference, Grenoble, France, February 2013.

[13] M. S. Sadabadi and J. Poshtan, "Identification of an Ill-Conditioned Distillation Column Process using Rotated Signals as Input", International Symposium on Advanced Control of Chemical Processes (ADCHEM 2009), Vol. 2, pp. 868-873, Istanbul, Turkey, July 2009.

[12] M. S. Sadabadi and J. Poshtan, "MIMO Rotated Input Design for Ill-conditioned Distillation Column Process", Proceedings of ICEE 2009, Vol. 7, pp. 339-343, Tehran, Iran, May 2009.

[11] M. S. Sadabadi and J. Poshtan, "Black Box Identification of Synchronous Generator using Hammerstein and Nonlinear Feedback Models", Proceedings of the ICEE 2009, Vol. 7, pp. 333-338, Tehran, Iran, May 2009.

[10] M. S. Sadabadi, M. Shafiee, and M. Karrari, "Continuous-Time System Identification Using Sine-Cosine Wavelet Based Modulating Function", ICEE 2008, pp. 107-111, May 2008, Tehran, Iran, May 2008.

[9] M. S. Sadabadi, M. Karrari, and O.P. Malik, "Identification of Synchronous Generator Using Nonlinear Feedback Model", Proceedings of the 17th IFAC World Congress, pp. 10371-10376, Seoul, Korea, 2008.

[8] M. S. Sadabadi, M. Shafiee, and M. Karrari, "Parameter Estimation of Two-Dimensional Linear Differential Systems via Fourier Based Modulation Function", Proceedings of the 17th IFAC World Congress, pp. 14385-14390, Seoul, Korea, 2008.

[7] M. S. Sadabadi, M. Shafiee, and M. Karrari, "Determination of Two-Dimensional ARMA Model Order Using Rank Test Based Approach", Proceedings of the 16th IEEE Conference on Control and Applications (CCA) Part of IEEE Multi-Conference on Systems and Control, pp. 1156-1160, Singapore, October 2007.

[6] M. S. Sadabadi, M. Karrari, and O.P. Malik, "Nonlinear Identification of Synchronous Generator Using Hammerstein Model with Piecewise Linear Static Maps", Proceedings of the IEEE Power Tech 2007, pp. 1067-1071, Lausanne, Switzerland, July 2007.

[5] M. S. Sadabadi, M. Shafiee, and M. Karrari, "A New Technique for Order Determination of Two-Dimensional ARMA Models", Proceedings of the 16th International Conference on Systems Science (SYSTEMS SCIENCE XVI), Vol. 1, pp. 456-462, Wroclaw, Poland, September 2007.

[4] M. S. Sadabadi, M. Shafiee, and M. Karrari, "AR Order Determination of a 2-D ARMA Model", Proceedings of the European Control Conference 2007 (ECC07), pp. 3877-3882, Kos, Greece, July 2007.

[3] M. S. Sadabadi, M. Shafiee, and M. Karrari, "Determination of the Order of the AR Part of a 2-D ARMA Model Based on MDL Criterion and Instrumental Variable Method", Proceedings of the ICEE 2007, pp. 130-135, Tehran, Iran, May 2007 (in Farsi).

[2] M. S. Sadabadi, M. Shafiee, and M. Karrari, "MA Order Determination of a Two-Dimensional ARMA Model Using Samples Correlation", Proceedings of the ICEE 2007, pp. 136-140, Tehran, Iran, May 2007 (in Farsi).

[1] M. S. Sadabadi, M. Karrari, and M. S. Akhavan Hejazi, "Nonlinear Identification of Synchronous Generator Using Hammerstein Model", Proceedings of the 21st International Power System Conference (PSC), pp. 533-541, Tehran, Iran, November 2006 (in Farsi).